Changing flood and landslide hazard
—
A meteorological perspective

Thea A. R. Turkington

PhD dissertation committee

Chair	
Prof.dr. A. Veldkamp	University of Twente
Promoter	
Prof.dr. V. Jetten	University of Twente
Assistant promoters	
Dr. C. J. van Westen	University of Twente
Dr.ir. J. Ettema	University of Twente
Members	
Prof.dr. G. van Steenhoven	University of Twente
Prof.dr. F.D. van der Meer	University of Twente
Prof.dr. T. Glade	University of Vienna
Prof.dr. S.M. de Jong	Utrecht University
Prof.dr. A. Klein-Tank	KNMI

This research was conducted under the auspices of the
Graduate School for Socio-Economic and Natural Sciences
of the Environment (SENSE).

ITC dissertation number 288
ITC, P.O. Box 217, 7500 AE Enschede, The Netherlands

ISBN: 978-90-365-4193-0
DOI: http://dx.doi.org/10.3990//1.9789036541930
Printed by: ITC Printing Department

UNIVERSITY OF TWENTE.

FACULTY OF GEO-INFORMATION SCIENCE AND EARTH OBSERVATION

CHANGING FLOOD AND LANDSLIDE HAZARD
—
A METEOROLOGICAL PERSPECTIVE

DISSERTATION

to obtain
the degree of doctor at the University of Twente,
on the authority of the rector magnificus,
prof. dr. H. Brinksma,
on account of the decision of the graduation committee,
to be publicly defended
on Thursday 22 September, 2016 at 11.00

by

Thea A. R. Turkington
born on December 02, 1983
in Vancouver, Canada

This dissertation is approved by:

Prof.dr. V. Jetten (promoter)
Dr. C. J. van Westen (assistant promoter)
Dr.ir. J. Ettema (assistant promoter)

Acknowledgments

This work would not have been possible without the support of many people. I would like to express my thanks to my colleagues for providing different perspectives as well as to my friends and family helping me keep perspective.

A big chunk of support came from CHANGES - the European Marie Curie research network in which this research took place (CHANGES = Changing Hydro-meteorological Risks as Analysed by a New Generation of European Scientists). The participants in CHANGES worked together to come up with unique solutions to a variety of challenges in assessing changing hazard and risk assessment, and provided the opportunity to situate this research within a wider framework of changing risk in Europe. Alongside climate changes, the focus of this research, other changes considered in the project included changes in land use and vulnerability. A big thank you must therefore go to the CHANGES team for giving me the opportunity to undertake this research and for all the support, data, and guidance along the way. And to the 14 other CHANGES early stage researchers: Korbinian, Romy, Ziga, Roxana, Haydar, Veronica, Kathrin, Zar Chi, Juliette, Tess, Marie, Vera, Kaixi, Roya, Irina, and Julian, thank you all for the fun times, hard work, and support throughout the CHANGES project and beyond.

A special thank you goes to my supervisory team. To my supervisors, Janneke Ettema and Cees van Westen, thank you for accepting me into this PhD journey and for all the guidance along the way. Janneke, as your first PhD student, I felt that in some ways we both grew together over this journey. Thank you for your honesty and for your positive encouragement to keep pushing onward and upward. Cees, thank you for your enthusiasm, the discussions, and seemingly limitless number of new ideas. To my promoter Victor, thank you for your support and the long, interesting discussions we had. Thank you also to my supervisors when on secondment Stephan Harrison (University of Exeter) and Peter Zeil and Stefan Kienberger (University of Salzburg). Thank you also to the Red Cross Climate Centre team, who provided valuable guidance in the final chapter.

My heartfelt thanks go to my fellow PhDs and colleagues. Thank you all for the encouragement, advice, and of course, the cake. Thank you to my colleagues in the ESA department, you were always open to

providing advice and guidance. To my fellow PhDs, including those in the wider SENSE community, you played a large role in making the whole PhD experience enjoyable. Particularly to my fellow ESA PhDs, Bastian, Islam, Effie, Hakan, Matthew, Saad, Riswan, Chenxiao, and Irena, as well as Fangyuan, Anandita, Maria, Elnaz, Mitra, Xi, Novi, Manuel, and Alby, thank you for all the laughs, encouragement, adventures, and photo shoots. To my fellow sport enthusiasts, including those in Run4Fun, you played a vital role in helping me work out any frustrations, as well as working off some of the cake.

A big hug and thank you goes to my family and friends in New Zealand and Canada. To my mum, Diane, and my dad, Dale, thank you for the support and for always believing in me. To my brother Rowan, thank you for the support, including helping with the cover. And finally to my husband Dayal, you had to put up with a lot over these past four years. I am forever grateful and look forward to what the future has in store for us. Thank you.

Summary

Despite the concern around climate change, understanding how hydro-meteorological hazards will respond in the future still faces many challenges. Climate change-hazard studies are undertaken to improve our understanding by combining future projections of various climate variables with hydro-meteorological hazard event characteristics. However, floods and landslides are rare events, which require a long record of both the climate and the hazardous events. Even if long records are available, the completeness of hazard inventories may be questionable, and inhomogeneity and trends in the climate data may be present. Furthermore, while heavy rainfall is a precursor for many flood and landslide events, the occurrence also depends on the spatial variability, antecedent precipitation and temperature, and properties of the landscape. Rain gauges measure rainfall at a particular point and can miss nearby intense, localized, convective rainfall that triggers hydro-meteorological hazards. Once a relationship is established between climate and hazards, it is not straightforward translating future climate change into changing hazard. The grid-sizes of climate models used for climate projections are too coarse for local hazard studies and to adequately represent the complex local topography. All these factors result in few climate change-hazard studies for mountainous catchments. However, climate change has the potential to alter hydro-meteorological hazards, and therefore overcoming the challenges is vital to help support decision makers and convey the seriousness of climate change in mountainous catchments.

This research addresses several of the challenges in developing climate change-hazard studies for mountainous catchments. Local climate projections for mountainous hydro-meteorological hazards were developed through the assessment of the triggering conditions of these events along with the climate change scenarios. Current and future triggering conditions were assessed from a climate or meteorological perspective, as opposed to considering other factors such as land cover change or mitigation works, which are out of the scope of this work. The types of hydro-meteorological hazards investigated were floods (flash floods, river/fluvial floods) and landslides (soil slides and debris flows). These hazards have been under-reported in climate research literature due to the small scale on which they occur relative to climate models, the difficulties in downscaling modelled precipitation in mountainous

catchments, incomplete hazard inventories, and limitations in defining the precise meteorological triggers. The European Alps is an ideal area to study these challenges as changes in the climate have already been observed and the region contains some of the longest climate records. Three study areas were chosen: the Barcelonnette Basin in the southeast of France, the Fella River Basin in the northeast of Italy, and the Salzach Valley in western Austria. The study areas have experienced numerous flood and landslide events and have more than 20 years of climate records. The three areas also have the potential to respond differently to future climate change, allowing for a spectrum of climate-change hazard studies to be developed.

The first step in developing climate change-hazard studies was to investigate the climate data to determine its quality and to compare the climate of the three study areas. It is important to understand the meteorological characteristics of each of the regions to gain an understanding of the current situation and to also understand the limitations of the data before further analysis. The climate data was assessed for changes in the records caused by non-climatic factors, such as the movement of a weather station, or new measurement techniques. The climate of the catchments was compared between the three study areas, with the Barcelonnette Basin the driest catchment, followed by the Salzach Valley. For the two study areas with climate records longer than 30 years, the Barcelonnette and Fella River basins, most temperature records showed trends consistent with warming, such as increases in the growing season length, and decreases in the number of days that do not exceed 0°C. The precipitation records had fewer and less consistent trends, with 10 out of 11 indices with significant trends in the Fella River basin showing an increase in heavy precipitation, while for Barcelonnette, only 1 out of 4 indices found significant trends indicate increasing heavy precipitation.

Various methods were tested for identifying the climate variables or proxies for hydro-meteorological hazards at the daily timescale. Fluvial (river) floods, flash floods and debris flows, and soil slides were first treated separately, as each hazard type may have unique meteorological triggers. All hydro-meteorological events were then grouped together to determine if there are particular large scale atmospheric conditions that lead to hydro-meteorological hazards in the area. Three sets of distinct temperature and precipitation conditions were identified for floods in the Barcelonnette Basin, indicating that multiple climate proxies are required. For flash floods and debris flows, extreme daily precipitation (>150 mm) in the Fella Basin could be used as a climate proxy, and the return period of daily precipitation as an indication of the return period for the hazards. However, the link for the Barcelonnette Basin was not as clear, with the most extreme daily precipitation events not associated with either a flash flood or debris flow. The link for soil slides was also not clear in the Barcelonnette Basin, although including temperature improved the results than using precipitation alone. Finally, atmospheric conditions with low pressure systems to the northwest of the Barcelonnette Basin had the highest association with hydro-meteorological events.

These situations brought moist northwesterlies over the area, and high precipitation amounts, as would be expected for hydro-meteorological hazards.

Due to the limitations in using precipitation directly for flash floods and debris flows in the Barcelonnette Basin, atmospheric indicators as proxies were assessed in more detail. In particular empirical thresholds were developed, which could be used in risk assessment, early warning systems, or climate change-hazard studies. The most important atmospheric indicators for the study area were Convective Available Potential Energy (CAPE) and specific humidity. CAPE is a measure of how much energy would be gained from taking a small parcel of air near the surface and nudging it upward. The results show that in general the atmospheric indicators perform better than using precipitation, although there is still a high level of uncertainty.

Two statistical downscaling approaches were considered bridge the gap between regional scale climate model data and the local scale of the climate change-hazard studies. The perfect prognosis approach was applied first, where an empirical relationship between the large-scale observed atmospheric variables and the local scale feature provided the basis for future projections. The second approach that was applied was Model Output Statistics, where corrections were applied to large-scale model data in the observed period, which were then used for the future projections. The results show that the Barcelonnette Basin had smaller increases in extreme precipitation and greater decreases in the wet day frequency than the Fella River Basin. However, the ability of the statistical downscaling methods to model mean precipitation values or wet day frequency were not necessarily representative of extreme values. Trends in future wet day frequency were also not indicative of trends in extreme precipitation. Finally, the results suggest that the MOS method applied was the preferable downscaling technique for extreme daily precipitation.

Based on the previous results, future climate projections were translated into future debris flow activity predictions for the Barcelonnette and Fella River basins. Future trends in debris flow activity were constructed based on bias-corrected climate projections using two proxies: daily precipitation and CAPE combined with specific humidity. Along with a comparison between the precipitation and atmospheric proxies, the future trends in debris flow activity were compared based on the climate models used, the Representative Concentration Pathways (RCPs), and the base period. For both basins, the future climate projections varied between no change in debris flow activity up to an increase of 6.0% per decade in days with debris flow occurrences towards the end of 21st century. In the Barcelonnette Basin, the base period and proxy had the biggest impact on the future number of debris flow days. In the Fella River Basin, the base period, RCP, and proxy used defined the future range. The results show that not only should the downscaling technique be considered when assessing future debris flow activity, but also the selection of proxy and base period used to determine the proxy.

As flood types may change differently under climate change, a new flood type classification method was demonstrated for the Barcelonnette Basin and the Salzach Valley. A weather generator combined with a rainfall-runoff model was used to create long records of discharge with a high number of flood events. These flood events were then clustered into different types based on temperature and precipitation. The results show that the method was able to reproduce the observed flood types in both catchments. Under future climate scenarios, the results identified changes in the distribution of flood types and characteristics of the flood types in both study areas.

In the final chapter, the information from a meteorological perspective on climate change-hazards studies was assessed for how it can be used to enable action by planners and decision makers. For action in the next decade, a better understanding about the current link between climate and hydro-meteorological hazards is useful not only for climate projections, but also for early warning systems, and in some instances longer term forecasts over weeks or months. The usability of future projections is discussed in terms of the uncertainty in climate projections, the inclusion of climate change-hazard studies into risk calculations, and identifying new hydro-meteorological hazards in a region. There are many challenges in developing climate change-hazard studies for floods and landslides, and even more when trying to take action based on the studies. Waiting for more information, more projections before action is taken may not be the answer. Perhaps the best approach for taking action at the local scale is to address current challenges along with researchers and end users working together to develop relevant climate change-hazard studies.

Samenvatting

Ondanks de toenemende bezorgdheid rondom klimaatverandering, staat het onderzoek naar de mogelijke toekomstige van klimaatverandering op hydro-meteorologische gevaren nog steeds voor grote uitdagingen. Onderzoek naar de gevolgen van klimaatverandering voor natuurgevaren, zoals overstromingen of aardverschuivingen in berggebieden, is gebaseerd op het combineren van toekomstprojecties van verschillende klimaatvariabelen met karakteristieken van hydro-meteorologische extreme gebeurtenissen. Echter, deze extreme gebeurtenissen zijn zeldzaam, en hun analyse vereist lange observatieperiodes van zowel klimaatgegevens als historische data van overstromingen en aardverschuivingen. Zelfs als deze gegevens beschikbaar zijn over een lange periode, kan het zijn dat de volledigheid van deze gegevens vragen oproept, bijvoorbeeld kunnen de klimaatgegevens inhomogeen zijn of trends vertonen. Hoewel extreme neerslaghoeveelheid meestal de oorzaak is van overstromingen en aardverschuivingen, spelen andere factoren ook een rol, zoals de ruimtelijke variabiliteit van neerslag, antecedente neerslag en temperatuur, en de eigenschappen van het landschap. Regenmeters, die de regenval op een bepaald punt meten, kunnen intensieve, gelokaliseerde, convectieve neerslag in de directe omgeving missen die wel de oorzaak zijn van hydro-meteorologische extreme gebeurtenissen. Als er al een relatie is tussen de gemeten klimaatgegevens en extreme gebeurtenissen is het nog niet eenvoudig om mogelijke toekomstige veranderingen in het klimaat te vertalen in veranderingen van deze gevaren. De resolutie van klimaatmodellen gebruikt om klimaat projecties te berekenen zijn te grof voor lokale gevarenbeoordelingen, omdat ze de complexe lokale topografie niet adequaat weergeven. De bovengenoemde aspecten maken het onderzoek naar de gevolgen van klimaatveranderingen op toekomstige natuurgevaren in berggebieden bijzonder complex en er zijn nog maar weinig complete studies op dit vakgebied gepubliceerd. De verwachting is dat klimaatverandering kan leiden tot veranderingen in hydro-meteorologische natuurgevaren in berggebieden, en het is daarom van groot belang om de bovengenoemde uitdagingen aan te gaan, om beleidsmakers beter te ondersteunen.

Dit onderzoek richt zich op een aantal van de uitdagingen om grootschalige klimaatprojecties te vertaling naar de mogelijke gevolgen voor natuurgevaren in bergachtige gebieden. Lokale klimaatprojecties

voor hydro-meteorologische gevaren in berggebieden zijn ontwikkeld door middel van de evaluatie van de triggers van deze natuurgevaren in samenhang met grootschalige klimaatscenario's. De huidige en toekomstige triggers zijn beoordeeld vanuit een klimatologisch of meteorologisch perspectief, waarbij andere mogelijke oorzaken, zoals veranderingen in landgebruik of de effecten van beschermende maatregelen, buiten de scope van dit onderzoek vielen. Het onderzoek beperkte zich tot bepaalde hydro-meteorologische gevarensoorten, namelijk overstromingen (flash floods en rivieroverstromingen) en aardverschuivingen (waaronder modderstromen en oppervlakkige afglijdingen). Er zijn relatief weinig publicaties over deze natuurgevaren binnen klimaatonderzoek, vanwege de lokale schaal waarop ze voorkomen ten opzichte van de grote schaal van klimaatmodellen, de moeilijkheden bij het downscalen van gemodelleerde neerslag in bergachtige gebieden en beperkingen bij het definiëren van de precieze meteorologische triggers. De Europese Alpen vormen een ideaal gebied om deze uitdagingen te bestuderen, omdat hier al klimaatveranderingen zijn geobserveerd en vanwege de lange periode waarvoor klimaatgegevens beschikbaar zijn. Drie studiegebieden werden gekozen: het Barcelonnette stroomgebied in het zuidoosten van Frankrijk, het bovenstroomse deel van het stroomgebied van de Fella rivier in het noordoosten van Italië, en de Salzach vallei in het westen van Oostenrijk. In deze studiegebieden zijn overstromingen en aardverschuivingen vaak voorgekomen en zijn klimaatgegevens beschikbaar over een periode van minstens 20 jaar. De drie gebieden reageren ook mogelijk anders op toekomstige klimaatverandering.

De eerste stap in het onderzoek naar veranderingen van natuurgevaren door klimaatverandering was kwaliteitsanalyse van beschikbare klimaatgegevens en het vergelijken van de klimatologie tussen de drie gebieden. Het begrijpen van de meteorologische kenmerken van elk van de regio's is belangrijk om inzicht te krijgen in de huidige situatie en in de beperkingen van de klimaatdata voor verdere analyse. De klimaatgegevens zijn beoordeeld op veranderingen in de meetreeksen veroorzaakt door niet-klimatologische factoren, zoals de verplaatsing van een weerstation, of nieuwe meettechnieken. Het klimaat van de stroomgebieden is vergeleken, waaruit bleek dat Barcelonnette het droogste stroomgebied is, gevolgd door het Salzach dal. De gevonden trends in temperatuur in de twee studiegebieden met klimaatarchieven langer dan 30 jaar, Barcelonnette en Fella, zijn in overeenstemming met globale trends, zoals een langer groeiseizoen en daling van het aantal dagen met temperaturen onder 0°C. De neerslaggegevens laten veel minder ruimtelijk consistente trends zien, waar 10 van de 11 extreem weerindices in het Fella gebied significante toename van extreme neerslag lieten zien was dit slechts het geval voor één van de vier in het Barcelonnette gebied.

Diverse werkwijzen zijn getest om te bepalen welke klimaatvariabelen als proxies gebruikt kunnen worden voor hydro-meteorologische gevaren op een dagelijkse tijdschaal. Rivieroverstromingen, flashfloods, modderstromen, en aardverschuivingen zijn eerst afzonderlijk beoordeeld, om-

dat ze verschillende triggers kunnen hebben. Alle hydro-meteorologische extreme gebeurtenissenzijn vervolgens gegroepeerd om te bepalen of er een link is met zekere grootschalige atmosferische omstandigheden zijn die de natuurgevaren veroorzaken. Drie specifieke combinaties van temperatuur en neerslag zijn geïdentificeerd als voorwaarden voor overstromingen in het Barcelonnette gebied. Een extreme dagelijkse neerslag van meer dan 150 mm kan worden gebruikt als drempelwaarde voor overstromingen en modderstromen in het Fella gebied met de herhalingstijd van de dagelijkse neerslag als indicatie van de herhalingstijd voor deze gevaren. Echter, deze link was minder sterk voor het Barcelonnette gebied, waar de meest extreme dagelijkse neerslag niet geassocieerd is met dergelijke fenomenen. De relatie tussen extreme neerslag en aardverschuivingen was ook niet duidelijk in het Barcelonnette gebied, hoewel de resultaten verbeterden toen naast neerslag ook gekeken werd naar temperatuursveranderingen. Tot slot, de hoogste associatie van overstromingen en aardverschuivingen was gerelateerd aan lagedrukgebieden ten noordwesten van het Barcelonnette gebied. Deze brachten vochtige noordwestelijke stromingen over het gebied, resulterend in hoge neerslagintensiteit die overstromingen en modderstromen kunnen veroorzaken.

Vanwege de beperkingen in het gebruik van directe neerslagmetingen voor de analyse van overstromingen en modderstromen in het Barcelonnette gebied, is er verder studie gedaan naar atmosferische indicatoren die gebruikt konden worden als neerslagproxies. Er zijn empirische drempelwaarden ontwikkeld, die gebruikt kunnen worden in gevarenanalyse, waarschuwingssystemen, of om de effecten te analyseren van klimaatverandering op de verandering van de frequentie. De belangrijkste atmosferische indicatoren voor dit studiegebied waren Convective Available Potential Energy (CAPE) en specifieke vochtigheid. CAPE is een maat voor de hoeveelheid energie die vrij komt met het opstijgen van een bepaalde hoeveelheid lucht vanaf het oppervlak. De resultaten tonen aan dat atmosferische indicatoren over het algemeen beter presteren dan de directe neerslagmetingen, hoewel er nog een hoge mate van onzekerheid is.

Twee statistische downscalingsmethoden zijn onderzocht om de kloof tussen regionale klimaatmodellen en de lokale schaal van natuurgevaar studies te overbruggen. Eerst is de zogenaamde "'Perfect Prognosis"' aanpak toegepast, waarin een empirische relatie tussen de grootschalige geobserveerde atmosferische condities en de gevaren op lokale schaal de basis was voor toekomstige projecties. De tweede benadering die is toegepast is de "'Model Output Statistics (MOS)"' aanpak, waarin correcties werden aangebracht aan klimaatmodel data in de referentie periode, die vervolgens werden gebruikt voor de toekomstprojecties. beide methoden laten zien dat voor het Barcelonnette studiegebied kleinere toename in extreme neerslag en een grotere daling in de frequentie van natte dagen te verwachten zijn dan voor het Fella gebied. Echter, het vermogen van deze statistische downscalingsmethoden om de gemiddelde neerslaghoeveelheden of frequenties van natte dagen

te modelleren is nog geen aanwijzing dat deze methoden ook toepasbaar zijn voor extreme waarden. Trends in de frequentie van toekomstige natte dagen waren ook niet indicatief bevonden voor trends in extreme neerslag. De resultaten suggereren dat de toegepaste MOS-methode de voorkeur geniet als downscalingstechniek voor extreme dagelijkse neerslag.

Op basis van de vorige resultaten, zijn de toekomstige klimaatprojecties vertaald in verwachtingen van debrisflow activiteit voor de Barcelonnette en Fella stroomgebieden. Toekomstige trends in modderstroom activiteit zijn geconstrueerd op basis van "'bias-corrected"' klimaatprojecties met behulp van twee neerslagproxies: dagelijkse neerslag en CAPE gecombineerd met specifieke vochtigheid. Daarnaast zijn de toekomstige trends in modderstroom activiteit is vergeleken wanneer er verschillende klimaatmodellen, de Representative Concentration Pathways (RCPs), en referentieperioden zijn gebruikt. De toename van dagen met modderstroom activiteit voor de verschillende toekomstige klimaatprojecties aan het einde van de 21^{e} eeuw varieerden in beide studiegebieden van 0% tot maximaal 6% per decade. De referentieperiode en gebruikte proxies hadden de grootste invloed op het geschatte aantal dagen met modderstroom activiteit in het Barcelonnette gebied, terwijl in het Fella gebied naast de bovengenoemde ook de gebruikte RCP's een grote rol speelden. De resultaten laten zien dat het van belang is om naast de downscaling techniek veel belang te hechten aan de selectie van de proxy variabelen en referentieperiode voor het schatten van toekomstige veranderingen in het aantal dagen met modderstroom activiteit.

Dit onderzoek ontwikkelde een nieuwe classificatiemethode voor overstromingen in de Barcelonnette en Salzach studiegebieden, aangezien overstromingstypes mogelijk kunnen veranderen onder invloed van klimaatverandering. Een weather generator in combinatie met een neerslag-afvoer model werden toegepast voor het genereren van lange afvoerreeksen met een grote hoeveelheid overstromingen. Deze overstromingen werden vervolgens gegroepeerd in verschillende types op basis van temperatuur en neerslag. Uit de resultaten blijkt dat deze werkwijze in staat is om de waargenomen overstromingentypen te reproduceren in beide stroomgebieden. De resultaten tonen voor beide gebieden veranderingen aan in de verdelingen van overstromingstype en karakteristieken onder toekomstige klimaatscenario's.

Het laatste hoofdstuk bespreekt hoe de verkregen informatie over mogelijke veranderingen in klimaatgerelateerde natuurgevaren kan worden gebruikt door planners en beleidsmakers. Als voorwaarde om tot actie over te gaan, is het nuttig om een beter begrip te krijgen hoe de relatie tussen klimaat en hydro-meteorologische gevaren gebruikt kan worden, niet alleen voor klimaatprojecties, maar ook voor waarschuwingssystemen, en in sommige gevallen voorspellingen op een termijn van weken of maanden. De bruikbaarheid van toekomstige projecties wordt besproken, waarbij aandacht gegeven wordt aan de onzekerheid in klimaatprojecties, het toepassen van klimaatverandering studies in risicoberekeningen,

en het identificeren van nieuwe hydro-meteorologische gevaren in een regio. Er zijn vele uitdagingen in de ontwikkeling van natuurgevaren-onderzoek gerelateerd aan klimaatverandering voor overstromingen en aardverschuivingen, en het vertalen van onderzoek in concrete actie is daar één van. Het is niet de beste aanpak om af te wachten tot er meer informatie, meer projecties en minder onzekerheid is voordat er tot concrete actie wordt overgegaan. De beste aanpak voor het nemen van actie op lokale schaal is wellicht om de huidige uitdagingen aan te pakken, en als onderzoekers en eindgebruikers samen te werken aan relevante oplossingen om de effecten van klimaatgerelateerde veranderingen van natuurgevaren effectief tegen te gaan.

Contents

Definitions

Atmospheric circulation patterns Patterns in different atmospheric fields, which in this work refer to those at the synoptic scale. These can patterns can be classified (atmospheric classification schemes) into discrete atmospheric circulation states or weather types.

Change-point Step or shift in a time series, caused by non-climatic factors.

Climate The statistical description in terms of the mean and variability of relevant meteorological variables over a period of time of at least 20 years (often 30 years).

Climate change An identifiable change in the climate from natural, external or anthropogenic origins.

Climate change, global Refers to widespread changes to the climate at the global scale, such as global mean temperature, shift of storm tracks, rather than local changes such as precipitation at a single grid box or rain gauge.

Climate change-hazard studies Climate change impact studies for hydro-meteorological hazards.

Climate change impact studies Any study or research that incorporates climate change information as an input (such as future projections for drought, floods, or landslides).

Climate change projections A statement about how a particular variable or parameter may change in the future due to climate change. Unlike a prediction, it acknowledges that significant changes in the boundary conditions are possible (such as changes in the greenhouse gas emissions).

Climate data A time series of meteorological measurements from which long term inferences of the climate can be made.

Climatology Summary of the climate for a particular area or areas.

Convective rainfall/precipitation Rainfall/precipitation from convective clouds, usually intense and with a short duration.

Current climate A general term representing the climate between 1950 and 2015.

Debris flow A rapid mass movement that is composed of soil, rock, organic matter, water and air.

Downscaling To take information at the large scale and make predictions on a smaller scale.

Extreme event A weather or climate occurrence that is at the tail end of range of observed values.

Exposure The presence of people, and/or economical, environmental, social, or cultural assets that could be adversely affected.

Flood Unless otherwise stated, overflow of water from a river channel or side stream/torrent (fluvial flood).

Flood, flash As above, but during which the rise in water level occurs over a short period of time (less than 24 hours). For the examined study areas, these floods occur predominately in the side stream/torrents.

Flash event A day where one or more flash floods or debris flows were recorded in the study area.

Hazard A phenomenon that has the potential to have an adverse effect on people or valuable assets (economical, environmental, social or cultural).

Hazardous event A phenomenon that had an adverse effect on people or valuable assets.

Historical period Time period over which direct observations of the climate or hazards are available.

Hydro-meteorological event A phenomenon with a hydrological, meteorological, or oceanographic component that has had an adverse effect.

Hydro-meteorological hazard A hazard that has a hydrological, meteorological or oceanographic component, often triggered by an meteorological event.

Hydro-meteorological trigger Unless otherwise stated, this terms refers to atmospheric or meteorological conditions (such as heavy rainfall) that lead to a hydro-meteorological hazard, generally floods and/or landslides.

Landslides The term landslide in isolation refers to any landslide type from Hungr et al. (2014), including debris flows, shallow landslides, and rock falls. If preceded by another term, e.g. shallow landslide, the term only refers the specific type or sub-set.

Natural variability Internal variability in the climate of non-anthropogenic origins, often greater when looking at smaller temporal and spatial scales.

Observation period Time period where instrumental measurements of weather are available, which varies depending on the type of instrument being discussed and the location.

Parameter A sub-set of a variable, such as daily precipitation or maximum 20 year daily precipitation.

Perfect prognosis A type of statistical downscaling, where a relationship is developed between coarse and fine scale observational data, without correcting for biases in the global climate models.

Precipitation Any form of water that falls to the surface, including rain and snow.

Precipitation, heavy Daily or sub-daily precipitation totals , generally with return period of 30 days or more.

Predictor (Coarse scale) variable used for predicting another variable, often at a finer scale.

Predictand The variable being predicted in statistical downscaling .

Proxy In this thesis, data that can be used in place of or to represent hydro-meteorological hazards. Terms such as atmospheric proxy or rain proxy, indicate that the data representing the hazards, e.g. atmospheric data or rainfall data.

Rainfall Liquid only precipitation.

Risk A combination of the likelihood of adverse phenomena happening and the consequence if it happens.

Synoptic situation The atmospheric conditions at the synoptic scale.

Synoptic scale The atmospheric scale that includes fronts, low and high pressure systems.

Vulnerability The predisposition to be adversely affected.

Weather station An observational station where weather conditions are observed and meteorological data recorded, including temperature, precipitation, pressure, humidity. Weather station data over a period of time is referred to as climate data.

Introduction 1

1.1 Changing hazard in the face of climate change: the need for climate change-hazard studies

In March 2015 the global atmospheric CO_2 concentration reached 400 ppm, corresponding to a likely long term increase of the global mean temperature of up to 2.3°C (Rummukainen, 2015). Already the global mean temperature has risen 0.8°C since pre-industrial times (Dai et al., 2015), and changes in the climate and environment have observed around the globe. Between 1951 and 2003, 70% of the global land area has had a decrease in the number of cold nights (Alexander et al., 2006). In the Northern Hemisphere, over two thirds of the land covered by observations has shown increases in the annual maximum daily and 5-daily rainfall amounts (Min et al., 2011). At the same time, the snow cover extent has declined over North America and Eurasia, particularly in spring (Déry and Brown, 2007). These and other changes in the climate will have a wide range of environmental impacts, including altering certain hazards (IPCC, 2012). To understand how a particular process may be altered by climate change and in turn how these changes may impact the environment and society, climate change impact studies are undertaken.

Climate change-hazard studies refers to climate change impact studies where the analysis considers the effect of climate change on hydro-meteorological hazards. These hazards are defined as phenomena with a hydrological, meteorological, or oceanographic component, which have the potential to have an adverse effect on people or assets (McBean, 2013). Hydro-meteorological hazards are often triggered by meteorological events, such as a period of intense precipitation over a few hours resulting in a flash flood, or drought caused by months of low rainfall and warmer temperatures. As hydro-meteorological hazards have a meteorological component, they have the potential to change under climate change.

There are a variety of reasons why climate change-hazard studies are needed. Information is required to support decisions around climate change alongside decisions about air pollution, food production, water management, risk mitigation, and other environmental challenges.

And while the mitigation of climate change is often considered a global problem, adaptation to change will occur at regional or local scales (Shapiro et al., 2010). The regional and local manifestations of climate change will not be equal to that at the global scale, and therefore climate change–hazard studies are needed to help bridge the gap.

Climate change-hazard studies are also needed to determine the sensitivity of a particular natural phenomena to climate change. For example, the decline of permafrost in Alpine catchments can lead to destabilization of slopes, but there is uncertainty about how much the snowpack needs to decrease and temperature to increase for this destabilization to occur. This example demonstrates how there needs to be a better understanding of the link between the natural phenomena and the climate. Phenomena that are more sensitive to climate change can then be prioritized with regards to climate change than those that are less or not sensitive.

Finally, climate change-hazard studies contribute not only to the advancement of science, but can convey the seriousness and importance of climate change to the general public. The target of keeping the global temperature rise below 2°C, or the hungry polar bear image, may be easier to dismiss for the general public or decision makers than a more local threat due to changes in natural hazard and risk. It was found that the visualization of local responses to decreasing snowpack in North Vancouver, Canada, influenced the emotional response and understanding of climate adaptation for the local inhabitants (Cohen et al., 2012). However, while climate change-hazard studies may be needed, the benefits of such studies depends on the skill of the researchers, how the results are communicated, and the quality of the studies.

Developing climate change-hazard studies involves combining future projections of climate variables with hydro-meteorological hazard inventories. However, there are a variety of challenges involved. Understanding the link between climate and hazard is not straightforward. Hazardous events are rare events, which require a long record of both the events and climate to establish any link. Even if long records are available, the completeness of hazard inventories may be questionable, and trends in the climate may be present. And while particular hydro-meteorological hazards such as flash floods and debris flows are caused by rainfall, capturing the rainfall amount is difficult. Rain gauges measure rainfall at a particular point and can miss nearby intense, localized, convective rainfall that triggers hydro-meteorological hazards. There are other meteorological factors that can trigger hazardous events as well, such as snowmelt, long or short duration rainfall, and it may not be clear which factor or combinations of factors are triggering hazardous events in an area.

Even with an established relationship between climate and hazard, it is not straightforward translating future climate change into changing hazard. Global Climate Models (GCMs) and Regional Climate Models (RCMs), on which future projections are based, are at a scale that is too coarse to adequately represent the complex local topography, or for use

in modelling the hydro-meteorological hazards. Therefore, downscaling of GCM or RCM data is required. There are a variety of downscaling techniques, each with their own advantages and limitations. Choosing the appropriate technique and climate models needs careful consideration, as the choice will likely affect the final climate projection.

Challenges in understanding the climate-hazard relationship and downscaling climate projections has meant there have been few climate change-hazards studies for landslides and flooding in mountainous catchments. In Europe, which contains some of the best areas for undertaking climate change-hazard studies due to long meteorological records (Auer et al., 2007) and hazard inventories (Stoffel et al., 2014), there have been a limited number of studies with inconsistent results. For example, a decrease in debris flows was projected for the French Alps due to temperature increases and decreases in precipitation (Jomelli et al., 2009), however in a study for Norway no consistent change was found due to uncertainties in extreme and antecedent precipitation (Melchiorre and Frattini, 2012). In studies comparing future projections for floods, results show that the meteorological triggers, such as snowmelt or rainfall, may change differently in the future (e.g. Arnell and Gosling, 2014; Benestad and Haugen, 2007; Stoffel et al., 2014). Climate change-hazard studies in mountainous catchments therefore need to determine the meteorological triggers for the particular area, and how they may change in the future.

Assessing changing hydro-meteorological hazard from a meteorological perspective is only part of the storyline of future flood and landslide hazard. Changes in the climate are not the only factors that can alter a hazard. Human activity has thought to have dominated historical changes in debris flow occurrence (Crozier, 2010). These activities include changing of vegetation or land cover, earthworks leading to slope changes, and construction of mitigation works, such as dykes or retention basins for landslide debris. A meteorological perspective, as presented in this research, should therefore be paired with changing land cover and mitigation works when considering a holistic view of future flood and landslide hazard.

1.2 Research objectives and framework

The general objective of this thesis is to develop local climate projections for hydro-meteorological hazards in mountainous catchments, through assessing triggering mechanisms and climate change scenarios from a meteorological perspective. Changes in land cover and mitigation works are out of the scope of this research. The types of hydro-meteorological hazards are investigated are pertinent to mountainous areas: floods (flash floods, fluvial floods) and landslides (soil slides, debris flows). These hazards have been under-reported in climate research literature due to the fine scale on which they occur relative to climate models, the difficulties in downscaling modelled precipitation in mountainous catchments, incomplete hazard inventories, and limitations in defining the

precise meteorological triggers. In this thesis, the climate change-hazard study is broken into five components as shown in Fig 1.1: analysing the climate data (A), identifying the link between climate and hazardous events (B), choosing the downscaling method (C), developing the climate change-hazard studies (D), and assessing the outcome (E). In particular, understanding the link between climate and hydro-meteorological events at a local level is undertaken prior to developing future projections, a part that is often absent in previous climate change-hazard studies. The specific objectives for each of the five components are listed below, with the corresponding letter for the research framework in Fig 1.1.

(A) Analyse climate records, including data quality, to assess the current climate and climate trends in each study area

(B) Identify meteorological proxies for hydro-meteorological hazards that can be used in climate change-hazard studies

(C) Determine the applicability of various statistical downscaling methods for use in climate change-hazard studies, focusing on extreme precipitation indices

(D) Develop local climate change projections for hydro-meteorological hazards in the future

(E) Evaluate the usability of such climate change-hazard studies for decision makers and society

To reach objectives A and B, long meteorological records (more than twenty years of continuous measurements) are required, which should be matched with substantial hazard inventories. Study areas that are expected to have a larger and differing response to global climate change are beneficial for objectives C and D.

1.3 Study areas

The European Alps are an ideal place to study the impact of climate change on hydro-meteorological hazards and associated triggers, having the data and characteristics required for the objectives outlined above. The European Alps contains some of the longest meteorological records for mountainous areas. Parts of the European Alps and surrounding region have been identified as a hot-spot for climate change (Giorgi, 2006). Furthermore, changes in the climate have already been observed. Since the 19^{th} century, the Greater European Alpine area has warmed twice as fast as the mean for the Northern Hemisphere (Auer et al., 2007), with the observed warming trend in Western Europe increasing faster than predicted (van Oldenborgh et al., 2009). The observed trends in precipitation have been less clear, with some Alpine regions recording an increase in seasonal precipitation and other areas a decrease (van den Besselaar et al., 2013). However, changes in average precipitation are not necessarily representative of changes in extreme values, with an increase in extreme precipitation noted in numerous areas (Klein Tank

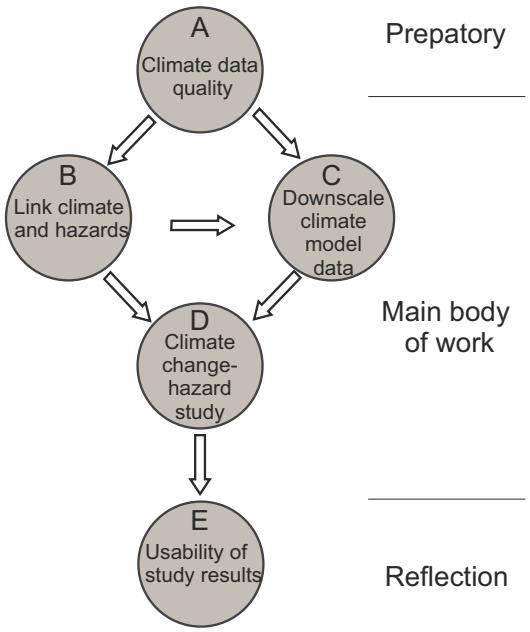

Figure 1.1 Framework for assessing climate change-hazard studies as covered in this thesis. The letters correspond to the five main objectives.

and Können, 2003; van den Besselaar et al., 2013). Furthermore, how the coarse scale climate changes effect the hydro-meteorological hazards at a finer scale is not clear.

Three European catchments are used in this work: the Barcelonnette Basin, France, the Fella River Basin, Italy, and the Salzach Valley, Austria. Each area has experienced numerous floods or landslide events in the recent decades and have more than 20 years of continuous meteorological measurements. The study areas are located in the Alps (Fig 1.2), with differences in size, land cover, and climate (Table 1.1). On average the northern side of the Alps (including the Salzach Valley) has a higher wet day frequency, while lower mean precipitation amount on wet days (Isotta et al., 2014). The northern portions also tend to have the highest daily rainfall totals in June and July, while in central and southern regions, such as north-eastern Italy, the highest rainfall generally occurs in September and October, and between May to October in the west (France, northwest Italy; Parajka et al., 2010). Therefore, hydro-meteorological hazards may change differently with respect to future climate change between the study areas. Changes in temperature and snowpack may be more important for hazards in mountainous climates, and changes in storm intensity more important for the Mediterranean climates. While the three areas may not be representative of the entire Alpine area,

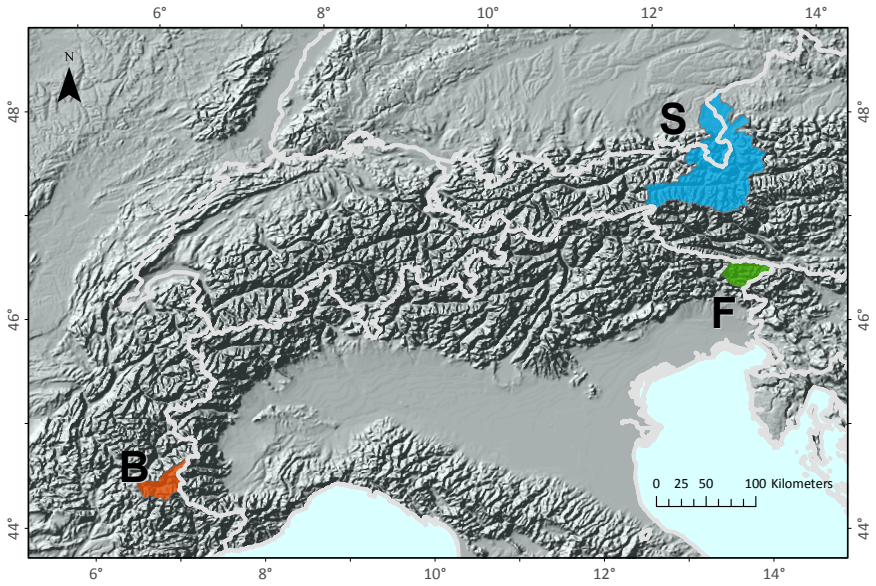

Figure 1.2 Location of the three study areas: Barcelonnette Basin (B, orange), Fella River Basin (F, green), and Salzach valley (S, blue), with country borders indicated in light grey. More detailed information can be found in Fig 2.1

they contain already extensive hydro-meteorological hazard inventories and may respond differently under future climate change due to their location, two conditions fundamental for obtaining the Sec 1.2 objectives.

1.3.1 Barcelonnette Basin, France

The Barcelonnette Basin resides in the Alps de Haute-Provence in the southern portion of the French Alps. The two largest villages in the region are Barcelonnette and Jausiers, both situated on the side of the Ubaye River. The area is a touristic centre, with ski resorts in winter months. The study area covers an area of 548 km^2, with the elevation ranging from 1100 to 3100 m.a.s.l. The geology consist of flysch, sandstone and black marls with parts of the slope covered by quaternary deposits, such as glacial moraine and colluvial deposits (Saez et al., 2012). The upper part of the catchment (above 1900 m) is either bare or grassland, with forests (60%) , agricultural (22%), urban (11%), and other (7%) covering the lower portions (Ramesh, 2013).

The Barcelonnette Basin is located in a dry intra-Alpine zone and experiences a mountainous climate with a strong Mediterranean influence (Remaître et al., 2011). There are between 100 and 130 freezing days per year at higher elevations. During the summer and autumn, intense, convective storms occur that have led to recorded precipitation amounts of more 40 mm/day. Heavy rainfall is also recorded in spring, and, when

Table 1.1 Summary of the three study areas (Barcelonnette Basin, Fella River Basin, and Salzach Valley). Further details on the climate are in Chapter 2.

	Barcelonnette B.	Fella River B.	Salzach Valley
Country	France	Italy	Austria
Size (km^2)	550	880	4640
Elevation range (ma.s.l.)	1100-3100	200-2800	410-3600
Main centres	Barcelonnette, Jausiers	Tarvisio, Pontebba	Salzburg
Population	4500	10000	45400
Land cover	Above 1900m: bare or grassland, below: forest (60%), agriculture (22%), urban (11%)	Forest (75%), bare surface (10%), grasslands (8%)	Predominately forest, grasslands
Climate	Dry, mountainous Mediterranean	Mediterranean/ mountainous Mediterranean	Mountainous climate (higher elevations), continental climate (lower elevations)

combined with an extensive snowpack, can lead to high discharge levels (Ramesh, 2013).

Climate and geomorphologic conditions of the valley have led to a variety of floods and landslides in the past 100 years (e.g. Cepeda et al., 2010; Flageollet et al., 1999; Remaître and Malet, 2010; Saez et al., 2013). During a spring warm spell in 1957, rapid snow melt and heavy rainfall combined to cause flooding in both Barcelonnette and Jausiers, as well as in the surrounding Cerveyrette and Maruieene valleys (Arnaud-Fassetta et al., 2005). More recently in May 2008, heavy spring rain again led to flooding and damage to buildings, bridges, and other infrastructure in the basin. Between 1950 and 2010 more than 90 debris flows have occurred within the area. Of the 26 torrents in the Barcelonnette Basin, 90% of these debris flows have occurred on the south-facing slopes (Fig 5.1, OMIV-Coordinator, 2012). One of the recent damaging events occurred in 2003, where a debris flow damaged six houses as well as a critical road crossing (Remaître and Malet, 2010).

The Barcelonnette hazard inventory was based on the catalogue by a subsection of the French Forest Office (RTM), which compiled a catalogue of historical hazards in the area since 1880. The long record of landslides and other hazardous events makes this study area a prime location for understanding the link between the climate and hydro-meteorological hazards (objective B). The RTM constructed the inventory through the systematic analysis of other existing catalogues supplemented by a thorough search of local historical archives and newspapers chronicles. The events reported in the catalogue correspond usually to hazardous events that resulted in damage, affected buildings or roads, and were located

near towns and villages. For most of the hydro-meteorological events, the information in the inventory includes: the precise or approximate location of the area affected, the time, date or period, the meteorological conditions, landslide type and the generic description of the rock types and associated soils within the triggering area.

Previous research has begun to investigate the link between hydro-meteorological hazards and climate in the area. Most hydro-meteorological hazards in the area are associated with snowmelt or high intensity summer storms, although the precise triggers have been difficult to determine (Flageollet et al., 1999). For example, Cepeda et al. (2010) established thresholds for debris flows based on sub-daily precipitation measurements that correctly predicted 86% of events. However, these debris flow events only accounted for 6% of all values above the threshold (equivalent to a high false alarm rate, see Chapter 5 for more information). Another threshold for total precipitation between December to March was able to provide a 80% probability of reactivated landslides, although many landslide reactivations occurred below the threshold (Saez et al., 2013). In each of these studies, precipitation was obtained from rain gauge(s) located at the bottom of the valley, and not necessarily representative of precipitation at higher elevations.

1.3.2 Fella River Basin, Italy

The Fella River Basin resides in the north-eastern corner of the Italian Alps, in the Friuli-Venezia Giulia autonomous region (FVG). There are a number of small communes along the river, the largest being Pontebba and Tarvisio. The study area covers 883 km^2, with an elevation range of 200 to 2800 m.a.s.l. The geology consists of limestone and dolomite covered by quaternary deposits. Approximately 75% of the study area and surrounding region is forested, 10% consisting of bare surface such as outcrops and scree deposits, 8% of grasslands, and 2% urban (Malek et al., 2014).

There are distinct variations in the climate between the seasons. During winter, precipitation is derived primarily from synoptic features, such as lows and fronts, whose frequency and intensity vary significantly from year to year (Ceschia et al., 1991). In the summer months, convective processes become more important for precipitation generation, with local daily totals exceeding 400 mm (Borga et al., 2007). Overall, the valleys that are aligned east-west have lower annual precipitation (approximately 500 mm), while others have higher annual precipitation, some exceeding 3000 mm annually (D'Agostino and Marchi, 2001).

The heavy precipitation, steep slopes, shallow mountainous soils, and the highly fractured rock associated with the high seismicity, make the north-eastern part of the FVG prone to flash floods, landslides and debris flows (Borga et al., 2007). In the last 40 years, there have been three major flooding events of the Fella River: 11 September 1983, 22 June 1996 and 29 August, 2003 (Borga et al., 2007; Chen et al., 2016). In August 2003 more than 400 mm of rainfall was recorded within 24 hours, leading

to a major flood of the Fella River as well as numerous debris flows, depositing 1 million cubic meters of debris at the bottom of the channels and valleys (Tropeano et al., 2004). There have been numerous other landslide events that have impacted society in the FVG region (Salvati et al., 2010). While there are fewer recorded hydro-meteorological events than in the Barcelonnette inventory, events such as in 2003 were greater in magnitude, and therefore may have disparate triggers and respond differently under climate change.

To undertake objective B, not only are known hazardous events required, but also sufficiently complete records of such events that contain the largest events. The Fella River flood and landslide inventory for 1950-2002 was obtained from the AVI Project (Guzzetti et al., 1994). The project collected the date and location of floods and landslides for the most affected areas in Italy, including this study area. Post 2002 dates were obtained through the Italian Civil Protection for the FVG region (http://www.protezionecivile.fvg.it/, last accessed 13th August, 2015).

Previous work has investigated the link between precipitation and hydro-meteorological hazards in the area and surrounding regions (e.g. Bacchini and Zannoni, 2003; Norbiato et al., 2009). For the 2003 event, a return period of between 200 and 1000 years was obtained based on the 3 to 12 hour rainfall data (Norbiato et al., 2009). To the east of the study area, Bacchini and Zannoni (2003) investigated relationships between rainfall and triggering of debris-flows using normalised rainfall total amount, intensity, and duration. Other studies that have developed thresholds for nearby or larger regions include Guzzetti et al. (2007) (central and southern Europe) and Brunetti et al. (2010, 2013) (Italy). However, to the author's knowledge, there has been little research understanding how future changes in precipitation will alter debris flows and other hydro-meteorological hazards for this catchment.

1.3.3 Salzach Valley, Austria

The Salzach Valley in Austria is located on the northern side of the Alps. The Salzach River drains a large part of the Eastern Alps in Austria. The study area is the largest of the three, with Salzach sub-catchment (ending in Salzburg) covering 4637km^2, and elevation between 415 and 3627 m a.s.l. Approximately 45400 inhabitants live in the catchment, with most of the people residing in Salzburg (Kienberger et al., 2009). The upper reaches of the catchment form part of the Northern Calcareous Alps, with quaternary deposits at the valley bottom varying between 190 and 340 m in thickness (Herbst and Riepler, 2006). The area is covered by predominately forest and alpine grassland, with less than 4% of the area containing ice, snow or permafrost (Lang et al., 2011).

The catchment covers a range of climate conditions. A mountainous climate is experienced at higher elevations, while lower portions, including Salzburg, are continental in climate. As the catchment is on the northern part of the Alps, it receives less annual precipitation than

the Fella River Basin. However, thunderstorms are prevalent throughout the catchment in summer and lead to locally high precipitation amounts over a short period (40-80 mm/day). Residing on the northern side of the Alps, and with a more continental climate than the other study areas, the Salzach Valley has the potential to respond differently to global climate change.

The Salzach Valley experiences a variety of hydro-meteorological hazards. Summer floods are more common than other seasons, including the August 2002 flood event where recorded discharge was the highest in the previous 100 years (Ulbrich et al., 2003), and more recently the June 2013 flood. Debris flows occur with a higher frequency than other areas in Austria, particularly in the southern portion of the catchment (Aulitzky, 1989). However, no sufficiently complete landslide inventory was obtained for this study area. Daily discharge measurements are also available, making it possible to study the link between climate and flooding hazard in more detail (objective B), and to develop climate change-hazard studies (objective D).

1.4 Structure of the thesis

The thesis is divided into two parts. The following three chapters (Chapters 2-4) explore with a broad lens the components in developing climate change-hazard studies (A-C in Fig 1.1). The second part of the thesis builds on these results, with a more in-depth focus on objective B and then developing climate change-hazard studies for objective D (Chapters 5-7). Chapter 8 concludes the work, addressing the issue of usability climate change-hazard studies (objective E). Further details on the chapters is given below. The letter in brackets refers to Fig 1.1.

Chapter 2 covers the climate records for each of the study areas. The quality of the data is assessed, followed by a comparison of the climate between study areas. The climate records are analysed for possible trends in the data, focusing on extremes. Understanding trends and non-climatic shifts in the climate records is vital for further work. (A)

Chapter 3 provides an overview of understanding the link between the climate and hazards through empirical analysis. Floods, debris flows and landslides are considered separately, with the final section considering all three hydro-meteorological hazards together in association with atmospheric circulation patterns. (B)

Chapter 4 considers how climate projections can be downscaled for use in climate change-hazard studies. Two statistical approaches, perfect prognosis and model output statistics, are compared. Precipitation is the main climate variable considered in this chapter, with the focus on extremes. (C)

Chapter 5 is the first of the in-depth chapters. The chapter investigates the use of atmospheric variables as proxies for debris flows and flash floods in comparison with precipitation. After the conclusion from earlier

chapters, atmospheric variables associated with heavy precipitation are considered as a potential alternative for rain gauge measurements. (B)

Chapter 6 builds on the previous chapter and compares how future projections of debris flows based on precipitation projections compare with those based on atmospheric variables. Consideration is given to the role of base period, as well as the climate model and emission scenario used. (D)

Chapter 7 considers floods under climate change in more detail. A new methodology to classify flood events into causal types is presented, with application for current and future periods. In particular, how the frequency and characteristics of the flood types changes in the future is considered for two catchments. (D)

Finally, Chapter 8 provides a summary of the research. Ideas on how this work and similar climate change-hazard studies can be used to reduce risk are introduced, returning to the question of why we need climate change-hazard studies for hydro-meteorological hazards, and how they can be useful to society. (E)

Climate Records: Homogeneity, extremes, and trends

2

2.1 Introduction

Changes in climate can alter hydro-meteorological hazards, especially in mountainous regions. Since the 19th century, the Greater European Alpine mean temperature has warmed twice as fast as the mean Northern Hemisphere temperature (Auer et al., 2007). Extreme precipitation in Southern Europe (below 49°N) has also increased, with previously 5 to 20 year daily precipitation events becoming more frequent (van den Besselaar et al., 2013). To analyse whether changes in the climate may have impacted hydro-meteorological hazards, the quality of the meteorological records needs to be sufficient and any non-climatic factors removed.

Long climate records are often plagued with discontinuities in their records masking actual trends in the climate. Generally, discontinuities arise in data from weather stations from four different causes: changes in location of the station, changes in the surroundings of the station, changes in observing practice, and changes in the instruments. As an example of changes in the area around the weather station, changes in the record of mean wind speed in Canterbury, New Zealand, were recorded due to vegetation growth and building construction (Aguilar et al., 2003). Gradual changes, such as changes over time in site characteristics, can be very difficult to determine, especially without any record of the changes in metadata. However, abrupt changes, such as moving the weather station, can be picked up by different homogeneity tests.

The objective of this chapter is to analyse the climate records for three Alpine study areas with a focus on extremes. Long time series are needed to assess extreme climate conditions, which are vital for assessing the link between the climate and hydro-meteorological events such as floods and landslides in subsequent chapters. A brief overview of the three study areas is included in Sec 2.2. Section 2.3 covers homogeneity tests for the three study areas. The resulting homogeneous time series are then compared between study areas with a focus on extreme values (Sec 2.4). This comparison of the climate may provide information on differences in observed hydro-meteorological event frequency between

study areas that is treated in subsequent chapters. Trends in the climate records are considered in Sec 2.5, as detected trends may provide insight into how the local climate and hydro-meteorological hazardous events are responding to climate change.

2.2 Climate records in the three study areas

As mentioned in Chapter 1, the three Alpine study areas considered were the Barcelonnette Basin, France, the Fella River Basin, Italy, and the Salzach Valley, Austria (Fig 2.1). A general overview of each study area is provided in Chapter 1, including a brief description of the geomorphologic conditions and major hydro-meteorological events. All three areas have more than 20 years of continuous daily temperature and precipitation measurements, as well as records of flood and landslide events. The location of the weather stations can be found in Fig 2.1. For each station, the height of the station, duration of daily precipitation and daily temperature records, the number of years with no more than four days with missing data (Y), and dates of weather station shifts (Metadata) are given in Table 2.1.

Records for the Barcelonnette Basin extend back to 1928 for precipitation, with five stations measuring daily precipitation and one temperature record. As station B-5 has less than 20 sufficiently complete years for precipitation, the precipitation record was not used. The Fella River Basin has over 30 years of climate data with six weather stations measuring temperature and precipitation, with an additional two measuring precipitation only. Unlike for the other study areas, no information was available about station relocation. For both the Barcelonnette and Fella River basins, daily temperature was calculated as the average of the daily maximum and minimum temperature. The Salzach Valley has 19 weather stations measuring precipitation, three of which also measure temperature. Information about station relocation was only available for 13 weather stations.

For the Fella River Basin, until the last decade the climate records were collected by volunteers, with varying standards in observation practices. In the past 20 years the climate records have undergone validation by the Italian Hydrographic Service, which included cross-checking the stations with neighbouring stations as well as annotating the records (personal communication). Annotations include whether the precipitation was snow and whether the value was an accumulation over multiple days or interpolated based on nearby stations. The accumulated and interpolated values may have influenced the precipitation record, therefore two datasets are used in this work: one including all accumulated and interpolated precipitation amounts (referred to as ‘full’), the other includes only direct measurements, excluding all annotated values (referred to as ‘reduced’).

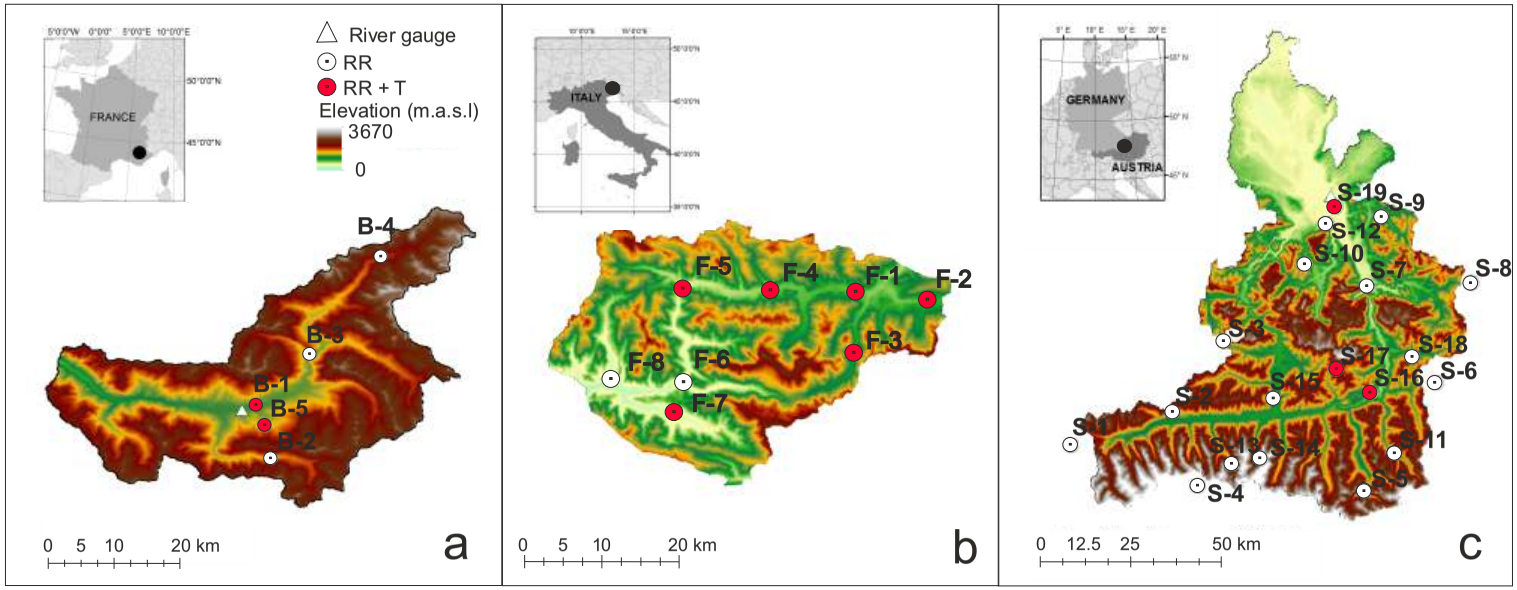

Figure 2.1 Map of the three study areas with the location of weather stations (a: Barcelonnette Basin, b: Fella River Basin, c: Salzach Valley). Stations with only precipitation are white, while stations that record temperature and precipitation are red. The station numbers correspond to those in Table 2.1.

Table 2.1 Length of weather station records for each study area for daily precipitation and temperature. Per station and variable the historical period (period) and number of years with less than four day missing (Y) is given. The height of the station is given in metres. The final column lists the known month and year where the location of the site changed (dash indicates no record available, and NC indicates no changes reported).

	#	Station Name	Height	Precipitation		Temperature		Metadata
				Period	Y	Period	Y	
Barcelonnette	B1	Barcelonnette	1155	1928-2010	66	1961-2010	46	1965,'71, '81, '97
	B2	Condamine	1325	1955-2004	49	–		-
	B3	St Paul	1903	1971-2010	36	–		1974
	B4	Uvernet	1660	1955-2010	55	–		NC
	B5	Jausiers	1510	1960-2010	19	1985-2008	22	NC
Fella River	F1	Tarvisio	725	1923-2011	72	1927-2011	73	–
	F2	Valico de Fusine	850	1971-2003	27	1975-2011	25	–
	F3	Cave del Predil	897	1927-2006	63	1949-2006	43	–
	F4	Malborghetto	733	1922-2011	82	1987-2011	22	–
	F5	Pontebba	568	1920-2011	77	1927-2011	68	–
	F6	Chiusaforte	400	1920-2005	60	–	–	–
	F7	Resia	469	1920-2011	80	1967-2011	42	–
	F8	Moggio Udinese	310	1935-2005	70	–	–	–
Salzach	S1	Gerlos	1250	1987-2010	24	–	–	1983, '84, '86
	S2	PaβThurn	1200	1987-2010	24	–		NC
	S3	Hochfilzen	960	1987-2010	24	–		1992,'03
	S4	Felbertauerntunnel	1650	1987-2010	24	–		NC
	S5	Böckstein	1140	1987-2010	24	–		1998
	S6	Flachau	910	1987–2010	24	–		NC
	S7	Golling–Torren	473	1987-2010	24	–		2002
	S8	Gosau	765	1987-2010	24	–		NC
	S9	Hintersee	750	1987-2010	24	–		NC
	S10	Bischofswiesen–Loipl	845	1987-2010	24	–		–
	S11	Hüttschlag	1030	1987-2010	24	–		2004
	S12	Glanegg	450	1987-2010	24	–		1996
	S13	Enzingerboden	1768	1987-2010	24	–		–
	S14	Schmittenhöhe	2102	1987-2010	24	–		–
	S15	Zell am See	767	1987-2010	24	–		–
	S16	St Veit	747	1987-2010	24	1987-2010	24	–
	S17	Dienten	1265	1987-2010	24	1987-2010	24	–
	S18	Hüttau		1987-2010	24	–		2001
	S19	Salzburg Airport	424	1987-2010	24	1987-2010	24	–

2.3 Homogeneity tests

2.3.1 Methodology

Homogeneity tests were performed on the climate records for the three study areas, the Barcelonnette Basin, the Fella River Basin, and the Salzach Valley. The temperature and precipitation records were assessed for abrupt shifts in the data (change-points), as shifts would affect subsequent analysis, such as frequency estimations and trend detection. As an example, Fig 2.2 highlights a change-point in the B-1 temperature record. The annual values of diurnal temperature range are given in black, with gaps indicating years with insufficient data. The red trend line shows a step indicating a potential change-point. The reliability of such change-points is especially important when looking for shifts when little or no metadata is available. However, there is no agreement regarding the most appropriate method to test for homogeneity in different climate variables, especially for daily values (Klein Tank et al., 2009). Therefore performing more than one test provides more confidence in the change-point detection. In this study, three homogeneity tests were used for detecting change-points: the Standard Normal Homogeneity test (SNHT), the Pettit test (Pettit), and the Penalized maximal f-test (F-test).

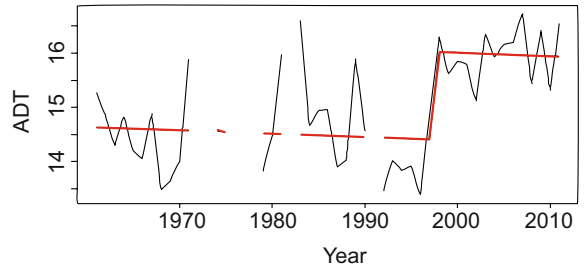

Figure 2.2 Example of a change-point for the B-1 temperature record using the annual diurnal temperature range (ADT, °C). Gaps in the black line indicated years with insufficient data. The step in the red trend line indicates a change-point.

The SNHT has previously been shown to be reliable in detecting change-points (e.g. Ducré-Robitaille et al., 2003; Reeves et al., 2007). The null hypothesis is that the time series consists of independently normally distributed data. This hypothesis is tested against the alternative that there is a change-point in the data using a likelihood ratio test (Costa and Soares, 2009). Major drawbacks of the SNHT are the assumption of a normal distribution for the data and that it does not allow for trends.

The Pettit test is a non-parametric test based on the earlier Mann-Whitney Test and therefore makes no assumption on the distribution of the data (Pettitt, 1979). The null hypothesis is that the time series

consists of independent and identically distributed data,tested against the alternative that there is a single change-point in the data (Costa and Soares, 2009).

The third homogeneity test, the F-test, uses an empirical approach to detect one or more change-points in a time series using the penalized maximal F-test (Wang, 2008). As with the SNHT, the F-test assumes that the data is normally distributed, while also accounting for first order autocorrelation or linear trends that may be present in climate data(Wang and Feng, 2010). However, the authors of the F-test note that this test should not be used for daily precipitation data, which is typically non-Gaussian (Wang and Feng, 2010).

Literature comparing different homogeneity tests showed the SNHT test is more sensitive to changes at the beginning and end of a record, while the Pettit test is more likely to pick up a change-point in the middle of the record (Wijngaard et al., 2003). The false alarm rate for the F-test was only slightly higher when a change was near the end of the distributions (Wang, 2008). Furthermore, while non-parametric test do not assume that the data are normally distributed, non-parametric tests are thought to be less powerful as ones where the underlying distribution of the data is known (Costa and Soares, 2009). Therefore, the Pettit test may be less sensitive to change-points than the F-test or SNHT, provided the time series have a Gaussian distribution.

Homogeneity in data can be tested using several indices per variable. Annual values are tested as autocorrelation in the data should be minimal due to the assumption that the data points are independent for the SNHT and Pettit tests. Furthermore, annual values reduce the variability in the record, making any trends or change-points easier to detect.

In this work, daily precipitation and temperature time series are tested for their homogeneity in all three study areas. The indices used to test for change-points are summarized in Table 2.2 and are based on indices from Wijngaard et al. (2003). The annual mean diurnal temperature range (ADT) represents characteristics of variations on a daily scale (Wijngaard et al., 2003). As only daily values were available for the Salzach Valley, average daily temperature was assessed instead. Two precipitation indices are assessed: the annual wet day count (WD) and annual very wet day count (VWD). Changes in WD are expected to represent overall changes in the precipitation record, while VWD are expected to determine changes in heavy precipitation events specifically. Annual snow day count (SD) assesses possible changes in recording snowfall. For example, automated weather stations that record snowfall can be heated to melt the snow, which can cause an underestimation of the snowfall. A second version of snow data count was only used for the Fella River Basin based on annotations by the observers (not available for the other areas). For all indices, years with more than four days with missing data are excluded from the time series, a common criteria when considering daily climate extremes (Klein Tank et al., 2009).

Four criteria are set to test whether a record could be considered as homogeneous:

Table 2.2 Indices used to test for change-points in the temperature, precipitation, and snow records.

Variable	Indices	Description
Temperature	ADT: Annual mean diurnal temperature range	Difference between maximum and minimum daily temperature averaged over one year
Precipitation	WD: Annual wet day count	Number of days per year with more than 0.99 mm of precipitation
	VWD: Annual very wet day count	Number of days per year with more than 19.99 mm of precipitation
Snow	SD: Annual snow day count	Number of days per year with more than 0.99 mm of precipitation and maximum temperature less than 3.01°C
	SDC: Annual snow days by comment	Number of days that the observer noted snow (Fella River only)

- If no test detects a change-point: homogeneous
- If only one test shows a change-point: likely homogeneous
- If two tests show a change-point at the same location: likely not homogeneous
- If all three tests indicate a change-point at the same location: not homogeneous

Based on the outcome of the homogeneity tests, records that are considered homogeneous are used for developing climate change-hazard studies. If the record is either not homogeneous or likely not homogeneous, the dataset is not used, or only part of the dataset where no change-point was detected. An exception is made for likely homogeneous records in a study area where there are few other homogeneous records, as well as no recorded changes in weather station location in Table 2.1.

2.3.2 Results and discussion

The results for the three homogeneity tests, Pettit, SNHT, and F-test, are shown in Table 2.3 for each weather station. Homogeneous stations are displayed in white, while any stations with detected change-points are shown in grey and change-point year (last two digits only). For the Fella River Basin where the full and reduced precipitation records were used, a light grey box with an asterisk indicates that only the full records contained any change-points and the reduced times series was assessed as homogeneous. Black boxes indicate stations where there was less than 20 years of sufficiently complete data (less than four days missing) and therefore not tested.

Table 2.3 Summary of Homogeneity tests Pt = Pettit test, SN = SNHT, Ft = F-test. White box: no change-point, dark grey: change-point(s) with the year indicated. Light grey: only full data set showed a significant change-point (Fella River precipitation and snow records only). Black boxes: not tested. B-5 is not included due to short time series. Years in bold indicate a change-point or likely change-point. Refer to Table 2.2 for abbreviations ADT, WD, VWD, SD, and SDC.

		Temperature			Precipitation						Snow					
		ADT			WD			VWD			SD			SDC		
		Pt	SN	Ft	Pt	SN	Ft	Pt	SN	Ft	Pt	SN	Ft	Pt	SN	Ft
Barcelonnette	B1	**97**	**98**	**97**												
	B2															
	B3															
	B4															
Fella River	F1				**42**	**42**				49	**88**	**88**	**88**	88		
	F2								01		**88**	**88**		**88**	**87**	
	F3										**88**	**88**		**88**	**00**	
	F4					42		**38**	**38**	**37**				**89**	**05**	
	F5	**93**	**96** &31		**42**	**42**						**88**	**85**		06	
	F6				34			**34**	**37**	**37**						
	F7			95	**39**	**41**	**41**		**37**	**37**	**84**	**87**				
	F8					38			38							
Salzach	S1															
	S2															
	S3															
	S4															
	S5							**02**		**98**						
	S6															
	S7							**00**		**00**						
	S8															
	S9															
	S10															
	S11				97											
	S12															
	S13						00	**02**	**03**							
	S14				**93**		**00**	**99**	**99**	**99**						
	S15	96														
	S16	96						**94**		**98**						
	S17															
	S18															
	S19															

2.3.2.1 Barcelonnette Basin

The single temperature record tested in the Barcelonnette Basin, B-1, likely contained a change-point in 1997-1998 (Fig 2.2). More than 10 years recorded ADT values lower than 15°C before 1997, while all values were higher after the change-point. A gap indicates years with more than four days of missing data. All three tests found a shift in the location

indicated in Fig 2.2. The change-point may have come from a shift in the site in 1997 (Table 2.1).

For the Barcelonnette Basin precipitation records, all four tested stations were found to be homogeneous. No change-points were detected in any of the records by any of the tests (Table 2.3). While stations B-1 and B-3 had moved location during the recorded period, changes caused by the relocation were not found in any of the three tests. The number of snow days at B-1 also contained no change-points. This was the only station where snow days were calculated as no other station recorded both temperature and precipitation.

Overall, the Barcelonnette Basin precipitation and snow records were considered homogeneous, with a change-point detected in the sole B-1 temperature record. The change-point in this temperature record was likely caused by a shift in the weather station location. The shift did not affect the precipitation record based on the homogeneity test results. No attempt was made to correct for the change-point in the temperature record as in the following chapters, daily values are important, and it is not straight forward to correct change-points at the daily scale. Therefore, either the B-1 temperature record should only be used up to 1996, or another dataset used for temperature in the Barcelonnette Basin. Station B-5 was not assessed due to the length of the record. For future work, precipitation records from stations B-1 to B-4 can be used.

2.3.2.2 Fella River Basin

In the Fella River Basin, all four out of six temperature records tested homogeneous, with the possible exceptions of F-5 and F-7. In the case of F-7, the record was likely homogeneous, as only the F-test found a significant change-point. For F-5, the Pettit and SNHT tests found change-points in the temperature data, indicating a change-point in the 1990s, and therefore likely not homogeneous.

Two types of precipitation records were tested for change-points: the full record, and the reduced record with all interpolated and accumulated values removed. Before 1943, three stations reported change-points in the full records and two in the reduced records (marked in bold in Table 2.3). No change-points were found in the reduced precipitation record after 1943 for all eight stations. When using the full record however, a change-point was detected in 1949 for the F-1 VWD time series and 2001 for the F-2 VWD time series. For station F-1, the F-test was the only test that found a change-point in the VWD record in 1949, and may be associated with the change-point found in the WD record in 1942. The SNHT detected a change-point for very wet days in F-2 in the full record, although this was not surprising as the change-point was near the end of the time series, a known sensitivity of the SNHT. Therefore, all reduced records for precipitation in the Fella River Basin are homogeneous from 1943 onwards, but only likely homogeneous for stations F-1 and F-2 using the full record.

All six records of snow days (SD and SDC) in the Fella River Basin had at least one test recording a change-point between 1984-1989, except for station F-4 (SDC only) and F-7 (SD only). For the SDC record, station F-7 was homogeneous, stations F-1 and F-5 were likely homogeneous, while stations F2, F3, and F-4 where likely not homogeneous. However, the F-test did not detect any change-points in the SDC records. The Pettit and SNHT tests do not account for a trend in the data, which if present in the SDC records, may lead to false identification of change-points. A similar result was found for the SD records, apart from F-4 that was homogeneous and for F-5. For station F-5, the F test and SNHT test found a change-point, making it unlikely that the presence of a trend in the data caused a shift. When comparing the SD and SDC record for F-5, SNHT found the change-point later in the time series between 2000 and 2006. The shift in the year of the change-point may be due to the SNHT being more sensitive to changes at the end of a time series. Overall, the snow records in the Fella River Basin were likely not homogeneous, whether it was calculated based on precipitation and temperature (SD) or the comments from the observers (SDC).

Change-points in the snow records may have come from differences in observational practices. It is expected that there may be small differences between the two snow day counts, SD and SDC, as not all days with snow may have been reported in the comments from observers (SDC) and the simple formula for determining a snow day (see Table 2.2). As all the records are collected by the same agency this shift could be a result from a change in observation methods and not a climate signal.

Overall, the temperature and precipitation records were either homogeneous or likely homogeneous for all temperature and precipitation records from 1943 onwards, except for the F-5 temperature record. However, change-points were detected in the snow records. These change-points may be from changes in observing practice, however as the F-test only found one significant change-point, a trend in snow days over time may have resulted in the SNHT or Pettit tests detecting artificial change-points. For the precipitation records, stations F-1 to 8 from 1943 onwards can be used in future work, along with the temperature records apart from station F-5.

2.3.2.3 Salzach Valley

For the Salzach Valley, the temperature record was homogeneous for station S-19 and likely homogeneous for the other two stations, S-15 and S-16. For station S-15 and S-16 only the Pettit test found a significant shift in 1996. It is possible that the Pettit test was over sensitive to the temperature change-point in the middle of the time series. No metadata was available for either station to confirm any station relocations.

For the Salzach Valley, 13 out of 19 precipitation records were homogeneous and another two were likely homogeneous (Table 2.3). For wet days, only station S-14 had two tests indicating a change-point in 1993 (Pettit) and 2000 (F-test). For very wet days, stations S-13 and 14 both

likely contained a change-point. Station S-14 also had all three test finding a change-point in 1999, confirming a change-point in the time series. Stations S-5, S-7, S-13, and S-16 also had two tests with change-points in the VWD time series, in each case the Pettit test along with either the SNHT or F-test. It is not surprising that the Pettit test found the most change-points between 1994 and 2002 in the precipitation records, as this test is most sensitive to changes in the middle of the time series.

The relocation of the stations S-5 and S-7 appears to have affected the precipitation records. Stations S-5 and S-7 were relocated in 1998 and 2002 respectively, close to the change-points found in Table 2.3. For stations S-13, S-14, and S-16, no information on relocation of stations was available to determine the cause for the change-point. The relocation of stations S-1, S-3, S-11, and S-18 appeared to have no effect on the homogeneity of the precipitation records.

The Salzach snow records tested homogeneous. None of the three stations for which SD time series could be calculated (S-15, S-16, and S-19) found a change-point. Therefore, the snow records can be used for further work.

Overall, the Salzach climate records are homogeneous or likely homogeneous except for station S-14. Stations S-5, S-7, S-13, and S-16 may contain a change-point in the very wet day precipitation time series, and therefore should be excluded when examining heavy or extreme precipitation. The three temperature records can be used for future work, as well as stations S-1 to 4, 6, 8 to 12, 15, 18, 19 for precipitation.

2.4 Exploratory data analysis: Comparison of the climate between study areas

2.4.1 Methodology

Exploratory data analysis (EDA) of the temperature and precipitation records is undertaken in this section to define and compare the climate of the three study areas. EDA investigates the major features of a dataset, providing insight without prior assumptions about the statistical properties of the data. Based onTukey (1977), EDA is concerned with the appearance of data, using both graphical and numerical summaries of the data to assess the average, spread and symmetry of the data (Wilks, 2011). Through such analysis, EDA can provide insight into the climate records and highlight underlying structure in the data, such as the magnitude–frequency relationship for precipitation. Furthermore, EDA can also highlight differences between datasets, relevant for this work as the climate of the study areas could influence hydro-meteorological triggers assessed in subsequent chapters. Variations in the climate can indicate that the three areas may respond differently to future climate change, a requirement for objectives C and D in Chapter 1.

Exploratory data analysis here covers the temperature and precipitation records. Precipitation is treated in more detail as it is considered

as a key factor in the triggering of hydro-meteorological hazards. First, an overview is given of the average daily temperature and 30-day precipitation totals that are compared between the study areas. Next, a more detailed numerical summary is given for both the annual precipitation and annual daily maximum precipitation (R_{1MAX}).

The parameters considered are the mean and maximum recorded value, skewness, and the Inter-Quartile Range (IQR). The Inter-Quartile Range, the difference between the 25% and 75% quartiles, was used as it is more resilient to outliers than the standard deviation. Skewness is assessed using the sample skewness coefficient, which enjoys widespread usage, and the Yule-Kendall index that is more robust and resilient to outliers (Wilks, 2011). From these results, the climate of each study area can be defined and compared.

In the final part of this section, the cumulative frequency distribution (CDF) for R_{1MAX} is assessed. The CDFs can be related to the return period for precipitation amounts, estimating the average recurrence interval between events of a similar magnitude. The CDF for R_{1MAX} is calculated both empirically (empirical cumulative distribution function, ECDF) and using the Generalized-Extreme Value distribution (GEV). While fitting the GEV is not strictly EDA as it assumes an underlying structure to the data, it allows for a comparison of the ECDF with a known distribution. GEV is based on the theory that the largest values from the same distribution will follow a known distribution, which does not depend on the original distribution (Wilks, 2011), and is frequently used for precipitation annual maxima (e.g. Buonomo et al., 2007; Min et al., 2011). The distribution assumes that the data it is derived from is not changing, an assumption that is invalidated if there is a trend in the data. The cumulative GEV-distribution function is:

$$F(x) = \exp\{-[1 + \frac{\alpha(x-\delta)}{\beta}]^{\frac{-1}{\alpha}}\} \tag{2.1}$$

where β is the scale parameter, α is the shape parameter and δ is the shift parameter. The ECDF can be written as:

$$F(x) = \frac{\#values \geq x}{n} \tag{2.2}$$

where n is total number of values.

The EDA is undertaken over the period 1971 to 2000 for the Fella River and Barcelonnette basins and 1987-2010 for the Salzach Valley. The B-1 temperature record is an exception, where 1961-1990 is used due to the change-point found in 1997/1998 (Sec 2.3.2.1). These time periods were selected so that the highest number of stations could be included in the analysis, as well as to adhere to the WMO climate normal of 30 years (Arguez and Vose, 2010). Longer time series may be affected by long term trends that would invalidate the assumption above for the GEV distribution. Only time series that were found to be homogeneous in

Sec 2.3 were used, reducing the final number of stations for each study area to 4 for the Barcelonnette Basin (B-1 to 4), 8 for the Fella River Basin (F-1 to 8, reduced time series), and 14 for the Salzach Valley (S-1 to 4, 6, 8-13, 15, 17-19).

2.4.2 Results and Discussion

Figure 2.3 displays the mean daily temperature (red), 30-day precipitation (blue) for all homogeneous stations. The average daily temperature values were similar between all three study areas, with the highest temperatures in July, and near freezing temperatures in December, January and February (red lines, Fig 2.3). The warmest average summer temperatures were recorded by station S-19 (19.98^oC), with the coldest winter temperatures at sites F-2 (-4.78^oC), S-15 (-3.34^oC), and S-16 (-2.42^oC). Colder winter and spring temperatures indicate a higher chance of snowfall (temperature $\leq 3^oC$), which may influence the occurrence of some hydro-meteorological hazards.

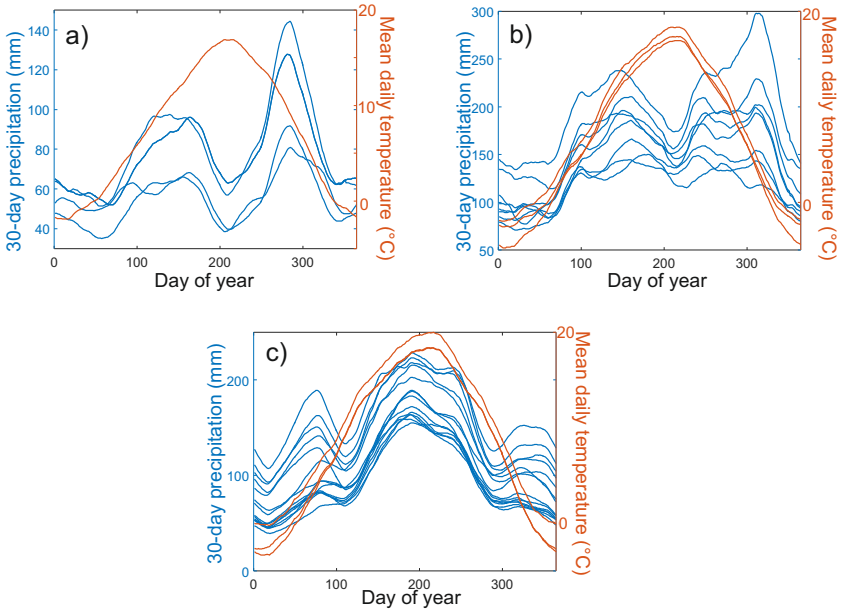

Figure 2.3 Mean daily temperature and running average 30-day precipitation for the Barcelonnette Basin (a, RR: 1971-2000, T: 1987-2010), the Fella River Basin (b, 1971-2000), and the Salzach Valley (c, 1987-2010) for the homogeneous stations listed in Table 2.3.

In the same Fig 2.3, the mean 30-day total shows dissimilar distributions of precipitation over the year between the three study areas (blue lines, Fig 2.3). The Barcelonnette and Fella River basins had two distinct peaks in precipitation and low 30-day totals during winter (December - February). The first peak occurred within April-June, with a second peak

in September-November. However, the average August precipitation in the Barcelonnette Basin reduces to winter levels, while for the Fella River Basin the August precipitation was still 30-60 mm higher than in winter. For the Salzach Valley, there was one main precipitation peak (May-July) and two minor peaks, one in March and one in November. All stations recorded the lowest precipitation over winter, although this amount may be underestimated in part due to the difficulty of measuring snow with rain gauges (see Sec. 2.3).

Table 2.4 provides a numerical summary of the annual total precipitation and R_{1MAX} for the stations in Fig 2.3. The highest average annual total precipitation was for the Fella River Basin (1440-2460 mm), followed by the Salzach Valley (1096-2035 mm) and then the Barcelonnette Basin (664-990 mm). The maximum R_{1MAX} amounts were again highest in the Fella River Basin (81-195 mm) compared with the Salzach Valley (45-84 mm) and the Barcelonnette Basin (46-69 mm). However, the overlap was larger between the Salzach Valley and the Fella River Basin for the annual totals than the R_{1MAX} amounts. The R_{1MAX} amounts contributed to a larger percent of the annual total precipitation for the Fella River and Barcelonnette basins (5.4-7.9% and 5.8-7.1% respectively) compared to the Salzach Valley (3.4-4.6%). Within each study area, the station that had the highest mean and maximum annual totals for an area also had the highest mean R_{1MAX} values (Barcelonnette: B-4, Fella River: F-7, Salzach: S-9). The only exception for the highest R_{1MAX} was for station S-12, which was 7% higher than S-9.

The distribution of R_{1MAX} amounts over the study areas varied. For the Barcelonnette Basin, the stations to the north east in Fig 2.1 (B-3 and B-4) had the highest precipitation amounts, as opposed to stations B-1 and B-2. For the Fella River Basin, the most southern station, F-7, had the highest precipitation amounts in Table 2.4. In contrast, the most northern stations, F-1, 2, 4, and 5, had the lowest annual total and R_{1MAX} amounts. These four stations were also at a higher elevation than station F-7. For the Salzach Valley, two stations in the north part of the catchment, S-9 and S-10, had the highest annual total and R_{1MAX} amounts. Station S-19 was further north of the two stations, although at a lower elevation (see Table 2.1). The stations that recorded the lowest average precipitation varied between parameters, with stations S-6, 11, and 18 in the east of the catchment recording the lowest annual total precipitation and stations S-1, S-2, and S-18 recording the lowest average R_{1MAX}. The spatial distribution was in part caused by the topography within the study area, as stations on the leeward side of the mountain ranges receive less precipitation than those on the windward side.

The skewness of the annual total and R_{1MAX} was assessed (Table 2.4). Positively skewed data indicates that there are frequent years with smaller precipitation amounts, and a few years with extreme high precipitation totals. The Fella River and Barcelonnette basins annual totals were all positively skewed based on the SCC test. However when using the Y-K test in the Fella River Basin, the range of values was 0.0-0.35, indicating that the median 50% of the data is either balance, or

Table 2.4 Summary of annual total precipitation and annual maximum daily precipitation (R_{1MAX}). The statistics compare the mean, the maximum observed value, the Inter-Quartile Range (IQR), Yule-Kendall test (Y-K) and skewness coefficient (skew). BB indicates the Barcelonnette Basin.

		Annual total				R_{1MAX}				
		Mean (mm)	Max (mm)	Y-K	Skew	Mean (mm)	Max (mm)	IQR (mm)	Y-K	Skew
BB	B1	704	1025	0.33	0.96	48.1	72.9	14.8	-0.11	0.51
	B2	664	992	0.52	0.32	46.7	83.0	10.8	0.30	1.13
	B3	939	1436	0.36	0.40	54.8	87.0	15.7	-0.13	0.61
	B4	990	1521	0.26	0.1	69.8	128.7	33.9	0.19	0.76
Fella River	F-1	1506	2114	0.21	0.57	81.0	126.8	28.6	0.49	0.50
	F2	1440	1852	0.03	0.36	81.5	178.5	24.5	-0.38	2.27
	F3	2062	2968	0.35	0.70	133.0	246.0	56.8	0.00	0.86
	F4	1533	2170	0.01	0.95	97.0	186.2	34.1	0.37	1.25
	F5	1814	2840	0.14	1.32	126.8	278.6	59.1	-0.04	1.38
	F6	2066	3006	0.29	1.24	152.6	229.7	76.5	-0.20	0.04
	F7	2460	3594	0.00	0.42	195.1	355.0	131.1	0.37	0.68
	F8	184	2940	0.10	1.10	138.5	276.6	71.2	0.16	1.15
Salzach	S1	1278	1524	-0.18	0.26	45.4	65.8	16.5	0.19	0.24
	S2	1206	1403	0.09	0.06	45.8	101.4	11.7	-0.03	2.46
	S3	1781	2161	-0.14	0.01	66.3	102.1	21.5	0.37	0.45
	S4	1403	1729	-0.22	0.20	55.6	94.0	19.3	0.23	0.68
	S6	1154	1422	0.23	0.76	49.5	81.2	18.8	0.42	1.04
	S8	1742	2027	0.14	-0.20	62.2	106.8	21.2	0.24	0.83
	S9	2035	2528	0.14	-0.13	83.8	137.0	33.3	0.23	0.81
	S10	1894	2198	0.21	-0.10	76.2	128.2	30.8	0.09	0.90
	S11	1096	1285	0.13	0.20	46.2	60.4	12.6	-0.33	-0.11
	S12	1550	1849	-0.37	-0.07	67.8	146.7	19.5	0.25	1.77
	S15	1175	1399	0.13	0.16	49.8	94.2	15.2	0.09	1.40
	S17	1480	1702	0.26	0.24	50.5	74.1	16.6	0.11	0.49
	S18	1138	1412	-0.18	0.58	45.7	70.5	22.4	0.12	0.48
	S19	1213	1506	0.38	0.33	55.5	101.5	27.2	0.33	0.69

only slightly skewed to the right. For the Salzach Valley, the range was balanced, -0.37-0.38, for the Y-K test and -0.20-0.76 for the SCC test. In most cases the SCC value was greater than that found with the Y-K, although this did not hold for stations S-8 and S-9, and stations S2, S-15, S-17, and S-19 were within 0.03 of each other. For R_{1MAX}, all but one station (S-11) were positively skewed using the SCC. Unlike the annual precipitation amounts, all study areas had a range of values between negatively and positively skewed based on the Y-K. Therefore, it appears that R_{1MAX} does not follow the same distribution as the annual total precipitation, and therefore changes in the annual precipitation will not necessarily account for similar changes in daily extreme precipitation.

Figure 2.4 displays the return periods for R_{1MAX} for each station, with a solid line for the empirical distribution and a dashed line for the best fit GEV-distribution. Steep curves indicate little increase in

precipitation for increasing return periods, while a more gradual curve indicates a faster precipitation increase with increasing return period. For the Barcelonnette Basin, the three stations in the south of the study area (B-1, B-2, B-3) were similar in shape and values. Station B-4 had more extreme precipitation amounts, in line with the mean and maximum R_{1MAX} amounts in Table 2.4. For the Fella River Basin, station F-5 had the largest shape value of any of the stations (0.07-0.25 compared with 0.78).The large shape value resulted in station F-5 having moderate precipitation amounts for high frequency events, but one of the highest precipitation amounts for low frequency events. The Salzach Valley had similar distributions to the Barcelonnette Basin, with many northern stations recording smaller extreme precipitation amounts than those in the south. Shown in more detail than in Table 2.4, S-12 has moderate precipitation amounts for high frequency events, but one of the highest values for the low frequency events (along with S-9 and S-10). Overall, as was found in Table 2.4, the highest R_{1MAX} amounts are found in the Fella River Basin, compared with the Barcelonnette Basin and Salzach Valley.

The differences between the empirical and GEV distributions for extreme values highlights the difficulty in determining return periods for extreme events. For all stations, the difference between the empirical and fitted distributions was small (<5 mm) for return periods less than three years, with differences increasing up to 40 mm for return periods greater than 20 years. For example, based on the GEV distributions in the Salzach Valley, the highest daily values would be expected from stations S-9, and S-10, rather than at S-12 as was observed. Another distribution may have an improved fit over the GEV, however this is not guaranteed.

Overall, the EDA has shown most precipitation falls during spring to autumn. All study areas record on average near zero precipitation amounts during December, January, and February. The average 30-day precipitation amount was distributed differently over the year between study areas, possibly leading to variations in time of year that hydro-meteorological events occur. Of the three sites, the Fella River Basin had the highest R_{1MAX} amounts and annual total precipitation. Differences in the precipitation distributions between stations may mean that all stations do not correlate equally with hydro-meteorological events. The values here can therefore be used as a reference for subsequent chapters, a basis from which the link between climate and hydro-meteorological hazard can be assessed.

2.5 Observed trends

2.5.1 Methodology

This section investigates trends in the temperature and precipitation records analysed in Sec 2.4. Trend analysis identifies trends in the data and can provide an indication about how the area is responding to global climate change. As hydro-meteorological events are often triggered by

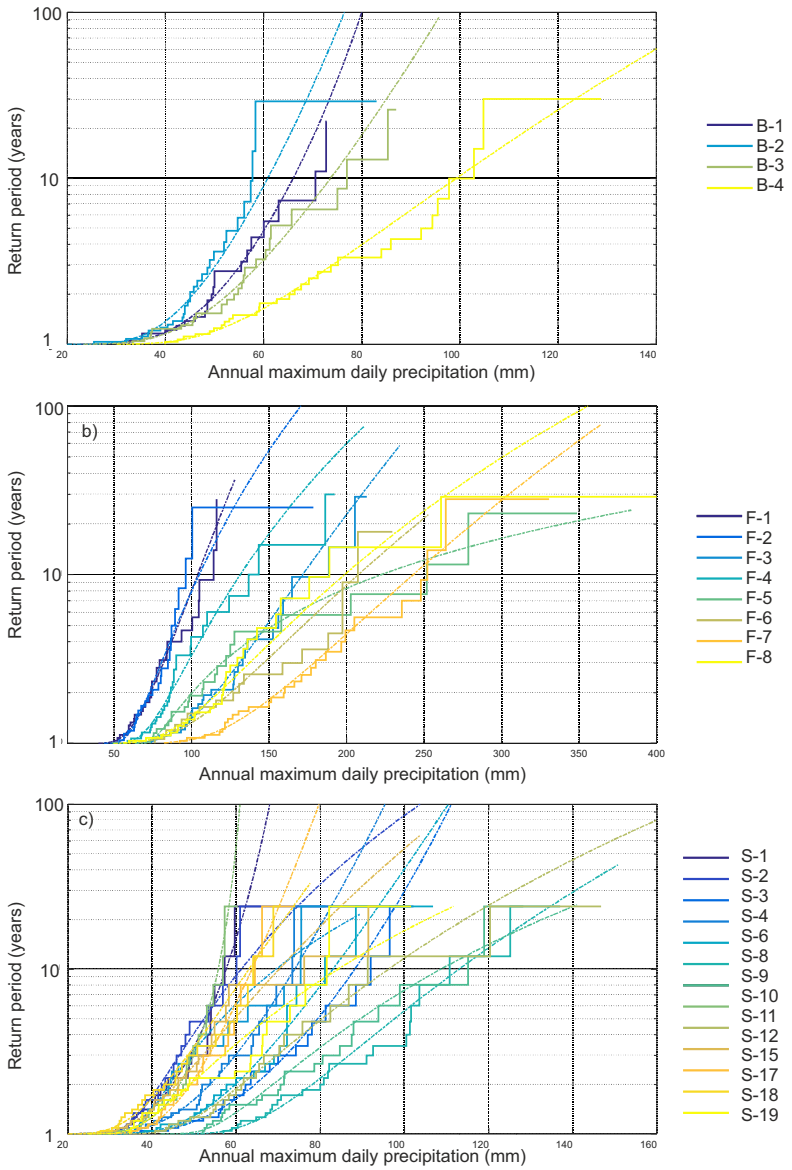

Figure 2.4 Annual maximum daily precipitation amounts for a) the Barcelonnette Basin 1971-2000, b) the Fella River Basin 1971-2000 and c) the Salzach Valley 1987-2010, for the homogeneous stations. The stair plots show the empirical return periods, while the dashed line plots the best fit GEV-distribution.

extreme conditions, such as extreme daily rainfall, trends for climate extremes should be assessed. However, trend detection in extreme values can be challenging. Frei and Schär (2001) found that in a 100 year long record, a frequency change by a factor of 1.5 could only be detected with a 20% probability for an event with a return period of 100 days. The probability of detecting such a trend in a shorter time series, such as those in Table 2.1, would be even less likely. Therefore, the focus here will be on moderate extremes (return periods < 1 year), increasing the likelihood of detecting trends, while providing results relevant for hydro-meteorological hazards.

Trends in 21 different climate indices were calculated, focusing on moderate extreme indices (Zhang and Yang, 2004). The indices are taken from the ETCDDI/CRD Climate Change indices, formulated by a number of international organisations (see Klein Tank et al. (2009) for more information). The significance of the trends was assessed using the Mann-Kendall rank correlation statistic (MK), as it makes no assumption about the distribution of the data, or that the trend is linear. The MK has be used to valuate trends in a variety of climate series, and found to be robust to the effect of outliers (Peterson et al., 2008).

For this section, only the Barcelonnette and Fella River basins were assessed. The 24-year records for the Salzach Valley were considered to be too short. Long time series are essential to insure that detected trends are not a result of interannual or decadal natural variability. The length of the Barcelonnette and Fella River basins time series are longer than the 30-year WMO climate normal (excluding F-2).

2.5.2 Results and Discussion

The trend for the climate indices are stated per station for the Barcelonnette and Fella River basins in Table 2.5. The indices cover extreme maximum and minimum temperature, growing season length, length of wet and dry spells, and measures of extreme and moderate extreme precipitation. Further details on the abbreviations and exact definition of the indices can be found in Appendix A.1 and Klein Tank et al. (2009). Colours in the table are used to indicate whether the increasing/decreasing trend is above the 5% (red/blue) and 10% (pink/light blue) significance level. Insignificant trends are represented by a grey colour. Some indices (black) could not be computed as there was either no data available or the length of the homogeneous record was less than thirty years. Here we focus on results that stand out or might be contradictive to a warming climate.

For the temperature related indices (first 10 indices in Table 2.5), most trends were indicative of a warming climate, such as fewer cold days and nights and more warm nights. There was one exception for the B-1 record. Station B-1 had a significant decrease (0.1°C per decade) for the monthly maximum value of daily maximum temperature (Max Tmax). The other temperature indices for the B-1 either had no significant trend, or one associated with a warming climate, such as a decrease in the

Table 2.5 Trends for 21 climate indices for the Barcelonnette Basin, and Fella River Basin for the homogeneous stations in Table 2.2. Red/blue boxes indicate increases/decreases at the 5% significance level, and pink/light blue at the 10% significance level. Grey indicates no significant trend, and black where no data was available or the record was too short (<30 years). R = precipitation, T = temperature, GSL =growing season length, DTR = diurnal temperature range, p = percentile, CCD = consecutive dry days, CWD = consecutive wet days. X = 25 mm for the Barcelonnette Basin and 50 mm for the Fella River Basin. Stars denote stations with smaller trends when using the full time series over the reduced time series.

	Barcelonnette				Fella River						
Indices	1	2	3	4	1	3	4	5	6	7	8
TMin> 20°C(days)								0.0		0.0	
TMax> 25°C(days)					0.3	0.3		0.4		0.9	
TMax< 0°C(days)					-0.5			-0.4		-0.4	
TMin< 0°C(days)	-0.1				-0.3			-0.3		-0.1	
GSL (days)	0.7				0.5			0.4		0.8	
Max TMax (°C)	-0.1				0.0	0.0		0.0		0.1	
Min TMax (°C)								0.1		0.1	
Max TMin (°C)						0.0		0.0		0.0	
Min TMin (°C)					0.1			0.1		0.1	
DTR (°C)						0.0					
Max 1dayR (mm)							0.7*	0.8*			
Max 5dayR (mm)							0.9*				
Intensity (mm/day)	-0.0										0.0
Days >10 mm											
Days >20 mm					-0.1						
Days >X (mm)	-0.0						0.0				
Max CCD											
Max CWD			0.1			0.0					
R95p (mm)	-0.9						2.7*	3.4*			
R99p (mm)							1.9*	24*			
Annual R (mm)											

number of days with a minimum temperature less than 0°C, and the growing season length (GSL). All Fella River temperature records had a significant increase in the number of days with a maximum temperature above 0°C. Most stations also had an increase in the GSL, apart from station F-3. Station F-3 has the highest elevation of the Fella River rain gauges, followed by F-2, which may have played a role.

For the precipitation related indices (last 11 indices in Table 2.5), the trends were less clear than for temperature. The indices with significant trends found decreasing moderate extreme precipitation for the Barcelonnette Basin, opposite to most trends for the Fella River Basin. For the B-1 record, the average intensity, number of days with rainfall above 25 mm, and the total precipitation amount greater than the 95th percentile (R95p) all decreased. The maximum number of consecutive wet days at station B-3 increased. Most precipitation indices showed no

significant change for the Fella River Basins, although stations F-4 and F-5 had five and three indices with significant increases in extreme precipitation respectively. In particular, the amount of precipitation greater than the 95^{th} and 99^{th} percentiles both increased significantly (1.9-3.4 mm/decade). Stations F-4 and F-5 were also two of the drier stations in the Fella River Basin (Table 2.4), which may indicate more uniform precipitation distribution over the area. One precipitation index for the Fella River Basin found a decrease in extreme precipitation: number of days greater than 20 mm for station F-1. Overall however, there were few (15) significant changes in the precipitation indices for the two study areas.

When using the full time series for the Fella River Basin, seven increasing trends in the extreme precipitation were reduced (indicated with stars in Table 2.5). The full time series included also accumulated measurements over multiple days. As there were no accumulated values in the last decade of the time series, inclusion of the accumulated, and possibly the interpolated values, masked the increase in directly recorded precipitation extremes.

The detected trends in the climate indices may have implications for hydro-meteorological hazards. Five of the six temperature stations found a significant increase in the growing season length, which may lead to a reduction of the number of days with snow. This increase in snow-free conditions may have implications for hydro-meteorological events in the region, altering the time of year when snowmelt- influenced hazards occur, as well as snow can act as a stabilising factor for landslides (Matsuura et al., 2003). All temperature records in the Fella River Basin saw a significant increase in days with maximum temperature greater than 25°C (Tmax > 25°C), which may increase the potential for severe convective storms, and hence flash floods and debris flows. While there were few significant changes in precipitation for the Fella River Basin, most indicated an increase in moderate extreme precipitation which may lead to an increase in hydro-meteorological events such as flash floods and debris flows. The only precipitation index that had a decrease was days greater than 20 mm. However the precipitation amount is not particularly high for the weather station (the average R_{1MAX} is 81 mm). For the Barcelonnette Basin, overall the precipitation in the study area had experienced little change over the observed period. There is the potential that changes in temperature and precipitation may have affected hydro-meteorological hazards in the Barcelonnette and Fella River basins, and therefore should be considered when assessing the link between climate and hydro-meteorological hazards.

2.6 Conclusion

Most of the precipitation and temperature records in the Barcelonnette Basin, the Fella River Basin (from 1943 onwards), and the Salzach Valley were homogeneous or likely homogeneous. The exception for the

Barcelonnette Basin was in the B-1 temperature record, which was homogeneous up to 1996. Five precipitation records in the Salzach Valley likely had change-points, although only S-14 had significant shifts in both wet days and very wet days. The homogeneity of snow day records was questionable for the Fella River Basin, and therefore snowfall days should only be used with care in future work. After removing stations that likely had change-points in precipitation, there were 4 homogeneous stations in the Barcelonnette Basin, 8 in the Fella River Basin (reduced time series), and 14 in the Salzach Valley.

Comparing the climate between the three areas, the Fella River Basin received the highest annual precipitation totals, as well as R_{1MAX}. The Barcelonnette Basin was the driest, with the Salzach Valley mean annual precipitation closer to the Fella River Basin, and closer to the Barcelonnette Basin for extreme precipitation. All three areas recorded the lowest precipitation amounts in the winter, although the peak precipitation differs between study areas. All temperature records had near zero temperatures for December, January, and February, during which time most precipitation would fall as snow. There was also variation between stations within a study areas, with differences as much as 175 mm for the 10 year return period precipitation events in the Fella River Basin, potentially due to topography and prevailing wind directions. The separation between the GEV and ECDF for low frequency precipitation events further highlights the challenges in defining precise return periods for extreme events. Overall, the results from this section can be used as a reference for work in subsequent chapters.

Changes in climate have been observed in the Barcelonnette and Fella River basins (the Salzach Valley was not assessed), although the results are mixed. Most observed changes in the temperature indices were consistent with warming, such as increases in the growing season length, number of days exceeding 25°C and a decrease in the number of days that do not exceed 0°C. The signal was less clear for station B-1. There were fewer changes in the precipitation indices, with 3 out of 4 significant trends for the Barcelonnette Basin indicating a decrease in heavy precipitation, and 10 out of 11 trends finding an increase in heavy precipitation in the Fella River Basin. The inclusion or exclusion of interpolated values clearly has an effect on the trend analysis for the Fella River stations, demonstrating the importance of data quality and homogeneity tests before trend analysis is undertaken. Future work assessing precipitation extremes should consider only using the reduced time series.

Increases of temperature extremes may have affected the homogeneity tests that do not account for trends in the data. Trend analysis showed that there was warming at station F-5, where only the SNHT and Pettit tests, which do not account for a linear trend, detected a change-point. Furthermore, the F-test that accounts for a possible trend found no significant change-points, except for station F-7.

Overall, the three study areas have multiple precipitation records that can be used in understanding the link between the climate and hydro-

meteorological events. Detected trends in the climate records indicate that changes have occurred in the Barcelonnette and Fella River basins, which may have already had an effect on historical floods and landslides. Variations in the climatology between areas indicate potential differences in the hydro-meteorological triggers. These ideas can be explored in the following chapter, using the results from this chapter as a foundation.

3 Meteorological proxies for hydro-meteorological hazards: thresholds and weather types

3.1 Introduction

There are numerous potentially important meteorological triggers for floods and landslides. Intense, short duration rainfall is often a trigger for flash floods and debris flows (e.g. Marchi et al., 2010; Smith et al., 2011), while heavy rainfall over multiple days can also lead to hazardous events (e.g. 3 days for shallow landslides Tiranti et al. (2013), 60 days or longer for deep seated landslides Borgatti and Soldati (2010); Martelloni et al. (2011), and 1-10 days for a range of landslide types including debris flows and mudslides Kirschbaum et al. (2015)). In mountainous catchments, snow and snowmelt can play a role (e.g. landslides: Borgatti and Soldati (2010); Saez et al. (2013); Stoffel et al. (2014), floods: McCabe et al. (2007); Hall et al. (2014)). Warmer temperatures have led to warming of permafrost and glacier retreat influencing slope stability and sediment availability for landslides (Huggel et al., 2012). Which of the above factors dominate however, needs to be assessed per study area.

There are various approaches in linking the climate with hydro-meteorological hazards, ranging from empirical statistical relationships to those based on physical models. Physical models can include most of known influences on the flood or landslide occurrence, including non-linear relationships. However, physical models can have extensive data requirements, and challenges in parameterization and calibration of conceptual and data models increase uncertainty in modelling procedures (Wagener et al., 2003). Over larger areas, or where there is poor data coverage, empirical thresholds can be used (e.g. Frattini et al., 2009; Berti et al., 2012; Brunetti et al., 2013). These thresholds define minimum or maximum conditions of triggering factors for a particular hazardous event (Frattini et al., 2009).

Physical models differ in complexity based on the physical processes included. In flood forecasting for both short and long term planning, rainfall-runoff models are generally used (Beven, 2012). These models

calculate the amount of rainfall that is converted to runoff based on mathematical models. Physical models for landslides are useful for individual study areas not more than a few square kilometres, where not only triggers such as rainfall are taken into account, but other factors as well, such as pore pressure and slope stability (Aleotti, 2004; Brunetti et al., 2013). In physical models for both floods and landslides, there are uncertainties in the parameters of the models, as well as in the initial and boundary conditions. However, and potentially more important for assessing hydro-meteorological triggers, it is not always clear from physical models what the climatic triggers are. An understanding of the appropriate meteorological proxies is especially needed when developing climate change-hazard studies, where a balance is needed between capturing the triggering process and what the climate projections are able to model adequately.

Therefore, empirical thresholds have continued to be developed alongside physical models. These thresholds can either exclude days with non-hazardous events (e.g. Caine, 1980; Brunetti et al., 2013; Marra et al., 2014; Nikolopoulos et al., 2014), or through a probabilistic approach where non-event days are included (e.g. Glade et al., 2000; Berti et al., 2012; Saez et al., 2013). A detailed review of empirical thresholds for debris flows and landslides can be found in Guzzetti et al. (2008).

Developed empirical thresholds or relationships can be used to assess the return period of the hydro-meteorological hazard. If a link is found between climate indices and hazardous events, the magnitude-frequency of the indices can be used as a proxy for the hazard. Recent approaches have moved beyond statistical based frequency of occurrence, to include classification of types of triggers (e.g. for flood types Merz and Blöschl, 2008), to account for non-stationarities in the records (e.g. Ouarda and El-Adlouni, 2011), or imperfect knowledge (e.g. Huard et al., 2010; Ouarda and El-Adlouni, 2011). The incorporation of factors beyond rainfall may provide additional information with regards to future climate change, as well as when looking at longer historical records or paleo-records. While the methods listed above are more complex than the traditional magnitude-frequency approach, they highlight challenges to take into account when assessing changes in hydro-meteorological hazard frequency.

Hydro-meteorological hazard trigger analysis is hampered due to limitations in observational networks. Flash floods can be one of the most dangerous flood types, yet they are often poorly documented and occur in ungauged basins (Gaume et al., 2009). Precipitation can vary greatly with altitude in mountainous areas, and, without extensive gauge networks or local radar, orographic processes can be difficult to determine (Tobin et al., 2011). Even extensive rain gauge networks can underestimate the rainfall during convection events, which often occur within 12 hours and over a limited area (Marra et al., 2014). To adequately record such convective events, measurements of sub-daily or even sub-hourly precipitation are needed. However, records of sub-daily precipitation are often not long enough for analysis of triggers (generally

less than 20 years). Uncertainty in the rainfall amount and intensity can therefore make it difficult to carry out trigger analysis (Nikolopoulos et al., 2014).

The link between climate and hazards may not be clear due to other environmental and non-environmental factors. Deforestation, urbanisation and agricultural practices all can alter flood regimes (Hall et al., 2014). Changes in flood patterns in the Mediterranean between 1301-2012 were mainly related to changes in land use and only partly by changes in precipitation (Barrera-Escoda and Llasat, 2015). The link with climate is often even less clear for landslides than for floods. Landslides are heterogeneous in nature, and therefore the precise climate parameter influencing the occurrence depends greatly on the location and can be difficult to determine (Dehn and Buma, 1999). Landslide occurrence depends on other factors such as soil properties, slope geometry, as well as characteristics of the upslope catchments (Dhakal and Sidle, 2004). The amount of debris or source material is difficult to estimate, increasing the uncertainty of the triggers for rock falls and debris flows (Jomelli et al., 2004). Besides the difficulties listed above, after a landslide many environmental factors change, such as slope and vegetation, which vary depending on the size and type of movement of the landslide (van Westen et al., 2006). Triggers involved in reactivation of a landslide may be different than the first initiation of movement (Borgatti and Soldati, 2010). Therefore, non-meteorological factors hamper attempts to understand precise links between hydro-meteorological hazards and the climate in addition to the limitations in observational networks.

This chapter assesses meteorological proxies for hydro-meteorological hazards for use in climate change-hazard studies and identifies research areas for further in-depth analysis. An overview of the hazard inventories for the study areas is given in Sec 3.2. Flood, debris flows, and soil slides are first assessed independently to allow for variation in the meteorological proxies and to account for differences in data availability and quality. Section 3.3 builds on the work of Merz and Blöschl (2008) by considering precipitation and temperature conditions surrounding high discharge days, which are used as an indicator for floods. Due to the fine temporal and spatial scale, debris flows and flash floods are considered together in Sec 3.4, focusing on a simple and probabilistic approach for empirical rainfall thresholds. Where a link with the climate can be determined, magnitude-frequency relationships for debris flows and flash floods are also considered. Soil slides are considered in Sec 3.5. Investigating the role of atmospheric circulation patterns on hydro-meteorological hazards, Sec 3.6 assesses occurrence of hydro-meteorological hazardous events between synoptic weather types. Section 3.7 provides overall conclusions around linking climate and hydro-meteorological hazards for the study areas considered.

3.2 Study areas

Two study areas with extensive flood and landslide inventories are considered in this work: the Barcelonnette Basin, France, and the Fella River Basin, Italy. Both areas have experienced numerous hydro-meteorological events and have more than 30 years of climate records. More information on climate data and maps of the study areas can be found in Chapter 2, and an overview of the hazard inventories in Chapter 1.

In the Barcelonnette Basin there were 204 hydro-meteorological events reported between 1930 and 2012, included flash floods, debris flows, landslides, and flooding of the Ubaye river. The majority of the events occur during the spring. In 1957, during a spring warm spell, rapid snow melt and heavy rainfall combined to cause flooding in Barcelonnette and Jausiers, as well as in the surrounding Cerveyrette and Maruieene valleys (Arnaud-Fassetta et al., 2005). More recently in May 2008, heavy spring rain again led to flooding and damage to buildings, bridges and other infrastructure in the basin. Outside of floods, June has the highest proportion of hydro-meteorological events, with a smaller number of debris flows, flash floods and landslides occurring in autumn. There are five weather stations in and around the basin; four with sufficiently complete records (Chapter 2).

For the Fella River Basin, 16 debris flows and landslide events were reported between 1980 and 2012. During this time, there were three major flooding events: September 1983, June 1996 and August, 2003 (Borga et al., 2007). The largest hydro-meteorological event occurred on the 29th of August, 2003 leading to more than 100 debris flows, as well as other shallow landslides, flash floods, and flooding of the Fella River. During the 2003 event, organized convection allowed for the continuous generation of heavy precipitation over parts of the Fella River Basin, with more than 390 mm recorded in 24 hours (Borga et al., 2007). The second largest hydro-meteorological event was in June 1996, where two consecutive storms led to flooding and numerous debris flows (Borga et al., 2007). The third largest event was in June 2011, a smaller event triggering fewer debris flows than either 1996 or 2003. The Fella River Basin receives higher annual and daily precipitation amounts than the Barcelonnette Basin (Chapter 2), with intensive, wide spread convective events in the summer months. The Fella River Basin has eight weather stations.

3.3 Floods and climate conditions in the Barcelonnette Basin

The objective of this section is to assess whether floods (represented by high discharge) occur under different meteorological conditions in the Barcelonnette Basin. Unlike for hazards such as debris flows or rock-falls, continuous measurements of discharge allow for magnitude-frequency

relationships to be developed directly, which can be extrapolated for unobserved events. However, this extrapolation may be unreliable if there are a variety of flood triggering mechanisms incorporated into the one magnitude-frequency curve (Merz and Blöschl, 2008). When assessing flood climate change-hazard studies, changes in flood types will have implications on both the local social and ecological systems (Gain et al., 2013; Garner et al., 2015). Therefore, if more than one flood type is identified, further work can be undertaken into incorporating changing flood types in climate change-hazard studies.

The Barcelonnette Basin study area is used for this work. Daily discharge measurements are available for 1970-2009, and are homogeneous based on the three tests in Chapter 2. The precipitation and temperature records from station B-1 (see Fig 2.1) were used.

3.3.1 Method

As a first step in assessing the link between climate and floods, a classical approach is applied. This method fits a curve to the flood observations. Here, the annual maximum daily discharge is extracted for the period 1970-2009, resulting in 40 flood events. While the annual maximum daily discharge is unlikely to correspond directly to flood events that resulted in damage, as some years discharge values may be low, or events missed due to multiple floods in one year, it is a relatively straight forward approach still used in flood frequency analysis (Bezak et al., 2013).

The second step is the classification of flood types. The classification is based on the work by Merz and Blöschl (2008), where five flood type groups were identified: flash floods (Type 1), short rain floods (Type 2), long rain floods (Type 3), rain on snow (Type 4) and snowmelt floods (Type 5). Details on the flood types can be found in Table 3.1 along with the expected response in the discharge measurements and precipitation and temperature conditions.

The flood types are classified automatically. In Merz and Blöschl (2008), floods were classified manually to allow for the observer to use a combination of sources of information, such as observational reports and meteorological records, as well as to allow for subtleties in the interactions between the meteorological triggers and flooding mechanisms. Rather than relying on manual classification, the flood events here are classified automatically based on the expected discharge response in Table 3.1. Floods are first divided into snow and non-snow influenced floods based on the time of year. Figure 3.1 displays the mean daily precipitation (blue), discharge (black) and temperature (red) over a year in the Barcelonnette Basin. The discharge is out of step with precipitation in the period April-July (Fig 3.1), which is defined here as the initial high discharge time (IHD). During the IHD, rising temperatures leads to snowmelt as well as periods of rainfall, with any resulting flood likely either Type 4 or 5. Once the flood events are separated into snow and non-snow influenced floods, the types are further split based on rate of increase for discharge.

Table 3.1 Flood types with explanation from Merz and Blöschl (2008) (description) compared with the expected response from discharge measurements and precipitation and temperature measurements

Type	Description	Expected hydrological response	Expected meteorological response
1. Flash	High intensity rainfall, where runoff is the main cause of flood and infiltration is less significant	Rapid increase in discharge from base flow	Extreme 24 hour or less rainfall totals. Antecedent conditions normal (on average)
2. Short rain	Short period of rainfall combined with previous rainfall saturating part of the catchment	Rapid increase in discharge from above base flow levels	Caused by high daily rainfall and higher than normal antecedent conditions
3. Long rain	Rainfall over several days or weeks leading to exceeding the storage capacity of the catchment	Gradual increase in discharge	Multiple days of rainfall, where the multi-day total rainfall is exceptionally high rather than the day of occurrence
4. Rain-snow	Rainfall on already existing snow cover. Increased discharge may be from antecedent snowmelt, increased snowmelt due to rain falling on the snow as well as runoff from the rainfall.	Rapid increase in discharge after a more gradual increase	Rainfall and increased discharge /saturation due to antecedent snowmelt
5. Snowmelt	Anomalous warm conditions lead to increased rate of snow melt up to a period of several weeks.	Gradual increase in discharge	Multiple days of rainfall, where the multi-day total rainfall is exceptionally high rather than the day of occurrence

The specific procedure for classification of flood types in the Barcelonnette Basin is as follows:

1. Separation of snow and non-snow influenced floods: any floods that occurred inside the IHD were classified as snow-influenced. The IHD was defined as the first time in the year discharge goes above base flow (6 m^3/s) for 50 days in a row, and ends when it goes below 6 m^3/s for two days consecutively after this peak. The dates of IHD vary from year to year. Flood events inside the IHD are classed as Type 4-5, outside these dates, Type 1-3 (from Table 3.1).
2. For non-snow influenced floods: If the previous day is near base

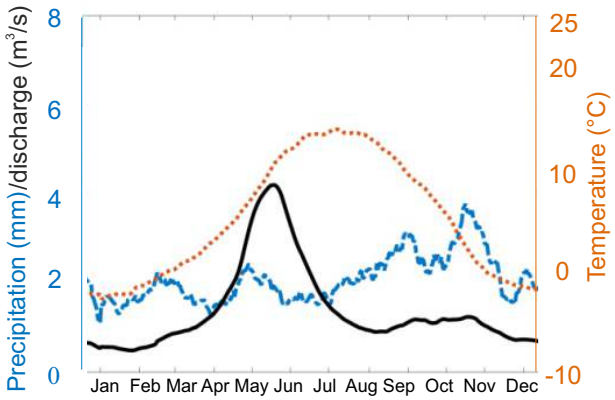

Figure 3.1 Mean daily discharge (solid black line), precipitation (dashed blue line), and temperature (dotted orange line) for the Barcelonnette Basin, 1988-2010

flow (<7 m^3/s), the event is classified as Type 1, if the previous day is near similar levels to the flood event (<5 m^3/s difference), the event is classified as Type 3, otherwise Type 2.

3. For snow influence floods: if the previous day was near similar levels to the flood event (<5 m^3/s difference), the event was classified as Type 5, otherwise Type 4.

Once the flood events are placed in one of the five groups in Table 3.1, the meteorological conditions for each group are assessed. Temperature and precipitation are used to compare with the expected meteorological response in the final column of Table 3.1. The parameters are 1, 5, and 30 day precipitation amounts, and 1, 5, and 20 day mean temperature values from station B-1 (Fig 2.1). For temperature, both normalized and absolute values are used, where the normalized values are calculated using:

$$\frac{T_j - \bar{T}_i}{s_i} \tag{3.1}$$

where T_j is the absolute temperature value, $\bar{T}_i$ is the mean temperature for the day of the year +/- 15 days, and s_i is the equivalent standard deviation.

3.3.2 Results and discussion

The annual maximum discharge days between 1970 and 2009 were classified based on the procedure above. Figure 3.2 shows the magnitude of the flood compared with the probability for each of the events, with the symbol indicating the flood type. Most of the flood events occurred

in the IHD (Snowmelt or Rain-Snow events), with only four flood events occurring outside this period. The largest two events, 30th May 2008 with a peak mean daily discharge of 17 m^3/s, and 11th June 1978 with 112 m^3/s, were classified Rain-Snow floods (Type 4), with the third highest, 111 m^3/s on 15^{3th} October 2000, a Short Rain flood (Type 2), followed by 100 m^3/s on 31st May 2001 classified as a Snowmelt flood (Type 5). The May 2008 event was 49 m^3/s greater than any other event between 1970 and 2009, and was the only flood during this period to cause significant damage (see Sec 3.2).

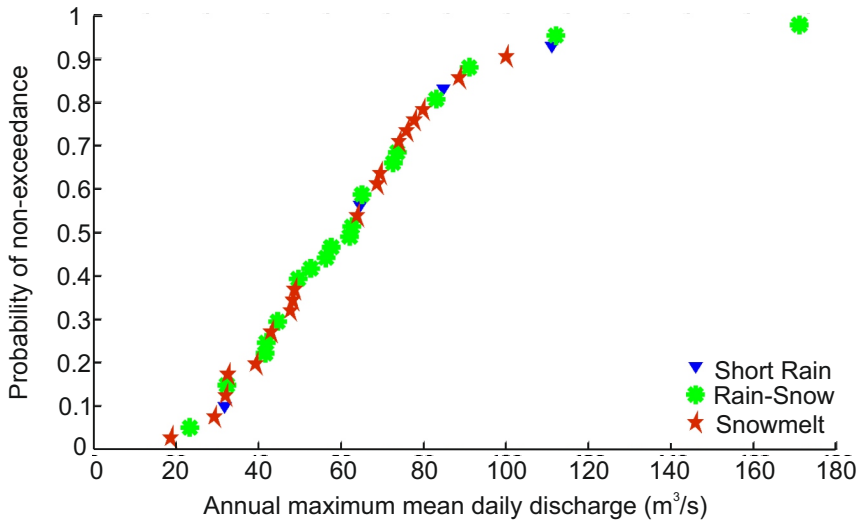

Figure 3.2 Annual maximum daily discharge for the Barcelonnette Basin 1970-2009, classified based on the flood types in Table3.1.

Once the flood events were classified into one of the five types, the temperature and precipitation parameters were calculated to compare with the expected meteorological conditions in Table 3.1. The temperature and precipitation for each of the observed flood types are summarised in Fig 3.3. Types 1 and 3 were not observed. For the three observed types of floods, Short Rain (Type 2) were significantly wetter and colder (excluding the daily temperature) than the other two flood types based on the two-sample Kolmogorov-Smirnov test. Snowmelt (Type 5) occurred under significantly drier daily and 5-day precipitation conditions, while Rain-Snow events (Type 4) were colder and drier than Type 2 events, and compared with Type 5, had significantly colder temperatures on the day of event and wetter daily and 5-day precipitation totals. Differences in the meteorological conditions between the flood types support the

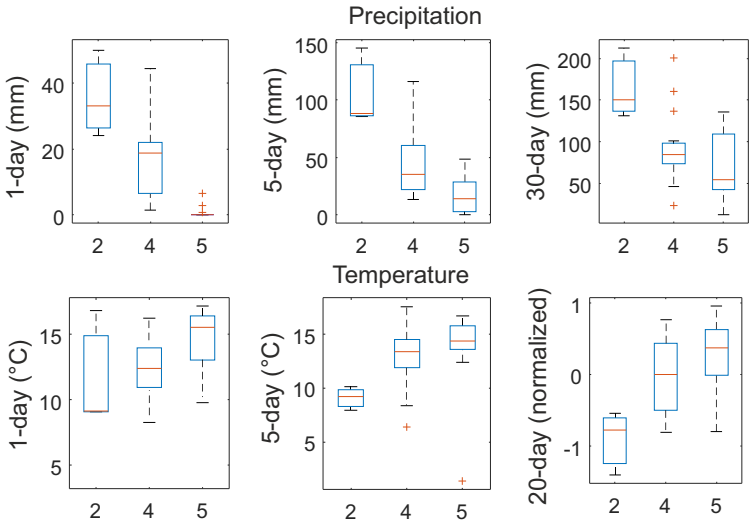

Figure 3.3 Box plot for each of the three observed flood types (Type 2, 4, and 5) for the daily, 5-day and 30-day precipitation amounts and mean daily, 5-day, and 20-day (normalized) temperature.

occurrence of more than one set of meteorological triggers for floods in the Barcelonnette Basin.

The Short Rain floods had the highest daily precipitation totals along with high antecedent precipitation, as would be expected from the precipitation response given in Table 3.1. However, as Short Rain floods were only observed four times, the observations in Fig 3.3 had a narrower range that then more frequently observed types. The precipitation on the day before Short Rain events was 24.2 mm or greater, with the 30 day antecedent precipitation total greater than 130 mm, unlike what would be expected in a flash type event. With regards to temperature, all four of the Short Rain events were on average colder than normal for the preceding 20 days. The average daily temperature was colder than the other observed flood types in the five days before the event, with similar temperatures on the day as Rain-Snow events.

For Snowmelt events, there was on average less precipitation than normal on the day before or the five days leading up to the event, as would be expected from the precipitation response in Table 3.1. However in 4 of the 18 events there was between 10 to 20 mm in the preceding 5 days, slightly higher than normal. The temperature during this period was normal (14°C) or above for these four events, indicating that the precipitation was likely rainfall, except in the case where the precipitation occurred during night (not assessed). These Type 5 flood events had the warmest average temperature for the 1, 5 and 20 day averages (Fig 3.3).

Only 3 of the 18 Type 5 events were not in line with the temperature and precipitation response in Table 3.1. These three events had colder than average 20-day temperatures (less than 0.10), which were also the three events with the greatest 30-day precipitation amounts. As the temperature was warmer in the five days preceding these three events (near or above normal), it is possible that with colder temperatures the precipitation increased the snowpack, allowing for more melting and increased discharge once the temperature warmed. Therefore the results were in line with the expected results in Table 3.1, except for the three events with colder than normal temperatures, possibly indicating a mix of Rain-Snow and Snowmelt.

Finally, most Rain-Snow events occurred under conditions expected in Table 3.1, although there were a wide range of conditions and some of the daily precipitation totals were smaller than expected. For Rain-Snow events, the precipitation recorded was half of what was observed preceding a Short Rain event for average daily and antecedent precipitation in Fig 3.3. While the upper range of the precipitation totals were similar, there was an event where only 3.1 mm was recorded the day before the event, and another event where 23.9 mm was recorded in the preceding 30 days, less than normal. This category displays a wide range of combinations of Rain-Snow events, where in some instances, the snowpack is smaller and therefore more precipitation is needed to increase the discharge to above normal levels. In other instances with a larger snowpack and more snowmelt, less rainfall and subsequent runoff are required. Overall the results for Rain-Snow were similar to what was expected in Table 3.1.

Changes to the flood type classification procedure may lead to differences in the distribution of identified flood types. By tightening the requirements of the IHD, a shorter IHD may have resulted in fewer Type 4 and 5 events. Furthermore, the distinction of near similar flood levels as less than $5m^3/s$ difference will have influenced the number of Type 2 vs Type 3 and Type 4 vs Type 5 events. More of the latter events would likely have been recorded if the allowed difference ($5m^3/s$) was increased. However, the procedure follows what would be expected from the discharge response in Table 3.1, with long rain and snowmelt floods observing more gradual increases in daily discharge than for Short Rain or Rain-Snow events.

The results here show that various flood types can be distinguished in the Barcelonnette Basin using discharge, precipitation, and temperature records. Short Rain events occurred under high precipitation and antecedent precipitation conditions, with temperature colder than normal for the time of year. Snowmelt events occurred after relatively little precipitation and warmer than average temperatures. Rain-Snow events occurred under a variety of precipitation and temperature conditions, indicating a possibly fuzzy boundary between the Types 4 and 5. This information is relevant for determining how floods and flood types may respond under future climate change.

3.4 Thresholds for debris flows and flash floods (flash events)

Unlike the flood events in Sec 3.3 where daily measurements of discharge were available, debris flow and flash flood events (flash events) are often treated as binary events. Hazard inventories provide information on the occurrence, with occasionally information about the size of the event (such as volume of debris or runout distance). Therefore, the common approach is to define thresholds, above which a flash event is more likely.

For debris flows and other types of landslides, rainfall thresholds are generally based on intensity, duration, or antecedent precipitation amounts (see list of precipitation parameters Table 3.2 and Guzzetti et al. (2008)). The parameters used depends on data availability and any information about possible triggering mechanism. In many instances, debris flows and flash floods are triggered by short intense rainfall with sub daily durations (e.g. Marchi et al., 2010; Brunetti et al., 2013). However, sub-daily rainfall records are often much shorter than daily records, making it difficult to acquire a threshold and determine its associated return period. Furthermore, the start and end of a rainfall event can be difficult to define, required for many of the parameters in Table 3.2 (Melillo et al., 2014).

Table 3.2 Precipitation parameters used in landslide thresholds.

Climate indices	Units	Reference
Rainfall duration	hr or days	Caine (1980)
Total rainfall during event	mm	Dhakal and Sidle (2004)
Daily (or multi-day) total rainfall	mm	Glade et al. (2000)
Average rainfall intensity	mm/hr	Caine (1980)
Peak rainfall intensity	mm/hr	Dhakal and Sidle (2004)
Antecedent rainfall	mm	Glade et al. (2000)

This section determines the applicability of using daily rain gauge measurements as proxy for flash events in the Barcelonnette Basin and the Fella River Basin, where a flash event is defined as a day with one or more flash floods or debris flows recorded. Precipitation is often used as a proxy for flash events, yet which records to use, and their correlation with flash events is not always clear. A particular focus is given to daily data, as sub-daily data is thought to be less reliable in climate models (Maraun et al., 2010), important when developing climate change-hazard studies.

First, the precipitation parameters are determined (Sec 3.4.1). These parameters are then used to calculate the frequency of the flash events based on the assumption that all precipitation events lead to flash events (simple approach, Sec 3.4.2). A probabilistic approach based on Berti et al. (2012) is then considered (Sec 3.4.3). The simple and probabilistic thresholds are calibrated using data between 1989 and 2003, with two validation periods, 1979-1988 and 2004-2010, extended to 2011 for

the Fella River Basin (due to data availability). Two validation periods are chosen, as non-climatic changes in the two study areas may have altered during the observational period, as well as changes in climate were observed in both study areas (see Chapter 2 for more information).

3.4.1 Determining precipitation parameters

There are a variety of precipitation parameters that can be used in precipitation thresholds using daily data (e.g. Table 3.2). Here, combinations of daily and antecedent precipitation were trialled to find the optimal precipitation parameters. The range of parameters included different weather stations and lengths of antecedent precipitation.

The accuracy of the thresholds was assessed using the confusion matrix with the four classifiers (Mason and Graham, 1999):

- True positives (TP): the number of correctly predicted events
- True negatives (TN): the number of correctly predicted number of non-events
- False positives (FP): the number of days where an event was predicted but did not occur
- False negative (FN): the number of events that were not predicted

The four classifiers were combined using the Matthew's correlation coefficient (MCC) to assess the quality of the thresholds (Powers, 2011):

$$MCC = \frac{TP \times TN - FP \times FN}{\sqrt{(TP + FP)(TP + FN)(TN + FP)(TN + FN)}} \tag{3.2}$$

The MCC is similar to the Pearson's product-moment correlation coefficient applied to contingency tables, and used when there is an unequal number of events to non-events (Powers, 2011). The MCC varies between -1 and 1, with a value of zero relating to a threshold that has no improvement over random selection, a value of 1 indicating perfect agreement, and -1 perfect disagreement.

For the threshold precipitation parameters, the MCC values for combinations of daily and antecedent precipitation in both study areas are in Fig 3.4. The records and precipitation combinations that had the highest MCC values are in yellow, with higher values for the Fella River Basin (0.50) compared with the Barcelonnette Basin (0.25). The dark blue colour indicates no correlation between the predictor and flash events.

The best predictor for the Barcelonnette Basin was the daily and 30-day antecedent precipitation for station B-1 with a MCC value of 0.17 (Fig 3.4). Stations B-3 and B-4 had the next best performance, with station B-2 having the lowest correlation between precipitation and flash events. An antecedent period of 25-35 days was associated with the highest MCC values for the stations, although in the case of B-1 and B-4, a 3-5 day antecedent period also had a weak positive correlation. The highest daily precipitation class (>25 mm) had a low MCC values for all stations due to none of the few events in this class being associated with a flash event in the calibration period.

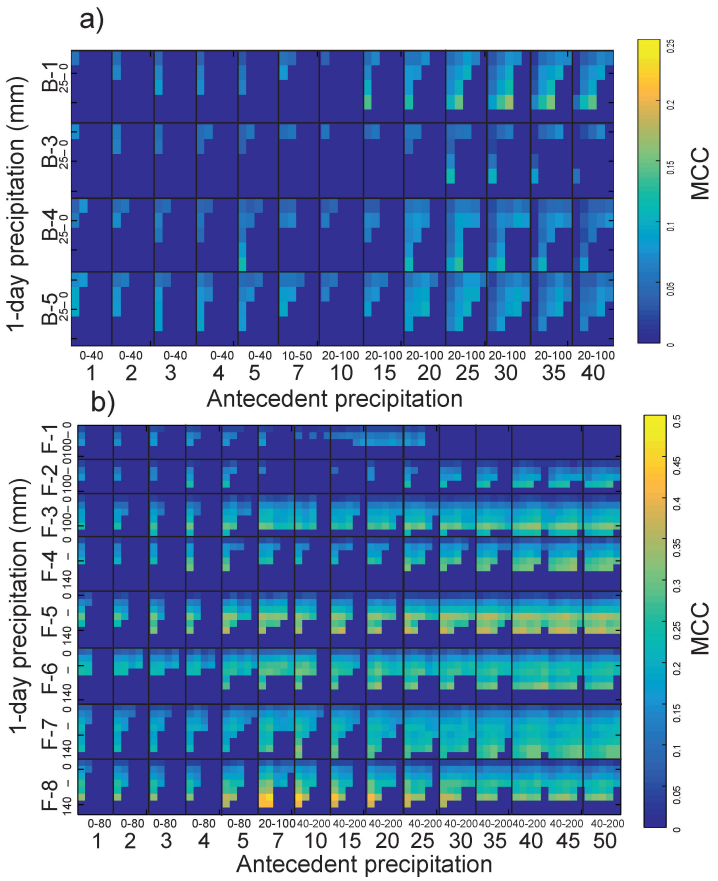

Figure 3.4 MCC value for combinations of daily and antecedent precipitation for the Barcelonnette Basin (a) and the Fella River Basin (b) with the threshold value for each of the stations in mm for the weather stations in Fig 2.1 for the period 1989-2003.

For the Fella River Basin, most stations saw an increase in the MCC value with increasing daily precipitation and longer antecedent periods (Fig 3.4). The station with the highest average MCC value was F-5 (0.20). Stations F-3, 4, and 8 had the next best average MCC value, with F-1 having the weakest correlation between precipitation and flash events. An antecedent period of 35-45 days had the best performance, except for F-8, where higher MCC values were obtained using 7-20 day totals. This weather station was furthest downstream site (Fig 2.1), and therefore may have only registered wide spread precipitation events.

Overall, the daily and antecedent precipitation were better proxies for debris flows and flash floods in the Fella River Basin than in the Barcelonnette Basin based on the MCC values. The best performing antecedent period for the areas differed, likely as result of its geometry

and size.

3.4.2 Simple approach for determining magnitude frequency relationships

After determining the optimal threshold parameters based on Eq 3.2, thresholds were developed based on return periods of precipitation based on the simple approach where all precipitation events above the threshold were considered to lead to one or more debris flows. For the more frequent events (return period $\leq$ 5 years), the empirical return period was calculated using equations 3.3 and 3.4:

$$R_{1d} = A + B \times R_{ant} \tag{3.3}$$

where R_{1d} and R_{ant} are the daily and antecedent precipitation respectively, and the return period (RP) was calculated using:

$$RP = \frac{n}{t_p} \tag{3.4}$$

where n is number of events above the threshold in Eq 3.3, and t_p is the time period over which the return period was calculated. Equations 3.3 and 3.4 were not used to calculate the return periods of greater than five years, as the return period become sensitive to the time period used for calibration.

In cases where the number of TPs is high while the number of FPs is low above the 5 year return period, Generalized Extreme Value distribution (GEV) was used. By fitting a distribution, it may give a more accurate estimate of the return periods of extreme events provided there is a good relationship between flash events and precipitation. The GEV was chosen as it has previous been used in other studies using the precipitation annual maxima (e.g. Buonomo et al., 2007; Min et al., 2011), as well as in Chapter 2. The GEV cumulative distribution function can be seen in Eq 2.1. To assess the uncertainty in the return periods, the maximum and minimum values based on the 90% confidence intervals were also calculated for particular quantiles (Geletu, 2007).

The magnitude of the flash events was also assessed. If precipitation was a good proxy for flash events, the magnitude of the flash events would increase with longer return periods. Therefore, a comparison of the magnitude of the flash events, approximated by the number of individual debris flows and flash floods per flash event, with the return periods was undertaken to further assess the applicability of using rain gauge records as a proxy for flash events.

For the Barcelonnette Basin, simple thresholds were obtained for return periods between 3 months to 5 years using the daily and 30-day antecedent precipitation at B-1. The number of flash and non-flash events above the thresholds can be seen in Fig 3.5a, where the thresholds were calculated based on Eq 3.4. While three flash events occurred above

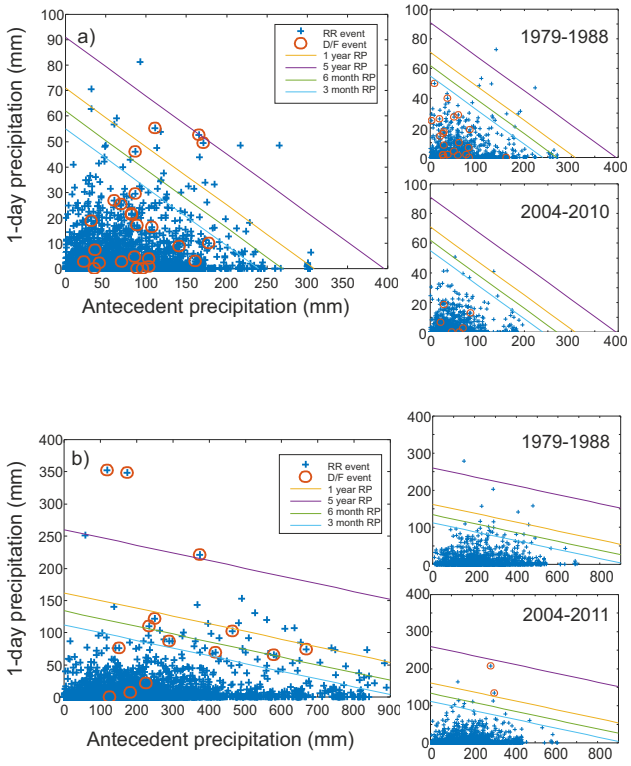

Figure 3.5 Empirical thresholds for the Barcelonnette Basin (a) and the Fella River Basin (b) based on daily precipitation (mm) and antecedent precipitation (30 days for Barcelonnette and 40 days for Fella River) (mm).

the 1-year return period threshold (yellow), the majority occurred with precipitation frequencies greater than every three months. For the two validation periods, 1979-1988 and 2004-2010, no debris flow events were observed to occur with extreme precipitation (return period greater than 3 months), although both these periods observed fewer days with extreme precipitation than in the calibration period. As no flash events were above the 5 year return period thresholds, precipitation could not be used as a proxy for flash events with higher return periods. Therefore GEV-based return periods were not developed.

It is possible that during the calibration period, more events occurred due to short duration rainfall in the Barcelonnette Basin, while in the validation periods there were other triggering factors, such as spring snow cover and snowmelt. Other possible triggering factors are supported by differences in the time of year in which the flash events occurred. In the calibration period, most events occurred between August and November; while in the second validation period (2004-2010), only one event occurred outside of June and July. For the first validation period

again more events occurred earlier in the year, with all events falling between May to September. As with the flood events in Sec 3.3, it is possible that there were various climate conditions that lead to flash events in the Barcelonnette Basin.

For the Barcelonnette Basin, the precipitation amount appeared to be a poor indicator for magnitude of the flash event. Most of the precipitation events only triggered one or two debris flows or flash floods (see Appendix B). However, for events where more than two were triggered, such as June 1992 and August 1988, the return period for the precipitation preceding these flash events was less than 3 months. Therefore, a magnitude-frequency relationship was not possible without either using other proxies or another measure for magnitude, such as volume or run-out distance. A full list of the flash events and associated return periods can be found in Appendix B.

For the Fella River Basin, daily and 40-day precipitation from F-5 was used along with Eq 3.4 to obtain thresholds for 3 months to 5 years, shown in Fig 3.5b. The three precipitation events above the 5 year return period threshold in calibration period were all associated with flash events. Of the 11 other flash events, 7 had return periods greater than 3 months, and 4 were even more frequent. In the validation period 2004-2011, two of the three most extreme precipitation events were associated with flash events. No flash events were recorded in the validation period 1979-1988, although it is possible in this period that a debris flow or flash flood occurred but was not recorded. Therefore, as with the Barcelonnette Basin, the validation periods perform poorer than the calibration period.

For the most extreme precipitation events in the Fella River Basin, further analysis was undertaken using the GEV distribution. The return period for each of the four flash events with the highest precipitation amounts are in Table 3.3 for F-4 and F-5. The second F-4 precipitation record was also used, as in the previous chapter, station F-5 had the most dissimilar GEV distribution, and may not be representative of the study area. Both stations show the event with the highest rainfall to have a return period of 110 years, with the confidence interval narrower for F-4 than for F-5. The second highest precipitation event for both stations was early June 1996, although the precipitation amount was much higher for station F-5 (349 mm) than for station F-4 (196 mm). The order of the third and fourth precipitation events changes between the stations, with F-4 having a longer return period for the 2011 event, while F-5 had a longer return period for the late 1996 event.

For the Fella River Basin, precipitation can be used to calculate magnitude-frequency relationships for flash events. The number of debris flows per flash event and the associated return period can be found in Appendix B. If the number of debris flows is taken as an indicator for the magnitude of the event, the less frequent precipitation events for the Fella River Basin have a higher magnitude (e.g. Chen et al., 2016). The largest event was in 2003; likely double the second largest event in early 1996. The 2011 event was a similar magnitude if not

Table 3.3 Return period in years for extreme events in the Fella River Basin based on Eq 3.3 (GEV estimate), and the upper and lower bounds of the 90% confidence interval and the empirical return period using 1952-2011 data.

		2003 event	1996 event (early)	2011 event	1996 event (late)
F-4	GEV estimate	110	23	13	2.4
	Lower	40	12	8	<2
	Higher	600	60	25	3
	Empirical	58	29	15	2.4
F-5	GEV estimate	110	105	9	34
	Lower	6	6	2	4
	Higher	>1000	>1000	11	250
	Empirical	52	26	4	13

greater than the late 1996 event: numerous debris flows were reported 2011 with only five in late 1996. This pattern more closely matches with that of the F-4 return periods. Therefore station F-4 appears to be a good proxy for the magnitude-frequency of debris flows for the Fella River Basin, as it both aligns better with debris flow magnitude (based on number of debris flows) as well as the GEV distribution had a better fit with the observed precipitation data.

Overall, the results show that rain gauge records are a better proxy for flash events in the Fella River Basin than for the Barcelonnette Basin. For the Fella River Basin, the three largest daily precipitation amounts were associated with multiple debris flows and flash floods. For the Barcelonnette Basin, no flash events occurred for the highest daily precipitation amounts. For both study areas however, precipitation is not a perfect predictor for flash events.

Furthermore, the return periods for precipitation and flash events varied based on the time period and method chosen. For both the Barcelonnette and Fella River basins, there were noticeable differences in the empirical frequencies of the precipitation events between the time periods in Fig 3.5. Even though the second validation period, 2004-2011, was shorter than the calibration period, it recorded significantly fewer extreme precipitation events. In the seven year period, only one event occurred above the 1-year return period for the Barcelonnette Basin and for the eight year period in the Fella River Basin, only three. Even though this may be from variations in the climate, it highlights difficulties in determining return periods for precipitation when records are not stationary.

3.4.3 Probabilistic approach

A probabilistic approach was also trialled, as precipitation is not a perfect predictor for flash events. A probabilistic approach assumes that there are other influencing factors besides the ones considered (in this case

precipitation), thereby assigning reliability into the threshold (Berti et al., 2012). It may account for precipitation parameters that are not included, such as differences in precipitation intensity at a finer resolution than recorded.

Bayes' theorem expresses the conditional probability of an event A, given a particular precipitation (or other) event B , $P(A|B)$ as:

$$P(A|B) = \frac{P(B|A)P(A)}{P(B)} \tag{3.5}$$

where $P(B|A)$ is the condition probability of B given A, and $P(A)$ and $P(B)$ are the unconditional probability of A and B respectively. Equation 3.5 can be reduced to (Berti et al., 2012):

$$P(A|B) \approx \frac{N_{(B|A)}}{N_A} \tag{3.6}$$

where $N_{(B|A)}$ is the number of precipitation events associated with landslides, and N_A is the total number of flash events. Equation 3.6 was calculated for 1989-2003, with 1979-1988 and 2004-2010 as the validation periods.

Using a probabilistic approach for the Barcelonnette Basin (1989-2003), the probability of a flash event increased as both the daily and antecedent precipitation increase. Figure 3.6 displays the probability of a flash event based on the daily and antecedent precipitation, where the highest probability of a flash event corresponds to moderately extreme daily and antecedent precipitation (50-60 mm for one day and 100-180 mm antecedent precipitation, occurring once in the calibration period). When only the daily or antecedent precipitation was high, the probability of a flash event was lower. However, when looking at the two validation periods (1979-1988 and 2004-2010) in Fig 3.6a, the daily and antecedent precipitation amounts were not observed in the second validation period and lower probabilities were observed in the first validation period. The period 1979-1988 had the highest probabilities for moderate daily precipitation amounts and low antecedent precipitation, although this may be realistic, it was contrary to what was found in the calibration period. Therefore, while the probabilistic approach appeared to provide good results in the calibration period, the results in the validation period lead to the conclusion that the probabilities threshold is highly dependent on the time period for the Barcelonnette Basin, and may not be reliable for extrapolation for the future.

Considering the probability of flash events for the Fella River Basin, Fig 3.6b shows the highest probability was associated with the highest daily precipitation amounts (1989-2003). All daily precipitation amounts greater than 150 mm were associated with flash events (Fig 3.6a, 1989-2003). Antecedent precipitation had little effect on the probability of flash events, as high daily and low antecedent precipitation still had 100% of precipitation events corresponding to flash events. Comparing the

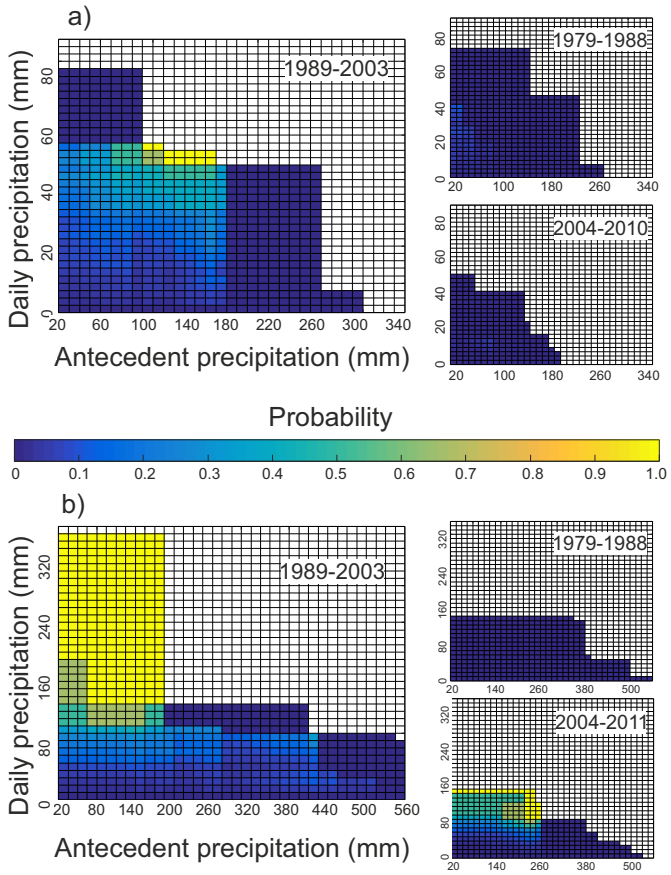

Figure 3.6 Probability of flash event for the Barcelonnette Basin using B-1 (a) and the Fella River Basin using F-4 (b) for the calibration (1989-2003) and validation periods (1979-1988, 2004-2010). Daily and antecedent precipitation conditions that were not observed are in white.

calibration period with second validation period, the period 2004-2011 had a similar pattern. While no flash events were observed in the first validation period, there were also no daily precipitation totals greater than 150 mm.

Overall, the probabilistic approach provided similar results to the simple thresholds, with the added ability to account for days above the threshold where no flash events were recorded. The Fella River Basin again had a stronger relationship between flash events and precipitation than the Barcelonnette Basin, with higher probability of occurrence. The results were dependent on the time period under which they were assessed, although the difference between calibration and validation periods was less for the Fella River Basin.

3.4.4 General discussion

Two approaches to linking precipitation with flash events were considered for the Barcelonnette and Fella River basins. The simple approach obtained a relationship between the magnitude and frequency of events for the Fella River Basin, although for the most frequent events (return periods less than 5 years), an empirical relationship based on flash events should be used due to non-flash events above the threshold. For the Barcelonnette Basin, while there was a positive correlation between flash events and precipitation, due to the high number of non-flash events above the thresholds, this method could not be used to determine the frequency of flash events based on precipitation.

As a comparison, the probabilistic approach accounted for precipitation not being a perfect predictor. Again precipitation was found to be a better predictor for flash events in the Fella River Basin than the Barcelonnette Basin. In the calibration period, antecedent precipitation appeared to be more important triggering factor for the Barcelonnette Basin than for the Fella River Basin. Figure 3.6 shows that the Fella River Basin recorded much higher daily precipitation amounts, all associated with flash events, and may be the reason why precipitation is a better predictor for this area than for the Barcelonnette Basin. However, the probabilistic threshold only considered the probability of a flash event above the threshold, not the probability of a missed event.

For both sections however, the difference between validation and calibration periods demonstrated that both the probability of extreme precipitation and flash events varies between time periods. For the probability of debris flows, some difference was due to the combination daily and antecedent precipitation not occurring, it is also possible that differences in study area, monitoring practice and other triggering or environmental factors influenced the occurrence of debris flows and flash floods. Lower recorded precipitation amounts in the Barcelonnette Basin may have made the probabilities fluctuate more due to these external factors.

The results highlighted challenges in determining the frequency of rare events. Long homogeneous records are needed for extreme values, although these can be difficult to obtain due to both non-climatic and climatic changes in the time series. For the stations F-4 and F-5, there were between 55-60 years of usable data where the time series was considered to be homogeneous and complete (see Chapter 2 for more information). Even so, the return periods of the most extreme events were highly uncertain, especially in the case of F-5, as has been found previously (e.g. Huard et al., 2010). The Fella River Basin stations had a significant increase in extreme precipitation between 1940 and 2011 (Chapter 2), leading to a possibly more frequent return period for the events in Table 3.3 if a shorter, more recent, time period was used. The return periods of the events therefore differ not only on the station used, but the time series to which the data was fitted, and meteorological parameters used.

3.5 Landslide thresholds for the Barcelonnette Basin

For soil slides, not only is precipitation a potential trigger (e.g. Segoni et al., 2014; Vennari et al., 2014), other factors such as temperature change (e.g. Chemenda et al., 2005), and snowmelt (e.g. Stoffel et al., 2014) are also important. It is possible that soil slides in the Barcelonnette Basin may occur under various conditions (similar to flood types in Sec 3.3), and therefore a single precipitation threshold may not be successful.

This section compares two approaches to establish a link between climate and soil slides using temperature and precipitation parameters. Thresholds are first developed based on discrete meteorological trigger types, such as rainfall, and snowmelt (Sec 3.5.1). A second method, anomaly detection, is trialled using a variety of temperature and precipitation parameters (Sec 3.5.2). As more soil slides were recorded in the Barcelonnette Basin than in the Fella River Basin, only the Barcelonnette dataset is used. The B-1 precipitation and temperature records were used.

3.5.1 Precipitation and temperature landslide thresholds

This section covers the performance of a simple threshold for soil slides based on only using precipitation compared to dividing soil slide events into three types: Rainfall (precipitation only, summer/autumn season), Rain-Snow (temperature and precipitation), and Snowmelt (no precipitation on the day of event or day before the event). As there may be multiple triggers, by splitting the inventory into groups, the aim is to improve the thresholds skill, as opposed to using only one threshold.

The method for the precipitation landslide threshold was similar to the selection of precipitation parameters in Sec 3.4.1. Various combinations of daily and antecedent precipitation were trialled, with the threshold with the maximum MCC value (Eq 3.2) chosen as the final threshold.

For the three thresholds, the hazard inventory was first split into soil slides that were likely influenced by snowmelt and those where snowmelt was unlikely to play a role. The division was based on the discharge records in Sec 3.3, using increased discharge during spring (IHD) as a proxy for the time of the year when snowmelt may trigger (partly) soil slides. Any soil slides with a daily precipitation amount greater than 5 mm were assumed to be Rain-Snow, with any soil slides below the 5 mm daily threshold assumed to be Snowmelt. It was assumed there was only one rainfall threshold. For each of the three types, the threshold values and antecedent periods are varied to maximise the MCC (Eq 3.2).

Using the criteria above, there were 13 Rainfall landslides, 5 Rain-Snow landslides and 12 Snowmelt landslides in the period 1989-2003. Compared with flood events in Sec 3.3, there were a higher proportion of Rainfall landslides compared with Rain-Snow and Snowmelt ones, highlighting differences in the triggering conditions between floods and landslides.

Based on the maximum MCC for the period 1989-2003, varying the antecedent period from 5-180 days and varying the threshold, the best performing meteorological type thresholds in the calibration period were: Rainfall threshold:

$$R_{1d} \geq 16mm, R_{55d} \geq 140mm \tag{3.7}$$

Rain-Snow threshold:

$$R_{1d} \geq 12mm, R_{10d} \geq 25mm, Tmax_{1d} \geq 6^{\circ}C \tag{3.8}$$

Snowmelt threshold:

$$Tmax_{2d} \geq 13^{\circ}C, Tmax_{10d} \geq 5^{\circ}C \tag{3.9}$$

where R_{1d} is the daily precipitation total on the day of the event, R_{xd} is the total antecedent precipitation over x days, $Tmax_xd$ is the maximum daily temperature on the x days up to and including the day of the event. The precipitation only threshold (all soil slide events during 1989-2003 are grouped together) was:

$$R_{1d} \geq 12mm, R_{50d} \geq 110mm \tag{3.10}$$

The number of soil slides above each of the thresholds (TP) can be seen in Table 3.4, as well as days above the threshold with no soil slides recorded (FP). The best performing threshold in the calibration period was the Rain-snow threshold with a MCC score of 0.280. However, during the two validation periods, none of the five soil slides events were above the threshold (FN, Table 3.4). The Rainfall threshold again had a positive correlation with soil slides. As with the Rain-snow threshold, none of the soil slides were above the threshold in the validation periods. The Snowmelt threshold had the lowest MCC value of 0.063, due to the high number of false positives. However, of the three types of threshold, the snowmelt threshold was the only one with soil slide events above the threshold in the validation period (three of the seven).

When comparing the results from the three meteorological type thresholds with the precipitation only threshold in the calibration period, division of the soil slides increased the MCC value. This supports the hypothesis that temperature records are important when considering meteorological triggers for landslides. The better MCC value may also be due to variations in meteorological triggering conditions for landslides between seasons, with lower daily rainfall amounts required due to previous snow cover and melt.

While there was varying success in the calibration period for the landslide thresholds, all landslide thresholds performed poorly in the validation periods (Table 3.4). It is possible that the triggers for soil slides differed between the validation and calibration periods, undermining the simple threshold approach as applied here. A long time series with a wide variety of climate conditions as well as an extensive inventory would be required, which is difficult to obtain. Another possible explanation is

Table 3.4 Confusion matrix results for the landslide thresholds, for the calibration period (1989-2004), and the validation periods (1979-1988 and 2004-2010).

Type	Period	TP	FP	FN	TN	MCC
Rainfall	1989-03	7	42	6	2240	0.270
	1979-88	0	10	3	1517	-0.004
	2004-10	0	5	1	1065	-0.002
Rain-snow	1989-03	4	25	1	3142	0.280
	1979-88	0	23	4	1053	-0.006
	2004-10	0	16	1	1054	-0.004
Snowmelt	1989-03	12	1554	0	1617	0.063
	1979-88	2	685	4	564	-0.030
	2004-10	1	614	0	456	0.026
Precipitation only	1989-03	10	1404	20	5328	0.151
	1979-88	1	44	12	3594	0.0035
	2004-10	0	38	3	2516	-0.004

that more complex mechanisms are governing the landslide movement, which are not captured using a simple approach (Martelloni et al., 2011). Therefore, while the simple threshold approach applied may have some benefit for determining meteorological triggers for landslides, the performance in the validation periods makes the simple threshold a poor proxy for future landslides.

3.5.2 Anomaly detection

A second technique based on the anomaly detection was undertaken to account for a range of cold, wet, dry, and warm conditions triggering soil slides, rather than distinct thresholds as in Sec 3.5.1. Anomaly detection (AD) is a technique to identify observations or events that do not conform to the rest of the dataset, and are therefore anomalous. Previously anomaly detection has been used for detecting landslides from satellite data (e.g. Lu et al., 2011; Dabbiru et al., 2015), although little work has focused on landslide triggers. Here, a simple semi-supervised anomaly detection technique based on a probability distribution model is applied as an initial assessment of the applicability of anomaly detection to determine landslide thresholds.

The steps were as follows:

1. The data was split in to three groups: calibration (2/3 of the dataset), validation (1/6), and cross validation (1/6). Any soil slides in the calibration period and the 20 days preceding were split between the validation and cross validation period.
2. For the calibration period, four precipitation parameters and one temperature parameter were fitted to Gamma, Weibull, Gaussian, GEV, Exponential and Generalised Pareto distributions, with the distribution with the best fit selected as the distribution for the parameter.

3. The multivariate probability density function was calculated for the calibration and validation dataset
4. For the validation dataset, the threshold value was found that gave the highest MCC value (high threshold). A second threshold was found that gave the highest MCC value with the added condition that at least 50% of the soil slides are more anomalous than the threshold value (low threshold).
5. Based on the threshold value from Step 4, the MCC values were calculated for the cross-validation dataset.

For this work, five parameters were chosen for the time period 1980-2009: daily precipitation, precipitation the preceding day, precipitation total 2-3 days before, the antecedent precipitation 4 to 24 days before the event, and the average temperature over the preceding 20 days, normalized based on day of year. Any days where the daily precipitation was less than 0.2mm were removed. The parameters are listed in Table 3.5, along with the best fit distribution type (Distribution) and associated probability density function.

Table 3.5 The distribution type and parameters for each of the five variables used in the anomaly detection with the associated probability density function. Days gives the day(s) for which the parameter was summed (precipitation) or averaged (temperature), counting backwards from the day of the event/non-event.

Indices	Day(s)	Distribution	Probability density function
Precipitation	0	Generalised Pareto	$\frac{1}{5.6}\left(1+0.43\frac{(x-0.1)}{5.6}\right)^{-1-1/0.43}$
Precipitation	1	Gamma	$\frac{1}{23.1^{1.11}G(1.11)}x^{0.11}e^{-x/23.1}$
Precipitation	2-3	Exponential	$\frac{1}{22.6}e^{-x/22.6}$
Precipitation	4-24	Generalised Pareto	$\frac{1}{70.2}\left(1+0.17\frac{x}{70.2}\right)^{-1-1/0.17}$
Mean normalized temperature	0-20	Generalised Extreme Value	$\frac{1}{0.94}\left(1+0.27\frac{(x-0.36)}{0.94}\right)^{-1/0.27-1}$ $exp\left(-1-0.27\frac{(x-0.36)}{0.94}\right)^{-1/0.27-1}$

The MCC values for the high and low thresholds using AD can be found in Table 3.6, along with the number of correctly precipitation landslides (TP) and missed events (FN). The high threshold had the highest MCC score, as well as a high probability of landslide (33%). However, the high threshold had no skill in the cross-validation dataset (MCC Tables 3.6), indicating over-fitting of the validation dataset. The low threshold represented the threshold with highest MCC value and the added condition that at least 50% of the landslide events were more anomalous than the threshold. The addition of at least 50% landslide events above the threshold lowered the MCC value considerably in the validation dataset.

For the low threshold however, while there was only a weak positive correlation (0.086), it performed equally during the cross-validation phase.

Table 3.6 MCC for best performing high and low thresholds using AD for the validation dataset (top) and cross-validation dataset (bottom).

	MCC	TP	FP	FN	TN
Threshold	Validation				
High: 0.0066	0.232	3	6	12	310
Low: 4.26e-4	0.086	11	167	4	149
	Cross-validation				
High: 0.0066	-0.045	0	12	19	320
Low: 4.26e-4	0.086	12	146	7	186

It is possible that the results in Table 3.6 could be improved by using other meteorological variables or parameters for AD. Only minimal analysis of combinations of daily and antecedent precipitation were trialled (up to 60 days), and variables such as wind direction were not included. Furthermore, while it was not undertaken during the initial assessment phase, principle component analysis could be undertaken before steps 1 -7 were performed to reduce any correlation between the variables. With further analysis, the higher MCC values may be obtained for new thresholds.

Overall there is potential that the results can be improved, even though the two thresholds performed poorly in the cross-validation dataset. The high threshold was unable to determine any of the 19 landslide events in the cross-validation period, which may be improved with the application of other meteorological proxies. The low threshold performed equally well in the validation and calibration periods, although had a low MCC value due to a high number of false positives. This lower threshold could therefore be used as a first indicator of potential soil slides, with further investigation required to separate landslide events from non-landslide events.

3.5.3 General discussion

Two approaches for developing meteorological thresholds or proxies for soil slides were developed, a simple threshold and threshold using anomaly detection. For both approaches, temperature was included as part of the proxy, indicating that landslides in the Barcelonnette Basin were triggered not just by rainfall, but also changes in temperature through snow and snowmelt. Correlations were found between the meteorological parameters and soil slides, although the correlations were weak and had little skill in the validation or cross-validation datasets.

For the simple approach, the results indicate different meteorological triggers for soil slides than flash events or floods. Besides the inclusion of temperature, both the precipitation only and rainfall thresholds used longer antecedent periods (50 and 55 days respectively) than what was found for flash events in Sec 3.4. The division of types for the soil slide

events indicated a higher percentage of rainfall-landslide events (37%) than rainfall flood events (10%). Therefore, even though the threshold should not be used as a proxy for future landslide hazards, the results provide some information on the meteorological triggering conditions.

By using the AD method, no prior division into various meteorological triggering conditions was required. The low threshold was also the only threshold in Secs 3.4 and 3.5 that had the same skill in the calibration/validation phase as the validation/cross-validation phase. However, as with the simple approach, the overall skill of the AD method was low (MCC less than 0.10 in both cross-validation datasets).

Challenges in linking landslides with the climate come from a variety of potential triggering mechanisms, such as localised convective storms, longer periods of rainfall, snowmelt, changes in temperature, as well as landslides are influence by other environmental and non-environmental factors. While the simple threshold and anomaly technique both performed reasonably in the calibration period, except for the precipitation only, rain-snow threshold, and the low AD threshold, the other thresholds failed to capture soil slides in the validation period. It is possible that triggering conditions in the Barcelonnette Basin were significantly different in the validation periods, and therefore require another set of meteorological triggering conditions or proxies.

3.6 Hydro-meteorological hazards and atmospheric classification schemes

Beyond investigating local precipitation and temperature records, there may be favourable atmospheric circulation patterns for hydro-meteorological events. Atmospheric classification schemes can be used to analyse such relationships (Schiemann and Frei, 2010; Dayan et al., 2012). Atmospheric classification schemes, or the individual weather types of which they are comprised, capture multiple atmospheric variables in 2D or 3D. The weather types can be classified using a manual approach, or through an objective automated approach (Huth et al., 2008). The benefits of using weather types include that precipitation does is not explicitly have to be used (e.g. Nuissier et al., 2011; Hoy et al., 2014) and that they can provide information about the mechanisms behind the hydro-meteorological triggers.

Examples of the use of atmospheric classification schemes include Northern Italy, where it was found that the weather types that generally cause floods in the area came from southerly winds bringing warm, moist air from over the Mediterranean (Parajka et al., 2010). In a UK study, more than 80% of recorded flood events were associated with 5 weather types from a total of 27 (Pattison and Lane, 2012). Wood et al. (2016) assessed weather types and landslides for the European Alps, and found that weather types that were associated with higher amounts of precipitation were also associated with a higher probability of landslides.

This work presents a first attempt of linking hydro-meteorological events with a smaller area, the Barcelonnette Basin, which was then expanded on by Wood et al. (2016).

This section investigates the applicability of atmospheric classification schemes for flood and landslide events in the Barcelonnette Basin. Unlike the previous sections where thresholds were developed, this section determines the probability of a hydro-meteorological event over a discrete number of weather types. Furthermore, Secs 3.3-3.5 used local weather station data, while this section considers coarse scale atmospheric variables.

3.6.1 Method

This section compares the Barcelonnette hazard inventory with atmospheric classification schemes from the COST733 project (http://cost733.met.no/). Each of the 34 core schemes were applied over three domains that included the Barcelonnette Basin: Europe (EU), Central Europe (CE), and the western Mediterranean (WM) (Fig 3.7). The number of individual weather types in each classification scheme varied from 4 to 40 individual weather types, and were calculated on a daily basis. There were five main techniques used for the schemes (Philipp et al., 2010):

- Subjective, where the classification depended on the decisions of an expert
- Threshold, where the weather types are separated by thresholds or borderlines
- Principle Component Analysis (PCA), as a preprocessing tool or as a classification tool (T-mode)
- Leader algorithms, uses key patterns at the centre of high density points or days
- Optimization, where weather types are based on clusters that are optimized based on a particular function

A full list of the 34 core classification schemes used can be found in Table 3.7 along with the number of weather types, variables used, and type of classification scheme. The ERA40 reanalysis dataset was used as input for the automated classification schemes at the 1°x1° resolution (Philipp et al., 2010). The automated classification techniques marked with a star in Table 3.7 had multiple versions available. Further information on the individual weather types and their development can be found in Philipp et al. (2010).

The Brier skill score (BSS) was used to assess the skill of the classification scheme regards to hydro-meteorological events. From Schiemann and Frei (2010), the BSS is:

$$BSS = \frac{\frac{1}{N}\sum_{i=0}^{I} N_i(y_i - \bar{y})^2}{\bar{y}(1-\bar{y})} \tag{3.11}$$

Table 3.7 Classification schemes from COST733, with short and long name and number of weather types (WT). Those marked with an asterisk had multiple versions of each classification & number of weather types (WT). MSLP = mean sea level pressure, Z= geopotential height, SFC = surface, W = u and v wind

		Short	WT	Variable	Long Name
Subjective	1	GWLo	11, 30	n.s.	Hess and Brezowsky WetterLagen
	2	OGWo	29	MSLP, Z500	Objective Hess and Brezowsky
	3	PECo	13	n.s.	PECzely
	4	PERo	31	n.s.	PERret
	5	SUEo	40	MSP, Z500, WSFC/500	SchUEepp
	6	ZMGo	43	n.s.	ZAMG
Threshold	7	GWT	8, 18, 27	MSLP	GrossWetterTypes
	8	JCT	9, 18, 27	MSL	Jenkinson-Collinson-Types
	9	LWTo	10, 18, 26	MSLP	Jenkinson-Collinson "Lamb Weather Types 2"
	10	LIT	9, 18, 27	MSLP	Litynski(LITADVE/LITTC)
	11	LITo	9, 18, 27	MSLP	Litynski (LITADVE/LITTC)
	12	WLK	9, 18, 28	W700, Z955/500, PW	WetterLagenKlassifikation
	13	WLKo	9, 18, 28, 40	W700, Z955/500	WetterLagenKlassifikation
PCA	14	KRZ	9, 18, 27*	Z500	Kruizinga (P27)
	15	KRZo	8, 18, 27	z500	Kruizinga (P27)
	16	PXE	variable	MSLP	PCA-extreme scores, Euclidean distance
	17	PXEo	variable	MSLP	PCA- extreme scores, Euclidean distance
	18	PCT	9, 18, 27*	MSLP	Obliquely rotated PCA, T-mode
	19	PCTo	variable	MSLP	Obliquely rotated PCA, T-mode
	20	PTT	9, 18, variable	MSLP	Orthogonally rotated PCA, T-mode
Leader	21	LND	9, 18, 27*	MSLP	Lund
	22	KIR	9, 18, 27	MSLP	Kirchhofer
	23	ERP	9, 18, 27*	MSLP	ERPicum
	24	ERPo	9, 10, 18, 27, 30*	MSLP	ERPicum
	25	PTSo	9, 18, 27, variable	MSLP, Z500	Petisco
Optimization	26	CKM	9, 18, 27*	MSLP	CKMeans
	27	NNWo	9, 18, 27, variable	MSLP, Z500	Neural Network 2d-topology
	28	SOM	9, 18, 27	MSLP	Self-Organizing Maps 1d-topology
	29	CAP	9, 18, 27*	MSLP	Cluster Analysis of Principal components
	30	CAPo	4, 9, 18, 27	MSLP	Cluster Analysis of Principal components
	31	PXK	variable	MSLP	PCA- eXtreme scores, K-means
	32	PXKo	9-10	MSLP	PCA-eXtreme scores, K-means
	33	SAN	9, 18, 27*	MSLP, Z952/500	Simulated ANnealing clustering
	34	RAC	9, 18, 27*	MSLP	RAndom Centroid classification

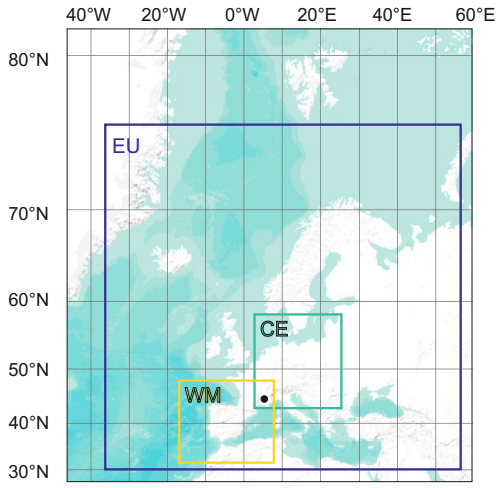

Figure 3.7 Outline of the three COST733 domains used in this work (EU, CE, and WM), with the location of the Barcelonnette Basin (black dot).

where y_i is the empirical frequency of hydro-meteorological events for weather type i, $\bar{y}$ is the frequency of hydro-meteorological events regardless of weather type, and N is the number of days. The BSS varies between 0 and 1, with 1 indicating that the classification perfectly splits event days from non-event days, and 0 indicating no skill.

The BSS was calculated over the period 1970 to 2002, as landslide databases have been found to be more reliable post 1970 (Wood et al., 2015). For each classification, the BSS was calculated annually and seasonally.

To determine if the BSS was significant, BSSs were calculated for the top three performing classifications using 1000 dummy inventories. The dummy inventories consisted of the same number of events in each month as in the Barcelonnette inventory on randomly generated days. Any BSS using the Barcelonnette inventory greater than 95% of BSS from the dummy datasets were assumed to be significant.

3.6.2 Results and discussion

From the COST733 dataset, the three atmospheric classifications with the highest average BSS were ERP (0.026), KRZo (0.021), and SUEo (0.021). The three best performing classifications were based on three techniques: subjective, leader, and PCA, respectively. The seasonal BSS and probability of hydro-meteorological event for each weather type in the classifications are given in Table 3.8. Mean sea level pressure charts are

Table 3.8 Percentage of days with one or more hydro-meteorological events for each weather type and BSS for three classifications, split into season (DJF = winter, MAM = spring, JJA = summer, and SON = autumn). For comparison, a hydro-meteorological event occurs in the Barcelonnette Basin on 0.27% of winter days, 1.58% of spring days, 2.27% of summer days and 1.03% of autumn days.

	ERP: WM				KRZo: CE				SUEo			
	DJF	MAM	JJA	SON	DJF	MAM	JJA	SON	DJF	MAM	JJA	SON
BSS	0.003	0.010	0.004	0.088	0.007	0.005	0.014	0.059	0.010	0.023	0.013	0.038
Percentage of days with a hydro-meteorological event for each weather type (%)	4.3	2.5	3.2	0.7	4.3	0.8	1.8	0.0	4.3	2.0	2.6	0.0
	0.6	1.3	2.2	1.0	0.6	0.7	0.8	0.0	0.6	3.1	3.5	1.8
	1.6	2.7	1.5	1.1	1.6	1.2	3.5	0.0	1.6	1.5	2.1	0.0
	0.0	2.4	5.3	0.4	0.0	2.7	8.0	0.0	0.0	2.0	4.9	0.0
	2.7	0.0	1.8	0.8	2.7	0.0	0.0	0.0	2.7	0.0	3.6	1.2
	0.6	0.0	2.2	1.8	0.6	2.0	2.0	0.9	0.6	0.0	1.6	0.6
	2.1	4.4	4.3	1.9	2.1	2.2	2.9	0.4	2.1	2.4	1.5	0.5
	0.0	2.5	1.4	0.6	0.0	0.9	0.7	0.0	0.0	0.6	1.8	0.0
	0.0	0.4	1.6	0.0	0.0	0.0	0.0	0.0	0.0	2.4	7.8	0.0
	0.6	0.0	1.8	0.7	0.6	1.6	2.2	0.0	0.6	1.3	1.6	2.7
	0.0	1.1	4.0	0.0	0.0	0.0	0.0	0.0	0.0	0.0	0.0	0.0
	0.0	1.3	0.0	1.6	0.0	0.0	0.0	0.0	0.0	0.0	1.4	1.6
	1.0	0.0	0.0	0.0	1.0	0.6	1.7	2.2	1.0	0.0	0.0	0.0
	0.0	2.0	9.1	2.8	0.0	1.4	1.8	0.0	0.0	0.0	0.0	0.0
	1.6	5.0	0.0	5.0	1.6	1.6	2.1	2.3	1.6	1.0	2.4	0.0
	1.4	0.0	0.0	0.0	1.4	0.0	20.0	100.0	1.4	7.7	5.6	1.5
	0.0	0.0	0.0	0.0	0.0	0.0	0.0	0.0	0.0	1.6	0.0	1.5
	0.0	0.0	-	0.0	0.0	1.7	11.5	0.0	0.0	0.0	2.2	0.0
	0.0	0.0	-	66.7	0.0	2.9	4.8	7.3	0.0	9.4	0.0	0.0
	0.0	0.0	-	0.0	0.0	3.2	5.3	2.3	0.0	0.0	2.9	0.0
	0.0	0.0	-	0.0	0.0	0.0	0.0	0.0	0.0	2.4	0.0	0.0
	0.0	0.0	-	0.0	0.0	1.7	1.3	0.9	0.0	0.0	0.0	4.0
	1.7	0.0	-	-	1.7	0.0	0.0	0.0	1.7	0.0	0.0	1.4
	0.0	-	-	-	0.0	0.0	4.3	0.0	0.0	0.0	1.3	0.0
	0.0	-	-	-	0.0	1.1	4.0	2.9	0.0	0.5	1.9	0.0
	0.0	-	-	-	0.0	1.1	2.4	0.0	0.0	0.0	0.0	20.0
	-	-	-	-	-	2.5	1.1	0.0	-	6.4	5.3	0.0
	-	-	-	-	-	2.1	0.0	4.4	-	1.4	0.0	2.6
	-	-	-	-	-	-	-	-	-	6.3	0.0	0.0
	-	-	-	-	-	-	-	-	-	0.0	0.0	0.0
	-	-	-	-	-	-	-	-	-	7.9	0.0	4.9
	-	-	-	-	-	-	-	-	-	2.0	5.9	6.0
	-	-	-	-	-	-	-	-	-	3.7	3.1	2.4
	-	-	-	-	-	-	-	-	-	5.4	6.3	0.0
	-	-	-	-	-	-	-	-	-	1.7	9.5	0.0
	-	-	-	-	-	-	-	-	-	0.0	0.0	33.3
	-	-	-	-	-	-	-	-	-	4.2	0.0	0.0
	-	-	-	-	-	-	-	-	-	1.6	1.8	3.0
	-	-	-	-	-	-	-	-	-	0.0	0.0	0.0
	-	-	-	-	-	-	-	-	-	0.0	0.0	0.0

shown in Fig 3.8 for selected weather types in Table 3.8.

The best performing atmospheric classification scheme, the ERP leader classification, was based on mean sea level pressure. This classification performed best in autumn, with a highest BSS of 0.088, followed by spring, with similar BSS values for summer and winter (Table 3.8). However, only the autumn BSS was significant. The highest probability for a hydro-meteorological event was for weather type 19 during autumn where four of the six occurrences of this type were associated with a hydro-meteorological event. Weather type 19 was associated with a low pressure system over southern England, resulting in a north-westerly flow over the Barcelonnette Basin and higher precipitation in France and the Alps (Fig 3.8a,b). These results are in line with what would be expected, as higher precipitation generally leads to higher probability of landslides and floods.

The KRZo threshold classification was based on the 500 hPa geo-

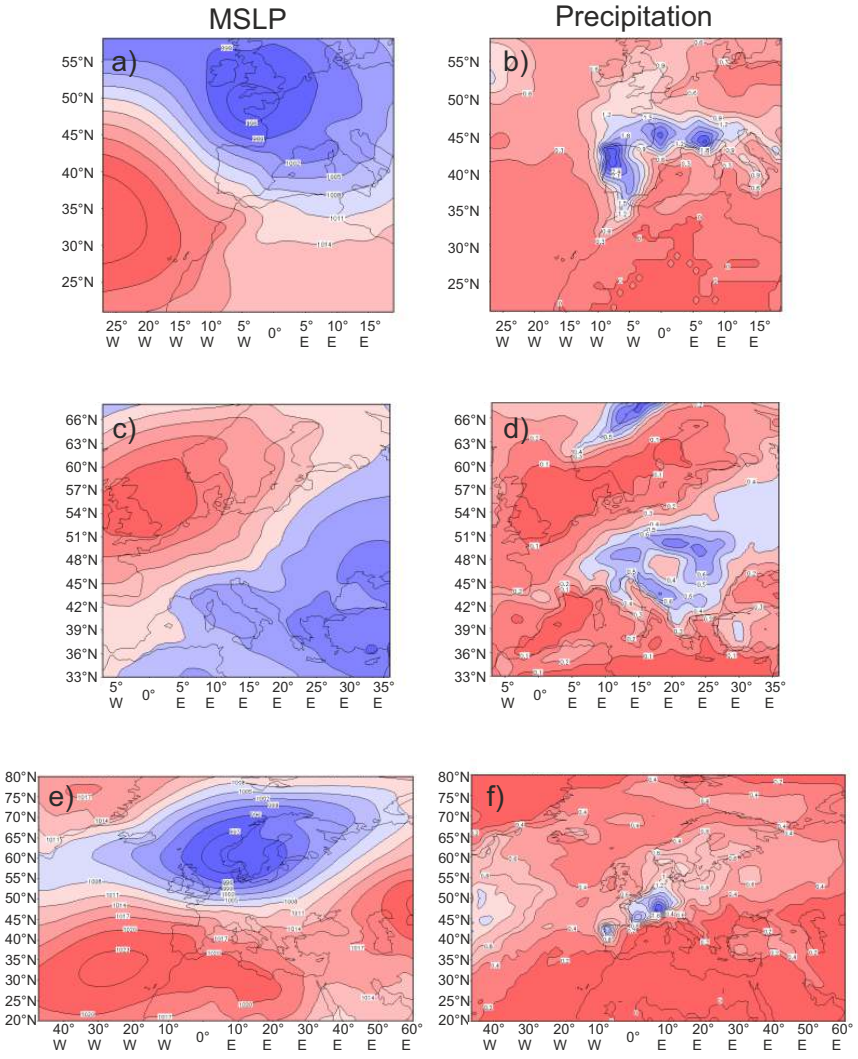

Figure 3.8 Mean sea level pressure charts (hPa) and precipitation (M) for classification ERP weather type 19 (a) and (b), classification KRZo weather type 16 (c) and (d), and classification SUEo weather type 16 (e) and (f), all for autumn. All weather types are associated with hydro-meteorological events.

potential height, and performed best in autumn with highest seasonal BSS of 0.059. The classification in summer had the second highest BSS value, followed by spring and winter (Table 3.8). However, as with ERP, only the autumn BSS was significant. The results for weather type 16 may have contributed to the high autumn BSS value. Weather type 16 occurred once in autumn, on a day with a hydro-meteorological event. In summer, this same weather type occurred five times, only one of which corresponded to a hydro-meteorological event. The mean sea level pressure for weather type 16 in autumn had an anticyclone between the United Kingdom and Scandinavia, with a trough just to the south of the Barcelonnette Basin, possibly increasing precipitation in the study area (Fig 3.8c,d).

The subjective SUEo classification used a threshold approach based on MSLP, 500 hPa geopotential height and u and v winds at the surface and 500 hPa (Table 3.7). The seasonal BSS values for SUEo were similar, with values ranging between 0.010 and 0.038, with the highest value again in autumn (Table 3.8). For this classification, the BSS for both spring and autumn were significant. Weather type 16 was associated with 11 hydro-meteorological events and a higher probability than normal for hydro-meteorological events across the seasons. Under weather type 16, high pressure to the SW of the Barcelonnette Basin and low pressure over Scandinavia results in a strong pressure gradient between these two features (Fig 3.8e,f). This would have led to a northerly flow over the area, and precipitation concentrated around the French Alps.

The BSS values were highest in autumn and lowest in winter for all of the three best performing atmospheric classifications. The low values in winter may have been due to the relatively low number of hydro-meteorological events reported during this season (8, or 0.26% of days). The classifications may have also been lower in winter, and other seasons, due to the variables used for the atmospheric circulations. For example, moisture fields were not included in the three best performing classifications, even though in summer, moisture fields are critical atmospheric field separating convective from non-convective days (Riemann-Campe et al., 2009). It is also possible that in spring, snow melt from warm temperatures was a critical field along with the dependence on antecedent conditions (see thresholds in Secs 3.4 and 3.5), although temperature would have been included indirectly through wind direction. Future work could extend the atmospheric circulations to include other atmospheric fields.

Overall, there was no clear best performing atmospheric classification for hydro-meteorological events in the Barcelonnette Basin, although a few favourable autumn weather types were determined. Most of these favourable weather types were associated with north-westerlies and higher precipitation for the study area. All three best performing weather types had these conditions in common, information that could form the basis of a proxy for hydro-meteorological hazards.

There are a number of avenues for future improvements. In this section, only day of occurrence is assessed, where antecedent conditions

may provide more information or have a better fit. Furthermore, by combining the weather types with more local conditions, such as atmospheric instability, the results may improve. It may also be beneficial to separate the classification based on hydro-meteorological hazards types (analogous to Secs 3.3-3.5). Separating the hazardous events would reduce the number of events in each category however, and may make it difficult to achieve significant results. Future work using inventories over larger areas for individual hydro-meteorological hazards may be more promising, such as in Wood et al. (2016).

3.7 Conclusion

There are a variety of approaches to identifying meteorological proxies for hydro-meteorological hazards. Here, various methods were explored for the different hazard types: floods (Sec 3.3), debris flows and flash floods (Sec 3.4), and soil slides (Sec 3.5). In Sec 3.6, weather types associated with higher probability of hydro-meteorological events (floods and landslides) were identified. For all sections the Barcelonnette Basin used as the study area, with the Fella River Basin also considered in Sec 3.4.

When considering flood events in the Barcelonnette Basin, Sec 3.3 showed that three flood types were associated with different precipitation and temperature conditions based on discharge records. Three types of high discharge days or floods were found: Snowmelt floods associated with warmer and drier antecedent conditions, Rain-Snow floods with a range of temperature and precipitation conditions, although generally wetter and not as warm as Snowmelt floods, and four Short rain floods associated with colder, wetter antecedent conditions. As distinct meteorological flood types were identified, Chapter 6 examines this subject in more detail, in particular how the flood types may alter as a result of climate change.

The Fella River Basin had the clearest link between daily precipitation and flash events (flash floods and debris flows) as seen in Sec 3.4. The three most extreme daily precipitation amounts were all associated with multiple flash events allowing the return periods associated with the precipitation to be used as a proxy for the flash event frequency. All daily precipitation totals above 150 mm and antecedent rainfall greater than 100 mm were associated with debris flows in both the calibration (1989-2003) and validation (2004-2011) periods. An increase number of debris flow followed the increase in extreme precipitation, strengthening the magnitude-frequency relationship using the GEV distribution. Even though there was a clear link between precipitation and flash in the Fella River Basin, there was uncertainty in the return period for the meteorological trigger, as the return period differed depending on the weather station, variables and time period used.

For the Barcelonnette Basin, the link between precipitation and flash events was less clear (Sec 3.4). The optimal daily and antecedent

threshold for flash events had a MCC value of 0.17 using an antecedent period of 30 days. Moderately extreme daily and antecedent precipitation were more likely to lead to flash events, as would be expected, but many flash events occurred with less precipitation. Furthermore, the days with the highest daily precipitation amounts were not associated with either a flash flood or debris flow. Therefore, it appears that while daily precipitation may be an indicator for flash events, it is not a consistent proxy. As a result, other meteorological variables are considered in more detail in Chapter 5.

For soil slides in the Barcelonnette Basin, the link between hydro-meteorological hazard and precipitation was also not clear. In Sec 3.5, the best performing threshold during the calibration period was for landslides triggered by rain and snow (MCC: 0.28), however during the validation periods, none of the five events were above the threshold. The Rainfall landslide threshold had the second best performance during the calibration period (MCC: 0.27), but again none of the four soil slides in the validation periods were above the threshold. The snowmelt threshold based only on temperature performed the worst (MCC: 0.06), although found three of the seven soil slides above the threshold in the validation periods. The high threshold from AD that performed well in the validation dataset failed to capture any events during the cross-validation. The lower threshold, with a low MCC value of 0.09 performed equally during validation and cross-validation. Overall, the low AD threshold performed the best, although further work is needed to reduce the number of false positives and increase the MCC score.

Finally, atmospheric circulation patterns in Sec 3.6 found a link between the climate and the hydro-meteorological events that did not rely on local meteorological records, and provided information about the governing atmospheric circulation patterns. Weather types that had the strongest link with hydro-meteorological hazards had low pressure systems to the northwest of Barcelonnette with moist north-westerlies, although for two of the three best preforming classifications only had significant BSS for autumn. Future work could consider dividing the hydro-meteorological hazards into types, as in Secs 3.3-3.5, although a larger study area may be needed to increase the number of hydro-meteorological events.

Precipitation may be a good proxy for hydro-meteorological hazards for areas where there are high daily precipitation amounts (in these areas greater than 150 mm); otherwise the link between hazard and precipitation was not always clear. By including other variables such as temperature or through weather types, the link between climate and hazard can sometimes be improved. Similarly, the triggers can differ between hydro-meteorological hazard types and even within a particular type (e.g. floods and soil slides). However, there is the possibility of over-fitting, and the meteorological triggers may vary over time. Therefore, care must be taken when determining the link between climate and hazard, particularly for use in climate change-hazard studies.

4 Comparison between downscaling methods for precipitation projections

This chapter is based on work undertaken for Turkington, T., Ettema, J. Malet, J.P., Remaître, A. and van Westen, C.J. (2014) Impacts of climate change on debris flows – what are some of the challenges? Conference paper for presentation: International Conference Analysis and Management of Changing Risks for Natural Hazards, Padua, Italy.

4.1 Introduction

To investigate how hydro-meteorological hazards may change in the future under climate change, global climate models (GCMs) are used to obtain projections of future climate. Modelling physical processes of the atmosphere, ocean, cryosphere, and land surface, GCMs produce projections for a swath of meteorological variables. However, many physical processes occur at a finer scale than can be directly modelled in GCMs, resulting in parameterization of the processes that introduces uncertainties. There is further uncertainty in the feedback mechanisms of some processes, such as clouds and radiation. These uncertainties result in a range of future climate projections among GCMs. Adding a number of emission scenarios or trajectories of future concentrations of greenhouse gases enhances the range of climate projections.

There is a scale discrepancy between the output from GCMs and what is needed for climate change-hazard studies. Global climate models typically have a horizontal resolution between 100 and 500 km, where horizontal resolution less than 10 km are often required for hydro-meteorological hazards. Furthermore, GCM resolution can result in poor representation of mountain topography. Dhakal and Sidle (2004) showed that by averaging precipitation over their study area, as in a coarse scale model, the likelihood of a landslide being triggered decreased. In an investigation of two floods in southern France, when the relief was removed from the numerical model, the amount of precipitation significantly decreased (Ducrocq et al., 2008). If GCM data is used directly,

it is likely that the precipitation or flood or landslide occurrence would be underestimated. Therefore before projections of precipitation can be used for climate change-hazard studies, downscaling of GCM data is required.

A variety of techniques have been developed to downscale GCM data, some of which may be applicable for climate change-hazard studies. There are two types of downscaling: dynamical downscaling based on finer resolution physical models, and statistical downscaling based on a statistical relationship between the coarse scale and finer-scale observations. Combinations of the dynamical and statistical downscaling can also be applied to utilize the advantages of both downscaling types.

Dynamical downscaling produces finer scale climate projections using regional climate models (RCMs) nested inside coarser GCMs. The finer resolution of the RCMs allows for more detailed topography, higher order of physical parameterization, and produces finer scale output. In recent years there have been an increasing number of coordinated climate projections for the regional level (for Europe ENSEMBLES, van der Linden and Mitchell (2009) and CORDEX, Jacob et al. (2014)). However, to obtain sub-10km resolution output required for climate change-hazard studies, it is not possible to use a single fine scale RCM nested inside the GCM. Multiple increasingly finer resolutions RCMs are needed, which increases the uncertainty due lateral boundary conditions between each RCM and the original GCM and may mask the climate signal (Déqué et al., 2012). Furthermore, biases still remain in the RCM output (Teutschbein and Seibert, 2012). To compensate for the difficulties using RCMs, statistical downscaling is often used as a relatively efficient way to translate GCM and RCM output to the local scale.

The two major underlying assumptions for any statistical downscaling method are (1) there is a relationship between coarse scale climate variables (predictors) and what occurs at the local scale (predictands) and (2) that this relationship will hold true in the future. While there has been speculation that the second assumption may not be valid (Hewitson and Crane, 2006), there is evidence that certain statistical downscaling methods can reproduce long term changes (Timbal et al., 2009). A wide range of predictors have the potential to be downscaled, including traditional predictors such as geopotential height and wind, as well as sea surface temperature and convective indices (Chen et al., 2010; Jacobeit et al., 2014).

Statistical downscaling methods can be grouped into three approaches: perfect prognosis, model output statistics (MOS) and weather generators (Maraun et al., 2010). Perfect prognosis methods develop empirical relationships between coarse scale observations and local scale features, which are projected into the future using GCMs and RCMs. MOS methods apply corrections to GCM or RCM output based on local observations to account for biases in the dynamical models. Weather generators are stochastic models that are designed to replicate statistical properties of the observations. As weather generators are also used to produce longer time series of observations, weather generators are

not strictly only a downscaling method. However as a statistical downscaling method, weather generators can be conditioned on coarse scale conditions.

The ability of any statistical downscaling method depends on the strength of the predictor-predictand relationship, the ability of the predictors to identify climate change signals, and whether the predictors can be reliably reproduced in climate models. When considering the appropriate method to use, care must be taken as to what conditions need to be preserved. These conditions include inter-site correlation between weather stations, autocorrelation, intra/inter annual variations, or consistency between variables such as temperature and precipitation. Furthermore, the ability of the method to downscale a mean meteorological parameter, such as wet day frequency, may not be an indication of how well the downscaling method captures extremes, often what is more important for hydro-meteorological hazards (see Chapter 3). Ultimately the most appropriate method for downscaling will depend on the purpose, the resources, and time available. Decisions have to be made on the downscaling method in the climate change-hazard study chain and these decisions should have a scientific basis (Déandreis et al., 2014).

The objective of this chapter is to determine the behaviour of wet day frequency compared with extreme precipitation indices for four downscaling methods based on two approaches. The 90^{th} and 99^{th} percentiles of daily precipitation represent the extreme precipitation indices, as high daily precipitation amounts can be a proxy for hydro-meteorological hazards. Two statistical downscaling approaches are applied. First, a perfect prognosis approach is applied using three methods: two analogue methods based on similar days in the observational record, and generalised linear models (Sec 4.3). A MOS method, quantile mapping, is applied in Sec 4.4. The results are intended to be used as an introduction to climate studies and a guide for the statistical downscaling method to use in subsequent chapters considering climate change-hazard studies.

4.2 Study area and data

Two study areas are considered: the Barcelonnette Basin, France and the Fella River Basin, Italy. Each area has more than 30 years of homogeneous daily rainfall (see Chapter 2 for more information). Long observational records are a requirement for successful application of statistical downscaling, as the end result depends on the strength of the predictor-predictand relationship assessed under a wide variety of conditions. Both study areas have recorded numerous flood and landslide events, required to develop climate change-hazard studies for hydro-meteorological hazards in subsequent chapters. Furthermore, the two study areas have the most dissimilar climate of the three areas considered in the thesis (Chapter 2) and therefore may respond differently under future climate change.

The Barcelonnette Basin is the drier of the two study areas with 75% of days recording less than 0.2 mm of precipitation. The annual precipitation is between 600 and 1000 mm per year, with the highest daily precipitation per year between 21 and 86 mm. For the days with 0.2 mm or more precipitation recorded (wet days), the 90^{th} and 99^{th} percentile values are 19.4 mm and 44.0 mm respectively. For this chapter, the Barcelonnette rain gauge was used (B-1, Chapter 2).

The Fella River Basin receives more precipitation than the Barcelonnette Basin: annual precipitation varies between 1400 mm in the north and 2200 mm in the south, and it is recording less than 0.2 mm of precipitation on 63% of days. The highest daily precipitation per year varies between 30 and 355 mm. For wet days, the 90^{th} and 99^{th} percentile values are 28.8 mm and 74.5 mm respectively. For this chapter, the Malborghetto rain gauge (F-4, Chapter 2) was used.

The current and future climate data for the perfect prognosis methods comprised of IPCC AR4 simulations, simulations from the ENSEMBLES European project (van der Linden and Mitchell, 2009), and reanalysis data. The GCMs used are listed in Table 4.1, along with the resolution of the model and emission scenarios. Two emission scenarios (SRES) were used: A1B and A2 scenarios. The A1B scenario contains moderate future emissions from rapid economic development, technological improvements, along with an eventually declining global population, while the A2 scenario has greater future emissions due to continuously increasing population, slow technological change and regional economic development (Nakicenovic et al., 2000). The ERA-40 reanalysis data was produced by the European Centre for Medium-Range Weather Forecasts and is available from September 1957 to August 2002 (Uppala et al., 2005).

Table 4.1 Perfect prognosis approach GCMs and SRES scenarios. For models where an abbreviation was used for the name, the abbreviation is given in brackets.

GCM	Institute	Resolution	SRES
BCCR-BCM 2.0 (BCM2)	Bjerknes Centre for Climate Research, Norway	1.9°x1.9°	A1B
			A2
CNRM-CM3 (CNCM)	Météo-France/Centre National de Recherches Météorologlques, France	1.9°x1.9°	A1B
			A2
UKMO-HadGEM2 (HADG)	Hadley Centre for Climate Prediction and Research/Met Office, UK	1.3°x1.9°	A1B

The climate data for the MOS method originated from the EURO-CORDEX dataset (Jacob et al., 2014). Table 4.2 lists the combination of RCMs and driving GCMs that were selected to cover a wide range of genealogy (Knutti et al., 2013). The resolution of the climate data and Representative Concentration Pathway (RCP) are included in the table. The RCPs were used as opposed to the SRES scenarios, as the CORDEX dataset includes the more recent model runs using the RCPs. A

Table 4.2 MOS approach RCMs, driving GCMs, RCPs, and resolution (Res). For models where an abbreviation was used for the name, the abbreviation is given in brackets.

Modelling centre or group	RCM	Res.	Driving model	Driving model institute	RCP
SMHI	SMHI-RCA4 (SM)	0.44°	CanESM2 (CE)	Canadian Centre for Climate Modelling and Analysis	4.5,8.5
			EC-EARTH (EC)	EC-EARTH consortium published at Irish Centre for High-End Computing	4.5,8.5
			IPSL_CM5A-MR (IP)	Institut Pierre-Simon Laplace	4.5,8.5
			CNRM-CM5 (CN)	Centre National de Recherches Météorologiques / Centre Européen de Recherche et de Formation Avancée en Calcul Scientifique	4.5,8.5
			GFDL-ESM2M (GF)	Geophysical Fluid Dynamics Laboratory	4.5,8.5
DMI	DMI-HIRHAM5 (DM)	0.44°	EC_EARTH (EC)	EC-EARTH consortium published at Irish Centre for High-End Computing	4.5,8.5
KNMI	KNMI_RACMO22E (KN)	0.44°			4.5,8.5

comparison of CO_2 concentrations for the two approaches showed that RCP 8.5 is similar to the A2 SRES scenario, while RCP 4.5 has lower CO_2 concentrations than A1B, similar to those from SRES scenario B2 (van Vuuren and Carter, 2014). No reanalysis data was required for the MOS method.

4.3 Perfect prognosis: Analogue and GLM methods

Perfect prognosis methods determine empirical relationships between coarse scale observations and local scale features (in this case precipitation) that is assumed to hold for future climate. Statistical relationships between the coarse scale and local scale are usually established through either regression or weather typing for perfect prognosis methods. Regression methods are based on a variety of multivariate statistical techniques to move from coarse scale to local precipitation. Weather typing methods identify a set of atmospheric conditions, circulation types, or weather regimes that are related to local precipitation. While the method used will depend on data availability, often there are still

trade-offs between the methods and no single perfect prognosis method is optimal.

As no corrections are applied to the climate model output in this approach, predictors used should be reasonably reproduced by the models (Gutiérrez et al., 2012). Predictors can be assessed by comparing the predictor variables from GCMs with available global observational datasets. However, not all well replicated variables will be good predictors for precipitation and may result in a weak relationship between the predictor and predictand when downscaling. Therefore, for any perfect prognosis method a balance needs to be made between the reliability of predictors in the climate model and their ability to capture precipitation.

This section considers three perfect prognosis methods for downscaling daily precipitation for use in assessing future hydro-meteorological hazard: two analogue methods as a weather type method and Generalized Linear Models (GLM) as regression method. All three perfect prognosis methods are applied using the Statistical Downscaling Portal (Gutiérrez et al., 2011).

4.3.1 Method

Analogue methods are one of the simplest downscaling methods (Zorita and von Storch, 1999; Gutiérrez et al., 2012). The methods select from the observational record the days that are most similar, or in the case of weather types, one of the previous observations for a particular weather type (Willems and Vrac, 2011). The advantage of these methods is that it is relatively simple to implement. However, the methods require long observational records from which to draw the analogues. Furthermore, by selecting predictands from the observational dataset, unobserved extremes are excluded. Analogue methods have been widely used in a variety of climate change impact studies (e.g. Teutschbein et al., 2011; Teng et al., 2012; Dayon et al., 2015). Two analogue methods applied here are:

AM1: Analogue method using the nearest neighbour, where the closest analogue in the historical record is chosen based on the predictor fields.

AM2: Analogue method using the weighted mean of the nearest 10 neighbours, where the weighted average of the 10 closest analogues are chosen based on the predictor fields.

Generalized Linear Models base the predictand on a linear set of predictors, where the predictand does not necessarily follow a Gaussian distribution. The method may be particularly useful for daily precipitation, which is often non-Gaussian (Maraun et al., 2010). As with the analogue method, GLMs require extensive observational records to obtain an accurate relationship between the predictor and predictand. The method is able to project unobserved extreme values. For these reasons, GLMs have been used to obtain future projections of precipitation (e.g. Hertig and Jacobeit, 2014; Pulquério et al., 2015). The GLM method applied here is:

GLM: Generalised Linear Model, with five principle components and 25 clusters, clustered using k-means.

The predictor-predictand relationship was developed using the ERA-40 dataset for the period 1961-2001. Seven predictor fields for the coarse scale were used: geopotential height, temperature, and specific humidity, all at 850 hPa and 500 hPa with an additional specific humidity field value at 700 hPa. All fields are readily available in both reanalysis and GCM datasets. As the Downscaling Portal uses publicly available data (GSOD, National Climatic Data Center) as predictands, the nearest weather stations were used and then corrected (the Barcelonnette Basin: Embrum, the Fella River Basin: Lienz).

The skill of each of the three perfect prognosis methods in the observational period was assessed using five indicators:

- Hit rate (HIR): proportion of wet days (precipitation greater or equal to 0.2 mm) that were correctly predicted, with values between 0 and 1, and 1 being a perfect score
- False alarm rate (FAR): proportion of dry days (precipitation less than 0.2 mm) that were incorrectly predicted, with values between 0 and 1, and 0 being a perfect score
- Spearman's rank correlation coefficient (r): dependence between observations and forecasts based on their rank, with values between -1 and 1, and 1 being a perfect monotone relationship
- Root mean square error (RMSE): average magnitude of the predictor errors, values equal or greater than 0, and 0 being a perfect score
- Kolmogorov-Smirnov test (KS p-value): compares the modelled and observed cumulative distribution functions with the null hypothesis that the two samples are from the same distribution, and a p-value less than 0.05 indicates different distributions

The HIR and FAR determined the accuracy of the modelled wet and dry days. The RMSE and r determined the skill of the method including the precipitation amounts. The KS p-value was used to compare the observed and modelled distributions without the serial correspondence required in the other tests. More information on the five indicators can be found in Gutiérrez et al. (2011).

Once the predictand-predictor relationship was established for the period 1961-2000, GCM data replaced the reanalysis predictor data to obtain projections for the observational period (1961-2000) and the future (2070-2100). The GCMs used from the Downscaling portal are listed in Table 4.1. In the observational period, the difference between the observed and modelled wet day frequency and extreme precipitation indices was assessed. The significance of the future trends in wet day frequency and extreme precipitation indices was assessed by resampling of the projections (1000 resampled datasets).

4.3.2 Results

Three perfect prognosis statistical downscaling method were applied for the Barcelonnette and Fella River basins: AM1, AM2, and GLM. Before a comparison of the extreme precipitation indices and wet day frequency, the overall skill of the perfect prognosis methods for precipitation in the observational period was assessed. Five tests were applied to determine the skill of each method based on the ERA-40 reanalysis data, with the results of each of the tests in Table 4.3.

Table 4.3 Skill of three perfect prognosis methods for the Barcelonnette and Fella River daily precipitation over the base period 1961-2000. The test were Hit rate (HIR), False alarm rate (FAR), Spearman's rank correlation coefficient (r), Root mean square error (RMSE), and Kolmogorov-Smirnov test (KS p-value).

	Barcelonnette				
	HIR	FAR	r	RMSE	KS p-value
AM1	0.41	0.20	0.23	7.63	0.99
AM2	0.92	0.69	0.36	5.60	0
GLM	0.37	0.21	0.16	8.48	0
	Fella River				
AM1	0.50	0.25	0.27	10.61	0.46
AM2	0.96	0.75	0.41	8.00	0
GLM	0.45	0.25	0.21	18.05	0

For the Barcelonnette Basin, the AM1 method had the best performing predictor-predictand relationship as it was the only method that had no significant difference between the distribution of the observed and predicted precipitation (KS p-value > 0.90). This method had the best performance predicting dry days (lowest FAR of 0.20) and the second best score in the remaining tests. The AM2 method performed the second best, with the highest r value and lowest RMSE (0.36 and 5.6 respectively), indicating the most similar values or rate of change of values with the observations. The number of correctly predicted wet days was high (HIR = 0.92), due to a much higher wet day frequency overall, as seen with the high FAR (0.69). The GLM had the poorest performance, apart from having a lower FAR than the AM2 method (0.21 compared with 0.69).

For the Fella River Basin, the AM1 was the best performing predictor-predictand relationship based on the results in Table 4.3 as with the Barcelonnette Basin, with no significant difference between the observed and predicted precipitation distributions (KS p-value >0.40) and a low FAR (0.25). As with the Barcelonnette Basin, the AM2 method had the second best performance, with the highest r value and lowest RMSE (0.41 and 8.00 respectively). This method had the highest HIR (0.96), however the AM2 method had the highest percentage of false alarms (0.75). The GLM method had a low FAR (0.25), although in every other test in Table 4.3 it had the poorest performance score.

While Table 4.3 considered the entire precipitation distribution using reanalysis data, Table 4.4 assessed the perfect prognosis methods using

the GCM data specifically for the wet day frequency and the heavy (90^{th} percentile) and extreme (99^{th} percentile) precipitation amounts. The percentage of days with 0.2 mm of precipitation or more is given (wet days), along with the threshold required to have the same wet day frequency as the observations ($Threshold_E$). The AM1 method was the closest to the observation wet day frequency for the Fella River Basin (average difference of -0.87%), while the GLM method was closest for the Barcelonnette Basin (average difference of 1.03%). The AM2 overestimated the wet day frequency by on average 40% and 45% for the Barcelonnette and Fella River basins respectively, more than double the observed frequency. The GLM method was the closest to the observed extreme precipitation indices for both catchments (average difference Barcelonnette: 7.51 mm, Fella River: -9.86 mm), as well as the heavy events in the Fella River Basin (average difference -5.57 mm). The AM2 method had the greatest difference, underestimating the heavy and extreme precipitation amounts for both catchments. Overall for the wet day frequency and extreme indices, the AM1 method performed better than the AM2 method for both catchments, but not as well as the GLM method when estimating extreme precipitation indices for the Fella River Basin. The AM1 performed worse than the GLM method for the Barcelonnette Basin, due to a greater difference in extreme precipitation amounts and wet day frequency from the observations.

Table 4.4 Comparison of precipitation indices for the Barcelonnette and Fella River basins for the period 1961-2000 based on the three perfect prognosis methods for the three GCMs: the percentage of wet days (precipitation $\leq$ 0.2mm), the equivalent threshold ($Threshold_E$; the threshold where the model data has the same wet day frequency as observed) , and the values for the 90^{th} and 99^{th} percentiles (based on $Threshold_E$).

	Barcelonnette									
	Obs	AM1			AM2			GLM		
		BCM2	CNCM	HADG	BCM2	CNCM	HADG	BCM2	CNCM	HADG
Wet days (%)	25.1	29.7	29.7	29.7	76.6	76.6	76.6	26.9	25.7	25.8
$Threshold_E$	0.20	0.51	0.33	0.25	3.14	2.92	2.83	0.45	0.55	0.50
90^{th} (mm)	19.4	20.0	17.8	18.7	8.5	7.8	7.9	19.8	21.2	18.8
99^{th} (mm)	44.0	36.8	32.7	39.3	12.3	12.1	12.3	53.93	50.8	49.8
	Fella River									
	Obs	AM1			AM2			GLM		
		BCM2	CNCM	HADG	BCM2	CNCM	HADG	BCM2	CNCM	HADG
Wet days	36.9	36.3	35.9	35.9	81.9	81.9	81.9	33.7	33.7	33.7
$Threshold_E$	0.2	0.07	0.05	0.05	3.11	2.87	2.80	0.05	0.05	0.05
90^{th} (mm)	28.8	22.0	21.5	21.8	11.6	11.7	12.4	22.3	24.0	23.4
99^{th} (mm)	74.5	55.1	58.8	67.2	19.8	21.0	21.4	62.7	66.3	64.9

Future changes in wet day frequency and heavy and extreme precipitation amounts are shown in Fig 4.1, with yellow and light green colours indicating drier or less extreme precipitation, blue indicating wetter or more extreme precipitation, and white indicating no significant change.

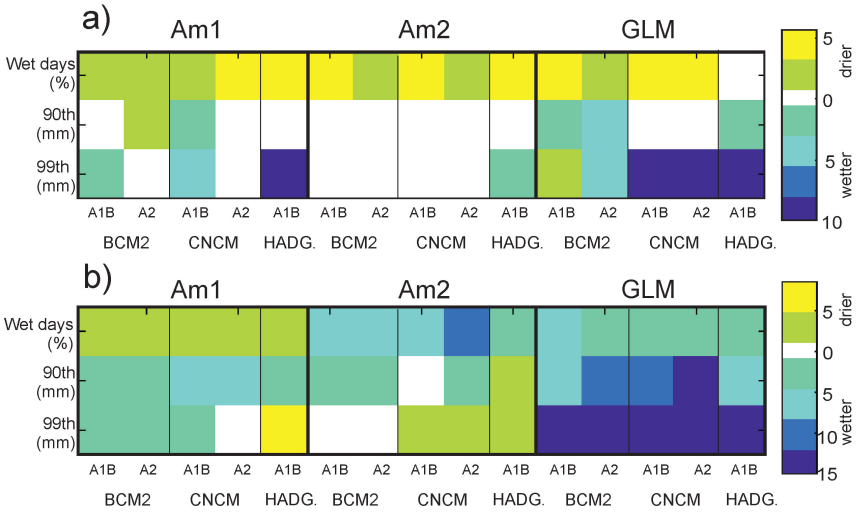

Figure 4.1 Change in future precipitation properties for Barcelonnette (a) and Fella River (b) based on the three perfect prognosis methods AM1, AM2 and GLM. The 90th and 99th (mm) gives the change in precipitation amount for the respective percentiles. Wet days gives the change in percentage of days that have more than 0.2 mm of precipitation. Blue boxes indicate wetter conditions (increase in precipitation amount or frequency), and yellow/green indicate drier conditions (decrease in precipitation amount or frequency). All changes are given for the period 2071-2099 relative to 1961-1989.

From this figure, the changes in the wet day frequency and extreme precipitation indices can be compared for the three perfect prognosis methods for the period 2071-2099 compared with 1961-1989.

For the perfect prognosis methods in the Barcelonnette Basin shown in Fig 4.1, the changes in wet day frequency were not representative of changes for the extreme precipitation indices. Fourteen out of 15 perfect prognosis based projections had fewer wet days in the future (top row Fig 4.1a) in contrast to extreme precipitation where there was either more intense daily precipitation or no significant change (subsequent rows in Fig 4.1a). All of the projections had a 0.5-5.5% decrease in wet days, except for one projection where there was no change (HadG-A1B using the GLM method). For the change of intensity, most projections of the 90th and 99th percentiles had either an increase in precipitation amounts (0-12 mm) or little change. The two exceptions were BCM2-A2 using the AM1 method (1 mm decrease in the 90th percentile precipitation amount) and BCM2-A1B using the GLM method (0.5 mm decrease in 99th percentile precipitation amount). Comparing the perfect prognosis methods, the GLM method had the greatest change in future projections, followed by the AM1 method. The AM2 method only had changes for the frequency of wet days and the 90th percentile, and the 99th percentile

precipitation amount with one projection (HADGEM2).

For the Fella River Basin, changes in wet day frequency were not consistently representative of changes in extreme precipitation. The Fella River Basin future projections depended on the perfect prognosis method used. The GLM projections had increases in wet day frequency (2-5.5%) and in precipitation amounts (90^{th} increase of 6.5-18 mm and 99^{th} increase of 17-89 mm). In contrast, the AM1 method had fewer wet days (1-2%), with increases in the 90^{th} percentile precipitation amounts (4.5-5.0 mm). The 99^{th} percentile amount decreased for HADG-A1B under AM1 (8 mm), with a small increase or no change for the other projections (0-3.5 mm). The AM2 technique had the largest increase in wet day frequency (3.5-9%), while for changes in extreme precipitation, the HADG-A1B projected decreases in amount, and either little change or increases for the other two GCMs. Therefore, while the changes in wet day frequency and extreme precipitation indices were in the same direction for the GLM perfect prognosis method, the results were inconsistent for the AM1 and AM2 methods.

4.3.3 Discussion

The choice of perfect prognosis method had a clear effect on how close the modelled values were to the observational daily precipitation amounts for the two study areas. The AM1 analogue method had the most similar observation chosen based on seven predictor fields and was most similar to the observed values when considering the entire distribution. This result is not unexpected, as the AM1 method only used observed values. As the GLM values were based on a linear set of predictands and not selected from the observations, the predicted precipitation amounts differed from the observations due to the imperfect predictand-predictor relationship. It is possible that other predictor fields may improve the results. Therefore, as neither the AM2 nor GLM method were able to reproduce a similar precipitation distribution as the observations (KS p-value), any future projections for these two methods become questionable.

When comparing the wet day frequency and extreme values, there were also differences between the methods. The AM2 analogue method had the weakest performance in Table 4.4. As the method was based on the average of 10 most similar observations, the precipitation amounts were smoothed out, which resulted in more wet days, yet lower heavy and extreme precipitation amounts. For the GLM and the AM1 methods, preferred method depended on the study area.

The inconsistency between the trend in wet day frequency and the trend in extreme precipitation indices for the two study areas suggests that changes in the number of wet days are not an indication for changes in future extreme precipitation. Other studies have also found that the direction of the trend for mean and extreme precipitation differed in some instances (e.g. for the Mediterranean using GLM, Hertig et al. (2013)), Portugal specifically, GLM, Pulquério et al. (2015)). Using a

variety of statistical downscaling techniques, including an analogue method and multiple linear regression method, Schmidli et al. (2007) found that for Europe in summer, mean precipitation decreased on average, while the 90^{th} percentile amounts stayed the same. A decrease in wet day frequency while an increase in the extreme precipitation indices suggests that more of the annual precipitation is derived from intense precipitation events, events that are often important for hydro-meteorological hazards. Therefore, changes in wet day frequency or other average precipitation indices are unlikely to be indicative of future changes in hydro-meteorological hazards and investigation of relevant meteorological parameters should be undertaken.

The ability of the three methods to model unobserved extreme precipitation amounts may have affected the projections of heavy and extreme precipitation, parameters important when considering future hydro-meteorological hazard. The only method that allowed for unobserved extreme values, GLM, had the largest increases in the future 90^{th} and 99^{th} percentile values with one exception (Barcelonnette BCM2-A1B). The ability to model unobserved precipitation amounts allows for a potentially unlimited increase in precipitation, although the further the precipitation amount is from observed amounts, the less reliable the results are. Both the AM1 and AM2 methods were restricted to observed values of precipitation, there by capping the 90^{th} and 99^{th} percentile at the highest observed precipitation amount in the calibration period.

When comparing the two study areas, the Barcelonnette Basin had more projections with a decrease in wet day frequency, while larger increases in extreme precipitation were found for Fella River. The Fella River Basin observes higher precipitation amounts in the observational period (Chapter 2), and this may partly explain the larger increases in the extreme indices, as the values in Fig 4.1 are given in absolute changes. However, the overall increase or decrease in extreme precipitation and wet day frequency was governed by the climate projections, and therefore the two study areas are expected to have differing responses to future climate change.

4.4 MOS: quantile mapping

The aim of MOS is to correct biases or errors in the models compared to observations and downscale to point scale. MOS therefore differs from perfect prognosis approaches as it attempts to remove biases in the existing models rather than using the observed coarse scale atmospheric variable. MOS methods include the delta method (e.g. Diaz-Nieto and Wilby, 2005), quantile mapping (e.g. Dobler et al., 2011; Finger et al., 2012; Themeβl et al., 2012), and bias correction and spatial downscaling (BCSD; e.g. Maurer and Hidalgo, 2008; Liu et al., 2012).

Not all MOS methods are equally applicable for hydro-meteorological hazards. The delta method applies a correction to the data so that both the observed and modelled datasets have the same mean value. This

delta method is one of the easiest methods to apply, however due to the simplistic nature, should only be used for mean precipitation conditions, as no correction is made for extreme precipitation or standard deviation (Teutschbein and Seibert, 2012). Quantile mapping matches the distribution of precipitation between the climate model and observations. No correction is made for the length of wet and dry spells, which may be important for certain hazards like flooding and drought. Furthermore, the method cannot downscale for multiple locations, unless used in combination with another technique that accounts for variability between sites. The BCSD method combines quantile mapping with spatial disaggregation to allow for variability at the sub-climate model grid scale, important when looking to downscale for multiple locations (Wood et al., 2004). As with other MOS methods, the BCSD makes no correction for inter-seasonal or inter-annual variations in climate outside of what is produced from the climate model. For hydro-meteorological hazards where sub-monthly precipitation is important and only one station is used, quantile mapping is therefore the appropriate method to use.

This section evaluates quantile mapping of RCM precipitation data for use in climate change-hazard studies. Fourteen projections of precipitation are obtained for the B-1 and F-4 precipitation records, a similar number of projections as in Sec 4.3. Only one rain gauge for each study area is examined for comparison with the perfect prognosis downscaling methods and negating the need for spatial disaggregation. While the ability of quantile mapping to reproduce the entire precipitation distribution is assessed, the focus is on heavy and extreme precipitation indices (90^{th} and 99^{th} percentile respectively) and changes in the wet day frequency.

4.4.1 Method

The quantile mapping method applied was based on Themeβl et al. (2012). There were two differences from Themeβl et al. (2012) in that the correction factors were applied on a monthly basis rather than a 31-day moving window and no frequency adaptation was applied. The monthly correction value was applied to account for seasonal variation in the precipitation distribution and to match the weather generator used in Chapter 7. Frequency adaptation may be needed when the RCMs overestimate the dry day frequency. However, most RCMs underestimate the dry day frequency and overestimate days with light precipitation, known as the drizzle effect (Maraun, 2013).

The quantile mapping method matches the empirical cumulative distribution function (ECDF) from the RCM data to the ECDF for the observational data. Theoretical distributions, such as the gamma distribution, were not used as a combination of two distributions is needed to best capture extreme precipitation (Breinl et al., 2014). From Themeβl et al. (2012), the corrected precipitation amounts ($Xcorr$) were calculated

using:

$$Xcorr_{t,i} = Xraw_{t,j} + CF_i \tag{4.1}$$

$$CF_i = ECDF_i^{obs,-1}(P_{m,j}) - ECDF_i^{mod,-1}(P_{m,j}) \tag{4.2}$$

$$P_{m,j} = ECDF_j^{mod}(Xraw_j) \tag{4.3}$$

where $Xraw_{t,j}$ is the precipitation amount on day t at point j, $Xcorr_{t,i}$ is the corrected RCM precipitation amount on day t for gauge i, CF_i is the correction factor at j with regards to i, and P is the probability of $Xraw$ based on the ECDF for daily precipitation amounts. The two ECDFs, $ECDF^{obs}$ and $ECDF^{mod}$ are the ECDFs for the observed rain gauge and RCM data respectively. For unobserved extreme precipitation amounts, the average from the larges five precipitation amounts was taken.

To assess the quality of the quantile mapping, each dataset was divided into a calibration (85%) and validation (15%) datasets from the period 1961-1990. The root mean squared error (RMSE) was calculated for both calibration and validation datasets. Bias correction was done for RCP4.5 and RCP8.5 datasets. Even though both model runs are identical for the observational period, the division into calibration and validation datasets was based on random selection, allowing correction factors to vary between the two RCPs. The KS p-value was calculated as in Sec 4.3. The other four skill tests in Sec 4.3 were not applied due to no autocorrelation between predicted and observed precipitation in the MOS approach.

The quantile mapping method was applied to each of the RCM projections in Table 4.2 for the period 2071-2100. As RCMs contain considerable noise on a single grid point (Fowler and Ekström, 2009), an average of nine grid boxes surrounding the rain gauge was taken. The ECDF was calculated for the observation period (1961-1990), and then applied to the future period (2071-2100). The absolute change in wet day frequency, 90^{th} and 99^{th} percentiles and probability of non-exceedance for the historical 90^{th} and 99^{th} values were calculated (as in Sec 4.3). The significance of the future trends was assessed by resampling of the projections (1000 resampled datasets).

4.4.2 Results

The output of 14 RCM projections from the CORDEX project were bias-corrected using quantile mapping. The calculations were applied to both the calibration (Cal) and validation (Val) data. Plotting the modelled precipitation against the observed precipitation for the calibration and

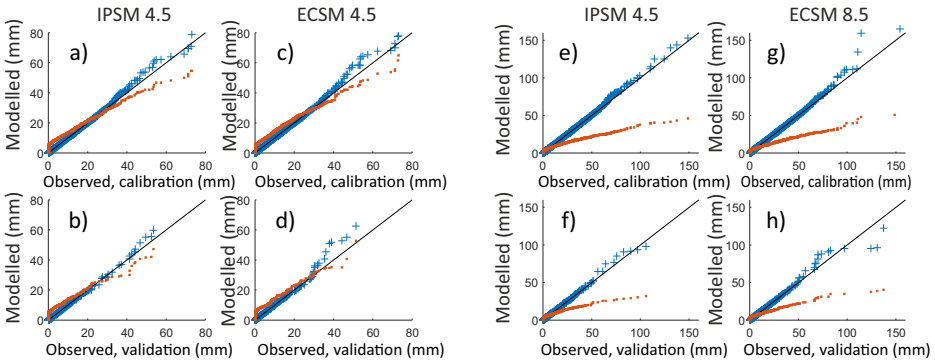

Figure 4.2 Quantile-quantile plots for the best and worst performing modelled precipitation based on the RMSE for the calibration (top) and validation (bottom) datasets. For B-1, IPSM4.5 performed the best (calibration a, validation: b), and ECSM4.5 had the highest RMSE value (calibration: c, validation: d). For F-4, the lowest RMSE was for IPSM 4.5 (calibration: e, validation: f) and the highest for ECSM 8.5 (calibration: g, validation: h). Uncorrected data are in orange, and bias-corrected data in blue crosses. The black line indicates a perfect match. All values are daily precipitation (mm).

validation data shows how the quantile mapping alters the modelled data for each quantile. Figure 4.2 contains quantile-quantile plots before (orange) and after (blue) quantile mapping. For a perfect match, all precipitation amounts would lie along the black line. Only models with the lowest RMSE value in Table C.1 (Barcelonnette: IPSM 4.5, Fella River IPSM 4.5) and highest RMSE value (Barcelonnette: ECSM 4.5, Fella River ECSM 8.5) are shown. For each model, quantile mapping improved the modelled precipitation, and there were no significant differences between the observed and corrected model precipitation as the KS p-value was greater than 0.85 for all models (see Table C.1 for the RSME values). Therefore, the quantile mapping method performs well for daily precipitation in the observational period.

For the B-1 precipitation record, the quantile mapping corrected the overestimation of low precipitation amounts and underestimation of high precipitation amounts, as seen with the blue corrected data closer to the black line in Fig 4.2 a. When considering the validation data, IPSM 4.5 corrected data is closer to the black line than the uncorrected data due to similar to over/underestimation as the calibration period (Fig 4.2b). The quantile mapping overcorrected for the higher ECSM 4.5 precipitation amounts in Fig 4.2d, as the uncorrected RCM validation data was closer to the observational data than in the calibration period. Overall the B-1 precipitation record after quantile mapping was closer to the observations, although there were still discrepancies between the observations and modelled data for higher precipitation amounts.

For the Fella River precipitation data in Fig 4.2e-h, the raw IPSM 4.5

and ECSM 8.5 data overestimate the low precipitation amounts (<10 mm) while underestimating the high precipitation amounts, in some instances by 100 mm. For the best performing projection (Fig 4.2e,f), the corrected IPSM 4.5 RCM data is within 5 mm of the observed precipitation for both the calibration and validation datasets. However, for the projection with the highest RMSE (Fig 4.2g,h), the two highest values were overcorrected in the calibration dataset, while they were undercorrected in the validation dataset. This under and overestimation demonstrate that the models did not consistently underestimate the extreme precipitation.

The performance of the quantile mapping method for the extreme precipitation indices and wet day frequency is shown in Table 4.5 with the wet day frequency before (wet days R) and after (wet days) quantile mapping along with the threshold required to have the same wet day frequency as the observations ($Threshold_E$). The raw wet day frequency (Wet days R) in each case greater than the observed wet day frequency, with a similar difference for both study areas. Due to the higher modelled frequency, no frequency adaptation was required. The precipitation amounts for the 90^{th} and 99^{th} percentile show that after correction, the modelled data is within 1.5 mm for the 90^{th} percentile and 10 mm for the 99^{th} for all models except for ECKN in the Barcelonnette Basin.

Table 4.5 Observational period precipitation properties based on the MOS method for the seven RCM projections: the percentage of wet days (precipitation 0.2 mm), the equivalent threshold ($Threshold_E$), and the 90^{th} and 99^{th} percentiles (based on $Threshold_E$). The values for each model are averaged over the RCP 4.5 and 8.5 runs for the period 1961-1990.

	Barcelonnette Basin							
	Obs	CESM	CNSM	GFSM	IPSM	ECSM	ECDM	ECKN
Wet days R	25.1%	74.2%	81.7%	81.5%	74.2%	71.8%	72.5%	70.2%
Wet days		26.7%	25.6%	26.2%	26.6%	26.5%	26.2%	26.2%
$Threshold_E$	0.2	0.30	0.30	0.30	0.55	0.30	0.25	0.38
90^{th} (mm)	19.4	18.3	19.1	19.5	19.3	19.2	18.4	18.4
99^{th} (mm)	44.0	46.4	48.1	50.7	46.6	53.9	53.1	55.4
	Fella River Basin							
	Obs	CESM	CNSM	GFSM	IPSM	ECSM	ECDM	ECKN
Wet days R	36.9%	78.8%	84.5%	82.6%	80.7%	76.1%	77.5%	76.0%
Wet days		34.7%	34.5%	36.0%	36.0%	34.1%	34.1%	35.2%
$Threshold_E$	0.2	0.13	0.15	0.25	0.25	0.12	0.10	0.20
90^{th} (mm)	28.8	28.9	28.7	27.6	29.7	29.1	29.0	27.9
99^{th} (mm)	74.5	79.7	82.5	74.8	81.4	74.8	78.6	79.5

The future MOS based projections for the wet day frequency and extreme precipitation indices are in Fig 4.3 for the period 2071-2100. Yellow and green indicate drier or less extreme precipitation, while blue for wetter or more intense precipitation projections. Parameters with no significant change based on the resampling are white.

When considering the future projections for B-1, most projections had fewer wet days in the future (top row Fig 4.3a), in contrast to increases

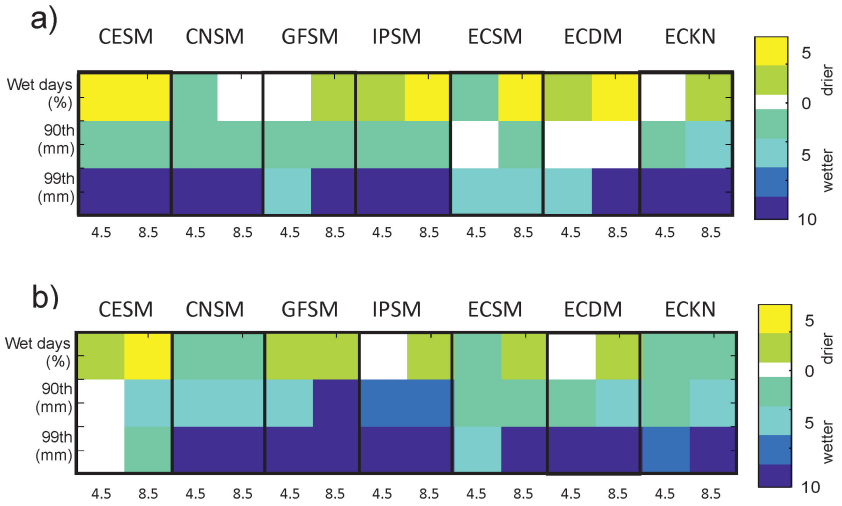

Figure 4.3 Change in future precipitation properties for the Barcelonnette Basin (a) and Fella River Basin (b) from 14 biased corrected projections with the RCM and GCM model listed above and the RCP below. The 90th and 99th (mm) gives the change in precipitation amount for the respective percentiles. Blue boxes indicate wetter conditions (increase precipitation amount or frequency), and yellow, green indicated drier conditions (decrease in precipitation amount or frequency). White boxes indicate no significant change. All changes are given for the period 2071-2100 in absolute values relative to 1961-1990.

in the extreme precipitation indices (subsequent rows Fig 4.3a). Nine projections had an increase in the percentage of dry days (1.0-5.0%), three with no change (CNSM 8.5, GFSM 4.5, ECKN 4.5), and two projections with a decrease of 1.0-1.5% (CNSM 4.5 and ECSM 4.5). No projection had a decrease in the 90th of 99th percentile amounts, although the ECSM and ECDM found no significant change. As would be expected, most model combinations (5 out of 7) found a greater change under the more aggressive RCP 8.5 than RCP 4.5. The two exceptions were CESM and CNSM where the results for the extreme precipitation indices were similar for the two RCPs and wet day frequency for CESM. The CNSM wet day frequency decreased under RCP 4.5 and observed no significant change under RCP 8.5.

For the Fella River Basin station F-4, all projections found either no change or an increase in precipitation amounts, with inconsistent changes projected for the percentage of wet days (Fig 4.3b). Seven projections had an increase of 1.5-4.5% of dry days, five had a decrease between 0.5-2.5% (CNSM both, ECSM 4.5, ECKM both), and two with no significant change (IPSM 4.5 and ECDM 4.5). Of the seven RCM-GCM combinations, all had an increase in heavy and extreme precipitation amounts (1-28.5 mm) apart from CESM. Under RCP4.5 CESM found no significant increase in extreme precipitation, although there was an increase with the more aggressive RCP 8.5. Six of the 7 model combinations followed the expec-

ted result of at least 1 of the wet day and extreme precipitation indices experiencing a greater change under RCP 8.5 than RCP 4.5. Only CNSM found similar results for the two RCPs, similar to the results for the Barcelonnette Basin.

4.4.3 Discussion

Quantile mapping was applied to 14 future projections of precipitation for the Barcelonnette and Fella River basins. The quantile mapping performed well, reducing the RSME in all validation datasets. There was also no significant difference between the corrected RCM precipitation distributions and the observational data.

To determine the applicability of quantile mapping for climate change-hazard studies, how the ability of the method to model extreme daily precipitation is vital. Quantile mapping improved on the modelled extreme values, although the results were less reliable when applied to the most extreme precipitation amounts. This reliability can been seen through the inconsistent differences between the RCM data and observational data in Fig 4.2. The differences may be related to the type of precipitation, with the climate models able to capture synoptic, driven precipitation better than convective precipitation. In this work, the average between the highest five correction factors was used, to try and reduce any spurious effects from only using the most extreme value. Furthermore, as the most extreme values were not considered in either study area, the discrepancies would not have affected future projections of the 90^{th} and 99^{th} percentile amounts. Therefore, while the quantile mapping may be less reliable for the most extreme values, the method improves on the raw modelled data, and is reliable for the moderate extreme values such as the 90^{th} amounts.

The discrepancy in changes for wet day frequency with changes for extreme precipitation indices suggest that mean precipitation parameters cannot be used to predict changes in the extreme precipitation indices. A decrease in wet day frequency and increase in precipitation intensity has been found for other regions using MOS approaches (e.g. Upper Danube River Basin, Europe and Brahmaputra River Basin, Asia, Dobler et al. (2011)), although changes in mean precipitation in the same direction as extreme precipitation have also been found (e.g. Denmark, Sunyer et al. (2012)). Therefore, changes in extreme precipitation need to be analysed as well as mean changes when considering climate change-hazard studies.

Overall future projections for the Barcelonnette Basin were drier, with 9 projections finding a decrease in wet day frequency between 1.0% and 4.5%. This drier trend was in contrast to an increase in the intensity of heavy and extreme precipitation (11 projections with increase of 1-4 mm for the 90^{th} percentile and all projections with a 4-19 mm increase for the 99^{th} percentile). For the Fella River Basin there was also an increase in the intensity of heavy and extreme precipitation from the projections (13 projections with an increase of 1.0-6.5 mm for the 90^{th} percentile

and 3-28 mm for the 99th percentile), although the change in wet day frequency was inconsistent. Therefore, apart from the most extreme precipitation amounts, quantile mapping was a relatively straightforward approach for developing precipitation projections for use in climate change-hazard studies and could capture the changes in both the wet day frequency and extreme precipitation indices.

4.5 General discussion

A perfect prognosis approach (Sec 4.3) and a MOS approach (Sec 4.4) were assessed for the applicability in climate change-hazard studies, particularly focussing on wet day frequency and extreme precipitation indices. The perfect prognosis approaches used primarily the IPCC-AR4 GCMs and the SRES scenarios, while the MOS approach used the CORDEX RCMS, which were nested inside the more recent Coupled Model Intercomparison Project Phase 5 (CMIP5) GCMs that used RCPs. Previous studies comparing the IPCC-AR4 models with the CMIP5 models showed only small improvements between the datasets (e.g. for cloud properties: Lauer and Hamilton (2013), temperature and precipitation: Joetzjer et al. (2013); Sun et al. (2015)). Representative Concentration Pathway 8.5 used in Sec 4.4 is similar to the SRES A1 scenario from Sec 4.3, although A1B is a more aggressive scenario than the RCP 4.5. Therefore, it is unlikely that differences between the MOS and perfect prognosis approaches are from the driving models and scenarios, and the two approaches can be compared.

Comparing the perfect prognosis with the MOS approaches, the precipitation distribution after quantile mapping outperformed the perfect prognosis approaches for the observational period. Only the AM1 method and the quantile mapping method had no significant differences between the modelled and observed precipitation. The RMSE was lower using quantile mapping than for AM1, AM2, or GLM. Part of the reason for the lower RMSE from quantile mapping was ordering precipitation amounts before the RMSE was calculated, where the perfect prognosis methods were based on a comparison of modelled and observed precipitation on a daily basis. It is possible that the perfect prognosis methods would have performed better with other predictors, although this is not guaranteed.

Capturing the most extreme precipitation amounts was challenging for both approaches. For AM1 and AM2, neither were able to project future daily precipitation amounts greater than what was observed as future amounts are drawn from observations. The one perfect prognosis approach that could project greater precipitation amounts, the GLM method, was unable to reproduce the observed precipitation distribution, and therefore was unreliable. For the quantile mapping method, new extremes could be projected although the results may not be reliable. While underestimation of extreme values is common for model data (Zolina et al., 2004), applying a correction can be difficult as the underestimation can vary significantly. This underestimation problem is also found when

trying to forecast extreme precipitation on the scale of hours to days (e.g. for streamflow forecasting, Cuo et al. (2011), for 2km resolution numerical weather prediction models, (Kain et al., 2008)). However, while capturing the most extreme values was difficult, particularly the MOS approach was able to reproduce the more moderate extremes, such as the 90^{th} and 99^{th} percentiles.

The downscaling approach affected the future precipitation projections (2071-2100), as seen in the average and range of future wet day frequencies and extreme precipitation indices in Table 4.6. The average of all the projections for the perfect prognosis and MOS methods are shown, along with the minimum and maximum projected change. For wet day frequency in the Barcelonnette Basin, the perfect prognosis methods projected drier futures than quantile mapping (a decrease of 3.5% compared to 1.8%), while the opposite was found in the Fella River Basin (an increase of 2.8% compared to a decrease of 0.4%). The increase in the extreme precipitation indices was greater with quantile mapping than the perfect prognosis methods for the Barcelonnette Basin, possibly due to more projections that allowed for unobserved extreme amounts. For the change in the 90^{th} and 99^{th} percentiles in the Fella River Basin, the AM1 and AM2 methods had less extreme precipitation compared to the GLM or quantile mapping method, apart from the CESM projections, with the mean values similar between approaches.

Table 4.6 Mean, minimum, and maximum of future projections for the 15 perfect prognosis based projections (PP) and 14 MOS projections (MOS) in Fig 4.1 and 4.3.

	Barcelonnette					
	Mean		Min		Max	
	MOS	PP	MOS	PP	MOS	PP
Wet days (%)	-1.8	-3.5	-5.0	-5.0	1.5	0.0
90^{th} (mm)	1.8	0.4	0.0	-1.0	4.0	4.0
99^{th} (mm)	10.4	3.1	4.0	-3.0	19.0	12.5
	Fella River					
	Mean		Min		Max	
	MOS	PP	MOS	PP	MOS	PP
Wet days (%)	-0.4	2.8	-4.5	-2.5	2.5	9.0
90^{th} (mm)	4.1	5.1	0.5	-1.0	9.5	18.0
99^{th} (mm)	14.3	14.3	0.0	-8.0	28.5	88.5

Other studies comparing perfect prognosis and MOS methods also found differences between approaches. For example in California, using a finer scale (2 km) RCM provided wetter projections than using perfect prognosis, possibly due to the model's ability to capture the North American monsoon (Pierce et al., 2013). For the Alps, RCMs had a stronger trend towards drier conditions compared to a variety of perfect prognosis techniques (Schmidli et al., 2007). Therefore, as with other studies, future precipitation projections depend on the method used. Future work could consider applying correction factors based on the

atmospheric situation, a combination between weather typing and MOS. Another alternative for climate change-hazard studies, as applied here, would be to not use the most extreme values, rather the 90^{th} or 99^{th} percentile levels. However, changes in the most extreme values will likely still be crucial for hydro-meteorological hazards. Therefore, the reliability of changes in the most extreme precipitation amounts should be carefully considered as the method selection affects future projections.

The ability of the method to downscale multiple variables, such as temperature and precipitation, varies between methods. As seen in Chapter 3, temperature can influence hydro-meteorological hazards and possibly should be considered when developing climate change-hazard studies. Of the methods considered here, the analogue method and quantile mapping can be extended to include temperature and other variables. When choosing the nearest neighbour, any other observations available such as temperature and wind speed, can be selected, maintaining a realistic relationship between the variables. Similarly for quantile mapping, other variables from the RCM projection, including temperature, can be chosen and corrected for biases. For the GLM method, it is not straightforward to include other variables. Using a separate GLM for temperature may not preserve the correlation its precipitation, although it is possible that the results for temperature could be conditioned based on the outcome for precipitation. Therefore, the inclusion temperature and possibly other variables, such as humidity and wind direction, is most straightforward for the analogue and quantile mapping of the methods considered.

4.6 Conclusion

Two statistical downscaling approaches were considered with respect to developing climate projections of wet day frequency and extreme precipitation indices for use in climate change-hazard studies: perfect prognosis and MOS. For the perfect prognosis approach, three methods were applied, an analogue method choosing the nearest neighbour, an analogue method choosing a weighted average of the 10 nearest neighbours, and a GLM. For the MOS approach, one quantile mapping method was applied. Each of the methods were applied to two study areas, the Fella River and Barcelonnette basins. The four methods were compared based on their performance on wet day frequency and 90^{th} and 99^{th} percentile precipitation amounts for the observational period and future period (2071-2100). Other factors, such as dry and wet spell length, were not considered and may have a different behaviour. The main conclusions are as follows:

- The ability of statistical downscaling method to model mean values or wet day frequency was not necessarily representative of extreme values. For the perfect prognosis approach, the two analogue methods performed the best when considering the entire distribution,

while the GLM method had 90th and 99th percentile values closer to the observed precipitation amounts for both study areas.

- Trends in future wet day frequency (2071-2100) were not indicative of trends in extreme precipitation for either catchment, further evidence that mean precipitation parameters are not representative of extreme precipitation.
- The two study areas responded differently under future climate change. Compared to the Fella River Basin, the Barcelonnette Basin had smaller increases in the extreme precipitation indices (B-1: -3.0 to 19.0 mm, F-4: -8.0-88.5 mm) and smaller increases in the wet day frequency (B-1: -5.0 to 1.5% of days, F-4: -4.5 to 9% of days).
- When considering wet day frequency and the 90th and 99th percentile precipitation amounts for the four downscaling methods, the quantile mapping performed the best for the two study areas based on the RMSE and the ability to model unobserved extreme precipitation amounts. The results suggest that quantile mapping is the better method to use in climate change-hazard studies where the trigger is extreme daily precipitation.

5 Empirical atmospheric thresholds for debris flows and flash floods in the southern French Alps

This chapter is reproduced as published in Turkington et al. (2014) with minor modifications

5.1 Introduction

A key component in risk assessments for natural hazards is quantifying the probability of occurrence in relation to specific intensities of the hazardous events. Intense short duration precipitation, long-lasting rainfall, and snowmelt are all potential triggers for hydro-meteorological hazards in mountainous areas in Europe (Brunetti et al., 2013; Sene, 2013). However, while rainfall is often an important element in triggering hydro-meteorological hazards, the actual atmospheric conditions are often complex, with very localized rainfall.

In the European Alps and Mediterranean region, debris flows are generally caused by heavy rainfall from either intense convection, or sustained heavy rainfall (Tarolli et al., 2012). Antecedent conditions, such as previous rainfall, snowmelt and evaporation, are also important, however they are often not collected or incorporated into the threshold (Guzzetti et al., 2008). Debris flows can be generated by a number of different causes, such as liquefaction of the toe part of landslides, blocking of channels, and accelerated erosion along gullies. Heavy rainfall may trigger debris flows and flash floods in the same channels filled with sediments (van Asch et al., 2013), and both events can be approached similarly in the threshold analysis. Within this paper we refer to rapid instantaneous events such as debris flows or flash floods as flash events.

The role of rainfall in triggering debris flows and flash floods can be examined using physically based models (e.g. Luna et al., 2011; van Asch et al., 2013). Through the use of hydrologic and stability models, these physical models take into account not only rainfall, but other factors such as pore pressure and slope stability (Aleotti, 2004). However, the models can be computationally costly and require extensive parameterization

and calibration. Therefore, the application of such models is often only feasible for relatively small areas, such as a single torrent or a few square kilometres (Brunetti et al., 2013).

For larger areas (tens of square kilometres upwards), empirical rainfall thresholds are more frequently used (e.g. Aleotti, 2004; Giannecchini, 2006; Frattini et al., 2009; Brunetti et al., 2010; Berti et al., 2012). Thresholds define minimum or maximum conditions of one or more triggering factors for a particular hazardous event (Frattini et al., 2009). The research focus in this field recently has been towards the development of objective and reproducible thresholds (Guzzetti et al., 2008). Methods include Bayesian inference, where the parameters of the threshold are fit using a probability approach (Guzzetti et al., 2007), and a Frequentist approach, based on the frequency of conditions that have resulted in landslides (Brunetti et al., 2010). A detailed review of empirical thresholds for debris flows and landslides can be found in Guzzetti et al. (2008).

For debris flows a typical approach is to define a threshold based on the intensity, duration or antecedent rainfall amounts (Guzzetti et al., 2008). Three examples of the general form of the rainfall threshold is as below (Eq 5.1), with three examples from Caine (1980) (Eq 5.2), Guzzetti et al. (2008) (Eq 5.3), and Cepeda et al. (2010) (Eq 5.4):

$$I = \alpha D^{\beta} \tag{5.1}$$

$$I = 14.82 D^{-0.39} \tag{5.2}$$

$$I = 2.20 D^{-0.44} \tag{5.3}$$

$$I = 29.14 D^{-1.34} \tag{5.4}$$

where intensity (I) is given in mm/hr, duration (D) in hours, and α and β are curve parameters.

Empirical rainfall thresholds rely on accurate rainfall measurements, often requiring sub-daily data (e.g. Aleotti, 2004; Giannecchini, 2006; Cepeda et al., 2010). However, as many hydrological and meteorological stations still collect only daily rainfall, fine resolution data is not always available. In mountainous areas, precipitation can vary greatly with altitude. Without extensive meteorological networks, the effect of orographic processes on the spatial variation of rainfall can be difficult to determine (Tobin et al., 2011). Therefore, in many threshold studies, many hazardous events are excluded from analysis. Brunetti et al. (2013) automatically excluded events where the closest rain gauge was more than 5 km away or there was not sufficient rainfall data, and in Meyer et al. (2012), 20% were excluded due to insufficient information.

Other challenges for empirical rainfall thresholds include having a detailed and sufficiently complete inventory of events, and deciding and defining the indicators to use in the thresholds. It also is often not clear how to define a rainfall event (when it starts and finishes), although recent papers have tried to address this (Brunetti et al., 2010; Berti et al., 2012). Finally, many of the empirical methods establish a threshold above which debris flows may occur, without considering non-event observations also above the threshold, as there are many more non-event days. Meyer et al. (2012) used only debris flow events to determine the threshold, then analysed the annual frequency of days above the threshold. As rainfall is not the only factor governing debris flows, there will likely always be uncertainty when defining rainfall thresholds (Berti et al., 2012).

One way to approach the significance of a threshold is using Bayesian probability (e.g. Berti et al., 2012). Bayesian probability takes into account the likelihood of an event given certain conditions. However, while Bayes' theorem is useful in determining the probability of an event above a certain threshold, it does not take into account the probability that an event would be below this threshold. So even if the probability of an event occurring above a particular threshold is high, many events may occur below this threshold.

The thresholds above all use rainfall directly, however, it is also possible to analyse the cause of heavy precipitation. Ingredients that can lead to precipitation include mechanisms for uplift of an air mass (such as heating at the surface or orographic lift), increased saturation of the atmosphere, or a mixing of two or more air masses (such as fronts and low pressure systems). Maddox et al. (1979) found for the US that 43% of flash floods were caused by local convection, while the rest were synoptically driven. Studies in the Mediterranean basin show heavy precipitation events are often caused by quasi-stationary local convection (e.g. Nuissier et al., 2008). Atmospheric indicators can summarize the principle atmospheric conditions leading to heavy rainfall for a particular area, depending on the different causal mechanisms.

While atmospheric indicators have not had widespread usage in threshold analysis for flash events, they have been used as indicators for heavy rainfall and downscaling climate projections. Trapp et al. (2009) used the product of convective available potential energy (CAPE) and deep-layer wind shear (DLS) as an indicator for severe thunderstorms. Nuissier et al. (2011) used synoptic weather types based on the Hess-Brezowsky Grosswetterlagen classification, as well as low-level moisture flux and low-level wind direction to detect heavy precipitation events in southern France. Other examples of using atmospheric indicators for heavy precipitation include: Schmidli et al. (2007), Chen et al. (2010), and Jeong et al. (2012). Identification of synoptic atmospheric conditions that lead to flooding has also been undertaken in a number of studies (e.g. Petrow et al., 2009; Parajka et al., 2010).

Atmospheric indicators can be obtained using reanalysis data from physically-based models. Using a forecast model combined with observa-

tions, reanalysis data is both consistent with atmospheric observations and the laws of physics (Dee et al., 2011). The weighting given to the observations differs depending on the quality of the observations. Less reliable fields, such as precipitation, are less dependent on observations than more reliable fields such as mean sea level pressure (Tapiador et al., 2012). However, the quality of the output is dependent on the skill of the underlying forecasting model. Overall though, reanalysis data provides a wide range of atmospheric variables that are both spatially complete and coherent (Dee et al., 2011).

Rather than rainfall thresholds from local weather stations, this research develops empirical atmospheric thresholds for debris flows and flash floods using atmospheric indicators to identify the potential heavy rainfall events, using 63 flash events in the Southern French Alps. The main advantages are that a dense observational rain gauge network is no longer required, and that there is no need to define explicitly a rainfall event. Furthermore, atmospheric thresholds can lead to a better understanding of the meteorological conditions that are related to the occurrence of debris flows and flash floods. Empirical atmospheric thresholds therefore may be an alternative to the conventional empirical rainfall thresholds where dense observational networks are not available, or where further investigation is required to the cause of the rainfall.

The structure of the chapter is as follows: first an overview of the study area and the dataset is given, followed by a description of the methodology to develop atmospheric thresholds. The methodology includes dividing the flash events into those caused by local convection, and those that are from more synoptically driven, widespread rainfall. Thresholds using weather station data are also generated for comparison. The results are then presented and discussed, with a conclusion on the main results and limitations of developing and using empirical atmospheric threshold for debris flows and flash floods.

5.2 Study area and data description

The Barcelonnette Basin, France from Chapter 1 was chosen as the study area (Fig 5.1). Previous investigation has found that hydro-meteorological events are generally associated with snowmelt and high intensity summer storms, although the precise triggering conditions have been difficult to determine (Flageollet et al., 1999). Four of the five weather stations are located close to the main river channel (Fig 5.1). Differing from Chapter 2, Station 5 refers to weather station Super-Sauze located at a higher elevation, and used as a comparison for the other four stations. Station 5 is located above the valley bottom at 1,950 m a.s.l. with summer only daily measurements between 1996 and 2004. Information on elevation, length of measurement series and variables for the stations 1-4 can be found in Table 2.1. The correlation between station 5 and the other four stations in summer is low: between 0.02 and 0.08, based on the Kendall's tau correlation coefficient (Kendall, 1970). The correlation between

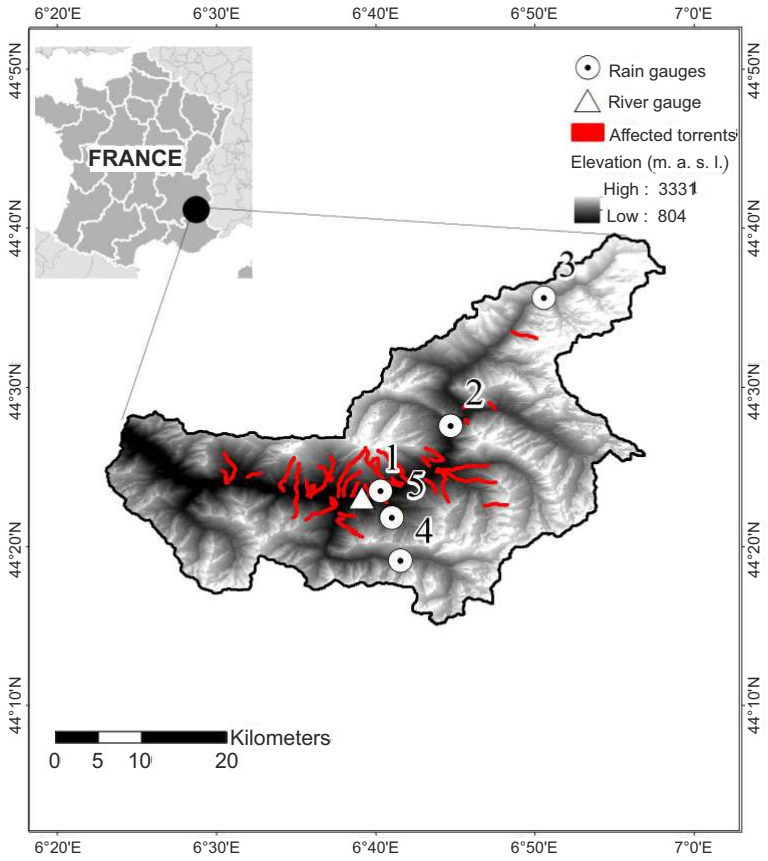

Figure 5.1 The study area including the location of rain gauges and a single river gauging station. Red lines depicts the affected torrents where debris flows or flash floods occurred between 1979 and 2010

stations 1 to 4 is higher: between 0.69 and 0.74. Further information on the homogeneity and climatology of the stations can be found in Chapter 2.

The Barcelonnette Basin has an extensive landslide, debris flow, and flash flood inventory. Information on the inventory compilation is in Chapter 1. The historical inventory contains 29 flash floods and 39 debris flows events observed between 1979-2010, which occurred between March and November (Fig 5.2). Tarolli et al. (2012) found a similar seasonal distribution of flash floods, with events generally occurring between August to November in the western Mediterranean. On average, discharge levels between September and November closely follows the mean precipitation intensity, while the discharge increases from March to July mainly due to snowmelt (Fig 5.2). As the basin is orientated west-east, north facing slopes are likely to retain snow longer than south

facing slopes.

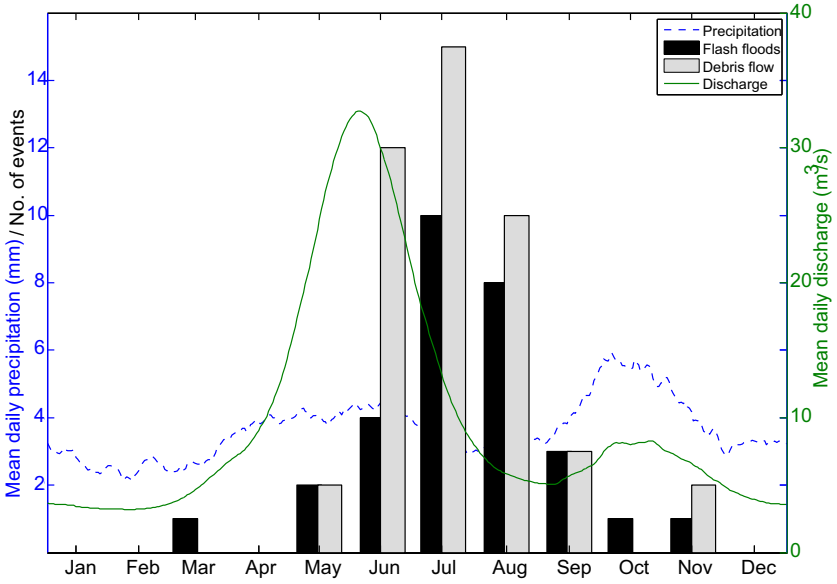

Figure 5.2 Running 30-day mean daily precipitation and discharge for the period 1979-2009, for the B-1 precipitation record and Barcelonnette river gauge in the Ubaye River. The bar graph displays the number of flash floods and debris flows observed between 1979 and 2010.

Cepeda et al. (2010) developed Eq 5.4 for debris flows based on hourly precipitation from Station 1. Only 7 debris flows were used, as the others occurred before sub-daily precipitation measurements were available (starting 1998), or the precipitation or inventory record was deemed to be not sufficient (Cepeda et al., 2010). For the threshold, 86% of the debris flow events used were correctly predicted, and 6% of rainfall events above the threshold resulted in a debris flows. However, no threshold was obtained using only the longer daily rainfall dataset. To obtain a threshold for a longer time period, other methods or datasets are therefore required.

ECMWF ERA-Interim reanalysis data is used for analysing the regional atmospheric variables. The data has a spatial resolution of 80 km (T255) covering the period 1979-2012 (Dee et al., 2011). More information about observation and data assimilation and model characteristics for ERA-Interim can be found in Dee et al. (2011). The study area is approximately half of one grid box, so only the grid box containing the study area and those directly beside it are used (nine in total). The variables chosen (Table 5.1) contain commonly used predictors for statistical downscaling precipitation from Global Climate Models at multiple atmospheric

pressure levels (Chen et al., 2010; Jeong et al., 2012). In addition, convective available potential energy (CAPE), deep layer shear (*DLS*), and soil moisture fields are also included. The first two are added as they might be indicative for convection (Marsh et al., 2009) and soil moisture as part of antecedent conditions. CAPE in particular is an estimate of the energy that a parcel of air would have at the surface if it was lifted. High positive CAPE values indicate that the air may be unstable and favourable for convection. A brief description of each of the variables is given in Table 5.1. Atmospheric indicators at 850 hPa and 700 hPa represent lower tropospheric conditions, while indicators at 500 hPa and 250 hPa represent the upper troposphere. The surface variables are available at 3 hourly time steps, with the others at 6 hourly time steps (Dee et al., 2011). *DLS* is estimated using the following equation and the surface wind fields ($u10m, v10m$) and 500 hPa wind fields ($u500hPa$, $v500hPa$) (Seltzer et al., 1985):

$$DLS = \sqrt{(u500 - u10)^2 + (v500 - v10)^2} \tag{5.5}$$

Table 5.1 ERA-interim variables used in this study, along with abbreviations used. A brief description of each variable is also given.

Variable	Pressure level	Description
Precipitation (R)	Surface	Rain and snow
CAPE	Surface	Estimate of instability of the atmosphere
Soil moisture (SWL)	Surface	Soil moisture for top layer (0-7 cm).
Specific humidity, (Q)	850 hPa, 700 hPa, 500 hPa	Atmospheric moisture
U&V wind	10 m, 850 hPa, 700 hPa, 500 hPa	Meridional (V) and zonal (U) wind speed
Temperature (T)	850 hPa, 700 hPa, 500 hPa, 250 hPa	Temperature
Vorticity (Vo)	850 hPa, 700 hPa, 500 hPa, 250 hPa	Local spinning motion of the air
Divergence (D)	850 hPa, 700 hPa, 500 hPa	Expansion or spreading out of a vector field

5.3 Methodology

This section explains a method to establish empirical thresholds for debris flows and flash flood events (flash events) based on regional atmospheric conditions or indicators from the reanalysis dataset. Two different thresholds are considered: (1) a probabilistic threshold based on Berti et al. (2012), determining the likelihood of a flash event using a

variety of indicators, and (2) a static threshold that takes into account the number of flash events below the threshold. Besides defining the threshold, the methodology also examines (a) if the local weather station network was adequately capturing the rainfall causing the event, (b) whether intense convection was the main rainfall source triggering the events, and (c) if other meteorological triggers, such as snowmelt, are relevant to triggering events in the study area. The three steps of the proposed methodology are:

Sec 5.3.1: Categorize events based on potential meteorological triggers

Sec 5.3.2: Select appropriate atmospheric indicators for each category

Sec 5.3.3: Compute the probabilistic and static thresholds and then apply these over a validation period

Based on the availability of the weather station data and reanalysis data, the period 1979-2010 was chosen as the focus study period. The years from 1989 to 2004 are used for calibration and two validation periods are selected, namely 1979-1988 and 2005-2010. By dividing the validation period into two segments, changes in data quality, such as measurement techniques or observational coverage, are expected to be reduced while maintaining a as long as possible data period. The probabilistic and static thresholds are also established using local weather station data for direct comparison with the empirical regional atmospheric thresholds.

5.3.1 Categorization of events

The proposed categories are based on the governing rainfall generation processes, with a secondary subdivision based on potential antecedent conditions. The four categories are: Ls - locally generated rainfall, spring, Lr - local rainfall, summer, Ss - synoptic rainfall, spring, and Sr - synoptic rainfall summer. The classification is based on Merz and Blöschl (2008), who identify five categories for river floods based on the type of rainfall and antecedent conditions such as snowmelt and rainfall over several weeks. The categories Ls and Ss assume snowmelt is an antecedent condition, while Lr and Sr assume no snowmelt. For this study, seasonal antecedent conditions (snowmelt or/and rainfall) are based on the average annual discharge pattern in Sec 5.2. From Fig 5.2, the discharge generally returns to near baseflow levels in July. Furthermore, the east-west orientation of the study area means that the south facing slopes will be snow-free earlier than the north facing slopes. Therefore, the spring events were defined as flash events between March and June for south facing slopes, and between March to mid-July for north facing slopes.

The rainfall generation processes are split into types where local conditions are driving the generation, or whether it is governed by the synoptic atmospheric processes. In Done et al. (2006), the authors estimate the rate at which CAPE is being removed by convective heating

as:

$$t_{CAPE} \sim \frac{CAPE}{dCAPE/dt} \tag{5.6}$$

where t_CAPE is the convective timescale and $\frac{dCAPE}{dt}$ is the rate of change of CAPE removed by convective heating.

Done et al. (2006) suggest that with convective timescales shorter than 6 hours the synoptic conditions are governing the instability of the atmosphere, while locally driven intense convection occurs when t_{CAPE} values are high. Non-convective precipitation would also have a low t_{CAPE} value, as $CAPE$ values are generally low (Molini et al., 2011). Applying the criteria by Molini et al. (2011), flash events with $t_{CAPE} > 6hr$ are classified as locally convective (L), and with $t_{CAPE} < 6hr$ corresponding to more equilibrium conditions (S).

Molini et al. (2011) and Done et al. (2006) further modified Eq 5.6 by estimating the latent heat release using the precipitation rate. However, as hourly rainfall rates are not available for any weather station before 1998, and Done et al. (2006) explain this is just a rough indication of the convective timescale, the version in Eq 5.6 is used.

The accuracy of the classification of rainfall generation type is dependent on the accuracy of CAPE from ERA-Interim. Molini et al. (2011) found, when comparing CAPE values from ERA-Interim with those from a near-by radiosonde, there was only modest correlation, with a coefficient of determination of approximately 60%. Differences would be expected however, when comparing the grid box average with a point location.

5.3.2 Indicator selection

Each day in the calibration period 1989-2004 is assigned a label as an event day (a day where one or more flash events were recorded), and non-event days (where no flash event was recorded). The atmospheric indicators that show a distinction between event days and non-event days can then be used in the development of atmospheric thresholds (Sec 5.3.3). The silhouette index (SI) is used to identify atmospheric indicators that best differentiate between the clusters of flash events and non-flash events. This index takes into account both the separation between the two clusters as well as the cohesion within the cluster (Rousseeuw, 1987). The index was developed as part of a tool to visualise the distinction between multiple clusters, and as a guide to the validity of the clustering and selection of number of clusters (Rousseeuw, 1987). It has since been used as a validation tool in classifying atmospheric conditions (e.g. Huth et al., 2008; Kannan and Ghosh, 2011; Kenawy et al., 2013).

An individual silhouette value determines how similar a point is to other points in its own cluster compared to points in other clusters (Rousseeuw, 1987). The SI is then the average of all the silhouette values

(Huth et al., 2008), with Eq 5.7 valid for two clusters:

$$SI = \frac{1}{2} \sum_{c=1}^{2} \frac{1}{n_c} \sum_{i=1}^{n_c} \frac{b_i - a_i}{max(a_i, b_i)} \tag{5.7}$$

where n_c is the number of observations in cluster c, b_i is the average Euclidean distance between an observation i and all observations in the other cluster and a_i is the average Euclidean distance between i and all observations in the same cluster.

The SI varies between -1 and 1. An individual silhouette value of 1 indicates that the observation is correctly classified as a flash or non-flash event, while a near zero value indicates that the observation could belong to either cluster, and negative values indicate misclassification (Ansari et al., 2011). The highest SI indicates the best clustering (Ansari et al., 2011). An overall SI value of 1 means that the clusters are compact and well separated from each other (Kenawy et al., 2013).

A worked example of the SI for floods in the Ubaye River is given. Days with high discharge values (flood days) are compared with no-flood days. The no-flood days chosen had similar event and antecedent rainfall amounts as the flood days. Figure 5.3 shows the individual silhouette values for flood days and no-flood days in the Barcelonnette Basin based on Q850 and U&V850. The left figure shows the individual silhouette values for each flood day are above 0, indicating they are more similar to the other flood days that the no-flood days. For the no-flood days, half of the days have positive silhouette values and are likely correctly classified. The other half has negative values, indicating they are more similar to the flood days. The figure on the right side plots the no-flood and flood days, and shows the separation between the two groups. It shows that generally flood days have higher specific humidity and more easterly winds compared with no-flood days.

The SI value is less reliable for clusters when there is a large difference between the number of flash and non-flash events. Therefore, x days are randomly selected to calculate the SI using the normalized atmospheric variables, where x is the number of flash events. This is repeated multiple times (10,000), with variables with the highest mean SI value selected for threshold analysis. Any atmospheric indicators that had more than 10% of SI values less than zero were discarded. In Sec 5.4.2, only the mean SI value is given.

As conventional thresholds are generally defined using two variables, the analysis is performed with the two best performing indicators. Furthermore, too many indicators could create noise, or lead to over-fitting of the data (Kenawy et al., 2013). The degree of correlation between atmospheric predictors also reduces the benefit of using many predictors (Hewitson and Crane, 2006). However, where the inventory of flash events is more substantial, three or more atmospheric variables could be used to improve the atmospheric threshold.

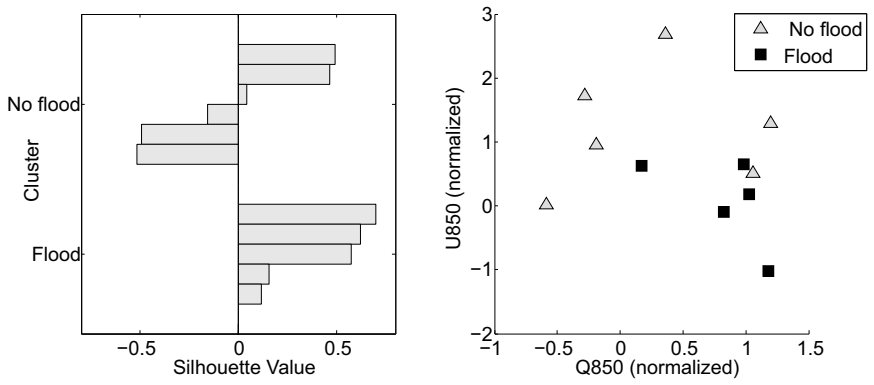

Figure 5.3 A worked example of calculating SI values. The right side plots the specific humidity at 850 hPa and U wind at 850 hPa for five flood days and six non-flood days. These values were then used to derive the individual silhouette values in the plot on the left.

5.3.3 Probabilistic and static thresholds

Bayes' theorem expresses the conditional probability of an event A, such as a flash event, occurring given some condition or conditions, B, such as atmospheric conditions (Eq 3.5 and 3.6). Using the two indicators from Sec 5.3.2 that had the highest SI value, the probability of a flash event occurring was calculated over the observed range of each of the indicator. This is similar to Berti et al. (2012), although extended to using atmospheric indicators.

A limitation of using probability of occurrence is that is does not take into account the percentage of flash events above the threshold. Therefore, a static threshold is also determined considering both the number of events above and below the threshold. A static threshold is taken to be a threshold where the values of the indicators remain constant. The indicators used for the static threshold are the same as for the probabilistic threshold.

A confusion matrix displays the performance of a prediction algorithm, such as a static threshold. The four classifiers in the confusion matrix(Mason and Graham, 1999) are:

- True positives (TP): the number of correctly predicted events
- False positives (FP): the number of events predicted, but where no event occurred
- False negatives (FN): the number of events that were not predicted
- True negatives (TN): the number of days that were correctly predicted as non-events

These classifiers can then be used to determine the correlation between the predicted and observed results using the Matthews Cor-

relation Coefficient (MCC; Eq 3.2). Although to our knowledge the MCC has not been used in rainfall threshold assessment, it has been used in bioinformatics, as an assessment tool where there are unequal numbers of events and non-events (Baldi et al., 2000; D'Este and Rahman, 2013).

The MCC is calculated for each combination of atmospheric indicators from the probabilistic threshold. The threshold with the highest MCC value is chosen as the static threshold, with the added condition in that at least 50% of the flash events are also above the threshold. These selection criteria are somewhat subjective, as the optimal threshold will depend on the application.

5.4 Results and discussion

5.4.1 Categorization of events

Table 5.2 shows the t_{CAPE} value (Eq 5.6) for all separate events in the period 1989-2004. In 66% of the events, local convection was considered to be the dominant meteorological trigger for flash events in the Barcelonnette Basin. The observed convective events occurred between the 1st of June and the 23rd November (numbers 5 and 13 in Table 5.2). The synoptic events occurred over a wider range of months, between March and November (numbers 9 and 1 in Table 5.2).

It is possible that some of the flash events are in the wrong category. Four of the nine synoptic events had no rainfall recorded in at least half of the stations 1-4, which would not be expected with widespread rainfall (numbers 3,4,6,8 in Table 5.2). However, any misclassification would likely only reduce the efficiency of the clustering (Sec 5.4.2), and the significance of the thresholds (Sec 5.4.3). Therefore we used the classification as indicated in Table 5.2 for the subsequent analysis.

5.4.2 Indicator selection

The two best performing indicators for the local convective events were CAPE and specific humidity at 700 hPa (Fig 5.4). These two indicators showed the highest SI value, 0.32. CAPE especially has been used before as an indicator for intense convection (Marsh et al., 2009), as it indicates atmospheric instability. Q700 is indicative of low-level moisture, which is also necessary for locally generated precipitation. Comparatively, the U&V winds showed very low SI values, indicating that wind conditions do not separate flash event days from non-event days. This was also true for DLS and soil moisture (SWL). The vertical integral of water vapour flux was also trialled, however the SI value was also low (not shown). Temperature, vorticity and divergence showed moderate SI values, between 0.10 and 0.25 depending on what other atmospheric indicator it was paired with. The moderate SI values separate the flash events from the non-event days somewhat, but not as much as CAPE and Q700.

Table 5.2 Classification of the flash events in the calibration period 1989-2003. The list contains the date of event, the t_{CAPE} value, and its category : Ls - local rainfall, spring Lr - local rainfall, summer, Ss synoptic rainfall, spring , Sr synoptic rainfall, summer.

	Local convection				Synoptic		
	Date	t_{CAPE}	Group		Date	t_{CAPE}	Group
1.	18/06/1989	7	Ls	1.	03/11/1991	-1	Sr
2.	14/08/1990	13	Lr	2.	02/06/1992	-1	Ss
3.	29/09/1991	46	Lr	3.	12/07/1993	0	Sr
4.	06/10/1991	24	Lr	4.	11/05/1994	0	Ss
5.	01/06/1992	19	Ls	5.	13/05/1994	0	Ss
6.	18/06/1992	93	Ls	6.	06/07/1996	0	Sr
7.	21/07/1992	8	Lr	7.	19/08/1996	1	Sr
8.	27/09/1992	9	Ls	8.	25/07/1997	0	Sr
9.	10/07/1993	12	Ls	9.	22/03/2001	0	Ss
10.	05/11/1994	77	Lr				
11.	28/08/1997	9	Lr				
12.	12/08/2000	9	Lr				
13.	13/08/2000	20	Lr				
14.	23/11/2000	8	Lr				
15.	26/07/2001	55	Lr				
16.	05/06/2002	27	Ls				
17.	23/06/2002	15	Ls				
18.	27/07/2003	10	Lr				
19.	05/08/2003	110	Lr				
20.	08/08/2003	20	Lr				

Figure 5.5 (top) shows that for all the synoptic events, only 10 indicator combinations were significant. To improve the indicator selection, the SI was calculated again further splitting the events into the Ss and Sr categories (Fig 5.5 middle and bottom). However this meant that there were only 4 to 5 flash events in each group. Therefore, any thresholds were unlikely to be as robust as for the local convection and weather stations, as there were fewer events to both calibrate and validate the thresholds.

Splitting the synoptic events into the Sr and Ss categories showed differences between the atmospheric indicators with the highest SI (Fig 5.5, middle and bottom). For Ss events, temperature at multiple pressure levels separated days with flash events from days with no flash events. This was in combination with 8-day average mid-level divergence, temperature, CAPE or specific humidity. The highest SI value of 0.21 was for temperature (3-day) and specific humidity (8-day), both at 700 hPa. These two indicators were then used as the basis of the thresholds in Sec 5.4.3. For the Sr flash events, the significant indicators were divergence at 850 hPa (daily), low level specific humidity, SWL, and 8-day average temperature (Fig 5.5). The highest SI of 0.42 for the Sr flash events

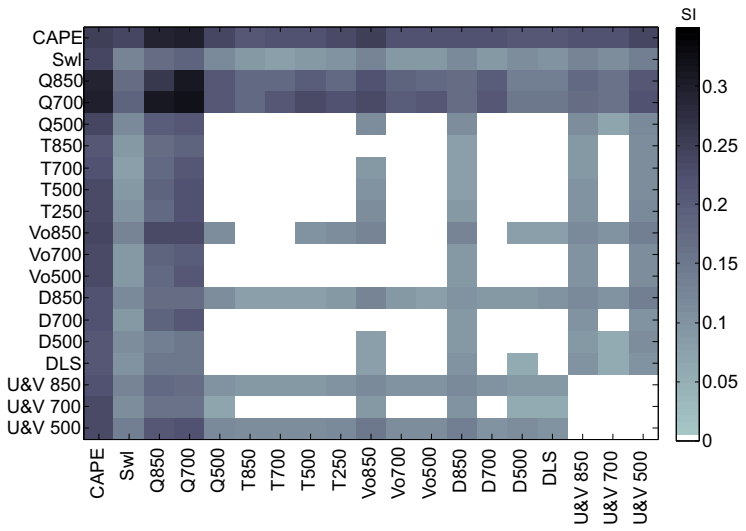

Figure 5.4 The SI value for each pair of atmospheric indicators in Table 5.1 for local convection events using daily values. Any value that was not significant at p = 0.05 level was given a value of zero.

corresponded to specific humidity and 8-day average temperature. Low level moisture (Q700 and Q850) again appeared to be a key atmospheric indicator. Low level temperature was also a key indicator, although only when Ss and Sr events were separated (Fig 5.5).

Finally, for the local weather station data, the highest SI value of 0.29 was for the 4-day and daily total rainfall based on the data from station 3. Other stations and combination of stations were tried, but all had lower SI values. These indicators were similar to those for debris flows in Jaiswal and van Westen (2009). Intensity and duration indicators are not used, as hourly data were not available before 1998. Also, previous attempts using daily data showed all flash events were below the thresholds Eq 5.2 and Eq 5.3.

5.4.3 Probabilistic and static threshold

5.4.3.1 Weather station thresholds

Using daily and 4-day rainfall amounts, there was increasing chance of flash events with higher rainfall totals. The highest probability of a flash event was 17% when the daily total is above 80 mm and the 4-day above 96 mm (Fig 5.6). This is lower than the maximum probability found in the study by Berti et al. (2012) of 40-60%.

While Fig 5.6 seems reasonable (more precipitation, more likely for a flash event to occur), there are a few limitations. There are 9 days with

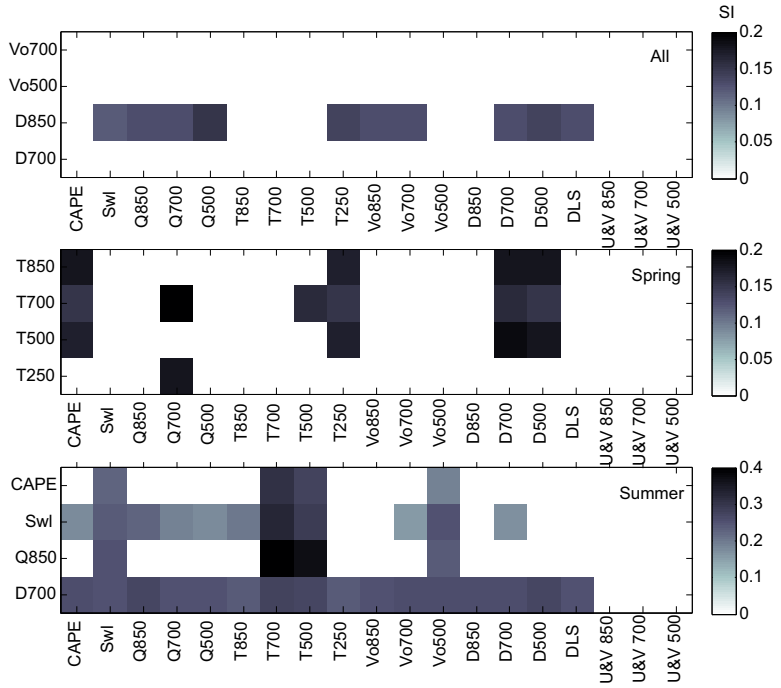

Figure 5.5 Top: The SI value for each pair of atmospheric indicators for all synoptic events using the daily value and the mean value over 10 days. Middle: The SI value for each pair of atmospheric indicators for the Ss events (3-day and 8-day average). Bottom: The SI value for each pair of atmospheric indicators for Sr using (daily value and 8-day average). Any value that was not significant was given a value of zero.

precipitation totals above 82 mm where no flash event was recorded and hence zero probability of flash occurrence. The lack of recorded events may have been because of low precipitation intensity, or the amount recorded by the rain gauge was much higher than for the rest of the study area. Spatial heterogeneity of rainfall may also be the reason why during the calibration period no precipitation was recorded for one flash event, and less than 10 mm for a further six flash events. From Fig 5.1, the affected torrents were in some instances more than 10km away from a rain gauge, which is especially problematic for localized convection where the precipitation is confined an area less than 10 km^2.

For the static threshold, the maximum MCC value during the calibration period, with at least 50% of events above the threshold, corresponded to the following Weather Station threshold ($Thres_{WS}$):

- $Thres_{WS}$: daily precipitation $>$ 20 mm and 4-day antecedent precipitation $>$ 22 mm

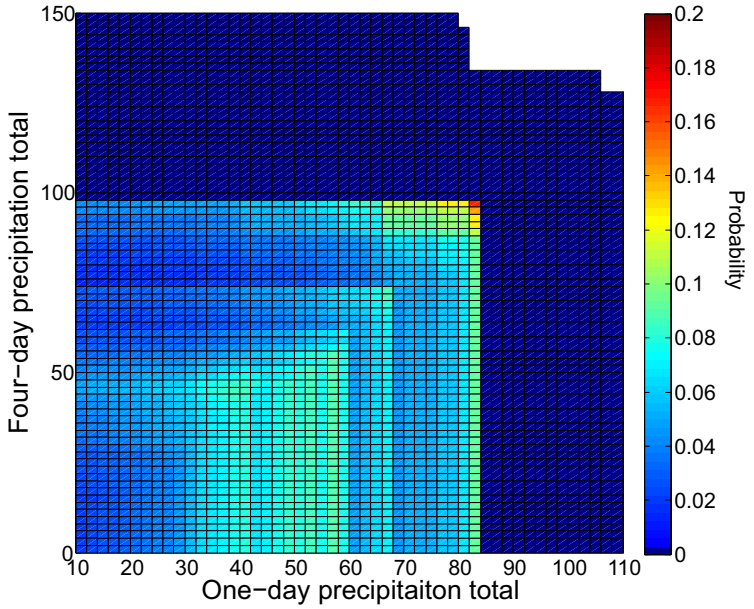

Figure 5.6 Probability of a flash event based on daily and 4-day precipitation totals from a local rain gauge. Dark blue indicates zero probability of occurrence.

The values for the static threshold are given in Table 5.3. Only 8.5% of the total number of days were above the $Thres_{WS}$ ((TP+FP)/(FN+TN)), while 55% of the flash events were above the $Thres_{WS}$ (TP/(TP+FN)). Somewhat surprisingly, 45% of the event days had less than 20 mm of rainfall. The percentage of the total number of days above $Thres_{WS}$ was slightly lower for the two validation periods (7.5% and 6.1% respectively), and the percentage of flash events drops even more (35.7% and 33.3% respectively). While the likelihood of a flash event still remains higher for days above the static threshold in the validation period, the drop in percentage of flash events above the threshold indicates differences in the triggering conditions between the calibration and validation periods. The torrents in which flash events occurred are generally closer to station 3 in the earlier validation period than the calibration period.

The results for the static threshold are comparable to those from other studies. Cepeda et al. (2010) found for the same study area that their threshold is exceeded on average 8.6 times per year, while 60% of debris flows are above the threshold (if including all debris flows between 1998 and 2010). While the percentage of correctly predicted events is similar, the percentage of false positives is only a third of the amount using Eq 5.4. The better performance of the rainfall threshold using hourly data from station 1 indicates that rainfall intensity is im-

Table 5.3 Results for the static threshold for the calibration period (1989-2003) and validation period 1 (1979-1988) and validation period 2 (2004-2010). The total number of days (TP+FN+FP+TN) is the same for the weather station and local convection. The number is lower for Ss and Sr, as they are only applied over spring and summer respectively.

	TP	FN	FP	TN	MCC
Weather station					
Calibration	16	13	412	5037	0.13
Validation 1	10	18	244	3381	0.10
Validation 2	2	4	145	2406	0.06
Local convection					
Calibration	15	5	332	5126	0.17
Validation 1	14	5	255	3397	0.18
Validation 2	4	1	171	2381	0.13
Synoptic -snowmelt					
Calibration	2	2	93	2198	0.10
Validation 1	1	2	105	1422	0.05
Validation 2	0	0	70	967	-
Synoptic -rainfall					
Calibration	3	2	193	2097	0.09
Validation 1	0	6	115	1409	0
Validation 2	0	1	60	1010	0

portant rather than daily amount. The daily total of 20 mm was in the range of Meyer et al. (2012), between 15–107 mm/day. The probability of static threshold exceedance was also similar to Meyer et al. (2012), whose threshold was exceeded between 0 and 77 days in a year (8.5% corresponds to 31 days a year).

5.4.3.2 Atmospheric thresholds: Local convection

Flash events during the summer and autumn period are more likely under high instability (CAPE) and high 700 hPa specific humidity (Fig 5.7). As both the instability of the atmosphere and low level moisture increase in Fig 5.7, the probability of a flash event also increases. The highest probability (100%) corresponds to CAPE values above 1100 J/kg and normalized Q700 greater than 1.45, although this was only observed once between 1989 and 2003.

For the static threshold, the maximum MCC value during the calibration period, corresponded to the following threshold ($Thres_L$):

- $Thres_L$: CAPE > 250 J/kg and normalized specific humidity at 700 hPa > 0.40

The confusion matrix results and MCC values are shown in Table 5.3. From this table it can be seen that 6.8% of the days are above $Thres_L$, compared with 75% of local convective flash events. In the validation periods, the percentage of days above $Thres_L$ rises to 7.8% (validation 1)

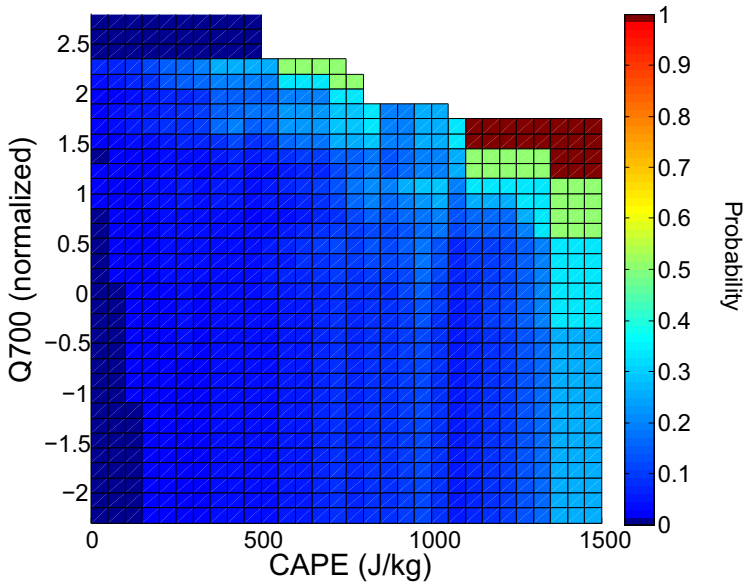

Figure 5.7 Probability of a local convection flash event based on atmospheric indicators CAPE and normalized specific humidity at 700 hPa (between 1989-2003).

and 7.3% (validation 2) and 71% and 80% for the local convection flash events.

Compared with the results in Sec 5.4.3.1, both the probability threshold and static thresholds perform better for the local convection than for the weather station threshold. In both validation periods, more flash events were above the $Thres_L$ than $Thres_{WS}$, with an even smaller number of FPs in the first validation period. Lower number of FP is important for early warning systems where the number of false alarms should be minimised.

While the CAPE value in $Thres_L$ was low for intense convection, similar limits have been found in other studies (e.g. for hail Niall and Walsh, 2005; Pistotnik et al., 2011, for heavy rainfall). Trapp et al. (2009) also found that availability of low level water vapour was a key component of changes in severe convection at mid-latitudes.

5.4.3.3 Atmospheric thresholds: Synoptic, spring

Figure 5.8 shows for Ss indicators, that with warmer 700 hPa temperatures and higher specific humidity the probability of flash event occurrence increases. Warm low to mid-level temperatures could be associated with melting of snow and high moisture levels could indicate rain. Fig-

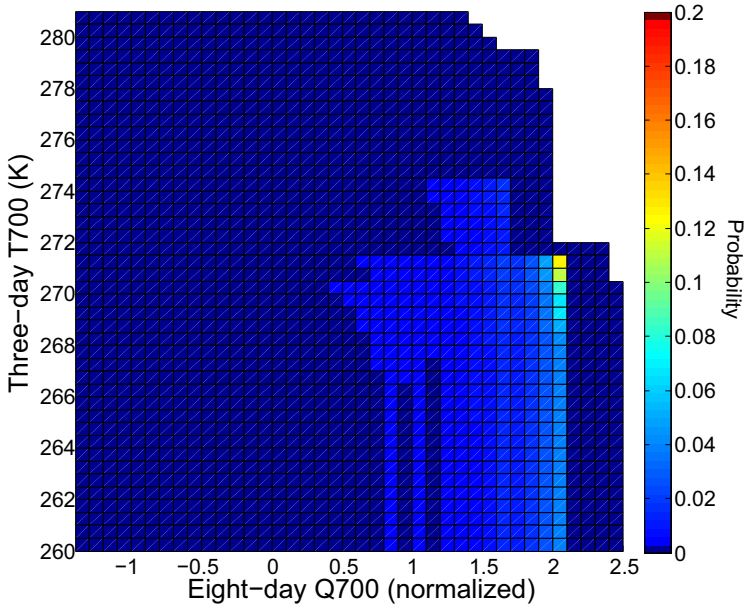

Figure 5.8 Probability of a flash event from spring synoptic rainfall based on 8-day mean specific humidity at 700 hPa and 3-day mean temperature at 700 hPa between 1989 and 2003.

ure 5.8 had similar probabilities of occurrence compared to $Thres_{WS}$, with the highest probability of occurrence of 12.5%. Similar to Fig 5.6, the most extreme days (days with the highest moisture and warmest temperature), were not associated with flash events.

Using the criteria in Sec 5.3.3 resulted in the following threshold ($Thres_{Ss}$):

- $Thres_{Ss}$:3-day mean temperature at 700 hPa > 271 K and 8-day mean normalized specific humidity at 700 hPa > 0.70

The values for the confusion matrix and MCC are in Table 5.3. Only 4.3% of days are above $Thres_{Ss}$, and 50% of the flash events. In the validation periods, the percentage of days above the threshold increased to 7.4% (validation 1) and 7.2% (validation 2), while only one of the three days in the first validation period was above the threshold. In the second validation period, there were no events in this category.

From $Thres_{Ss}$, if the 3-day average temperature at 700 hPa (lower troposphere) is above 271 K, then the majority of the study area would be at above freezing temperatures. While snow could still fall at the highest elevations, it is likely that it would rain in lower regions, and that any snow on the ground may melt. The second requirement of $Thres_{Ss}$, specific humidity at 700 hPa being higher than normal, also indicates possible rainfall. Therefore, $Thres_{Ss}$ indicated possible snowmelt and rainfall as triggers for flash events.

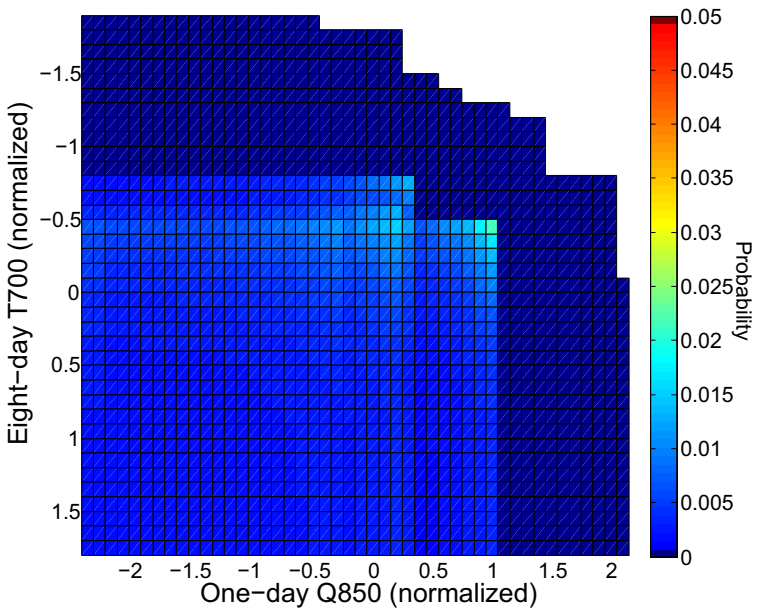

Figure 5.9 Probability of a flash event from summer synoptic rainfall based on 8-day mean temperature at 700 hPa and 3-day mean specific humidity at 850 hPa between 1989 and 2003. The y-axis is inverted to highlight that the figure represents the probability of a flash event given that T700 is less than the particular value and Q850 is greater than a particular value.

While both Fig 5.8 and $Thres_{Ss}$ made physical sense, the atmospheric threshold for synoptic-spring events did not perform well in the validation periods. This may have been due to the small number of events, and the number of indicators trying to capture the atmospheric triggering conditions.

5.4.3.4 Atmospheric thresholds: Synoptic, summer

Synoptic flash events in summer generally occurred with eight days of lower than normal temperature at 700 hPa, and increased specific humidity at 850 hPa (Fig 5.9). As Sr flash events are associated with colder temperatures, compared to warmer temperatures for Ss flash events, this explains why T700 does not have a significant SI value when Sr and Ss are grouped together (Sec 5.4.2). The probability of occurrence for this category was lower than any of the previous groups, with a maximum of 2%.

The Sr static threshold using the above atmospheric indicators corresponded to the following threshold ($Thres_{Sr}$):

- $Thres_{Sr}$: normalized specific humidity at 850 hPa > 0.15 and 8-day mean normalized temperature at 700 hPa < -0.40

The final group of values in Table 5.3 shows the performance of the above threshold. During the summer (July - November), 9.3% of days were above $Thres_{Sr}$, and 60% of synoptic summer flash events. However, the percentage of days above the threshold dropped in the two validation periods (8.1% and 5.9%), and no flash events were above the threshold.

Colder temperatures during a summer synoptic flash event are not unreasonable. Lower temperatures in summer may be associated with a front passing or cooler temperatures from prolonged cloud cover (and potentially rainfall). Similar to the other three atmospheric categories, high specific humidity indicated higher atmospheric moisture and more likely rain. However, $Thres_{Sr}$ was unsuccessful in the validation period. It could be that different synoptic conditions lead to flash events in the two validation periods, or that the events were misclassified.

5.4.3.5 General discussion

As with any empirical threshold, accuracy and completeness of the inventory and climate data are important. During the classification and subsequent threshold analysis, it is possible that flash events were misclassified. The spatial and temporal resolution of ERA-Interim was not fine enough to explicitly resolve convection. Therefore, parameterization schemes are used, with Dee et al. (2011) showing improvements in the convection parameterization from earlier reanalysis products. Furthermore, as CAPE values take into account instability over the depth of the troposphere, CAPE values may be underestimated when convection is confined to a shallow layer (Niall and Walsh, 2005). As found in Sec 5.4.1, it is likely that some events may have been misclassified as local convection or as synoptic.

The number of flash events limits the inferences that can be drawn from the results from this chapter. The difficulty of developing atmospheric thresholds with few calibration events was borne out with the synoptic thresholds failing to capture the synoptic flash events in the validation period. However, for the convective flash events, the atmospheric threshold still captured 75% events in the validation periods. Furthermore, grouping all 63 flash events together, the atmospheric threshold still performs better than the weather station, although by a smaller margin.

Atmospheric thresholds, like most empirical thresholds, are reliant on near-complete inventories, and only speculations can be made about what may happen under unobserved conditions. Therefore, these methods cannot completely replace physically based models and other threshold analysis techniques. However, for the Barcelonnette Basin where local convection appears to be the main meteorological trigger of flash events, the atmospheric threshold improves on the local rainfall threshold. This methodology therefore has a potential to work in other areas where rainfall observations are not available, or not complete enough for the traditional empirical rainfall threshold.

5.5 Summary and conclusions

The objective of this research was to develop empirical thresholds for rainfall triggered debris flows and flash floods using atmospheric indicators for the Barcelonnette Basin, France. Similar to rainfall thresholds, these thresholds could be used in risk assessment, early warning systems, or climate change-hazard studies. Using both atmospheric indicators and weather station data, two types of thresholds were obtained: a probabilistic threshold and a static threshold, based on classification statistics and specifically the MCC value. The main conclusions are as follows:

- In general the atmospheric indicators performed better than the weather station threshold (average MCC value of 0.16 compare with 0.10, and higher probability of occurrence). They also performed better than rainfall thresholds using hourly data.
- The most important atmospheric indicators were CAPE and specific humidity at 700 hPa. Both fit with convective precipitation being the main driver.
- Intense locally driven convection appears to be the main meteorological trigger for flash events in the study area (over 66% of events). Under these conditions, precipitation can be confined to a small area, and may explain why high precipitation amounts were not always recorded by the local weather stations.
- Even though the atmospheric thresholds performed better, there was still a high level of uncertainty in both the probabilistic thresholds and the static thresholds. This was especially true for the synoptic rainfall events.
- The number of observed events limits any statistical inference in the thresholds obtained, although this is partly mitigated using a validation dataset.
- The methodology needs to be trialled in other locations. It may be that in areas where there is a stronger relationship between the local weather stations and rainfall at the location of the flash events that intensity - duration thresholds are more suitable.

Assessing debris flow activity in a changing climate

6

This chapter is a modified version of Turkington et al. (2016). Duplications are removed, and parts of the supplementary material are included.

6.1 Introduction

Debris flows are a common mass movement hazard in mountainous areas, with extreme rainfall the most common trigger for fatal debris flows (Dowling and Santi, 2014), although snowmelt can also contribute in spring. For the Alps, the main trigger of debris flows is high intensity, short duration rainfall (Schneuwly-Bollschweiler and Stoffel, 2012; Stoffel et al., 2014; van den Heuvel et al., 2016). Under future climate change, it is likely that increases in extreme rainfall will alter debris flow frequency (Winter et al., 2010). A better understanding of how the frequency of debris flow days may change in the future is vital, especially for planning decisions in such mountainous environments, where often the settlements are located on alluvial fans.

Different meteorological proxies have been used for debris flow occurrence. Rainfall intensity-duration thresholds are often applied to determine minimum rainfall conditions under which debris flows may occur, and can be seen as a proxy for debris flow activity (Guzzetti et al., 2008; Nikolopoulos et al., 2014). However, while debris flows are often preceded by intense rainfall, capturing the rainfall in mountain catchments can be difficult due to the lack of rain gauges or poor coverage by weather radar in mountainous regions (Nikolopoulos et al., 2014; Pavlova et al., 2014). Therefore, other meteorological proxies for debris flow occurrence can account for deficiencies in precipitation records, either without (e.g. Turkington et al., 2014) or alongside rainfall (e.g. Paranunzio et al., 2016; Rulli et al., 2007). Temperature has been used where snow and thaw can contribute to debris flow occurrence (e.g. Paranunzio et al., 2016), or to distinguish between snow and rain (e.g. van den Heuvel et al., 2016). Previous work demonstrated that atmospheric variables, such as specific humidity (Q) combined with atmospheric instability through Convective Available Potential Energy (CAPE), can be used as proxies

for debris flow occurrence, especially for those triggered by intense convective rainfall unrecorded by a rain gauge (Turkington et al., 2014).

For future projections, General Circulation Models (GCMs) are considered primary tools for climate change impact studies (Kendon et al., 2010), for rainfall, humidity, as well as CAPE (Romps et al., 2014). Recent studies assessing the quality of GCMs have found that the models can replicate most of the changes in the historical climate (Brands et al., 2013; Sillmann et al., 2013). GCMs also replicate the observed increase in the annual daily maximum rainfall, an important parameter for debris flows, although the GCMs underestimate the rainfall magnitude (Asadieh and Krakauer, 2015). Furthermore, while GCMs provide the basis for future climate projections, model resolution is often at a much coarser scale than most debris flow source areas, restricting the use of GCM precipitation directly.

By downscaling the global projections using regional climate models (RCMs), changes in the relevant meteorological variables can be examined at a finer scale. This is especially important for mountainous regions where orographic processes are not always adequately captured in the global models. For the Alps, finer resolution climate models improved the spatial representation of precipitation compared to GCMs (Christensen et al., 2009), and simulate reasonably well mean and heavy precipitation (Rajczak et al., 2013). However, the projected changes in precipitation also depend on the driving GCM (Kjellström et al., 2011; Nikulin et al., 2011). Furthermore, RCMs at grid resolution 25-50 km are still coarser than cloud-resolving models, with biases remaining in precipitation (Rajczak et al., 2013). Therefore, the use of multiple RCMs in climate change-hazard studies is advised.

Previously, a limited number of climate change-hazard studies focused on debris flows, with inconsistent results. Changes in heavy summer precipitation is expected to reduce the number of debris flows in the Massif des Ecrins, France (Jomelli et al., 2009). For the Swiss Alps, Stoffel et al. (2014) also found a decrease in intense summer precipitation, although the authors discuss the possibility of unprecedented debris flows due to changes in stability of rock glaciers. Melchiorre and Frattini (2012), using changes in extreme precipitation from a variety of climate models, found a wide spread of future results and concluded that accurate quantification of changes in the number of debris flows was not possible.

This paper assesses future projected changes in debris flow activity in two European Alpine areas based on meteorological proxy, GCM, RCM, and Representative Concentration Pathways (RCPs) for the period 2010-2100. Although it is well established that numerous climate models and downscaling techniques are required for climate change-hazard studies (Déqué et al., 2012; Dobler et al., 2013), this chapter examines their contributions for debris flows specifically. Furthermore, this chapter examines the role of meteorological proxy on future debris flows using not only precipitation, but also CAPE combined with humidity, to capture instability and moisture needed to sustain deep convection. An ensemble

of 64 projections based on three RCMs, six driving GCMs, two RCPs, and two base periods (1950-1979 and 1980-2009), are used to compare future debris flow activity in the Barcelonnette Basin (France) and the Fella River Basin (Italy). An additional eight projections derived from CAPE and Q using four GCMs and two RCPs are also obtained. Ultimately, this work aims to determine the importance of choosing meteorological proxies in climate impact studies for debris flows.

6.2 Data and methodology

6.2.1 Study areas

To examine the role of meteorological proxies in assessing future debris flow activity, study areas need to have both long continuous precipitation records and sufficiently complete debris flow inventories. The two European alpine areas considered in this work fulfill these criteria: the Barcelonnette Basin, France and the Fella River Basin, Italy (Fig 2.1). Both have daily precipitation records covering 1950-2009, and were exposed to numerous documented debris flows (Barcelonnette: 99 over 66 days, Fella River: 335 over 24 days). The areas are known to have high intensity rainfall as primary trigger for debris flows, allowing for similar meteorological proxies to be used in both areas (Borga et al., 2007; Remaître and Malet, 2010). Sub-daily rainfall, although often a precursor for debris flows, was not considered due to the short available records and because daily rainfall totals are considered more reliably reproduced in climate models (Maraun et al., 2010). Further information on the study areas can be found in Chapter 1, with analysis of the climate data in Chapter 2.

6.2.2 Meteorological proxies for debris flows

Two meteorological proxies for debris flow activity (days with at least 1 debris flow) were considered: one using observed daily precipitation amounts (rain-proxy) and a second based on modeled CAPE and specific humidity at 750 hPa (QCAPE-proxy). The rain-proxy was chosen as precipitation is a dominant trigger of debris flows. As rain gauges are very local and often non-catchment representative, the QCAPE-proxy was used to mimic the mesoscale atmospheric conditions leading to heavy local convective precipitation. Turkington et al. (2014) showed that a QCAPE-based proxy could outperform daily precipitation and multiple day precipitation amounts as a proxy for debris flows in the Barcelonnette Basin. QCAPE-proxy was derived from ERA-Interim reanalysis dataset, for the period 1979-2011 (Dee et al., 2011). Mixed layer CAPE was calculated based on 18 levels from the reanalysis data of temperature, specific humidity, and geopotential height at 00, 06, 12 and 18 UTC as daily CAPE values were considered as insufficient to resolve deep convection (Romps et al., 2014).

For both daily proxies, a probabilistic approach (Berti et al., 2012) was applied to determine the relation between the meteorological event and debris flow activity. While many methods result in deterministic thresholds, a probabilistic approach has previously been proposed, due to other non-meteorological conditions triggering debris flows (Berti et al., 2012). From Bayes theorem, the conditional probability ($P(A|B)$) that one or more debris flows (debris flow day, A) occur due to a particular meteorological event (B), were derived using Eqs 3.5 and 3.6.

For the rain-proxy, the probability of a debris flow day was computed for six rainfall bins. The rainfall bins were allowed to differ between study areas as non-climatic factors, such as land cover or geology, make local proxy-debris flow relationships catchment dependent (Guzzetti et al., 2008). The probabilities were determined for summer (JJAS) and yearly to separate rainfall-only events from ones possibly influenced by snow and snowmelt. Long records of precipitation and debris flows allowed the rain-proxy to be computed for two base periods, 1950-1979 and 1980-2009. For QCAPE six bins were created based on a combination of CAPE and Q values, with bins bounded by the lowest and highest CAPE and Q values observed on a debris flow day. Based on ERA-interim data availability, QCAPE-proxy was computed for the base period 1980-2009. To test if the probability of debris flow days for both proxies was greater than chance, a Monte Carlo simulation was undertaken. 10,000 dummy debris flow datasets were randomly generated using the same number of dates as observed debris flow days, and the probability of a debris flow day in each bin was calculated. Any probability used in the proxy that was greater than 95% of the runs for a particular bin was assumed to be significant.

6.2.3 Future climate projections

To assess the impact of future climate on debris flow frequency, the choice of climate model and RCP were considered as potential uncertainties along with the choice of proxy and base period. Where possible, GCM models were selected based on their varying ability in representing climate extremes in the historical record (Sillmann et al., 2013), as well as differences in model genealogy (Knutti et al., 2013). For the rain-proxy, three RCMs in combination with two RCP scenarios (RCP4.5 and RCP8.5) driven by up to six GCMs were used for building an ensemble of 32 climate scenarios for period 2010-2099 from the EURO-CORDEX project (Jacob et al., 2014). The models selected are listed in Table 6.1.

For the QCAPE-proxy, four GCMs with RCP4.5 and RCP8.5 scenarios made an ensemble of eight climate scenarios (Taylor et al., 2011) as RCM data did not have sufficient information to assess CAPE accurately. The models are listed in Table 6.2. All the models have temperature and specific humidity available at six hour time steps with 20 or more vertical levels. The models were also used in another climate impact study assessing future changes in CAPE (Romps et al., 2014). For each GCM, RCP scenarios 4.5 and 8.5 were selected.

Table 6.1 Regional climate models and driving GCMs used for precipitation, including the resolution of the output (Res). The abbreviation for the RCM model is given in parentheses.

Modelling group	RCM model	Res.	Driving model	Driving model institute	RCP
SMHI	SMHI-RCA4 (SM)	0.44°	CanESM2	Canadian Centre for Climate Modelling and Analysis	4.5,8.5
			EC-EARTH	EC-EARTH consortium published at Irish Centre for High-End Computing	4.5,8.5
			IPSL_CM5A - MR	Institut Pierre-Simon Laplace	4.5,8.5
			CNRM-CM5	Centre National de Recherches Météorologiques / Centre Européen de Recherche et de Formation Avancée en Calcul Scientifique	4.5,8.5
			GFDL-ESM2M	Geophysical Fluid Dynamics Laboratory	4.5,8.5
			MPI-ESM-LR	Max-Planck Institute for Meteorology	4.5,8.5
DMI	DMI-HIRHAM5 (DM)	0.44°	EC-EARTH	EC-EARTH consortium published at Irish Centre for High-End Computing	4.5,8.5
KNMI	KNMI_RACMO22E (KN)	0.44°			4.5,8.5

Table 6.2 CMIP5 GCM models used for CAPE- based proxies

Model institute	GCM Model	Resolution (longitude x latitude)	Vertical levels	RCP
Canadian Centre for Climate Modelling and Analysis	CanESM2	128x64	35	4.5,8.5
Centre National de Recherches Météorologiques	CNRM-CM5	256x128	31	4.5,8.5
Geophysical Fluid Dynamics Laboratory	GFDL-ESM2M	144x90	24	4.5,8.5
Institut Pierre-Simon Laplace	IPSL	144x143	39	4.5,8.5

For realistic climate change scenarios, both RCM and GCM data have to be corrected for biases (Gudmundsson et al., 2012). Quantile-mapping was applied based on Themeβl et al. (2012). Empirical cumulative distribution functions (CDFs) of climate models were mapped to the CDFs from the observed data for each month of the year over 1950 to 2009 for the rain-proxy and 1980-2009 for the QCAPE-proxy. Bias-correction was applied to the RCM data for the rain-proxy. For the QCAPE-proxy, the calculated CAPE values were corrected for biases, rather than the individual temperature and humidity profiles. Two sizes of the area for quantile mapping are assessed for its impact on future debris-flow days: 0.5°x0.5° and 2.0°x2.0°. The debris flow day frequency based on GCM and RCM datasets was calculated based on the yearly probability computations as described in Sec 6.2.2.

6.3 Results

Bias-corrected climate change projections for two meteorological proxies, rain-proxy and QCAPE-proxy (Sec 6.3.1) were used as basis for future projections of frequency of debris flow days (Sec 6.3.2).

6.3.1 Meteorological proxies for debris flows

Using the rain-proxy, the probability of debris flow days generally increased with higher daily rainfall totals for both base periods and in both regions (Fig 6.1 and Table D.1). The probability of a debris flow days was significant for all rain-proxy bins except for the lowest rainfall bin and the second lowest rainfall bin for the Fella River Basin (Table D.5). In the Barcelonnette Basin the highest yearly probability (43.5%) was associated with the second highest rainfall bin (40-50 mm) for the base period 1980-2009 and not with the highest observed rainfall. The probability of a debris flow day for each of the rainfall bins in summer was also always equal or higher than the probability over all seasons. The higher absolute number of debris flow days (Table D.2) observed in the later base period explains the higher probability associated with certain rain-proxies in Fig 6.1. For the Fella River Basin, the second base period had 17 more debris flow days than the first base period. The increase in debris flow days was partly due to changes in precipitation, as using the first base period rain-proxy, 0.4 more debris flow days would be expected in 1980-2009, or an increase of 2.1 days using the second base period rain-proxy. Between 1950 and 1979 the Fella River Basin did not record rainfall over 150 mm, while two large rainfall events in 1996 (192 mm) and 2003 (354 mm) triggered more than 200 debris flows, explaining non-values in last bin for first base period and over 66.7% probability for the second base period. For the Barcelonnette Basin, the first base period rain-proxy predicts a decrease of 2.5 debris flow days between 1950-1979 and 1980-2009, and 7 days for the second period rain-proxy. The predicted decrease in debris flow days between 1950-1979 and 1980-

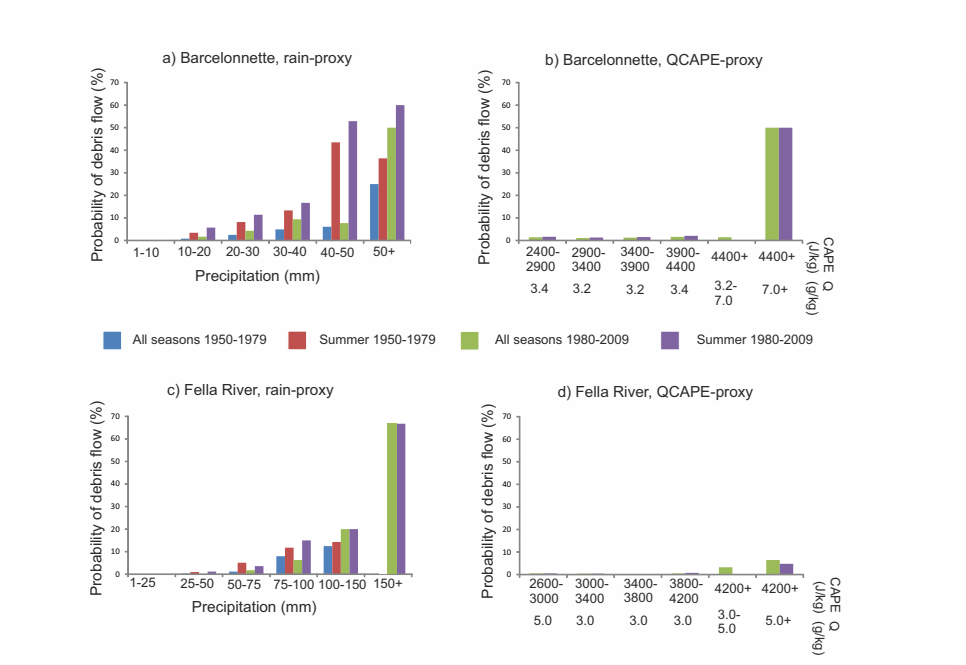

Figure 6.1 Probability of a debris flow day for the rain-proxy (left) and QCAPE-proxy (right)

2009 contrasts the observed increase of 32 debris flow days during the same period.

For the QCAPE-proxy, CAPE values over 4400 J/kg in combination with high humidity values (>7.0 g/kg) had the highest probability for debris flow days in the Barcelonnette Basin, while the values for the Fella River Basin were over 4200 J/kg and 5.0g/kg (Fig 6.1 and Table D.3). The probability of a debris flow day was significant for all QCAPE proxy bins for the Barcelonnette Basin, although only for the two highest and second lowest bin for the Fella River Basin (Table D.5). The summer debris flows were all associated with high humidity, while spring and autumn debris flows occurred under lower humidity conditions. The QCAPE-proxy did not perform as well for the Fella River Basin as for the Barcelonnette Basin, due to the lower probability of debris flow days for the highest QCAPE bins.

6.3.2 Future debris flow frequency

6.3.2.1 Rain-proxy based debris flow projections

Using the rain-proxy, the number of debris flow days increased in most future projections compared to the period 1950-1979 for both the Barcelonnette and Fella River basins during the 20th and 21st century (Fig

6.2a). For the Barcelonnette Basin, the mean relative trend of debris flow days from all projections is 2.4% per decade (%d^{-1}) for the period 1950-2099. Most projections (48 out of 64) showed a small positive trend (1-5%d^{-1}), whereas 5 projections showed a larger positive trend (5-6.2%d^{-1}) and 11 have no trend (less than 1%d^{-1}). For the Fella River basin, the future projections had an even larger increase of 4.6%d-1 for 1951-2099. Here, 28 out of 64 projections increased between 5.0 and 11.4%d^{-1}, while 32 projections showed an increase in the number of debris flow days between 1 and 5%d^{-1} and 4 had no trend (less than 1%d^{-1}).

For the Barcelonnette Basin, the relative future trend in debris flow days was most sensitive to the base period and the driving GCM or RCM, rather than the area for quantile mapping or RCP (Fig 6.2). The base period used (1950-1979 or 1980-2009) for the rain-proxy significantly affected the relative increase in the number of debris flow days (Fig 6.2c). The first base period had a greater trend (3.0%d^{-1}) compared to the second base period (1.7%d^{-1}). However, based on Table D.2, the absolute number of debris flow days would be smaller in the future using the earlier base period (21.6 debris flow days for 2070-2099, compared with 56.5 debris flow days for 2070-2099 using the second base period). Of less importance was whether a larger area of 2°x2°, similar to GCM grid-size, or a reduced area of 0.5°x0.5° was used for quantile mapping. The larger area led to an increase in debris flow days of 2.8%d^{-1}, compared to 2.0°%d^{-1} for the reduced area (Fig 6.2b). Based on the two-sample Kolmogorov-Smirnov test (Massey, 1951), the two groups were not significantly different at the 5% significance level. When comparing RCPs, the average trend was 2.4%d^{-1} for both RCPs (Fig 6.2d). The trend for the RCP depended on the driving GCMs; the driving GCM MPI-ESM-LR had a larger positive trend under RCP8.5, where EC-EARTH had a less pronounced trend under RCP8.5. Looking at projections using RCM SHMI-RCA4 driven by different GCMs (Fig 6.2e), the mean increase in number of debris flow days was highest using CNRM-CM5 (orange, 4.9%d^{-1}), and was significantly higher than the other five groups (1.7-2.9%d^{-1}). The projections by three RCMs driven by EC-EARTH differed by the end of 21st century, with the DMI-HIRHAM5 RCM showing a significantly smaller increase than with the other two RCMs (Fig 6.2f).

For the Fella River Basin, the range in projected relative number of debris flow days based on the rain-proxy was considerable larger than the Barcelonnette Basin by 2100 (Fig 6.2). Additionally, the factors impacting the future trend were different. For the Fella River Basin, the relative trend was most sensitive to the base period and the RCP scenario, and not to the choice of RCM or GCM. The different base periods resulted in a significantly different average trend of 5.2%d^{-1} for 1950-1979 and 3.9%$d^{-1}$for 1980-2009 (Fig 6.2c). The stronger trend using 1950-1979 was partly due to the lower absolute number of debris flow days in this period (Table D.2). The difference between base periods is largest using GCM EC-EARTH model, with a more than doubling of the trend depending on the base period for both RCPs. This was in line with the general trend, where the average increase in number debris flow days was significantly

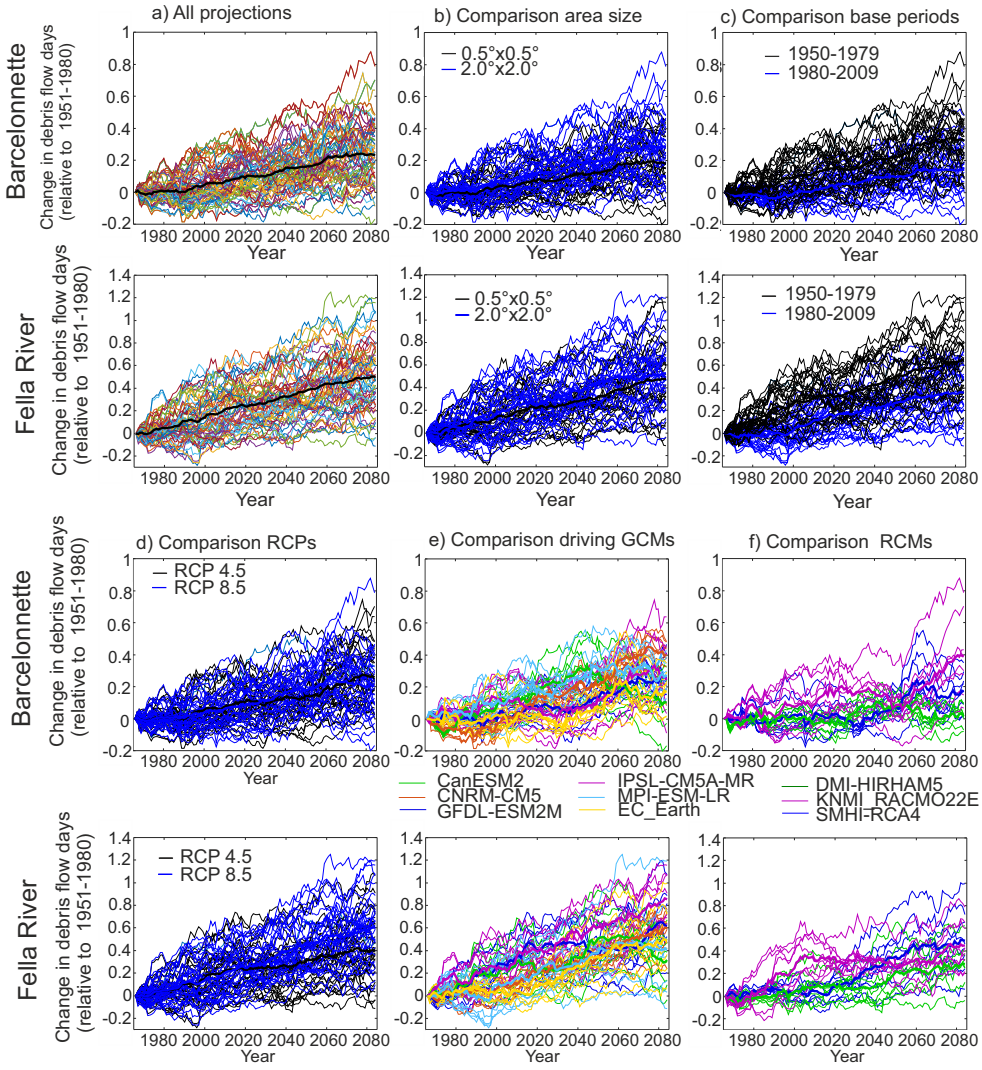

Figure 6.2 Change in number of debris flow days using rain-proxy, for all projections (a, with mean projection in black), and b, c, d, and e plot projections for comparison, with d, only using RCM SMHI-RCA4 and for e, only the EC-EARTH GCM was used (bold line indicates mean projection)

greater under RCP8.5 (5.6%d^{-1}) than RCP4.5 (3.5%d^{-1}) as seen in Fig 6.2d. The area for quantile mapping did not result in two significantly different groups; trends of 5.0%d^{-1} for 2°x2° area and 4.1%d^{-1} for 0.5°x0.5° area, respectively (Fig 6.2b). For the GCMs driving RCM SHMI-RCA4, the trend varied between 4.0%d^{-1} (CanESM2) and 6.8%d^{-1} (IPSL-CM5A-MR) (Fig 6.2e). Similarly, the RCM choice was of less importance to the relative trend, with no significant differences between the three RCM models (Fig 6.2f).

6.3.2.2 QCAPE-proxy based debris flow projections

For both study areas, the QCAPE-proxy showed a significantly smaller increase in future debris flow days than the rain-proxy projections, 0.3%d^{-1} against 3.6%d^{-1} for the rain-proxy for the Barcelonnette Basin (Fig 6.3a) and 1.2%d^{-1} for the Fella River Basin compared with 4.1%d^{-1} using the rain-proxy (Fig 6.3b). However, mean QCAPE-proxy projections were based on fewer scenarios than the rain-proxy (8 versus 32) due to absence of two base periods and lack of RCM projections. Therefore, Figs 6.3c, d, e, and f compare directly projections from the same GCM using QCAPE-proxy and rain-proxy for both RCP scenarios.

For the Barcelonnette Basin, most QCAPE-proxy projections showed similar changes in debris flow days compared to rain-proxy, but of smaller magnitude. For CanESM2, the QCAPE and rain-proxies were most in line with each other: all projections are in the range of 1.8-4.4%d^{-1}. CNRM-CM5 projections both had the largest increase in debris flow days for both proxies. Using GFDL-ESM2M, the QCAPE-proxy found a decrease to no change whereas the rain-proxy found an increase in debris flow activity. QCAPE-proxy for IPSL_C5A-MR RCP8.5 had the largest overall decrease in debris flow days of 1.4%d^{-1}.

For the Fella River Basin, generally the QCAPE-proxy projections showed a similar change as the rain-based proxy, although the CanESM2 QCAPE-proxy increased more than the rain-proxy, while for all other GCMs, the rain-proxy had a larger increase. Using GFDL-ESM2M, the QCAPE-proxy projections showed an earlier onset of decrease in debris flow days, resulting in an average decrease of 1.1-2.7%d^{-1} . The largest increase in debris flow days was based on the CanESM2 GCM, with an increase of 4.0 and 5.2%d^{-1} for RCP 4.5 and 8.5 respectively.

6.4 Discussion and conclusion

Using the rain-proxy results in a higher future debris flow activity compared to the QCAPE-proxy. Both proxies show an increase in the probability of debris flow days with increasing values: a general increase using observed daily precipitation, where the QCAPE-proxy provides a clear threshold above which debris flows are more likely. The differences may be due to the proxies being associated with different atmospheric conditions. The QCAPE-proxy is representative of short-lasting convective rainfall systems existing in a mesoscale humid environment triggering

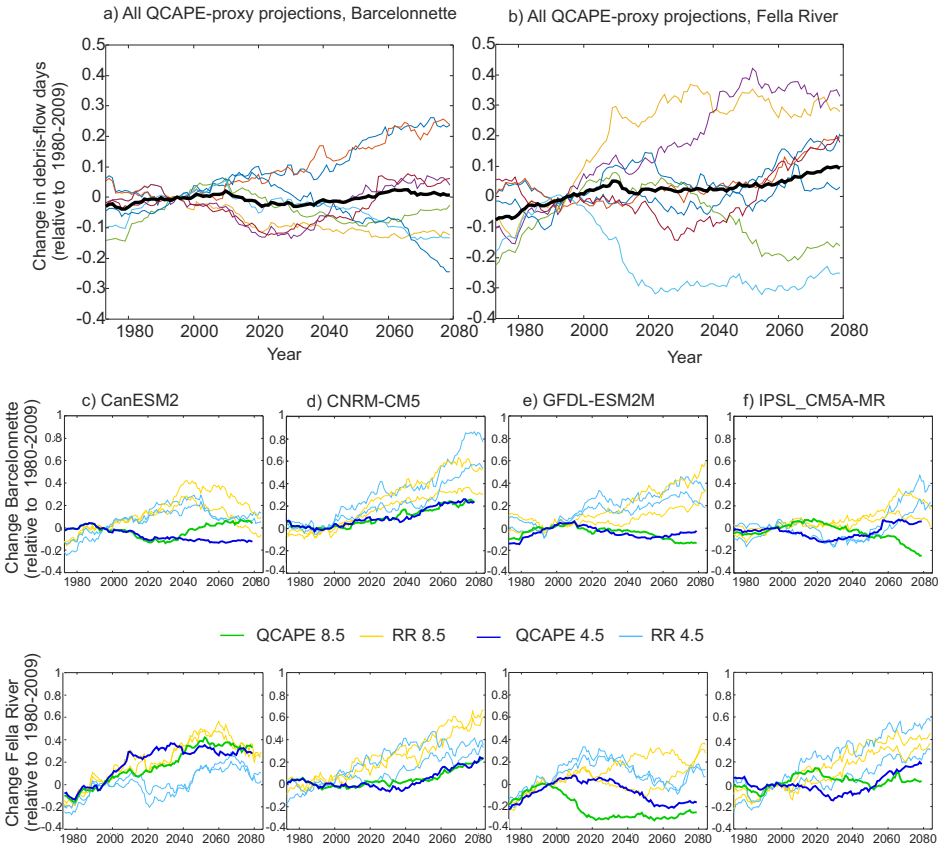

Figure 6.3 Change in debris flow days using QCAPE-proxy a) and b) with the mean change in debris flow days is in black, c-f compare each of the QCAPE-proxy projections with the rain-proxy projections from the same GCM, where the projection using RCP 4.5 is in green (QCAPE-proxy) and yellow (rain-proxy), and using RCP 8.5 in dark blue (QCAPE-proxy) and light blue (rain-proxy)

debris flows (Turkington et al., 2014). The rain-proxy includes all synoptic conditions producing sufficient rainfall to trigger a debris flow as it is based on observational records. These conditions range from slow moving low pressure systems causing multiple days of rain to short duration convection cells. For the Barcelonnette Basin, high QCAPE values have as high a probability as the highest rain-proxy values, which suggests that QCAPE-proxy might serve here as an alternative for rain-based projections. The QCAPE associated probability is lower for the Fella River Basin (6%) compared to the Barcelonnette Basin (50%) and to the rain-proxy (67%). Likely, in the Fella River Basin, atmospheric instability and specific humidity at 750hPa are not able to separate well the convective events that may or may not trigger debris flows.

In both areas, the absolute increase in number of future debris-flow

days is greater using the more recent base period, under the assumption that the relationship between debris flows and proxies is constant. However, the relationship has apparently changed from 1950-1979 to 1980-2009, as the number of debris-flow days increased more than predicted by the same rain-proxies in both study areas. Reasons for lower probabilities for the base period 1950-1979 versus 1980-2009 include underreporting of events in the earlier period, or non-climatic changes, along with past climate change. Historically, European landslide inventories are thought to become stable from 1970 onwards (Wood et al., 2015), and observed changes in debris flows may have been dominated by human mitigation factors (Crozier, 2010). Another factor that may alter the proxy-debris flow relationship is changes in sub-daily precipitation intensity, as the same amount of precipitation over a shorter period of time is more likely to trigger a debris flow (e.g. Guzzetti et al., 2008). As a non-climatic actor, changes in sediment availability might impact the relationship between a proxy and debris flows as changes in permafrost resulted in unprecedented debris flows (Stoffel et al., 2014). Additional factors, such as the role of snowmelt and future mitigation works, are not taken into account in this work.

The area for quantile mapping had a smaller effect on debris flow frequency than base period. Generally the internal variability in the climate has a larger contribution to the climate signal on smaller scales (Hawkins and Sutton, 2011), and may be the reason why the 2°x2° area for quantile mapping shows a slightly larger increase in debris flow days for both study areas. Although a larger area may not be as representative of local changes, such as in the Barcelonnette Basin, which is drier than the surrounding area.

The results here demonstrate that a probabilistic approach in combination with quantile mapping is capable of translating climate change scenarios into future debris flow activity. The projections displayed a wide range of results for future debris flow frequency, similar the findings of Melchiorre and Frattini (2012). Projected changes in the number of debris flow days however cannot be used directly in hazard and risk assessments, as they require a relation between the frequency of occurrence and the spatial distribution of debris flow intensities. To convert the results into useful hazard data would require more detailed information about the change in magnitude of debris flow events, which was not considered and is an avenue for future work in both study areas.

In this study, future climate projections are translated into future debris flow activity for two Alpine catchments. All projections show either an increase or little change in the number of days with debris flows, where the increase is greater for the Fella River Basin (QCAPE-proxy: $1.2\%d^{-1}$, rain-proxy: $4.6\%d^{-1}$), compared to the Barcelonnette Basin (QCAPE-proxy: $0.3\%d^{-1}$, rain-proxy: $2.4\%d^{-1}$). The projections depend strongly on the base period and proxy used, and to a lesser extent GCM, RCM, RCP, and area for quantile mapping. Therefore the base period and proxy used should be carefully considered when developing future projections of debris flow activity.

7 A new flood type classification method for use in climate change-hazard studies

This chapter has been submitted as: Turkington, T., Breinl, K., Ettema, J., Alkema, D., and Jetten, V. (under review)A new flood type classification method for use in climate change impact studies, with minor modifications

7.1 Introduction

Climate change will alter flooding around the globe, and therefore an increasing number of studies are modelling the impact of climate change on floods, with the focus generally on changing flood magnitude and frequency (Booij, 2005; Gain et al., 2013; Raff et al., 2009). However, future projections of the meteorological triggers, including heavy precipitation and snowmelt, may change differently and alter the characteristics of the flood events (Hall et al., 2014). As a result, factors associated with the causal type of flood such as seasonality and triggering conditions should be addressed next to the change in frequency or magnitude of floods. Classifying flood events into different types can place flooding into a wider climate context and help with exploring changes in future flood events. Changes in flood types will have implications on both the local social and ecological systems and are therefore important to consider when assessing future changes in flooding (Gain et al., 2013; Garner et al., 2015).

Flood types can be distinguished based on the meteorological conditions of a flood event, such as amount and distribution of precipitation, as well as antecedent conditions, such as snow depth and soil moisture. Nied et al. (2014) identify three different approaches to describe flood events: (1) based on the flood event description, (2) linking the flood with atmospheric circulation patterns, and (3) classification into flood types. The first category describing the specific flood events covers studies with a detailed examination of a particular event (e.g. the Danube flood in 2013 Blöschl et al. (2013), the Mississippi River flood in 1993 Kunkel et al. (1994), and the Himalayan flood in 2013 Dube et al. (2014)). The

second approach uses coarse scale atmospheric circulation patterns to identify similar atmospheric triggering conditions that are linked with the probability of flood occurrence (e.g. Bárdossy and Filiz, 2005; Delgado et al., 2014; Pattison and Lane, 2012; Prudhomme and Genevier, 2011). In the final approach, individual flood events are clustered into different categories based on generating processes of the events (e.g. Gaál et al., 2012; Merz and Blöschl, 2008; Viglione et al., 2010).

Of the three approaches for identifying flood types, the applicability of the method depends on the purpose. The description of flood events allows for a singular flood event to be examined, without necessarily a long record of events. However, the variables considered vary between case studies, in part due to different data availability, making it difficult to compare between case studies (Nied et al., 2014). Widely applied classification based on atmospheric conditions is hampered due to the small number of actual flood events relative to the overall number of days (Nied et al., 2014; Prudhomme and Genevier, 2011), particularly on the local or regional scale where maybe only a handful of observed flood events occurred over the past 100 years. Both the second and third categories have the potential to be used in climate change-hazard studies, provided there are sufficient flood events, and that climate models are able to reproduce the necessary atmospheric variables. Even with long complete records, a relationship between flood events and coarse scale atmospheric circulations cannot be determined in many cases. Therefore, the classification approach (approach 3) will be applied here, as the characteristics of the flood events are of concern in assessing the impact of climate change on flood types.

The variety of approaches to cluster flood events leads to different flood types. The approach to cluster flood events depends on the region and triggering conditions as well as the data available. Merz and Blöschl (2003) clustered flood types manually allowing a combination of different sources of information to be used. They classified the flood events into five types: flash floods, short rain, long rain, rain-on-snow, and snowmelt floods. Nied et al. (2014) used the previous classification of five flood types, and then compared the soil moisture and atmospheric circulation patterns between flood types, highlighting the importance of antecedent conditions for the different flood types. Alila and Mtiraoui (2002) clustered flood events based on ENSO, storms (monsoonal storms, frontal storms and dissipating tropical cyclones), with either two or three clusters for each classification for south-east and central Arizona in the USA. Viglione et al. (2010) included catchment excess rainfall as part of the flood response for different flood types in the Kamp catchment, Austria, while Gaál et al. (2012) clustered different Austrian catchments including the month when it occurred. In each of these studies, to obtain sufficient number of flood events, either less severe flood events were included or a large study area was defined, incorporating discharge measurements from multiple locations a catchment or catchments. Therefore, we introduce the use of a weather generator in combination with conceptual rainfall-runoff model to generate long time series of discharge to

classify flood types.

Little research has been done on how causal flood types explicitly will change in the future, while recent literature provides evidence that flood types will change along with potential indicators to use in classifications. Arnell and Gosling (2014) found decreases in magnitude of spring floods for central Europe as a result of smaller discharge peaks from rainfall than the previously snowmelt-generated ones. Possible future changes in flood seasonality have also been identified in Switzerland due to changes in rainfall, snow accumulation, and snowmelt (Köplin et al., 2014). Current trends in rain-on-snow floods in the western United States have a range of significant increasing and decreasing trends (McCabe et al., 2007). In the future, parts of the same area are expected to shift from snow dominated winters to rain dominated winters (Nolin and Daly, 2006). An increase of high temperature and heavy rainfall in Norway also indicates an increase in winter/spring snowmelt floods (Benestad and Haugen, 2007; Vormoor et al., 2015). While none of these studies considered changing flood types explicitly, they demonstrate that changes in precipitation, both rainfall and snowfall and melt have the potential to alter flood types in a catchment.

This paper presents a methodology developed to classify flood types particularly for use in climate change-hazard studies as it creates and analyses long records (meteorological and flood events). To obtain sufficiently long records of flood events for objective flood type classification, a multi-site weather generator is coupled with the HBV rainfall-runoff model. The flood events are extracted from the resulting 1200 years of generated data, where a flood is defined as days with discharge that could potentially lead to flood situations. In particular the discharge levels corresponded to the 2 (bank full flow), 10, and 25 year return periods, with longer return periods were not considered in order to limit spurious extrapolations. The flood events are separated into different flood types based on extreme meteorological triggering conditions and flood timing (Sec 7.2). To illustrate the developed methodology, two European catchments are used as test sites with different sizes and dominant flood types (Sec 7.3 and 7.4). In this chapter we apply the methodology to future climate projections and on the past climate (Sec 7.5), allowing new flood types to be identified that were absent in the past. Four different climate projections are analysed for each catchment for the period 2070 -2099 to demonstrate how changes in the future climate may alter flood types in the future. Sections 7.6 and 7.7 discuss and conclude the findings.

7.2 Method

In any classification method, a sufficient number of events is required to allow for clustering. In the case of flood events within a single catchment there are often only a handful of events. While other studies work around this through the using multiple catchments, this paper aims

to classify the flood types within a catchment by producing synthetic data based on observational records. Long time series of meteorological and hydrological data is generated using a combination of a weather generator (Sec 7.2.1) and model of discharge (Sec 7.2.2). Once this synthetic time series is generated for past and future climate, clustering of different flood types can be done (Sec 7.2.3). A flow diagram of the method is contained in the appendix (E.1).

7.2.1 Weather generator

The semi-parametric daily-multisite weather generator from Breinl et al. (2014) was utilized to generate long time series of daily temperature and precipitation values to serve as input for the rainfall-runoff model. The multi-site precipitation algorithm uses a univariate Markov process to represent sequences of daily snapshot of precipitation amounts for multiple point locations within the catchment. The weather generator was used in a so-called Reduced State Space setup (see Breinl, 2016; Breinl et al., 2014) to reduce the duplication of observed precipitation sequences. Precipitation amounts were generated by pure resampling of observations, instead of using parametric distribution functions for precipitation amounts as applied in Breinl et al. (2014). Parametric distributions were not applied due to the complexity of altering compound distributions under future climate scenarios. For the temperature, mean daily temperature was generated by autoregressive-moving-average processes (ARMA). The weather generator was set up monthly to account for seasonality of precipitation and temperature. In total, 1200 years of daily temperature and precipitation were generated to drive the conceptual rainfall-runoff model (see Sec 7.2.2) for the observed period, as well as for each of the selected future climate projections.

The multi-site weather generator has been successfully applied for the historical period in Alpine catchments by Breinl (2016). It was found that the weather generator handles the spatial variability of precipitation between rain gauges well, with a slight tendency to underestimate extreme dry spells, which is a well-known issue of Markov based weather generation algorithms. The mean number of dry and wet days were well simulated.

To generate future projections of precipitation, the time series of the resampled observational period values were first generated by the weather generator and then the values replaced with the projected precipitation amounts by reshuffling to maintain temporal and inter-site statistics. Future temperature projections were generated by adding the projected monthly mean temperature shift to the observations, a common technique in climate change-hazard studies (e.g. Steinschneider and Brown, 2013; Tao and Zhang, 2011). These generated time series are fed to the HBV model to simulate future discharge.

7.2.2 HBV model

The conceptual HBV rainfall-runoff model was used to model historical and future discharge based on observational records and future climate model data (Bergström, 1976). The HBV model was selected as it represents the main runoff generating processes, and due to the low computational costs, it can be used to generate discharge time series longer than 1000 years. The model has also been used in numerous previous studies (e.g. Booij, 2005; Das et al., 2008; Gao et al., 2012; Steele-Dunne et al., 2008). For this study, the HBV-light model (version 4.0.0.6) from Seibert and Vis (2012) was applied. The model was used in a semi-distributed setup, with a single catchment sliced into ten elevation zones for distributed snow modelling a well as three groundwater boxes. The HBV-light model uses time series of daily precipitation, daily mean temperature, and daily discharge data for calibration. For historical period, multi-site precipitation from the weather generator in Sec 7.2.1 was averaged through Thiessen polygons, which turned out to be sufficient compared to other methods such as Kriging with external drift (Breinl, 2016). The potential monthly evaporation was calculated after Thornthwaite (1948), as has been used in previous studies in combination with the HBV model (e.g. Bergström et al., 2001; Akhtar et al., 2008; Timalsina et al., 2015).

The HBV model was calibrated and validated based on 20 years of observed temperature, precipitation, and discharge as a 20 year period has been assessed to be sufficient length for use in climate change-hazard studies (Vaze et al., 2010). Further details on the calibration and validation process as well as the model performance in both catchments can be taken from Breinl (2016). After model calibration, synthetic discharge (1200 years) was generated by feeding the temperature and precipitation time series from the weather generator in Sec 7.2.1 into the HBV model. This was done for both the past and future periods. As different magnitude flood events may have differences in flood type characteristics, three discharge magnitudes were used. These were based on the 2 (bank full), 10, and 25 year return period amounts (Q2, Q10, Q25) and were calculated empirically based on the annual maximum daily discharge values.

7.2.3 Classification: Flood types

The two most important considerations in clustering flood types are the selection of meteorological indices, and how to cluster the flood events based on these indicators. Flood types in mountainous catchments include different combinations of intense-short-duration rainfall, high antecedent rainfall decreasing catchment storage, and snow cover and melt (Merz and Blöschl, 2008). The clusters should reflect these types, and therefore indicators should be able to capture differences.

The indicators representing four different components of flood generation were: 1) short (daily) duration precipitation, 2) antecedent pre-

cipitation over two or more days preceding the flood event, 3) daily and antecedent temperature, both absolute values and normalized temperature values based on time of year, and 4) day of the year (DOY). The precise antecedent precipitation and temperature indicators were selected based on their correlation with daily discharge. The period of antecedent precipitation that had the highest correlation with discharge was selected, varying the period from 2 to 60 days before the flood. Temperature in combination with precipitation may identify rainfall as opposed to snowfall, while warm spring temperatures indicate snowmelt, and high temperatures in summer and autumn the possibility of convective precipitation. DOY could indicate possible snow cover and snowmelt, or other seasonally varying phenomena. For temperature, the period was allowed to vary from 1 to 60 days, using both absolute and normalized values due to the strong seasonal signal. Temperature was normalized (T_{mn}) on a daily basis using:

$$T_{mn} = \frac{T_m - \bar{T}_m}{s} \tag{7.1}$$

where $T_m$is the daily mean temperature, $\bar{T}_m$ is the average daily mean temperature for all values for the same day of the year, and s is the standard deviation for all values for the same day of the year.

To cluster the flood events into different types the indicators were analysed by k-means clustering. K-means clustering is an unsupervised clustering technique that separates events or variables into different groups. Previous uses include classification of groups of catchments with similar precipitation and flood regimes (Parajka et al., 2010), as well as classifying atmospheric circulation patterns (Huth et al., 2008). The iterative process groups each event into the cluster with the closest centroid, after which the centroid is recalculated based on the mean values of all the events in the cluster. The flood types were clustered for each return period (Q2, Q10 and Q25) using two to all four indicators.

The silhouette index (SI, Rousseeuw (1987)) was used to evaluate the quality of the flood type clusters and determine the final number of clusters. The SI for each cluster can be calculated using:

$$SI = \frac{1}{n_c} \sum_{i=1}^{n_c} \frac{b_i - a_i}{max(a_i, b_i)} \tag{7.2}$$

where n_c is the number of flood events in cluster, b_i is the average Euclidean distance between an observation i and all observations in the next closest cluster, and a_i is the average Euclidean distance between i and all other flood events in the same cluster. SI values vary between 1 and -1, with positive values when they are likely to be correctly classified, negative when the likely belong in another cluster, or near zero for no particular cluster.

The final flood type classification was selected based on the classification with the highest average *SI* value from 7.2. It is possible that particular flood types are not observed at all return periods, or there may not be a clear distinction between the more frequent flood types. Therefore, for each study area the final flood type cluster indicators and number of clusters/types were allowed to vary between return periods.

Two different approaches were applied to assess how the flood types may change in the future. For both approaches, 1200 years of future discharge were generated using weather generator enforced by the future climate projections for temperature and precipitation and the HBV model. The first approach was to detect changes in the distribution of historical flood types as a change in dominant flood type may have an impact on the vulnerability or exposure of an area to flooding. To assess the change in distribution, the flood events (Q2, Q10, Q25) were identified based on the historical discharge amounts, allowing the relative change in flood frequency to be calculated. The future flood events were placed in the closest historical cluster. A change in the distribution of flood events between the clusters indicates possible changes in the dominant flood type or types in the future.

The second approach repeated the flood type classification using future discharge to allow for new flood types to emerge. To maintain the same number of flood events for clustering, the discharge return periods are re-calculated based on future discharge. The clustering is repeated, based on the four indicators and average SI value. Both the number and the characteristics of the flood types can be compared to the historical flood types to assess changes in future flood type characteristics. The projected temperature values were normalized based on the historical time series, so as to assess the difference in temperature between the historical and new future flood types.

7.3 Study area

Two study areas were selected to demonstrate the applicability of the methodology under different conditions: the Barcelonnette Basin (548 km^2) in the southern French Alps and the Salzach Valley (4637 km^2) in Austria (Fig 7.1). Further information on the study areas can be found in Chapter 1 and Chapter 2.

Salzach Valley and Barcelonnette Basin differ in size and average annual precipitation (Chapter 2), they also differ in flood seasonality as shown in previous flood hazard studies (Salzach: Stanzel et al. (2008), Barcelonnette: Ramesh (2013)). The Ubaye River in the Barcelonnette Basin generally experiences spring flood events, where warm rain amplifies elevated river levels due to snowmelt (Ramesh, 2013). Summer flood events are more common for the Salzach Valley, which includes the August 2002 flood event where the discharge was the highest in the previous 100 years (Ulbrich et al., 2003). More recently in June

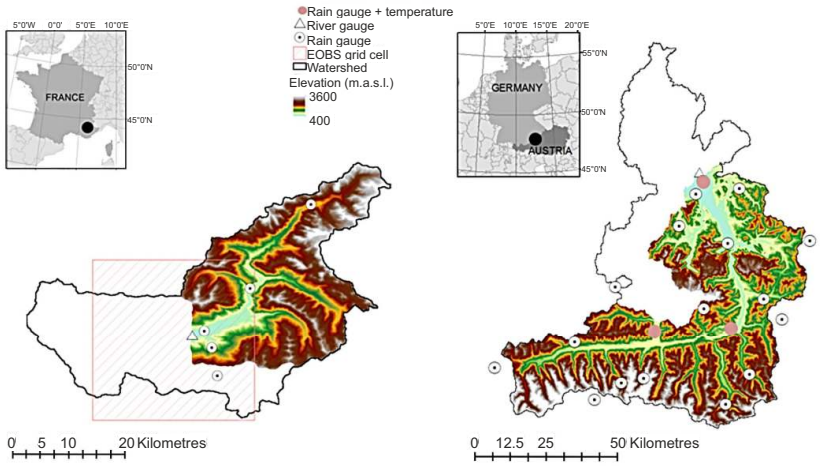

Figure 7.1 Map of the two study areas with the location of the rain and river gauges, including locations where temperature was also measured. The size and location of the EOBS grid cell is also shown for the Barcelonnette Basin.

2013, the Salzach Valley recorded high discharge after four days of high precipitation with high antecedent soil moisture (Blöschl et al., 2013).

7.4 Data selection

The Barcelonnette Basin and Salzach Valley are covered by a hydrological network with more than 20 years of measurements. The Barcelonnette Basin contains 4 rain gauges and measurements of mean daily discharge covering the period 1971–2004. Observed gridded data from the ENSEMBLES project was used for temperature (E–OBS, Haylock et al. (2008)), due to missing data and change-points in the temperature record for the catchment (Chapter 2). E–OBS data have been successfully used in previous flood related studies (e.g. Freudiger et al., 2014; Ionita et al., 2014). The Salzach Valley contains 18 rain gauges, 3 temperature gauges, and measurements of mean daily discharge for the period 1987-2010. For input into the HBV model the arithmetic mean of multiple temperature station was used for the Salzach Valley as it resulted in higher model efficiency coefficients compared to using a single, centrally located, temperature gauge. To calibrate the HBV model, a ten year period was selected (Salzach: 2001–2010, Barcelonnette: 1995–2004). The validation period was for Salzach: 1988-1997, and for Barcelonnette: 1971-1980. Both calibration periods contained significant flood events: 2002 in Salzach and 2003 in Barcelonnette.

For future flood type analysis over the period 2070-2099, 4 future

projections were selected from a set of 15 future climate projections. Four projections were selected to analyse future flood types to maintain a manageable number of future projections, as well as using many projections can tend to highlight the central tendency, rather than extreme conditions (Raff et al., 2009). The full set of 15 projections originate from the EURO-CORDEX dataset (Jacob et al., 2014). Model output from three RCMs (SMHI-RCA4, DMI_HIRHAM5, KNMI-RACMO22E) driven by four different GCMs (ICHEC-EC_EARTH, MOHC-HadGEM2_ES, IPSL-CM5a_MR, MPI-ESM_LR) and two representative concentration pathways, RCP4.5 and RCP 8.5, were selected to cover a wide range of genealogy (Knutti et al., 2013). The 15 projections are listed in Table 7.1. From the set of 15, 4 projections were selected using the method by Raff et al. (2009). This method is based on the mean temperature and precipitation projected changes compared to the historical period, averaged over the catchment. Mean changes in temperature and precipitation were used so that the results are not biased towards one particular flood type, for example through selecting changes in extreme precipitation or spring temperature. The selected projections represent combinations of warmer, milder, drier, and wetter conditions for the time period 2070-2099.

Table 7.1 Selected projections giving the driving GCM, RCM, output resolution (Res), and RCPs.

	GCM	RCM	Res	RCP
1	ICHEC-EC-EARTH	SMHI-RCA4	0.44°	4.5
2	ICHEC-EC-EARTH	SMHI-RCA4	0.44°	8.5
3	ICHEC-EC-EARTH	SMHI-RCA4	0.11°	4.5
4	ICHEC-EC-EARTH	DMI_HIRHAM5	0.44°	4.5
5	ICHEC-EC-EARTH	DMI_HIRHAM5	0.44°	8.5
6	ICHEC-EC-EARTH	DMI_HIRHAM5	0.11°	4.5
7	ICHEC-EC-EARTH	KNMI-RACMO22E	0.44°	4.5
8	ICHEC-EC-EARTH	KNMI-RACMO22E	0.44°	8.5
9	MOHC-HadGEM2_ES	SMHI-RCA4	0.44°	4.5
10	MOHC-HadGEM2_ES	SMHI-RCA4	0.44°	8.5
11	MOHC-HadGEM2_ES	SMHI-RCA4	0.11°	8.5
12	IPSL-CM5A_MR	SMHI-RCA4	0.44°	4.5
13	IPSL-CM5A_MR	SMHI-RCA4	0.44°	8.5
14	MPI-ESM-LR	SMHI-RCA4	0.44°	4.5
15	MPI-ESM-LR	SMHI-RCA4	0.44°	8.5

A bias correction method was utilized for the four selected projections for each catchment, as model biases may still remain in RCM data even though they reasonably reproduce meso-scale atmospheric features (Frei et al., 2006). For this work, the empirical-quantile mapping technique (EQM) from Chapter 4 was chosen. The bias correction methodology for precipitation was based on Themeβl et al. (2012), which has been successfully applied in hydrological climate change-hazard studies (e.g. Dobler et al., 2012; Finger et al., 2012). The correction factors were calculated monthly, as RCMs biases may differ between seasons (Frei

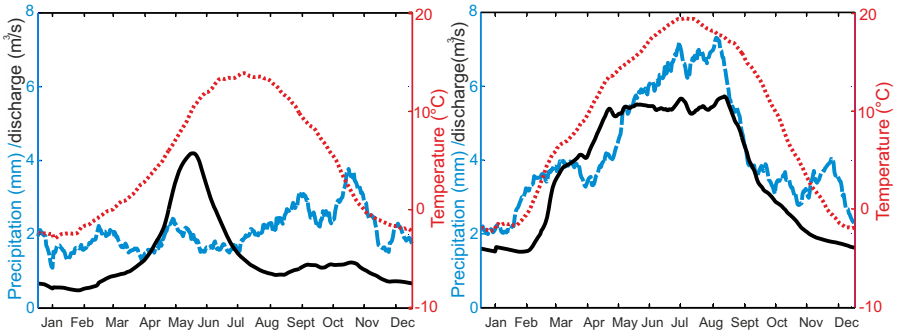

Figure 7.2 Mean daily discharge (solid black) from the HBV model, with mean temperature (red dots) and precipitation (blue dash) from the weather generator. Left: Barcelonnette for the period 1988-2010. Right: Salzach for the period 1971-2004.

et al., 2006), as well as to align with the weather generator (Sec 7.2.1). Further information on the method can be found in Chapter 4, Sec 4.4.

7.5 Flood typing

The generated time series from the combination weather generator and HBV model are described in Sec 7.5.1, including the results for the observational period as well as the future projections. These time series form the base for the classification of flood types along with the indicators selected using the observational data. As the catchments have different flood characteristics, the applicability of the flood type classification is shown per catchment (Barcelonnette in Sec 7.5.2 and Salzach in Sec 7.5.3) for past and future climates.

7.5.1 Data input for classification

7.5.1.1 Historical period and indicators

The generated discharge, precipitation and temperature for the historical period in both catchments are characterized in Fig 7.2. The discharge time series was generated after calibrating the HBV model. The average Nash-Sutcliffe efficiency (Nash and Sutcliffe, 1970), computed as performance indicator for the HBV model, was 0.87/0.82 for Salzach and 0.82/0.74 for Barcelonnette for the calibration/validation period. As the HBV model has been tested for both catchments, details on comparison with observational records can be found in Breinl (2016).

In the Barcelonnette Basin, the average daily precipitation was stable thought the year (1-2 mm) with a small peak in October/November (3

mm). In the Salzach Valley there was a clear seasonal signal, with the average daily precipitation lowest in December and January (2 mm) and increasing to 6-7 mm in July and August. The temperature shows the same annual variation for the two regions, with a higher maximum average temperature in the Salzach Valley. As a representation of extreme precipitation for the two catchments, the average annual maximum daily precipitation from the weather generator was 45.2 mm for Barcelonnette and 42.3 mm for Salzach.

The mean daily discharge for the Barcelonnette Basin peaks in spring, with a second smaller peak in the autumn. The second peak aligns with the peak precipitation period, while the first discharge peak may be associated with snowmelt. For the Salzach Valley, the mean discharge and precipitation are highest from late spring to early autumn. An increase in discharge around April/May, not matched in the mean precipitation amounts, was likely caused in part by snowmelt. Higher discharge values in the Salzach Valley could be explained by the difference in size compared to the Barcelonnette Basin.

The selection of exact indicators was based on the correlation with discharge using the generated time series of precipitation, temperature, and discharge (Fig 7.2). Various antecedent periods were tested as indicators in both catchments. The 15-day total precipitation and 5-day normalized temperature had the highest correlation with discharge for the Salzach Valley (correlation coefficients of 0.61 and 0.60 respectively). For the Barcelonnette Basin, the antecedent period used for precipitation was 35 days and 4 days for normalized temperature (both with a correlation coefficient of 0.42). As the antecedent normalized temperature had a higher correlation with discharge for both study areas, it was used as a potential indicator instead of absolute temperature values. Table 7.2 lists the potential indicators for the classification of flood types.

Table 7.2 Potential indicators for classification of flood types for the Barcelonnette Basin and Salzach Valley.

	Description	Definition	
		Barcelonnette	Salzach
R	Short precipitation	Daily total (mm)	Daily total (mm)
Ra	Antecedent precipitation	35-day total (mm)	15-day total (mm)
Tna	Temperature	4-day mean temperature (normalized)	5-day mean temperature (normalized)
DOY	Day of the year	Days from 31^{st} Dec	Days from 31^{st} Dec

7.5.1.2 Future period

The mean changes in precipitation and temperature in each catchment for 15 different bias-corrected climate projections are shown in Fig 7.3. All projections show an increase in the average annual temperature for the future (2070-2099) compared to the historical period (Barcelonnette:

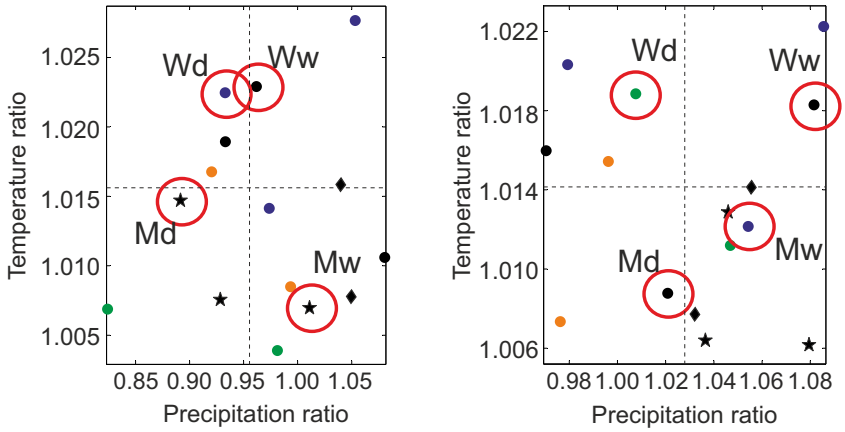

Figure 7.3 Projection temperature and precipitation ratio comparing the period 2070-2099 with observational period with Barcelonnette Basin (left) and the Salzach Valley (right). The selected projections circled in red are for the following combinations: mild dry (Md), mild wet (Mw), warm dry (Wd) and warm wet (Ww). The colors represent the different driving GCMs: black ICHEC-EC_EARTH, blue MOHC-HadGEM2_ES, green IPSL-EM5a_MR, orange MPI-ESM_LR, and the different RCMs are represented with different symbols: circle SMHI-RCA4, star DMI_HIRHAM5, diamond KNMI-RACMO22E.

1971-2004, Salzach: 1987-2010). The largest increase in temperature for both study areas was more than 2.0% using the MOHC-HadGEM2_ES-SMHI-RCA4 combination. For precipitation, the Barcelonnette Basin shows most projections with drier conditions, while for the Salzach Valley most projections show the area becoming wetter. To reduce the number of future projections, four were selected for each study area using the method proposed by Raff et al. (2009). The SMHI-RCA4 with ICHEC-EC_EARTH as driving GCM were selected for both catchment (red circle Fig 7.3), with the DMI_HIRHAM5 and ICHEC-EC_EARTH as the other model combination for Barcelonnette, and SMHI-RCA4 and IPSL-EM5a_MR for Salzach.

The eight projection circled in red were then fed to the weather generator and HBV model to produce four times 1200 years of generated data for both the Barcelonnette Basin and the Salzach Valley. Figure 7.4 shows the mean daily precipitation, temperature, and discharge per projection for the period 2070-2099. For Barcelonnette, all projections have the highest mean precipitation amounts in September and October, extending into August under the Wd projection. Furthermore, besides Wd, the other projections show a clear seasonal variation in precipitation with two peaks: one in September-October (3-6 mm/day) and a second minor peak in March-May (2-3 mm/day). The temperature had the same annual variation as in the historical period, although warmer by 1-2°C,

except for the winter temperatures for the two warmer projections (Wd and Ww). For the Wd and Ww projections, the temperature was 5-7°C higher than in the historical period elevating the mean temperature to above freezing. The changes in temperature and precipitation led to a smaller spring discharge peak than observed in the historical period, particularly for the Wd projection, and higher discharge amounts from October to November.

For the Salzach Valley, the seasonal variation of mean precipitation varied between the four future projections in Fig 7.4, with the Md projection being most similar to the historical period. The Mw and Ww projections had an increase in the average daily precipitation of 7-8 mm for July and August. For the Wd projection, there were two precipitation peaks of 5-6 mm, one in February to March and the other in June to September. The temperature showed a similar distribution as the historical period with a 2-4°C increase for the milder projections, Md and Mw, and a 4-6°C increase for the warmer projections, Wd and Ww. For future discharge, the amount either stayed the same or increased for March to April, with lower discharge between June and October. There was a second discharge peak in three of the projections occurring in July to August for Mw and Ww projections and September to October for the Md projection.

7.5.2 Barcelonnette Basin flood types

7.5.2.1 Historical period (1971-2004)

Per return period the dominant flood types in the Barcelonnette Basin were determined for the historical period 1971-2004. The indicators that independently gave the highest correlation with discharge were: daily precipitation (R), antecedent 35-day precipitation (Ra), and antecedent 4-day normalized temperature (Tna) in combination with the day-of-year (DOY). Figure 7.5 shows the flood types where DOY versus precipitation is plotted (a) as well as the silhouette value per event (b). For Q2, flood events were classified into two groups: a small cluster later in the year with higher daily rainfall amounts (Type 1) and a second larger cluster earlier in the year (Type 2; Fig 7.5a). For the Q2 floods, the combination of daily precipitation, temperature and day of the year gave an average SI score of 0.94, indicating a near perfect separation between the two groups. Using the same set of indicators and number of clusters, the SI values for Q10 and Q25 were both 0.85. However further analysis on Q10 and Q25 identified a third group that split the Type 1 floods into two smaller clusters. The two clusters also add the antecedent 35-day precipitation as an indicator and provided a more compact range of conditions under which the flood events occurred. The average SI score changed to 0.68 for the Q10 floods and 0.73 for the Q25 floods. The majority of individual SI values were above 0.5 in Fig 7.5b, indicating that these flood events were most similar to other flood events in their cluster. However, when introducing three flood types some SI values

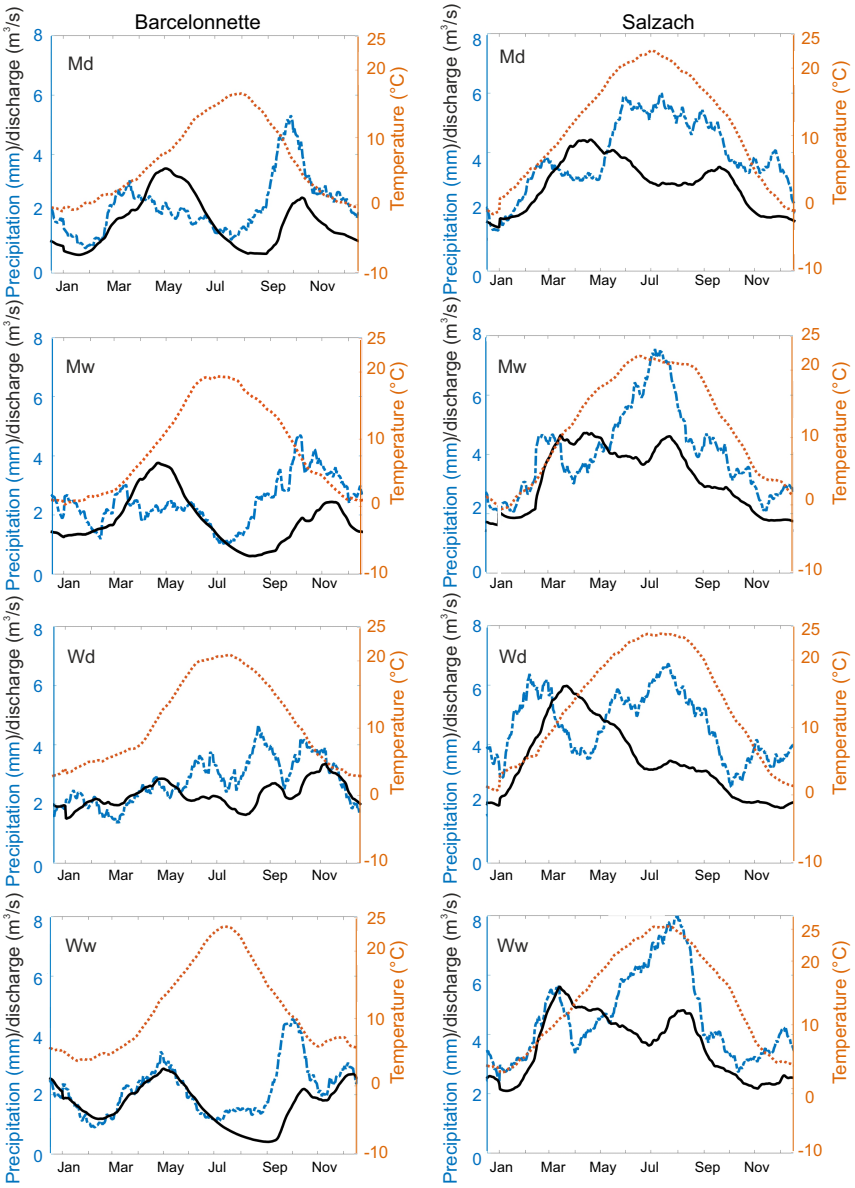

Figure 7.4 Mean daily discharge (solid black) from the HBV model, with mean temperature (red dots) and precipitation (blue dash) from the weather generator. Left: Barcelonnette Right: Salzach. Both for the period 2070-2099 and for each of the four projections Md, Mw, Wd, and Ww.

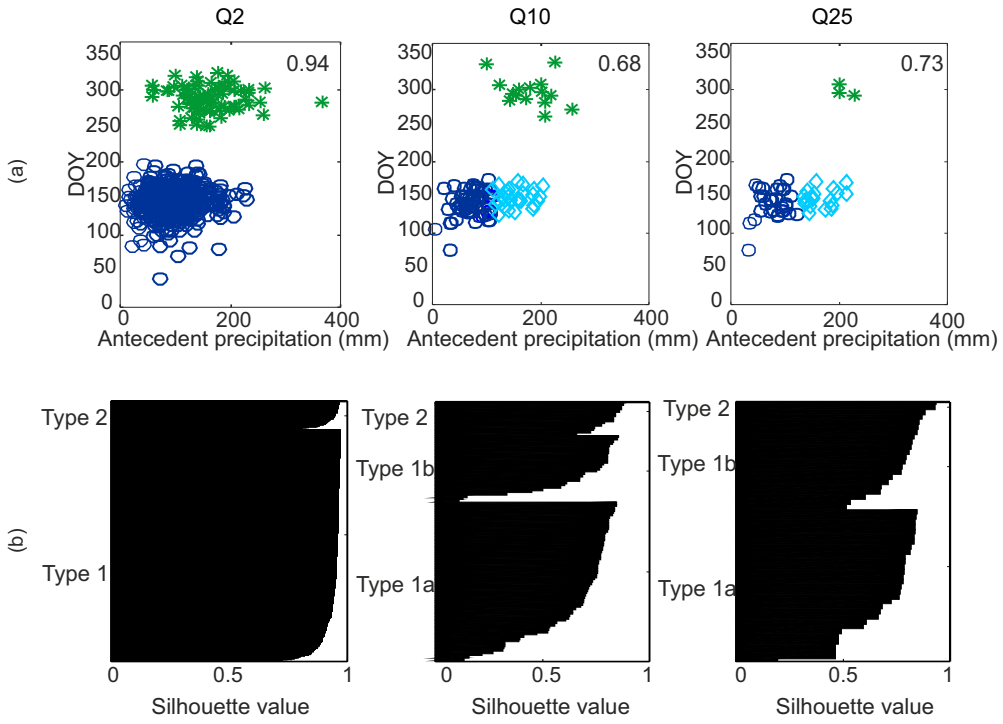

Figure 7.5 Clustering of flood types for the Barcelonnette Basin (A) with the individual silhouette values (B) for the historical period. Green stars indicate Type 2, blue circles Type 1/1a, and light blue diamonds for Type 1b flood events. In each instance, only the antecedent and DOY indicators are shown.

dropped to near zero, particularly for Q10 floods, indicating that there is no preferred cluster for these flood events. The average SI value and cluster centre values per indicator are listed in Table 7.3 per return period and flood type.

For all return periods, Type 2 floods occurred between September and December with higher than normal temperatures. The warmer temperatures indicated that the rainfall may come from warmer convective events. The associated mean daily precipitation amounts are 44.5 mm, 53.2 and 45.6 mm for Q2, Q10 and Q25, respectively (Table 7.3); values close to the observed annual daily maximum precipitation. The related antecedent precipitation mean values increased with increasing return period indicating higher soil moisture that may lead to more runoff during the short rain events.

Type 1 floods occurred between March and July. Compared to Type 2 floods, Type 1 floods had a lower Tna, but still generally higher than

Table 7.3 Cluster centre values for the different flood types for the Barcelonnette Basin under the historical climate. R is the daily precipitation amount, Ra is the 35-day antecedent precipitation and Tna is the normalized 4-day antecedent temperature. The values in bold are used for the cluster centres.

Barcelonnette flood type centres													
Type	Q2				Type	Q10				Q25			
	R	Ra	Tna	DOY		R	Ra	Tna	DOY	R	Ra	Tna	DOY
1	15.6	87	1.0	146	1a	30.1	71	1.8	142	40.7	78	1.5	141
					1b	23.3	152	0.7	150	21.7	165	1.3	149
2	44.5	159	1.5	294	-	53.2	170	1.7	298	45.6	210	1.9	299

normal (Table 7.3). The warmer temperatures in spring may have been associated with increased snowmelt, rain on snow, or more rainfall rather than snowfall. The daily precipitation amounts for this flood type were lower than for Type 2 floods (Fig 7.5a and Table 7.3), but higher than the mean values in Fig 7.2. Therefore it is unlikely that there were snowmelt floods in the Barcelonnette Basin, a type outlined by Merz and Blöschl (2008), rather, two groups of Rain-Snow floods (here labelled Type 1a and Type 1b) separated by antecedent precipitation amounts. Type 1b floods had higher antecedent precipitation with lower daily precipitation compared to Type 1a, as can be seen in Fig 7.5 and Table 7.3. As the temperature indicator covered a shorter time period than the antecedent precipitation, it is not possible to assess whether all the precipitation is snow or rain using the indicators alone. Further investigation of the HBV output data of a select number of the Q25 Type 1b floods showed lower temperatures the preceding weeks, only warming to above normal temperatures in the days before the flood event. In these instances, increased precipitation likely built up the snowpack, especially at higher elevations, which eventually melted and increased the discharge levels. Type 1 floods accounted for more than 90% of the flood events in the generated time series, with an equal split between Type 1a and Type 1b for Q10 and Q25.

As a performance check, the characteristics of the above generated flood types were compared with floods documented in the catchment. The highest measured discharge amount between 1970 and 2010 was in May 2008, and had similar values for the indicators as the flood Type 1a for Q25. The recorded daily precipitation was more than 40 mm at the rain gauges in Fig 7.1, with above normal temperature. Considering high observed discharge events, most Q2 events occurred during the March to July period, with only three events that could be classed as Type 2 events. Based on the observed times series, it was not possible to discern Type 1a and Type 1b floods, as there were only four measured Q10 floods and one Q25; too few to cluster. The comparison shows that types of floods captured by the flood classification method appear to be similar to those observed in the Barcelonnette Basin.

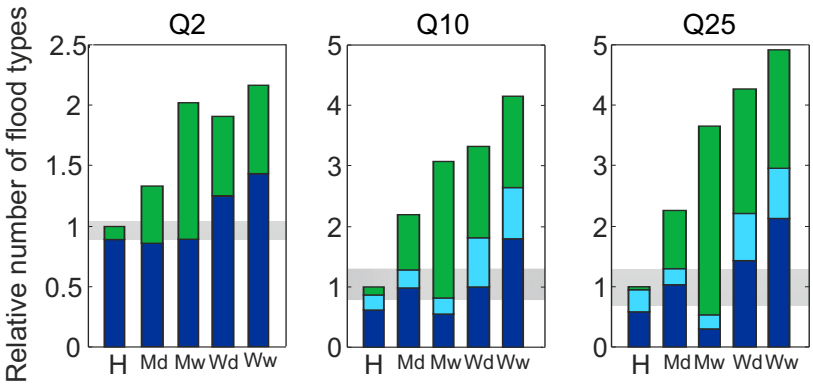

Figure 7.6 Approach 1: Number of high discharge events relative to the historical period, split into flood type (blue = Type 1/1a, light blue = Type 1b, green = Type 2, H = for the historical period). The horizontal grey box indicates the 99% random sampling range from the historical period. Amounts above 1 indicate an increase in overall flood frequency and below 1 represents a decrease. The Q2, Q10, Q25 refer to the discharge amount in the historical period. Md, Mw, Wd, and Ww correspond to the projections selected in Fig 7.3.

7.5.2.2 Future flood types (2070-2099)

The future flood types were first analysed for changes in the flood type frequency compared to the historical period (approach 1). Figure 7.6 shows the relative change in number of flood events for each flood type and return period with the historical period (H) as reference (the grey band indicating the 99% random sampling range of historical time series). For the Barcelonnette Basin, all four projections for Q2, Q10, and Q25 events had in increase in overall flood frequency in 2070-2099, as the total length of each bar is greater than the grey horizontal band in Fig 7.6. The overall increase was due to a strong increase in the number of Type 2 floods (green) for all projections: a flood type that accounted for less than 10% of the events in the historical period. The increase in these events primarily came from an increase in the daily precipitation during autumn (see Fig 7.4). There was no consistent change projected in Type 1 for Q2 and Types 1a and 1b for Q10 and Q25. Overall, there was a potential shift in flood types from Type 1 to Type 2 floods.

In the second approach, future flood type clusters were re-classified to account for potential changes in the climate of the catchment that alter the flood types themselves. The centre values of the clusters are in Table 7.4 for each projection (Wd, Ww, Md and Mw). Fig 7.7 shows the clustering of flood types based on the indicators DOY and daily rainfall for each return period and climate scenario. The individual SI values are in Appendix E.2.

The future flood types in the Barcelonnette Basin were similar to those

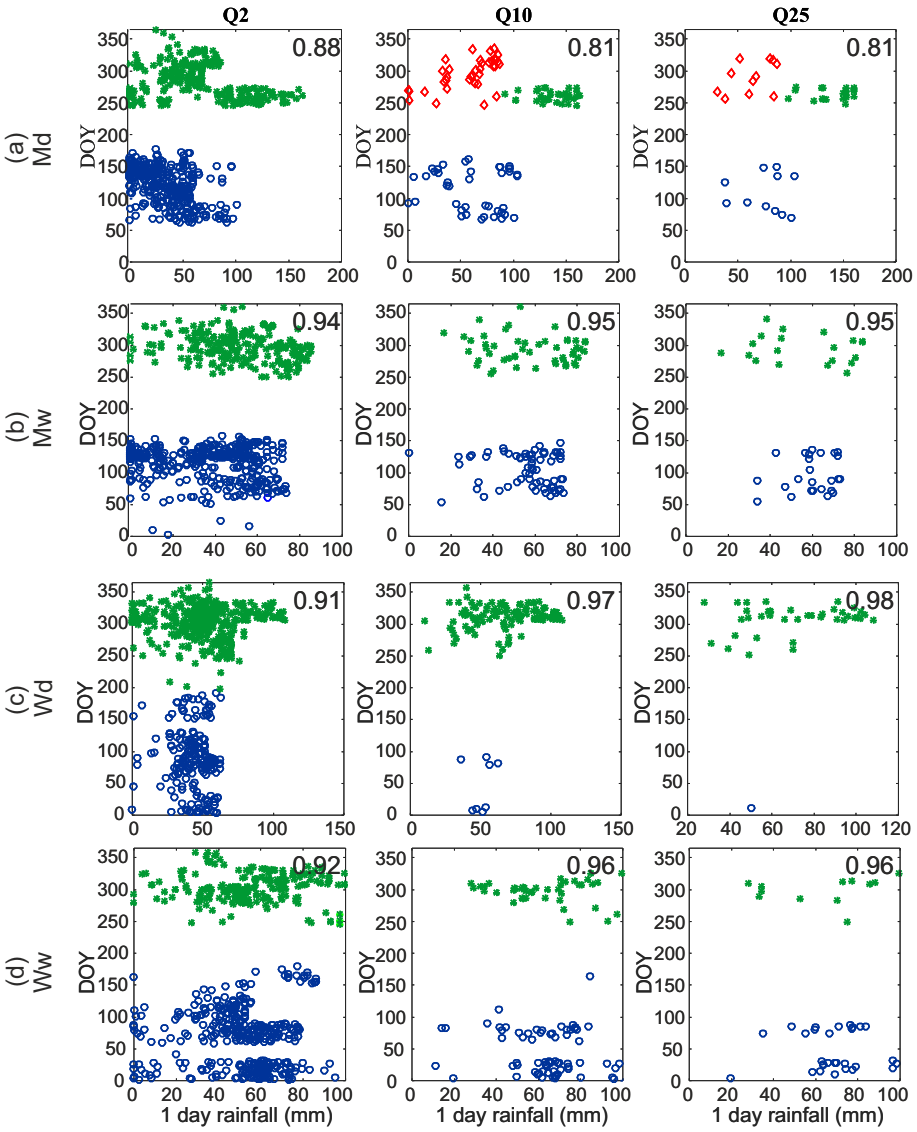

Figure 7.7 Clustering of future flood types for the Barcelonnette Basin for the period 2070-2099 per selected projection. Green stars indicate Type 2 floods, blue circles Type 1 floods, red diamonds for Type 3 floods with indicator daily rainfall on the x-axis and indicator DOY on the y-axis. The average SI value is shown the in top right corner.

Table 7.4 New cluster centres for future flood types in the Barcelonnette Basin (2070-2099) for the four future projections. R is the daily precipitation amount (mm), Ra is the 35-day antecedent precipitation (mm) and Tna is the normalized 4-day antecedent temperature. The values in bold are used for the cluster centres.

		Q2				Q10					Q25			
	Type	R	Ra	Tna	DOY	Type	R	Ra	Tna	DOY	R	Ra	Tna	DOY
Md	1	32	105	1.9	122		62	110	2.2	114	77	123	3.0	108
	2	66	148	1.8	285	2a	137	98	1.7	261	140	146	2.0	264
						2b	58	219	2.3	297	63	249	1.9	290
Mw	1	36	84	2.9	115		56	90	2.9	105	60	102	3.1	97
	2	51	167	2.8	296		57	204	3.0	293	56	239	3.1	295
Wd	1	43	101	4.1	90		51	95	4.4	47	50	153	4.5	11
	2	51	168	3.6	303		68	189	3.7	311	71	208	4.0	308
Ww	1	51	99	4.1	67		63	121	4.6	45	69	143	4.7	47
	2	55	171	3.5	303		62	219	3.9	297	63	242	3.8	299

in the historical period, except for projection Wd (Fig 7.7). Under Wd, Q2 events occurred throughout the year, as opposed to the defined spring and autumn periods observed historically. The three projections Mw, Ww, and Md showed two distinct periods of the year with flood events, as seen with the separation in the DOY between the Type 2 and Type 1 floods in Fig 7.7. Under the Md projection, Type 2 could be split for Q10 and Q25 floods, where Type 2a experienced higher daily precipitation amounts and lower antecedent precipitation than Type 2b flood events (Fig 7.7a and Table 7.4). All four future projections resulted in fewer Type 1 floods and a separation could no longer be made between Type 1a and 1b floods as in the historical period. For the Q2 events, the average SI value was similar to the historical period, while Q10 and Q25 had higher average SI values than in the historical period, indicative of a clearer separation between the future flood types.

Although similar clusters were detected in the future for the Barcelonnette Basin, shifts in timing and cluster centre values for indicators were projected. The two warmer projections (Wd and Ww) had Type 1 flood types occurring earlier in the year than historically (on average in March, as opposed to May from the generated flood events or the May 2008 flood event). Type 2 floods occurred on average at the same time of the year as found in the historical data, although some of the Q2 floods occur in December in all projections (Fig 7.7), which was not seen in the historical period (Fig 7.5a). For all projections, the cluster centre values for daily precipitation were higher (Table 7.4) than the historical values (Table 7.3). The antecedent precipitation amounts were lower. All temperature values were on average much warmer than in the historical period, consistent with a warming climate.

7.5.3 Salzach Valley flood types

7.5.3.1 Historical period (1987-2010)

For each return period the dominant flood types in the Salzach Valley were determined for the historical period 1987-2010. The indicators that gave the highest correlation with discharge were daily precipitation (R), antecedent 15-day precipitation (Ra), and antecedent 5-day temperature (Tna). Figure 7.8 shows the DOY and precipitation per flood event (a), as well as the silhouette value for each event (b). For the Q2 floods using all four indicators, there were two flood types from the classification. The first type were flood events earlier in the year with warmer than normal temperatures and moderate daily precipitation (Type 1). A second type occurred later in the year with higher daily precipitation and normal or colder than normal temperatures (Type 2; Fig 7.8a). The average SI value for this classification was 0.68. The separation between clusters became more distinct for the Q10 and Q25 flood events, with average SI values of 0.84 and 0.74 respectively. Antecedent precipitation was also not used for the Q10 and Q25 events to classify the clusters, due to lower SI values (0.79 and 0.44 respectively if included). For the Q25 flood events, the Type 2 events could be split into two clusters, ones with lower daily precipitation amounts and cooler temperatures that occurred earlier in the year (Type 2a) and flood events with higher daily precipitation amounts and temperatures near normal (Type 2b). Most of the silhouette values imply a good fit with values above 0.5 in Fig 7.8b, however, especially for Q2 events, there are near zero values, demonstrating that some flood events did not clearly fit in a particular flood type. The average SI value and cluster centre values for each of the indicators are listed in Table 7.5.

Table 7.5 Cluster centre values for the different discharge magnitudes for the Salzach Valley under the historical climate. R is the daily precipitation amount, Ra is the 15-day antecedent precipitation and Tna is the normalized 5-day antecedent temperature. The values in bold are used for the cluster centres.

Salzach flood type centres													
Type	Q2				Q10				Type	Q25			
	R	Ra	Tna	DOY	R	Ra	Tna	DOY		R	Ra	Tna	DOY
1	**31**	**153**	**0.95**	**125**	**35**	137	**1.4**	**94**	-	**36**	146	**2.0**	**84**
2	**43**	**232**	**-0.27**	**220**	**48**	246	**-0.5**	**215**	2a	**41**	284	**-0.5**	**192**
									2b	**53**	272	**-0.1**	**240**

For all return periods, Type 2 flood events occurred between July and October, with Type 2a events occurring between July and August and Type 2b between August and October (Q25 only). All Type 2 floods had on average daily precipitation amounts higher than the average annual daily maximum, except for the Type 2a events that were slightly lower (Table 7.5). The temperature was generally cooler than normal for these events, indicating that the rainfall may have originated from low pressure systems, rather than local convection. However, for the Type 2b events,

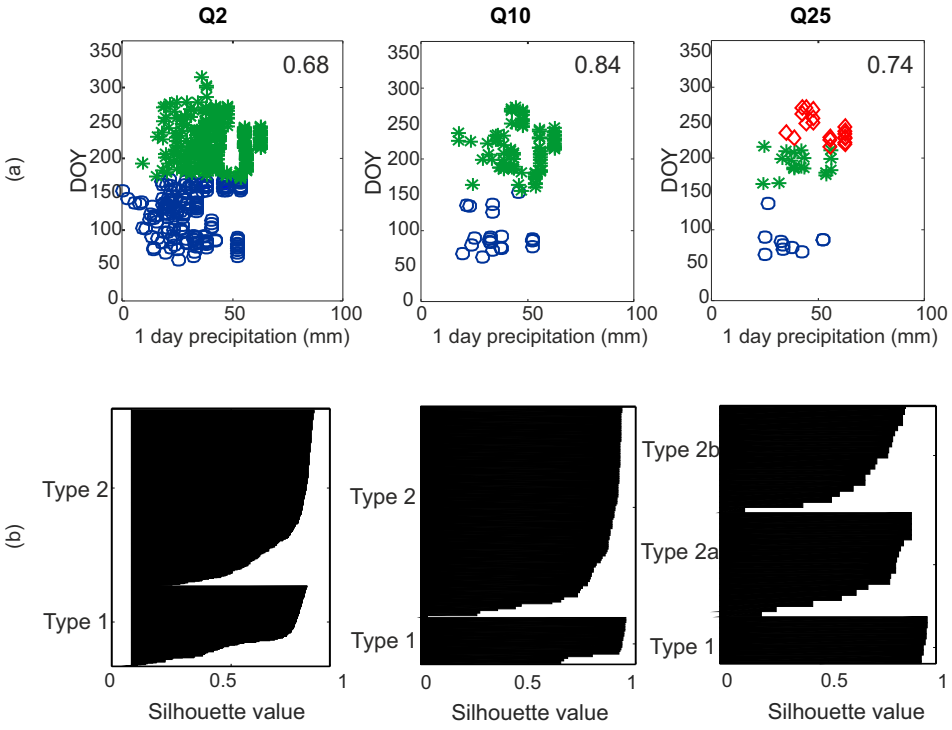

Figure 7.8 Clustering of flood types for the Salzach Valley (A), with the individual silhouette values (B). Green stars indicate Type 2/2a, blue circles Type 1, with red diamonds for Type 2b flood events. Only the R and DOY indicators are shown.

the temperatures were on average near normal, possibly due to a more balanced mixture of synoptically driven rainfall triggered flood events and local convective rainfall triggered flood events. Overall the Type 2 flood events were the dominant flood type in the generated time series for the Salzach Valley, accounting for more than 65% of the flood events.

Type 1 flood events occurred between March and July, with most of the Q10 and Q25 floods occurring between March and May. The average daily rainfall and antecedent precipitation were the same between the three return periods for this type, with the daily rainfall between 30-36 mm higher than normal for this time of year, but lower than the average annual daily maximum. The 15-day antecedent precipitation was on average 135-155 mm, double the average amount. The temperature was warmer than normal for all Type 1 events (Table 7.5), indicating that warmer temperatures in spring may be associated with increased snowmelt, or more rainfall rather than snowfall, as in the Barcelonnette

Basin. The cluster centre values for the temperature indicator also increased with increasing return period (Table 7.5), indicating either more snowmelt, or more rapid snowmelt. Overall, Type 1 flood events accounted for 10-35% of the total Q2, Q10, and Q25 floods in the Salzach Valley.

The characteristics of the generated flood types was compared with real flood events documented in the Salzach Valley. For the August 2002 flood event, the daily rainfall amounts in some places exceeded the 100-year return period amount, with heavy precipitation also recorded in the weeks before the event (Ulbrich et al., 2003). These are characteristic of the Type 2 flood events described in Table 7.5 and Fig 7.8a, although slightly earlier in the year than average for the generated data. More recently the early June 2013 flood occurred after three days of heavy precipitation combined with high antecedent moisture conditions in part due to snowmelt (Blöschl et al., 2013). This flood bares resemblance to the Type 1 flood events, where snowmelt appears to play a role, alongside heavy precipitation and higher than normal antecedent precipitation. Overall, the flood types captured through the classification of generated data appear to be similar to the observed flood types.

7.5.3.2 Future flood types 2070-2099)

The change in frequency of each of the flood types was analyzed first (approach 1). Figure 7.9 shows the relative change in number of flood events for each flood types and return period compared to the historical period (H). For each return period, three projections of flood events show an increase in overall frequency, with only the Md total bar length below the grey horizontal band in Fig 7.9. The Md projection was also unique between projections for the individual flood types, where the milder, drier projection had a decrease in Type 2 flood events and no change in Type 1 flood events. For the other three projections, Mw, Wd, Ww, each flood type increased in frequency, although the increase was small for Type 2a events for the Q25 Mw projection. For all return periods, the Type 1 flood events had the greatest increase in frequency, becoming the dominant flood type. For the two warmer projections, Wd and Ww, there were still more Type 2 flood events than Type 1. Overall the results for the Salzach Valley show that the distribution of flood types may shift to more events earlier in the year, although Type 2 flood types remained the dominant type, except in the Mw projection.

In approach 2, the future flood types were re-classified to account for possible changes in flood type characteristics by 2070-2099. The centre values for the indicators for each projection (Md, Mw, Wd, Ww) and return period are in Table 7.6. Figure 7.10 shows the clustering of flood types based on the indicators DOY and daily rainfall, with the individual SI values in Appendix E.2.

For the Salzach Valley, there was a larger difference between the historical and future flood types compared with Barcelonnette. The most similar flood types from the Md projection retained the Type 1 and

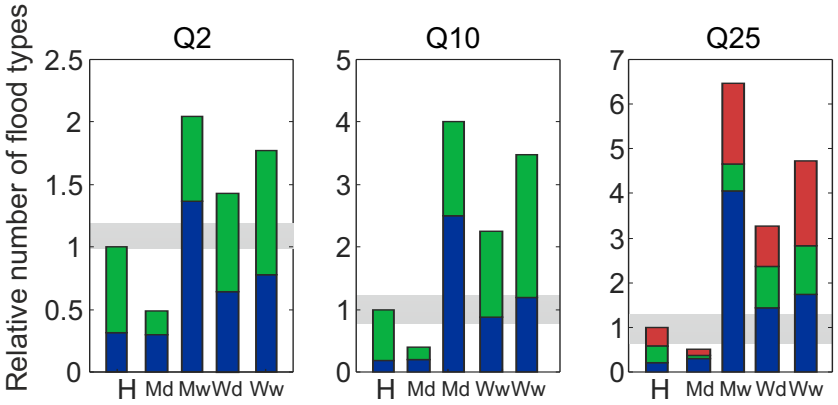

Figure 7.9 Approach 1: Number of high discharge events relative to the historical period, split into flood type (blue = Type 1, green = Type 2/2a, red = Type 2b, H = for the historical period). The horizontal grey box indicates the 99% random sampling range from the historical period. Amounts above 1 indicate an increase in overall flood frequency and below 1 represents a decrease. The Q2, Q10, Q25 refer to the discharge amount in the historical period. Md, Mw, Wd, and Ww correspond to the projections selected in Fig 7.3.

Type 2 events, although they occurred over a larger portion of the year (Fig 7.10a). The Mw projection future flood type characteristics had the largest contrast from the historical period (Fig 7.10b). This was the only projection that did not use DOY in all of the flood type classifications (Table 7.6). Four flood types were identified for Q2 events based on only temperature and daily precipitation, with the flood events that had the highest daily precipitation and coldest normalized temperature occurring in spring. Only two flood types were defined for the Q10 events, one group only occurring in spring, with higher daily precipitation amounts, and a second group that occurred throughout the year with higher antecedent precipitation. For the Q25 flood events, three types were identified with the inclusion of the DOY indicator. For the two warmer projections, Wd and Ww, between two and four clusters were found based on daily precipitation, temperature, and DOY with higher daily amounts (Fig 7.10c, d). Flood types 2a and 1 were similar to the flood types 2 and 1 from the historical period. However, in both cases a third type, Type 2b, was also observed, occurring in November and December with abnormally high temperatures, much later in the year than observed in the historical period. For the Wd projection, a fourth type, Type 2c, was also observed and occurred in June. As with the Barcelonnette Basin, all temperatures were higher than normal, as would be expected in a warmer climate.

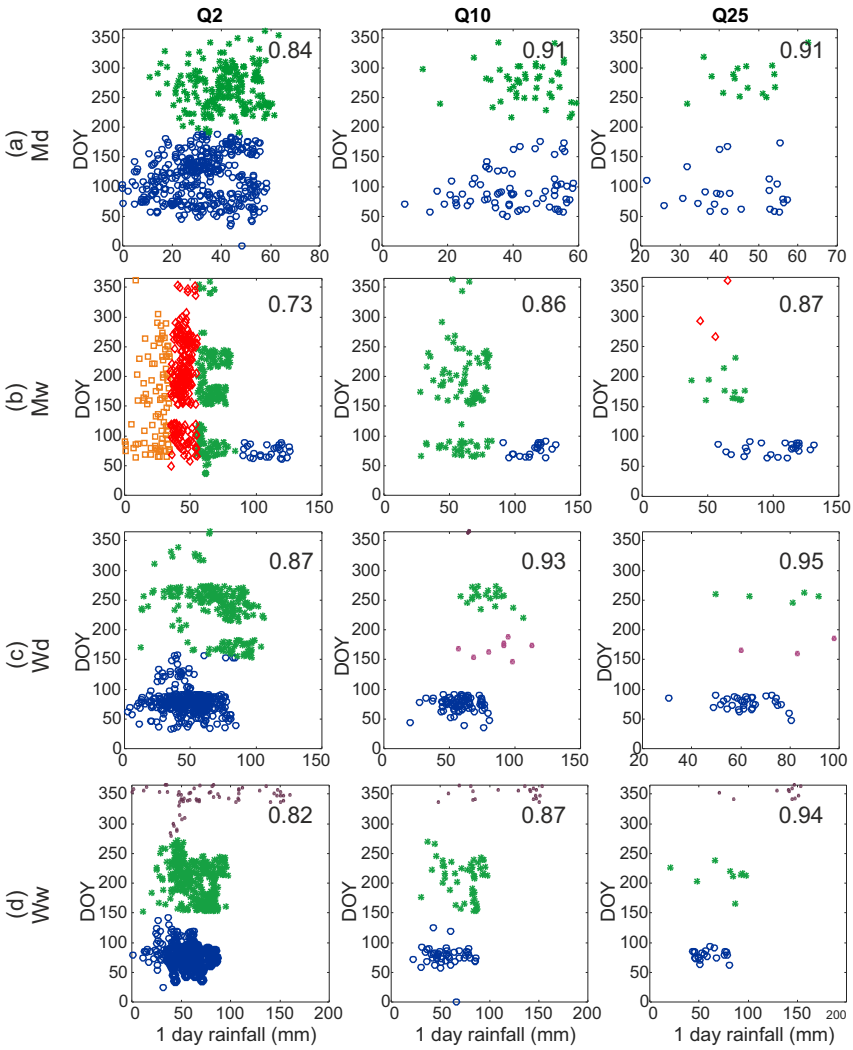

Figure 7.10 Clustering of future flood types for the Salzach Valley for the period 2070-2099 per selected projection. In the case of two flood types, green stars indicate Type 2/2a floods, blue circles Type 1 floods. In other cases, orange boxes = Type 3a, red diamonds = Type 3c and green stars = 3b, and purple small stars are Type 2b/c floods. The indicators shown are daily precipitation on the x-axis and indicator DOY on the y-axis. The average SI value is shown the in top right corner.

Table 7.6 Cluster centre values for the different discharge magnitudes for the Salzach Valley under the historical climate. R is the daily precipitation amount (mm), Ra is the 15-day antecedent precipitation (mm) and Tna is the normalized 5-day antecedent temperature. The values in bold are used for the cluster centres.

	Type	Q2				Type	Q10				Type	Q25			
		R	Ra	Tna	DOY		R	Ra	Tna	DOY		R	Ra	Tna	DOY
Md	1	**32**	74	**1.6**	**115**	-	**40**	82	**2.1**	**96**	-	**44**	95	**2.0**	**92**
	2	**42**	94	**1.1**	**265**	-	**44**	114	**1.4**	**275**	-	**47**	123	**1.9**	**281**
Mw	1	**109**	52	**0.6**	74	-	**113**	58	**1.2**	**78**	-	**101**	164	4.4	**80**
	3a	**24**	115	**1.6**	**160**	2	**60**	132	**1.1**	164	2a	**65**	177	4.5	**179**
	3b	**66**	87	**1.3**	**167**										
	3c	**45**	113	**1.3**	193						2b	**55**	217	4.4	**306**
Wd	1	**48**	85	**2.7**	**78**	-	**58**	114	**2.7**	**75**	-	**62**	141	**2.8**	**77**
	2	**69**	103	**2.2**	**237**	2a	**79**	132	**2.3**	**256**	2a	**74**	173	**2.2**	**256**
						2b	**57**	116	**4.6**	**364**					
						2c	**86**	138	**1.6**	**167**	-	**80**	149	**1.7**	**171**
Ww	1	**51**	75	**2.3**	**84**		**56**	105	**2.7**	**78**		**59**	135	**3.3**	**79**
	2a	**65**	122	**2.7**	**203**	-	**74**	151	**2.8**	**208**	-	**75**	186	**2.8**	**212**
	2b	**77**	92	**3.5**	**342**	-	**118**	102	**3.7**	**352**	-	**132**	92	**4.0**	**352**

7.6 Discussion

The developed flood type classification methodology was able to define the main historical flood types for both tested catchments as a result of temporal data expansion by using weather generator combined with the HBV rainfall-runoff model. Separation between flood types based on the SI value depended on both the catchment characteristics, as well as the number of flood events in the cluster. The separation was less clear for lower return period floods (Q2) in the Salzach Valley than the Barcelonnette Basin, which could be linked to the two distinct precipitation and discharge peaks in Barcelonnette that were absent in Salzach (Fig 7.2). Generally, there was an increase in SI values between the flood types with higher return periods, for both catchments and as well as for historical as future periods. A reason could be that more frequent discharge events can occur in a wider range of conditions, while the extreme flood event conditions only occur under specific combinations of indicator values, possibly linked to certain atmospheric situations such as atmospheric blocking leading to persistent rain over the catchment.

The developed methodology employs four types of indicators using only temperature and precipitation data from the weather generator and the DOY. The selected indicators have strongest correlation with generated discharge, but could limit the number of flood types. Other flood types, such as snowmelt, may be difficult to capture with only temperature and precipitation indicators (Gelfan, 2010). It is possible that new indicators should be used for clustering future flood events or other catchments. Using other indicators as well as antecedent periods for the temperature, precipitation, and DOY may alter the mean indicator values

per flood type, and possibly the flood types themselves. No weighting was applied to the indicator values, although this may be a viable option where the separation between clusters is less clear. However, for both test catchments most of the silhouette values were greater than 0.5, indicating that these two frequently measured meteorological variables, temperature and precipitation, can be used to distinguish two or three clearly different flood types.

Previous work shows that hydrologic future projections are potentially sensitive to the GCM, RCM, rainfall-runoff model and downscaling method used (e.g. Dobler et al., 2012; Wood et al., 2004). Here, climate model projections were selected based on mean changes in temperature and precipitation (Sec 7.4), although Figs 7.6 and 7.9 do not show consistent changes in flood types between the selections beyond the milder, drier projections showing the least number of flood events. These differences suggest that selecting projections based on mean changes in temperature and precipitation may not directly relate to the changes in flood types, although selecting the mean values reduces the assumptions on the governing factors for flood events. The selected indicators assume that the GCMs and RCMs were able to project future changes in precipitation, while GCMs are known to have limited skill in capturing factors driving regional precipitation, which would affect future projections of precipitation, and therefore flood types in this study (Asadieh and Krakauer, 2015; Merz et al., 2014). Furthermore, the weather generator assumed no change in autocorrelation, or inter-site correlation, rather focusing on changes in precipitation amounts as well as temperature. Spatial changes in precipitation can in some instances cause greater changes in discharge amounts than temporal changes (Perdigão and Blöschl, 2014). Not changing the autocorrelation might partly explain why the Type 2b floods saw a larger increase in frequency compared to those with larger antecedent precipitation (Type 2a). However, future projections in temperature and precipitation amounts still led to changes in the dominant flood types in a catchment as well as the flood frequency, although the range of future flood frequencies and flood types for the study areas may actually be greater than presented here. A more detailed study in changing flood types for a particular area should possibly consider more projections, as well as changes in land use and other catchment characteristics, as this may also influence future flooding.

Two approaches were provided to assess changes in the flood types under four future climate scenarios. These approaches were complementary to each other as one estimates changes in frequency of the historical flood types, where the second assesses whether future precipitation and temperature would lead to (dis)similar flood types compared to the historical period. Changes in the dominant flood type can have implications for local land use practices. For example, in the Barcelonnette Basin during summer the flood plains are used for farming and camping, as the historical flood events have occurred during spring. However, if summer and autumn floods become the dominant flood type, as projected in Sec 7.5.2.2, this will have implications for exposure in the area. Changes in

the characteristics, as in approach two, are also important, such as the decrease in the temperature indicator for the Type 1 floods in the Mw projection, even under a warmer climate.

Flood types for the historical period may be inherent to the combination of weather generator and specific rainfall-runoff model, enforced by historical observational records of precipitation and temperature. Two flood types were found, Type 1 and 2, which are similar to Rain-Snow and Short Rain floods respectively as classified in Merz and Blöschl (2008). Other flood types listed in the previous work, Snowmelt and Long Rain, were not distinguished through the flood type classification. Instead, in cases where there were three or more flood types, the types generally split one of the main clusters, based on which was the dominant flood type in the catchment. Even when considering the new flood types for 2070-2099 the Rain-Snow and Short Rain floods remained the two clear flood types from Merz and Blöschl (2008), even if the characteristics of the flood type were different. It is possible that a flood type, such as Snowmelt, could trigger only discharge with shorter return periods in the catchments, and not generate high discharge levels. The ability of the method to capture snowmelt floods could be confirmed through future work in a catchment where these flood types occurred.

While to the author's knowledge there has been little coverage of changes in future flood types for Alpine catchments, the results found here are similar to other studies for the two catchments. Hall et al. (2014) concluded that an increase in future extreme precipitation events with mean precipitation increases over northern Europe and decrease in southern areas will results in different changes in flood frequency between catchments in the future. For the Barcelonnette Basin, Saez et al. (2013) hypothesized that future warming could enhance snowmelt during the spring, although from the results in Sec 7.5.2 this appears to be offset by the decrease in antecedent precipitation. The increase in temperature in both Fig 7.4 and Table 7.3 is consistent with future warming in the area (Malet et al., 2007; Rousselot et al., 2012). For the Salzach Valley, previous work found no clear trend in flood frequency (Dobler et al., 2011), although the authors commented that higher spring temperatures could lead to more frequent flood events in this season. The similarities between this work and previous studies implies that the even with the limitations of method outlined above the method produces reasonable results using relatively straightforward method.

7.7 Conclusion

This chapter demonstrated a methodology developed for detecting present and future flood types. Long time series of discharge were generated using a weather generator coupled with a rainfall-runoff model to provide sufficient flood events for classification into different causal types. The types were determined to be sufficiently different based on the silhouette index. Future climate scenarios were assessed using bias

correction of different RCM climate projections and to train the weather generator. The methodology was applied in two European Alpine catchments, the Barcelonnette Basin and the Salzach Valley, for both the historical period, and the future period (2070-2099).

The flood type classification was based on a set of temperature and precipitation indicators as well as day of the year. In this work, the selection of indicators was based on correlation with historical discharge. The findings showed that the methodology was able to reliably reproduce the observed flood types for the two catchments. Care is needed in the selection of the indicator values however, as the variables used will affect the final flood types.

When looking at the future projections, both study areas showed potential changes in the distribution of flood types, as well as the types themselves. For the Barcelonnette Basin, flood events may shift from Rain-Snow (Type 1) dominated floods to Short Rain (Type 2), a type that currently accounts for less than 10% of flood events. Re-clustering of flood types shows changes in the characteristics of the flood events, with higher average daily precipitation amounts and flood events both later and earlier in the year in the future. For the Salzach Valley, Short Rain (Type 2) floods may remain the dominant flood type, although it is possible there is an increase in Rain-Snow floods (Type 1), and overall flood frequency. Re-classifying the future flood events for this catchment also found changes in the flood type characteristics with events occurring throughout the year, and in some instances particularly higher daily precipitation in spring. Although only a limited number of climate projections were considered, the results showed the potential of the methodology developed to assess a large range of possible future changes in flood types for the catchments.

Therefore, this methodology identifies realistic flood types, and can be used to assess future changes in flood types. The methodology has potential to be applied to higher return periods and other catchments as long as the observational records of precipitation, temperature, and flood events are of good quality and length. Changes in flood types are an important consideration for future research as the changes will have an impact on the local social and ecological systems and have implications for future flood management.

8 Changing hydro-meteorological hazard: steps towards action

8.1 Introduction

Climate change will alter the occurrence of hydro-meteorological hazards, but precisely how and what actions can be taken is less clear. Already between 2004 and 2010 there were more than 30,000 fatalities due to non-seismically triggered landslides, primarily in Asia and developing nations (Petley, 2012). In addition, flash floods have led to a high number of fatalities in recent years (Doocy et al., 2013). Compounding the problem for flash floods and landslides is that climate change is projected to be particularly important for mountainous areas (Carey et al., 2012). Climate change-hazard studies use climate projections to understand how hydro-meteorological hazards may change in the future. However, in the development of climate change-hazard studies many assumptions and simplifications are made, along with the inherent uncertainty in the climate projections. Therefore, how can the information in climate change-hazard studies, such as changes in future hazard or improved understanding of the link between climate and hazard be used for, or in, enabling action?

Examples from West Africa, India, and the United States have already shown how action can be taken with better forecasts and utilization of the forecasts under the current climate. In 2008 in West Africa, the International Federation of Red Cross and Red Crescent Societies implemented a set of pre-established actions based on seasonal rainfall forecasts, successfully saving lives and resources in the subsequent flood season (Braman et al., 2013). A lead time in some cases up to a month allowed for disaster response training to be provided, transportation of emergency stocks to key areas and contingency plans were put in place (Braman et al., 2013). Due to better forecasts and improved warning systems, 800,0000 people were evacuated ahead of cyclone Phailin in India (Ghosh et al., 2014) and the evacuation of some vulnerable people and pre-position of search teams was completed ahead of Hurricane Sandy in the United States (Powell et al., 2012). Examples of better understating and utilization of forecasts demonstrate how climate-hazard information can lead to action, which can potentially translate into similar sorts of

action based on climate change-hazard studies.

Therefore, this work introduces some of the ways in which climate change-hazard studies can enable action. Landslides and flash floods are considered in particular, as the events have received less focus from the climate community, compared to other hazards such as river floods, heat waves and drought. A summary of the main conclusions from the previous chapters is given first (Sec 8.2). The following section provides a look at how these and other results can be used for action in the coming decade and for changes in the climate that have already occurred (Sec 8.3). A better understanding about the current link between climate and hydro-meteorological hazards (Sec 8.3.1) is useful not only for climate projections, but may also be useful for early warning systems (Sec 8.3.2), and longer term forecasts over weeks or months (Sec 8.3.3). The usability of future projections is then discussed in Sec 8.4, covering uncertainty in climate projections (Sec 8.4.1), adding climate change to risk calculations (Sec 8.4.2), and how to incorporate previously unprecedented, new hazards in a region (Sec 8.4.3). In each of the sections the focus is on the triggers of the different hydro-meteorological events, as opposed to the vulnerability or exposure to hazard that are out of the scope of this work.

8.2 General conclusions

Starting with the identification of clear meteorological proxies for hydro-meteorological hazards was vital for climate change-hazard studies. The proxies differed not only between the hydro-meteorological hazards, but also causal factors, location, spatial extent and time of year. For the study areas considered in the thesis (the Barcelonnette Basin, France, the Fella River Basin, Italy, and the Salzach Valley, Austria), debris flows and flash floods were mostly triggered by short duration, intense rainfall, while soil slides and floods had a stronger relationship with precipitation over a longer period of time. The length of relevant antecedent period varied between location and hazard. Antecedent precipitation influences the groundwater levels and soil moisture, both of which affect slope stability. For flash floods and debris flows, higher saturation at shallow depths may also lead to more runoff. In Chapter 3, an antecedent period of 30-40 days had the highest correlation with observed debris flows, while for soil slides, the antecedent period of 50 days or longer was more appropriate for the Barcelonnette Basin. The longer antecedent periods for soil slides may be linked with the increasing role of higher groundwater levels for deeper landslides (Ibsen and Casagli, 2004; van Asch et al., 1999), or that the snowpack and subsequent melt has a larger influence on landslides. Warm spring time temperatures can be linked to soil slides (Chapter 3) and flood (Chapter 7) occurrence, likely due to type of precipitation (rain or snow), and snowmelt for the Barcelonnette Basin and the Salzach Valley increasing the soil moisture, or possibly through freeze and thaw cycles (e.g. Mateos et al., 2012).

For slide-type landslides, it was difficult to find a reliable meteorological proxy, possibly due to the variety of potential triggering conditions. In the Barcelonnette Basin, some soil slides were associated with anomalous high daily and antecedent rainfall, others with anomalously high temperatures in spring (snowmelt), as well as combinations of the two (Chapter 3). These differentiations may have been from different sub-types of landslides, although due to the limited number of events dividing the dataset further was not possible. Therefore, without extensive records, and repeated events, a significant relationship between these localized phenomena and the climate was difficult to determine. It may be possible elsewhere to determine a link between climate and soil slides from which climate projections can be developed. Another alternative is to combine projections of temperature and precipitation with stability modelling (e.g. Chiang and Chang, 2011; Melchiorre and Frattini, 2012). However, an understanding of the meteorological conditions leading to a landslide would still be required to adequately downscale the climate data.

For debris flows and flash floods, the events and associated triggers can occur on scales (<10km^2) that make atmospheric proxies better predictors of these events than observed rainfall. The correlation of daily rain gauge data with debris flow and flash flood occurrence for the Barcelonnette Basin was weaker than for the Fella River Basin (Chapter 3). The lower correlation was likely due to the localized nature of convection in the French study area. For this reason, indicators for atmospheric instability and moisture were found to have a better correlation with debris flow occurrence than rainfall (Chapter 5).

In identifying meteorological proxies for hydro-meteorological hazards, the multiple homogeneous precipitation records were available for the three study areas (Chapter 2). The long climate records required can contain shifts in the data caused by non-climatic factors. While there were likely shifts in the three study areas, each study area had at least three homogenous precipitation records longer than 20 years. Furthermore, detected trends in the Barcelonnette and Fella River basin records may have impacted historical hydro-meteorological events. However, as the weather stations were located at lower elevations the records may not be representative of the entire Alpine area. Therefore, analysis of the climate records for change-points and trends should be undertaken before assessing the link between the climate and hydro-meteorological hazards.

The ability of statistical downscaling methods to capture changes in wet day frequency was not representative for changes in extreme precipitation. Statistical downscaling is a method often used to develop finer scale projections of key meteorological variables, yet not all methods are able to adequately capture the extreme precipitation indices require for climate change-hazard studies. Of the four methods trialled in Chapter 4, two analogue methods, a generalized linear model and quantile mapping, quantile mapping had the best performance for the Barcelonnette and Fella River basins. Therefore, quantile mapping was

the suggested method to use when extreme daily precipitation is the main meteorological proxy or trigger.

When developing local climate change projections for debris flows, the decision whether to use atmospheric indicators or rain gauge data had a significant impact on the future occurrence (Chapter 6). Other factors that had a significant effect on the increase of future debris flow occurrence were the base period, representative concentration pathway, and climate model. For the two study areas in Chapter 6, the Barcelonnette and Fella River basins, the area from the climate models for downscaling had little impact on the future debris flow occurrence. Therefore, when developing future projections the base period and proxy (in this case atmospheric variables or rain gauge data) should be considered carefully.

Future changes in flood distribution were found to vary in frequency and in triggering conditions (Chapter 7). For the Barcelonnette Basin, certain projections showed a shift from spring time floods through a combination of rainfall and snowmelt, to floods during summer and autumn from short duration rainfall. If there is a change in causal flood type, this may affect the flood characteristics, such as a more rapid increase of water levels from short rain floods, as well as the exposure due to flooding at different times of the year. During summer, flood plains are often used as temporary campsites in the Barcelonnette Basin, putting more lives at risk in the future. Changes were also found for the Salzach Valley, including an increase in Rain-Snow floods that may be counter intuitive to a warming climate. Therefore in the context of future hydro-meteorological risk, changes in frequency of events should be considered alongside changes in types of hazards.

Changes in land use and other socio-economic factors at the study area scale were not considered when developing future projections. Human mitigation factors have dominated historical changes in debris flows (Crozier, 2010), and will likely contribute to future changes. However, the objective of the research was to provide a meteorological perspective to changing flood and landslide hazard, and the inclusion of changes from land use and other such factors would make it difficult to differentiate the changes driven by future temperature and precipitation. Although it is acknowledged that changes in climate will likely affect vegetation, such as the migration of species to higher elevations, and would be an avenue for future research in the study areas. Therefore, the projections developed here do not reflect the future hydro-meteorological hazard for the study areas, but potential changes from trends in precipitation and temperature.

In the end, future projections were obtained for debris flow occurrence (Chapter 6) and river floods (Chapter 7) by first determining the relevant meteorological proxies over three catchments in Europe. Future projections for other types of landslides were not developed, due to the complexity in relating landslide occurrence to the climate (Chapter 3). When developing the climate projections, assumptions were made, and changes in land use and other socio-economic factors were not considered. Therefore, the results here provide an indication of future

changes in hydro-meteorological hazards for particular areas in the European Alps, although there may still be surprises.

8.3 Starting point for potential actions: Changed climate and actions for the next decade

The usability of results such as those outlined in Sec 8.2 refers not only to action to adapt or mitigate future climate change, but also for potential action over the short term. This section reviews a few of the lessons learnt around identifying meteorological proxies, and how these lessons can be used for actions in the next decade.

8.3.1 Understanding the current system

Understanding the relationship between the hazard and the triggers is the building block from which action can be taken, both for current and future risk. The triggers for flash floods and landslides vary between seasons, locations, and even on inter-annual time scales. Therefore, research will need to focus, in at least some cases, on the local relationship between hazard and triggers before it can be used for actions such as part of an early warning system (EWS). From this relationship, the appropriate forecast data can then be used to develop hourly, daily weekly or even monthly to seasonal forecasts. While the traditional methods based on inventories and rain gauge data will likely still play a role in developing climate hazard-relationships, techniques including remote sensing data and numerical weather prediction (NWP) output should become increasingly important.

Developing and maintaining inventories of recent landslide and flash flood events is vital. Inventories are often poor, making it difficult to determine the triggering factor or temporal probability of the events (van Westen et al., 2006; Modrick and Georgakakos, 2015). In cases such as hurricanes, landslide or flash flood occurrence may not be reported and any subsequent damages erroneously attributed to the hurricane or triggering event (Anderson et al., 2011). Even so, there have been recent attempts to develop global landslide inventories (e.g. Petley et al., 2005; Kirschbaum et al., 2010) or as part of a wider disaster inventory (e.g. *DESINVENTAR.org*, n.d.). These inventories may form a basis for a better understanding of the link between climate and hydro-meteorological hazards around the globe, as well as for understanding the risk.

The most widely used method in defining thresholds for landslides and flash floods is based on rainfall (e.g. Guzzetti et al., 2008; Lainas et al., 2015; Zhuang et al., 2015). In particular, the thresholds are based on the intensity-duration of rainfall, where the duration ranges between 1 to 100 hours (e.g. Guzzetti et al., 2008), although possibly longer for landslides (e.g. Brunetti et al., 2010). Antecedent rainfall could be used, where the antecedent period can be as long as 120 days (e.g. Zêzere et al., 2005; Doglioni et al., 2012; Garcia-Urquia and Axelsson, 2015).

The duration of the antecedent period differs based on lithological, climate and slope conditions, with incompleteness in the rainfall and landslide records adding to the uncertainty in the threshold (Guzzetti et al., 2007). For thresholds in catchments with snowfall, snow cover and snowmelt should also be taken into account (Gourley et al., 2014). For example, Meyer et al. (2012) developed intensity-duration thresholds for Norway using water supply from rainfall and snowmelt, based on both temperature and precipitation, or using temperature and precipitation values in the thresholds directly, as in Chapter 3. However, there are a number of limitations using rain gauge-based thresholds. The thresholds are generally applicable for local or regional areas and are not necessarily transportable to neighbouring or similar catchments (Zhuang et al., 2015). Normalizing rainfall may help, although normalized rainfall thresholds can still differ between regions (Meyer et al., 2012). Furthermore, even in Europe where there is a dense network of rain gauges, rain gauges located at lower elevation can underestimate the triggering events where there is complex topography (Borga et al., 2014). Therefore, other approaches are now being undertaken using other information besides rain gauges to determine the relationship between the climate and hazard, and should continue to be developed more in the future, alongside rain gauge based thresholds.

In recent years remote sensing and NWP data have been utilized to improve the understanding of triggering conditions for landslides and flash floods. Satellite based precipitation measurements provide monitoring over large areas, although there are limitations due to the temporal sampling of the data, spatial resolution, as well as measurement and retrieval errors (Tao and Barros, 2013). Weather radar has also been used to try and account for deficiencies in rain gauge networks, such as in a study using historic radar observations of similar air mass conditions to predict orographic rainfall up to 6 hours (Panziera et al., 2011). However, weather radar can still underestimate extreme rainfall due to observational problems in mountainous areas and is not widely available (Marra et al., 2014). Atmospheric indicators from reanalysis data can be used as alternatives for rain gauge based thresholds (Chapter 5), especially as the parameters can be implemented in early warning systems. Correlating landslide activity with atmospheric circulation patterns is being undertaken (e.g. Chapter3 and Wood et al., 2016), although this is still limited by incomplete inventories at the country or regional level. Therefore, by using remote sensing and reanalysis NWP data, thresholds for hydro-meteorological hazards may be developed for areas where the rain gauge data is poor, although there are still limitations in using this data.

In developing any relationship between climate and hazard occurrence, other influencing factors should not be neglected. While rainfall may be the main trigger for debris flows, sediment sources are required and may limit the occurrence of the hazard (Borga et al., 2014). Slope conditions will change after a landslide and affect the susceptibility of future landslides, a reason why modelling slope-stability is still important for

understanding the landslide triggers at the local scale (Liao et al., 2011; Wu et al., 2015). Changes in land use and human activity may also alter landslide susceptibility in a region. For example, better management with regards to surface and household water led to a reduction in landslides in the Eastern Caribbean without any changes in the climate or other mitigation measures (Anderson et al., 2011). Therefore, it may not always be possible to obtain a clear link between climate and hazardous events and careful consideration is needed about what is actually triggering landslides and flash floods in an area.

Even with all the challenges outline previously, a link between hydro-meteorological hazards and the climate can be found in some instances. This link can then be used as part of early warning systems, along with monitoring, communicating risk and other aspects of early warning systems. The following two sections review some of the early warning systems that have been proposed for flash floods, debris flows and landslides that use rainfall or other climate information on the scale of minutes to days (Sec 8.3.2), as well as possible pathways for midrange forecasts (weeks to months, Sec 8.3.3).

8.3.2 Early warning systems (minutes to days)

Early warning systems for landslides and other hydro-meteorological hazards can be divided into three types: (1) based on rainfall forecasts (2) based on real time monitoring of landslide and flood discharge and (3) community based monitoring. Type 1 is based on rainfall forecasts, where a particular warning is provided based on the different rainfall threshold levels. For example, in Hong Kong, warnings are given based on the Hong Kong Meteorological Centre and the Geotechnical Engineering Office (Cheung et al., 2006). Type (2) are based on real time in-situ measurements, such as those that measure movement for landslides and discharge for flooding. This type of EWS is very localized, and often need maintenance. The final type (3) trains local communities to recognise early signs of problems, such as cracks for landslides, or in the case of floods, warn people downstream. This section will focus primarily on type (1) EWS.

Early warning systems based on simple thresholds as discussed in Sec 3.1 are used due to the good trade-off between low complexity and skill, as well as high uncertainty in extreme rainfall predictions (Borga et al., 2014; Alfieri and Thielen, 2015). Often the EWS are for large areas and provide a warning similar to a weather warning. An European precipitation index based on forecasted precipitation amount and duration has been proposed for flash floods (Alfieri and Thielen, 2015). On a global scale there is research towards satellite-based now-casting for landslides where thresholds based on the intensity and duration of rainfall are combined with static susceptibility maps for warnings for landslides (e.g. Kirschbaum, Adler, Hong, Kumar, Peters-Lidard and Lerner-Lam, 2012). The thresholds were applied on a regional basis using Guzzetti et al. (2008), as regional thresholds performed better than using a single

global threshold. However, the performance of rainfall thresholds can vary over time due to more data or non-climatic changes in the catchment, and should be updated periodically (Rosi et al., 2015). Therefore, thresholds similar to those developed in this thesis can be used as part of an early warning system when combined with readily available forecast or satellite data, and should be considered for areas where more extensive monitoring is not possible.

Advances in numerical weather prediction models and monitoring techniques have led to the development of various experimental early warning systems for flash floods and landslides. Examples include probabilistic forecasts for rapid surface flooding in the UK to account for positional and temporal uncertainty in the extreme rainfall (Hurford et al., 2012), a monitoring network for debris in Southwest China to measure rainfall along with different slope conditions (Huang et al., 2015), and satellite-based rainfall estimates combined with NWP output and rainfall-runoff model for flash floods warning in Klang River basins, Malaysia (Wardah et al., 2008). For landslides, combining rainfall forecasts with slope-stability models is also paving the way for better landslide prediction (e.g. North Carolina: Liao et al. (2011), southern Italy: Grelle et al. (2014), and Seoul, Korea: Kim et al. (2014)). While each of these efforts depends on varying amounts of data, all required extensive study at the local scale to determine correct levels for warnings. In each case there is also a trade of between false alarms (event predicted but does not occur), with missed events (event occurs, but was not predicted). In particular, the accuracy of early warning systems depends strongly on the monitoring and forecasting capabilities of an area, which can still be difficult for extreme rainfall (Borga et al., 2014).

8.3.3 Midrange forecasts (weeks to months)

Midrange or seasonal forecasts can be used for a variety of actions as they provide a longer lead time than the previous early warning systems. As the midrange forecasts are for longer term, they are normally based on general trends (e.g. wetter, drier), or atmospheric circulation patterns, as opposed to early warning systems that are more specific about location, timing and rainfall amount. Still, midrange forecasts provide the opportunity to review emergency plans, stock pile appropriate resources, and review mitigation works such as clearing retention basins and clearing bottlenecks.

For seasonal forecasts of landslides and flash floods, there needs to be a better understanding between atmospheric patterns and landslide occurrence before such midrange forecasts can be utilized. Currently, many seasonal forecasts are based on different observed climate phenomena such as El Nino/La Nina, North Atlantic Oscillation (NAO) and Pacific-North American pattern (PNA) (e.g. Wang et al., 2010; Rajeevan et al., 2012). However, there has been little research comparing landslide frequency and atmospheric patterns. Kirschbaum, Adler, Adler, Peters-Lidard and Huffman (2012) found that the ENSO in the early part of 2010

may have played a role in the increased landslide activity globally for 2010. Landslides associated with long lasting rainfall in Lisbon, Portugal have also been linked with the three month NAO (Zêzere et al., 2005). Particular weather types have also been tentatively linked to debris flows in the southern Swiss Alps, which in turn can be related to the NAO (Toreti et al., 2013). It is possible that warnings may be given for landslides linked to cumulative or antecedent rainfall of a month or longer, however, at this stage more research is needed linking the hydro-meteorological hazards with seasonal climate patterns.

Another avenue is the development of midrange forecasts in relation to external events that increase the susceptibility of a region to landslides, such as a fire or earthquake. Rainfall thresholds for post-fire debris flows were found to be lower than for debris flows in unburned sections (Cannon and DeGraff, 2009; Lainas et al., 2015). Similarly for earthquakes, the Wenchuan earthquake, China led to the abundance of source material for rainfall-induced debris flows or shallow landslides in the years following the event (Tang et al., 2012). Other examples include the 1999 Chi-Chi earthquake in Taiwan (Lin et al., 2004), and the 2005 Kashmir earthquake, Pakistan (Saba et al., 2010), although in the latter case the frequency of landslides returned to pre-earthquake levels within a few years of the event (Khan et al., 2013). And after the April 2015 Nepal earthquake, there is heightened fear in mountainous and hill communities in Nepal that more landslides could occur during the current monsoon season (Khazai et al., 2015). Although currently the country does not have the capacity to provide such early warning. Therefore, there is potential to provide midrange forecasts for landslides and flash floods as part of a cascading or multi-hazard approach, which may be more viable than seasonal forecasts for the hydro-meteorological events, particularly in the short term.

8.4 Starting point for potential actions: Acting now for changes beyond the next decade

Research studying future hydro-meteorological events is likely beneficial for the advancement of science, but it is less clear what actions can be taken based on these assessments. Even with a complete reduction of greenhouse gas emissions, there will be changes in the climate for the future, affecting the frequency, magnitude location and timing of hydro-meteorological events. If there are increases in the frequency, it will affect the ability of communities to recover after a disaster (Labadie, 2011). The biggest opportunity for decision making and action for environmental stresses related to climate change, such as hydro-meteorological hazards, may be at the regional or local level (Barron, 2009). However, obtaining climate impact assessments for every region exposed to hydro-meteorological hazards is likely impossible, if even beneficial due to the uncertainties in the projections. Therefore, this section looks at three

different aspects of understanding future hydro-meteorological hazard: the uncertainty of future projections, incorporating climate change into risk calculations, and new hazards.

8.4.1 Uncertain future-quantifying the uncertainty

Alongside the uncertainties in linking the climate with hydro-meteorological events, future projections of climate extremes often show a wider range of future possibilities than for mean conditions, such as average temperature. This uncertainty comes from uncertainty in the model, the initial state, observations, downscaling, translating emissions to concentrations, the socio-economics behind emission scenarios and feedback from climate change that then alter emissions (van der Linden and Mitchell, 2009). Much of the uncertainty in the climate is irreducible (Dessai and Hulme, 2004). Studies often look to 2100 to obtain a significant trend, such as in Chapter 6 and 7, however at this timescale, human influence becomes more important, increasing the uncertainty (Weaver et al., 2013). Climate models are also not optimized for extreme precipitation, an important trigger of flash floods and debris flows (Cabello et al., 2011). Furthermore, climate change impact studies often take a linear approach and do not consider the complex interactions and feedbacks in the systems (Falloon et al., 2010). Therefore, should communities prepare for particular scenarios, or just work on increasing resilience?

Capturing a wide variety of future scenarios may be a way to quantify some of the uncertainty, and has led to the development of probabilistic projections. Ensemble approaches use multiple projections from different models, different initial conditions, or with perturbations of parameters in climate models. One example are the set of probabilistic climate projections for the UK under climate change (UKCP09; Street et al., 2009). The probabilistic projections address to a various extent uncertainty from natural variability, modelling, and emissions. The range of projections are obtained through using multiple climate models and perturbation of the models, as well as using multiple emissions scenarios (Murphy et al., 2009). User guidance is also provided to highlight that multiple projections should be used and with different emission scenarios. Murphy et al. (2009) also highlight that the probability is the degree to which each climate projection is supported by the evidence available, based on the current understanding and observations. Since becoming available, the UKCP09 dataset has been used in a variety of climate change impact assessments for the UK (e.g. building performance: Tian and de Wilde (2011), water resource planning: Christierson et al. (2012), future wind hazard: Blenkinsop et al. (2012)). However, when assessing the UKCP09 probabilistic projections for adaptation planning, Tang et al. (2012) found that the ability of decision makers to use the data depended on their scientific competence and familiarity with climate information.

Another approach presented by Vano et al. (2015), selects climate scenarios based on impact relevant sensitivities, such as change in pre-

cipitation or temperature. As it is often not possible to include all available projections in an assessment, a subset are selected based on the application. Vano et al. (2015) provide two examples: one for hydrological sensitives, and another for vegetation carbon sensitivities. For the hydrological example, perturbations of the historical temperature and precipitation data are applied to a hydrological model to determine the sensitivity for a particular catchment. As catchments can have different responses to the same temperature or precipitation change, GCMs can be selected based on those that would have a varying effect on the discharge for a specific catchment, overall reducing the number of climate model projections that need to be downscaled and fed into the hydrological model. Care is needed when selecting the models however, the sensitivities for mean conditions, such as mean streamflow outlined above, may not necessarily be the same for extremes, which are of interest in climate change-hazard studies.

Both of the approaches above are based on the current (incomplete) knowledge of the future. Therefore, proposals have also been put forward to address the different sources of uncertainty separately, such as inherent uncertainties, model uncertainties and method limitations (Déandreis et al., 2014). However, as was raised by Tang et al. (2012), whatever approach is taken depends on the ability for users to interpret the results. During the work of this thesis, the preferred approach became to select relevant climate scenarios, without assigning likelihood. While a variety of climate projections are available through projects such as CORDEX or CMIP5, to translate these into projections for hydro-meteorological hazards is both computationally costly and time consuming. Even if multiple projections are obtained, the projections will not be able to determine what projection or scenario is most likely. Therefore, probabilistic projections for hydro-meteorological hazards should be restricted to those that have an understanding of climate science, to prevent inappropriate action.

8.4.2 Risk

The natural step after developing projections of changing hydro-meteorological hazard may seem to be to include these as possible future scenarios in risk calculations. The frequency of a particular hazardous event could be altered to match future projections, allowing projected future risk to be calculated. A long term view is also needed for planning of both structure and non-structural mitigation measures, such as retention basins and land use planning. Risk maps combine the likelihood of a particular hazard with the impact for a particular area. By including climate scenarios into risk and risk maps, it may lead to the incorporation of climate information into decision making and highlight that changes in climate change occur alongside changes in vulnerability and exposure (Labadie, 2011).

An example incorporation of climate change in risk calculations can be found for flood defences in the Netherlands. In 2000, a new policy dir-

ective 'Room for the River' outlined that the Netherlands should prepare for future peak discharges based on changes in sea level rise and rainfall (van Stokkom et al., 2005). The approach includes not only considering future climate change, as well as other factors including citizen awareness, responsibility for different tasks, and coordination of knowledge (van Stokkom et al., 2005). Based on the IPCC climate scenarios, three scenarios for flood defence design were given, with the middle scenarios used for the design (Slomp, 2012). The scenarios provided the basis from which the cost for river and coastal flood management for conditions under the future climate could be calculated, such as dike reinforcement and river widening (Aerts and Botzen, 2012).

There are risks in including climate change information in risk calculation, however. There is a limit to what downscaling can do, and what is needed for risk maps may not be at the scale that end-users need (Déandreis et al., 2014). The size of the catchments considered in the Netherlands above are much larger than the catchments considered in mountainous catchments, and are not subjected to all of the same challenges outlined in Sec 8.2. Furthermore, the climate projections contain subjective uncertainty, different than uncertainty in the current risk map process, and therefore care is needed (Dessai and Hulme, 2004). Furthermore, misinformation could lead to mal-adaptation (Tall et al., 2013). From the conclusions in this PhD research, a top-down approach of developing climate change-hazard projections for mountainous areas for direct as part of risk calculations is not an advisable way to proceed due to the high uncertainty of the projections involved.

An alternative to using risk maps from the point of view 'predict then act' is to for climate change projections to be used as scenario generators, or test cases, in a bottom up approach (Weaver et al., 2013). The developed scenarios can be used to help determine under what conditions policies or protective measures fail. This approach requires clearly defining and working with the end-users, as it is likely that a climate expert cannot decide alone what the relevant questions for a region are. An example is the development of almost worse case scenarios. As the worse-case scenario is unknown, the addition of the word 'almost' highlights for the end user or decision maker the incomplete knowledge about the future.

Finally, even if limitations in the downscaling of relevant climate information cannot answer these questions, possible changes in landslide and flash flood risk may be used to convey the seriousness and importance of the impact of climate change as part of the risk discussion. For example, visualization of changing snow pack in North Vancouver, Canada, under climate change was done to highlight awareness of changes landslide, forest fire and other risks (Cohen et al., 2012). Using climate change information to show where there may be an increase (or decrease) in hydro-meteorological risk in the future without providing absolute values reduces the chance of mal-adaptation.

Therefore, while inclusions of climate change in risk calculations may still be questionable, particularly for hydro-meteorological hazards in

mountainous areas, climate experts working with end users could lead to the development of relevant climate scenarios or test cases. Lempert and Schlesinger (2000) argue that the question that should be asked is not 'what will happen in the future?', rather 'what actions should we take, given that we cannot predict the future?'. The climate-hazard test cases, instead of deterministic projections, can help communities understand the options given changes in the climate (Meyer, 2011).

8.4.3 New system-new hazard

Not all changes in hazard are simply a change in frequency or magnitude, however. There can also be new hazards, such as a new hazard of rock falls or debris flows from warming temperatures causing destabilization of slopes. Even if an area experiences a variety of hydro-meteorological hazards, it is possible that the future characteristics of the hazard may change, as found in Chapter 7. Through exploratory modelling it may be possible to identify surprise or special cases in the system behaviour (Weaver et al., 2013). Or by assessing more than just changes in frequency of extreme precipitation, other changes in the climate may indicate possible new types of hazards. This section will outline some of the ways in which surprises may occur or have occurred in mountainous catchments. The surprises are summarized in Table 8.1, which outlines the change in the climate, the effect on the catchment, and the change in the hydro-meteorological hazard.

Table 8.1 A selection of possible surprises for climate change-hazard studies

Climate change	Environment	Hydro-meteorological hazard
Warmer temperatures	Thawing permafrost, retreat of glaciers	New debris flows, rockslides or avalanches
Warmer and drier conditions	Increases in forest fires (also linked to thunderstorms)	New precipitation threshold for debris flows
Longer growing season	Upward migration of vegetation	Changes in slope stability (debris flows, shallow landslides)
Sequences of extremes (e.g. extreme rainfall after droughts)	More wet/dry cycles over a period of time, leading to more weathering	Changes in slope stability

Persistent increases in mean temperatures can lead to the uncovering of glacial sediments and thawing of permafrost, leading to debris flows, as well as transport of heat to the subsurface can alter slope stability leading to rock slides or avalanches (Huggel et al., 2012). From 2009 onwards, the frequent rock falls on the north east face of Ritzlihorn, Switzerland are likely due to thawing permafrost (Huggel et al., 2013). In April 2007, warming of permafrost as well as very warm temperatures

in the preceding months led to a large (0.3 x106 m^3) rock slope failure Monte Rosa, Italy (Fischer et al., 2013). Ice cover of the east face of Monte Rosa had begun to decrease rapidly from 1988 onwards (Fischer et al., 2013). It was hypothesized that the warmer summer temperatures between 2003 and 2007 caused warming in the bedrock, and coupled with the spring heat wave that Europe experiences in the weeks before the failure, led to the rock slope failure (Huggel et al., 2010). In August 2005 one of the largest debris flows in the Swiss Alps in the 20^{th} Century occurred in Rotaui-Guttannen, with a total volume of 500,000m^3 (Huggel et al., 2012). Previous retreat of the glacier exposed large reservoirs of sediment and combined with warm temperatures and heavy rainfall, resulted in a debris flow that dammed the Aare River and caused extensive flooding in a nearby village (Huggel et al., 2012). These examples show how mountainous areas may see new hazards due to changes in permafrost and glacial retreat, which will continue in the future with further warming.

Warming temperatures can lead to other changes in mountainous areas. These changes may include the upward migration of vegetation, changing the stability of the slope (Beniston, 2003). During the 20^{th} century, forested plant species saw a shift to higher optimum elevations in Europe (Lenoir et al., 2008)). Vegetation can increase slope stability, although it depends on the type of vegetation and properties of the slope (Schwarz et al., 2010). There may also be an increase in forest fire intensity or extent (Dale et al., 2001). Section 8.3.3 outlined how wide spread forest fires can lead to an increase in debris flow. Warmer and drier conditions with climate change could lead to an increase in forest fires, potentially counteracting any upward migration of species (Dale et al., 2001).

There are other changes in climate that could bring about surprises in future hydro-meteorological hazards. The the occurrence of more wet and dry spells can also reduce the stability of a slope, or increased wind could lead to further evaporation and cracks in slopes (Crozier, 2010). The shift of storm tracks could lead to significant increases in rainfall in areas where there were previously few landslides or floods. Although previous research has found it difficult to relate landslides with atmospheric circulation patterns (Sec 3.3), Zêzere et al. (2005) were able to establish a relationship between landslides and the NAO in Portugal due to the position of storm tracks over the study area. While it may not be possible to consider all potential new hazards, by considering changes that have already been observed in similar areas, or through exploratory modelling, climate change-hazard studies may be able to identify surprises in the climate system.

Finally, when a new system emerges, such as through new hazards or different triggering mechanism, these changes may inhibit a community's ability to predict the hazardous events. Already it has been noted that the changes in climate has limited the Inuit elder's ability to predict weather in the Arctic (Weatherhead et al., 2010), along with examples from other regions (e.g. New Zealand, King et al. (2008)) . If climate

change-hazard studies can identify possible new hazards or changes in the system, they can make communities aware of and plan for new challenges they may face in the future.

8.5 Conclusion

There are many challenges in developing climate change-hazard studies for landslides and other hydro-meteorological hazards, and even more when trying to take action based on the assessments. Learning more about the link between climate and the hazard may not only improve climate projections, but can also be used in early warning or mid-range forecasts. Current work to improve global landslide inventories and the use of satellite data make these methods potentially applicable over a wider area. When looking to the future, the inclusion of adaptation plans for hydro-meteorological hazards will mean that these hazards are considered a key role in adapting to future climate change. However, tailored climate information should come from cooperation between climate experts and users. Consideration should also be given to potential new hazards in an area, particularly as local communities may be unfamiliar in how to respond to such events. However, there is no simple relationship between more information and better decisions (Weaver et al., 2013). Waiting for more information, more projections before action is taken may not be the answer. Perhaps the best approach for taking action at the local scale is to address current challenges along with researchers and end users working together to develop relevant climate change-hazard studies.

Bibliography

Aerts, J. and Botzen, W. (2012). Climate adaptation cost for flood risk management in the netherlands, *Storm Surge Barriers to Protect New York City*, American Society of Civil Engineers, pp. 99–113.

Aguilar, E., Auer, I., Brunet, M., Peterson, T. and Wieringa, J. (2003). Guidelines on climate metadata and homogenization, *Technical report*, World Meteorological Organization, Geneva, Switzerland.

Akhtar, M., Ahmad, N. and Booij, M. (2008). The impact of climate change on the water resources of hindukush-karakorum-himalaya region under different glacier coverage scenarios, *J Hydrol* **355**: 148–163.

Aleotti, P. (2004). A warning system for rainfall-induced shallow failures, *Eng Geol* **73**: 247–265.

Alexander, L., Zhang, X., Peterson, T., Caesar, J., Gleason, B., Tank, A. K., Haylock, M., Collins, D., Trewin, B., Rahimzadeh, F., Tagipour, A., Kumar, K. R., Revadekar, J., Griffiths, G., Vincent, L., Stephenson, D., Burn, J., Aguilar, E., Brunet, M., Taylor, M., New, M., Zhai, P., Rusticucci, M. and Vazquez-Aguirre, J. (2006). Global observed changes in daily climate extremes of temperature and precipitation, *J Geophys Res* **111**: D05109.

Alfieri, L. and Thielen, J. (2015). A european precipitation index for extreme rain-storm and flash flood early warning, *Meteorol Appl* **22**: 3–13.

Alila, Y. and Mtiraoui, A. (2002). Implications of heterogeneous flood-frequency distributions on traditional stream-discharge prediction techniques, *Hydrol Process* **16**: 1065–1084.

Anderson, M., Holcombe, E., Blake, J., Ghesquire, F., Holm-Nielsen, N. and Fisseha, T. (2011). Reducing landslide risk in communities: Evidence from the eastern caribbean, *Appl Geogr* **31**: 590–599.

Ansari, Z., Ahmed, W., Azeem, M. and Babu, A. (2011). Quantitative evaluation of performance and validity indices for clustering the web navigation sessions, *World of Computer Science and Information Technology Journal* **1**: 217–226.

Arguez, A. and Vose, R. (2010). The definition of the standard wmo climate normal: The key to deriving alternative climate normals, *B Am Meteorol Soc* **92**: 699–704.

Arnaud-Fassetta, G., Cossart, E. and Fort, M. (2005). Hydro-geomorphic hazards and impact of man-made structures during the catastrophic flood of june 2000 in the upper guil catchment (queyras, southern french alps), *Geomorphology* **66**: 41–67.

Arnell, N. and Gosling, S. (2014). The impacts of climate change on river flood risk at the global scale, *Climatic Change* pp. 1–15.

Asadieh, B. and Krakauer, N. (2015). Global trends in extreme precipitation: climate models versus observations, *Hydrol Earth Syst Sci* **19**: 877–891.

Auer, I., Böhm, R., Jurkovic, A., Lipa, W., Orlik, A., Potzmann, R., Schöner, W., Ungersböck, M., Matulla, C., Briffa, K. and et al. (2007). Histalp-historical instrumental climatological surface time series of the greater alpine region, *Int J Climatol* **27**: 17–46.

Aulitzky, H. (1989). The debris flows of austria, *Bulletin of the International Association of Engineering Geology - Bulletin de l'Association Internationale de Géologie de l'Ingénieur* **40**: 5–13.

Bacchini, M. and Zannoni, A. (2003). Relations between rainfall and triggering of debris-flow: case study of cancia (dolomites, northeastern italy), *Nat Hazard Earth Sys* **3**: 71–79.

Baldi, P., Brunak, S., Chauvin, Y., Andersen, C. and Nielsen, H. (2000). Assessing the accuracy of prediction algorithms for classification: an overview, *Bioinformatics* **16**: 412–424.

Bárdossy, A. and Filiz, F. (2005). Identification of flood producing atmospheric circulation patterns, *J Hydrol* **313**: 48–57.

Barrera-Escoda, A. and Llasat, M. (2015). Evolving flood patterns in a mediterranean region (1301-2012) and climatic factors - the case of catalonia, **19**: 465–483.

Barron, E. (2009). Beyond climate science, *Science* **326**: 643.

Benestad, R. and Haugen, J. (2007). On complex extremes: flood hazards and combined high spring-time precipitation and temperature in norway, *Climatic Change* **85**: 381–406.

Beniston, M. (2003). Climatic change in mountain regions: A review of possible impacts, *Climatic Change* **59**: 5–31.

Bergström, S. (1976). *Development and application of a conceptual runoff model for Scandinavian catchments*, Department of Water Resources, Engineering, Lund Institute of Technology, Lund, Sweden.

Bergström, S., Carlsson, B., Gardelin, M., Lindström, G., Pettersson, A. and Rummukainen, M. (2001). Climate change impacts on runoff in sweden - assessments by global climate models, dynamical downscaling and hydrological modelling, *Climate Research* **16**: 101–112.

Berti, M., Martina, M., Franceschini, S., Pignone, S., Simoni, A. and Pizziolo, M. (2012). Probabilistic rainfall thresholds for landslide occurrence using a bayesian approach, *J Geophys Res-Earth* **117**: F4.

Beven, K. (2012). *Rainfall-Runoff Modelling: The Primer, 2nd Edition*, Wiley-Blackwell.

Bezak, N., Brilly, M. and Šraj, M. (2013). Comparison between the peaks over threshold method and the annual maximum method for flood frequency analyses, *Hydrolog Sci J* **59**: 959–977.

Blenkinsop, S., Zhao, Y., Quinn, J., Berryman, F., Thornes, J., Bake, R. and Fowler, H. (2012). Downscaling future wind hazard for se london using the ukcp09 regional climate model ensemble, *Climate Res* **53**: 141–156.

Blöschl, G., Nester, T., Komma, J., Parajka, J. and ao, R. P. (2013). The june 2013 flood in the upper danube basin, and comparisons with the 2002, 1954 and 1899 floods, *Hydrol Earth Syst Sci* **17**: 5197–5212.

Booij, M. (2005). Impact of climate change on river flooding assessed with different spatial model resolutions, *J Hydrol* **303**: 176–198.

Borga, M., Boscolo, P., Zanon, F. and Sangati, M. (2007). Hydrometeorological analysis of the 29 august 2003 flash flood in the eastern italian alps, *J Hydrometeorology* **8**: 1049–1067.

Borga, M., Stoffel, M., Marchi, L., Marra, F. and Jakob, M. (2014). Hydrogeomorphic response to extreme rainfall in headwater systems: Flash floods and debris flows, *J Hydrol* **518**: 194–205.

Borgatti, L. and Soldati, M. (2010). Landslides as a geomorphological proxy for climate change: A record from the dolomites (northern italy), *Geomorphology* **120**: 56–64.

Braman, L., van Aalst, M., Mason, S., Suarez, P., Ait-Chellouche, Y. and Tall, A. (2013). Climate forecasts in disaster management: Red cross flood operations in west africa, 2008, *Disasters* **37**: 144–164.

Brands, S., Herrera, S., Fernández, J. and Gutiérrez, J. (2013). How well do cmip5 earth system models simulate present climate conditions in europe and africa?, *Clim Dynam* **41**: 803–817.

Breinl, K. (2016). Driving a lumped hydrological model with precipitation output from weather generators of different complexity, *Hydrolog Sci J* **61**.

Breinl, K., Turkington, T. and Stowasser, M. (2014). Simulating daily precipitation and temperature: a weather generation framework for assessing hydrometeorological hazards, *Meteorol Appl* **22**: 334–347.

Brunetti, M., Luino, F., Vennari, C., Peruccacci, S., Biddoccu, M., Valigi, D., Luciani, S., Cirio, C., Rossi, M., Nigrelli, G., Ardizzone, F., Palma, M. and Gussetti, F. (2013). Rainfall thresholds for possible occurrence of shallow landslides and debris flows in italy, *in* M. Schneuwly-Bollschweiler, M. Stoffel and F. Rudolf-Miklau (eds), *Dating torrential processes on fans and cones*, Springer, Netherlands, pp. 327–339.

Brunetti, M., Peruccacci, S., Rossi, M., Luciani, S., Valigi, D. and Guzzetti, F. (2010). Rainfall thresholds for the possible occurrence of landslides in italy, *Nat Hazard Earth Syst Sci.* **10**: 447–458.

Buonomo, E., Jones, R., Huntingford, C. and Hannaford, J. (2007). On the robustness of changes in extreme precipitation over europe from two high resolution climate change simulations, *Q J Roy Meteor Soc* **133**: 65–81.

Cabello, A., Velasco, M., Barredo, J., Hurkmans, R., Barrera-Escoda, A., Sempere-Torres, D. and Velasco, D. (2011). Assessment of future scenarios of climate and land-use changes in the imprints test-bed areas, *Environ Sci Policy* **14**: 884–897.

Caine, N. (1980). The rainfall intensity: duration control of shallow landslides and debris flows, *Geogr Ann A* **62**: 23–27.

Cannon, S. and DeGraff, J. (2009). The increasing wildfire and post-fire debris-flow threat in western usa, and implications for consequences of climate change, *in* K. Sassa and P. Canuti (eds), *Landslides - Disaster Risk Reduction*, Springer Berlin Heidelberg, pp. 177–190.

Carey, M., Huggel, C., Bury, J., Portocarrero, C. and Haeberli, W. (2012). An integrated socio-environmental framework for glacier hazard management and climate change adaptation: lessons from lake 513, cordillera blanca, peru, *Climatic Change* **112**: 733–767.

Cepeda, J., Colonnelli, S., Kronholm, K. and et al. (2010). Statistical and empirical models for prediction of precipitation-induced landslides, *Report D1.5, SafeLand:Living with landslide risk in Europe*, p. 137pp. **URL:** *http://www.safeland-fp7.eu/results/Documents/D1.5_revised.pdf*

Ceschia, M., Micheletti, S. and Carniel, R. (1991). Rainfall over friuli-venezia giulia: High amounts and strong geographical gradients, *Theor Appl Climatol* **43**: 175–180.

Chemenda, A., Bouissou, S. and Bachmann, D. (2005). Three-dimensional physical modeling of deep-seated landslides: New technique and first results, *J Geophys Res-Earth* **110**: F04004.

Chen, L., van Westen, C., Hussin, H., Ciurean, R., Turkington, T., Chavarro-Rincon, D. and Shrestha, D. (2016). Integrating expert opinion with modelling for quantitative multi-hazard risk assessment in the eastern italian alps, *Geomorphology* .

Chen, S., Yu, P. and Tang, Y. (2010). Statistical downscaling of daily precipitation using support vector machines and multivariate analysis, *J Hydrol* pp. 13–22.

Cheung, P., Wong, M. and Yeung, H. (2006). Application of rainstorm nowcast to real-time warning of landslide hazards in hong kong, *WMO PWS workshop on warnings of real-time hazards by using nowcasting technology*, WMO PWS Workshop on Warnings of Real-Time Hazards Sydney, Australia.

Chiang, S. and Chang, K. (2011). The potential impact of climate change on typhoon-triggered landslides in taiwan, 2010-2099, *Geomorphology* **133**: 143–151.

Christensen, J., Rummukainen, M. and Lenderink, G. (2009). Formulation of very-high-resolution regional climate models, *in* P. van der Linden and J. Mitchell (eds), *ENSEMBLES: Climate Change and its Impacts: Summary of research and results from the ENSEMBLES project*, Met Office, Hadley Centre, Exeter, United Kingdom, pp. 47–58.

Christierson, B., Vidal, J. and Wade, S. (2012). Using ukcp09 probabilistic climate information for uk water resource planning, *J Hydrol* pp. 48–67.

Cohen, S., Sheppard, S., Shaw, A., Flanders, D., Burch, S., Taylor, B., Hutchinson, D., Cannon, A., Hamilton, S., Burton, B. and Carmichael, J. (2012). Downscaling and visioning of mountain snow packs and other climate change implications in north vancouver, british columbia, *Mitigation and Adaptation Strategies for Global Change* **17**: 25–49.

Costa, A. and Soares, A. (2009). Homogenization of climate data: Review and new perspectives using geostatistics, *Math Geosci* **41**: 291–305.

Crozier, M. (2010). Deciphering the effect of climate change on landslide activity: A review, *Geomorphology* pp. 260–267.

Cuo, L., Pagano, T. and Wang, Q. (2011). A review of quantitative precipitation forecasts and their use in short- to medium-range streamflow forecasting, *J Hydrometeorology* **12**: 713–728.

Dabbiru, L., Aanstoos, J. and Younan, N. (2015). Earthen levee slide detection via automated analysis of synthetic aperture radar imagery, *Landslides* .

D'Agostino, V. and Marchi, L. (2001). Debris flow magnitude in the eastern italian alps: data collection and analysis, *Phys Chem Earth Pt C* **26**: 657–663.

Dai, A., Fyfe, J., Xie, S. and Dai, X. (2015). Decadal modulation of global surface temperature by internal climate variability, *Nature Climate Change* **5**: 555–559.

Dale, V., Joyce, L., McNulty, S., Neilson, R., Ayres, M., Flannigan, M., Hanson, P., Irland, L., Lugo, A., Peterson, C., Simberloff, D., Swanson, F., Stocks, B. and Wotton, B. (2001). Climate change and forest disturbances: Climate change can affect forests by altering the frequency, intensity, duration, and timing of fire, drought, introduced species, insect and pathogen outbreaks, hurricanes, windstorms, ice storms, or landslides, *BioScience* **51**: 723–734.

Das, T., Bárdossy, A., Zehe, E. and He, Y. (2008). Comparison of conceptual model performance using different representations of spatial variability, *J Hydrol* **356**: 106–118.

Dayan, U., Tubi, A. and Levy, T. (2012). On the importance of synoptic classification methods with respect to environmental phenomena, *Int J Climatol* **32**: 681–694.

Dayon, G., Boé, J. and Martin, E. (2015). Transferability in the future climate of a statistical downscaling method for precipitation in france, *J Geophys Res-Atmos* **120**: 1023–1043.

Déandreis, C., Pagé, C., Braconnot, P., Bärring, L., Bucchignani, E., de Cerff, W., Hutjes, R., Joussaume, S., Mares, C., Planton, S. and Plieger, M. (2014). Towards a dedicated impact portal to bridge the gap between the impact and climate communities : Lessons from use cases, *Climatic Change* **125**: 333–347.

Dee, D., Uppala, S., Simmons, A., Berrisford, P., Poli, P., Kobayashi, S., Andrae, U., Balmaseda, M., Balsamo, G., Bauer, P., Bechtold, P., Beljaars, A., van de Berg, L., Bidlot, J., Bormann, N., Delsol, C., Dragani, R., Fuentes, M., Geer, A., Haimberger, L., Healy, S., Hersbach, H., Hólm, E., Isaksen, L., Kållberg, P., Köhler, M., Matricardi, M., McNally, A., Monge-Sanz, B., Morcrette, J., Park, B., Peubey, C., de Rosnay, P., Tavolato, C., Thépaut, J. and Vitart, F. (2011). The era-interim reanalysis: configuration and performance of the data assimilation system, *Q J Roy Meteor Soc* **137**: 553–597.

Dehn, M. and Buma, J. (1999). Modelling future landslide activity based on general circulation models, *Geomorphology* **30**: 175–187.

Delgado, J., Merz, B. and Apel, H. (2014). Projecting flood hazard under climate change: an alternative approach to model chains, *Nat Hazard Earth Syst Sci* **14**: 1579–1589.

Déqué, M., Somot, S., Sanchez-Gomez, E., Goodess, C., Jacob, D., Lenderink, G. and Christensen, O. (2012). The spread amongst ensembles regional scenarios: regional climate models, driving general circulation models and interannual variability, *Clim Dynam* **38**: 951–964.

Déry, S. and Brown, R. (2007). Recent northern hemisphere snow cover extent trends and implications for the snow-albedo feedback, *Geophys Res Lett* **34**: L22504.

DESINVENTAR.org (n.d.). `http://http://www.desinventar.org/`. Accessed: 2016-03-27.

Dessai, S. and Hulme, M. (2004). Does climate adaptation policy need probabilities?, *Clim Policy* **4**: 107–128.

D'Este, C. and Rahman, A. (2013). Similarity weighted ensembles for relocating models of rare events, *in* Z. Zhou, F. Roli and J. Kittler (eds), *Multiple Classifier Systems*, Springer Berlin Heidelberg, pp. 25–36.

Dhakal, A. and Sidle, R. (2004). Distributed simulations of landslides for different rainfall conditions, *Hydrol Process* **18**: 757–776.

Diaz-Nieto, J. and Wilby, R. (2005). A comparison of statistical downscaling and climate change factor methods: impacts on low flows in the river thames, united kingdom, *Climatic Change* **69**: 245–268.

Dobler, A., Yaoming, M., Sharma, N., Kienberger, S. and Ahrens, B. (2011). Regional climate projections in two alpine river basins: Upper danube and upper brahmaputra, *Advances in Science Research* **7**: 11–20.

Dobler, C., Bürger, G. and Stötter, J. (2013). Simulating future precipitation extremes in a complex alpine catchment, *Nat Hazard Earth Syst Sci* **13**: 263–277.

Dobler, C., Hagemann, S., Wilby, R. and Stötter, J. (2012). Quantifying different sources of uncertainty in hydrological projections in an alpine watershed, *Hydrol Earth Syst Sci* **16**: 4343–4360.

Doglioni, A., Fiorillo, F., Guadagno, F. and Simeone, V. (2012). Evolutionary polynomial regression to alert rainfall-triggered landslide reactivation, *Landslides* **9**: 53–62.

Done, J., Craig, G., Gray, S., Clark, P. and Gray, M. (2006). Mesoscale simulations of organized convection: Importance of convective equilibrium, *Q J Roy Meteor Soc* **132**: 737–756.

Doocy, S., Daniels, A., Murray, S. and Kirsch, T. (2013). The human impact of floods: a historical review of events 1980-2009 and systematic literature review, *PLoS Currents* **5**.

Dowling, C. and Santi, P. (2014). Debris flows and their toll on human life: a global analysis of debris-flow fatalities from 1950 to 2011, *Nat Hazards* **71**: 203–227.

Dube, A., Ashrit, R., Ashish, A., Sharma, K., Iyengar, G., Rajagopal, E. and Basu, S. (2014). Forecasting the heavy rainfall during himalayan floodingâĂŤjune 2013, *Weather and Climate Extremes* **4**: 22–34.

Ducré-Robitaille, J., Vincent, L. and Boulet, G. (2003). Comparison of techniques for detection of discontinuities in temperature series, *Int J Climatol* **23**: 1087–1101.

Ducrocq, V., Nuissier, O., Ricard, D., Lebeaupin, C. and Thouvenin, T. (2008). A numerical study of three catastrophic precipitating events over southern france. ii: Mesoscale triggering and stationarity factors, *Q J Roy Meteor Soc* **134**: 131–145.

Falloon, P., R. and Betts (2010). Climate impacts on european agriculture and water management in the context of adaptation and mitigation-the importance of an integrated approach, *Sci Total Environ* **408**: 5667–5687.

Finger, D., Heinrich, G., Gobiet, A. and Bauder, A. (2012). Projections of future water resources and their uncertainty in a glacierized catchment in the swiss alps and the subsequent effects on hydropower production during the 21st century, *Water Resour Res* **48**: w02521.

Fischer, L., Huggel, C., Kääb, A. and Haeberli, W. (2013). Slope failures and erosion rates on a glacierized high-mountain face under climatic changes, *Earth Surf Proc Land* **38**: 836–846.

Flageollet, J., Maquaire, O., Martin, B. and Weber, D. (1999). Landslides and climatic conditions in the barcelonnette and vars basins (southern french alps, france), *Geomorphology* **30**: 65–78.

Fowler, H. and Ekström, M. (2009). Multi-model ensemble estimates of climate change impacts on uk seasonal precipitation extremes, *Int J Climatol* **29**: 385–416.

Frattini, P., Crosta, G. and Sosio, R. (2009). Approaches for defining thresholds and return periods for rainfall-triggered shallow landslides, *Hydrol Process* **23**: 1444–1460.

Frei, C. and Schär, C. (2001). Detection probability of trends in rare events: Theory and application to heavy precipitation in the alpine region, *J Climate* **14**: 1568–1587.

Frei, C., Schöll, R., Fukutome, S., Schmidli, J. and Vidale, P. (2006). Future change of precipitation extremes in europe: Intercomparison of scenarios from regional climate models, *J Geophys Res-Atmos* **111**: D06105.

Freudiger, D., Kohn, I., Stahl, K. and Weiler, M. (2014). Large-scale analysis of changing frequencies of rain-on-snow events with flood-generation potential, *Hydrol Earth Syst Sci* **18**: 2695–2709.

Gaál, L., Szolgay, J., Kohnová, S., Parajka, J., Merz, R., Viglione, A. and Blöschl, G. (2012). Flood timescales: Understanding the interplay of climate and catchment processes through comparative hydrology, *Water Resour Res* **48**: W04511.

Gain, A., Apel, H., Renaud, F. and Giupponi, C. (2013). Thresholds of hydrologic flow regime of a river and investigation of climate change impact-the case of the lower brahmaputra river basin, *Climatic Change* **120**: 463–475.

Gao, H., He, X., Ye, B. and Pu, J. (2012). Modeling the runoff and glacier mass balance in a small watershed on the central tibetan plateau, china, from 1955 to 2008, *Hydrol Process* **26**: 1593–1603.

Garcia-Urquia, E. and Axelsson, K. (2015). Rainfall thresholds for the occurrence of urban landslides in tegucigalpa, honduras: An application of the critical rainfall intensity, *Geogr Ann A* **97**: 61–83.

Garner, G., Loon, A. V., Prudhomme, C. and Hannah, D. (2015). Hydroclimatology of extreme river flows, *Freshwater Biol* **60**: 2461–2476.

Gaume, E., Bain, V., Bernardara, P., Newinger, O., Barbuc, M., Bateman, A., Blaškovičová, L., Blöschl, G., Borga, M., Dumitrescu, A., Daliakopoulos, I., Garcia, J., Irimescu, A., Kohnova, S., Koutroulis, A., Marchi, L., Matreata, S., Medina, V., Preciso, E., Sempere-Torres, D., Stancalie, G., Szolgay, J., Tsanis, I., Velasco, D. and Viglione, A. (2009). A compilation of data on european flash floods, *J Hydrol* **367**: 70–78.

Geletu, A. (2007). Solving optimization problems using the matlab optimization toolbox, *Tutorial*.

Gelfan, A. (2010). Extreme snowmelt floods: Frequency assessment and analysis of genesis on the basis of the dynamic-stochastic approach, *J Hydrol* **388**: 85–99.

Ghosh, S., Vidyasagaran, V. and Sandeep, S. (2014). Smart cyclone alerts over the indian subcontinent, *Atmos Sci Lett* **15**: 157–158.

Giannecchini, R. (2006). Relationship between rainfall and shallow landslides in the southern apuan alps (italy), *Nat Hazard Earth Sys* **6**: 357–364.

Giorgi, F. (2006). Climate change hot-spots, *Geophys Res Lett* **33**: L08707.

Glade, T., Crozier, M. and Smith, P. (2000). Applying probability determination to refine landslide-triggering rainfall thresholds using an empirical antecedent daily rainfall model, *Pure Appl Geophys* **157**: 1059–1079.

Gourley, J., Flamig, Z., Hong, Y. and Howard, K. (2014). Evaluation of past, present and future tools for radar-based flash-flood prediction in the usa, *Hydrolog Sci J* **59**: 1377–1389.

Grelle, G., Soriano, M., Revellino, P., Guerriero, L., Anderson, M., Diambra, A., Fiorillo, F., Esposito, L., Diodato, N. and Guadagno, F. (2014). Space-time prediction of rainfall-induced shallow landslides through a combined probabilistic/deterministic approach, optimized for initial water table conditions, *B Eng Geol Environ* **73**: 877–890.

Gudmundsson, L., Bremnes, J., Haugen, J. and T.Engen-Skaugen (2012). echnical note: Downscaling rcm precipitation to the station scale using statistical transformations & a comparison of methods, *Hydrol Earth Syst Sci* **16**: 3383–3390.

Gutiérrez, J., San-Martín, D., Brands, S., Manzanas, R. and Herrera, S. (2012). Reassessing statistical downscaling techniques for their robust application under climate change conditions, *J Climate* **26**: 171–188.

Gutiérrez, J., San-Martín, D., Cofiño, A., Herrera, S. and Manzanas, R. (2011). User guide of the ensembles downscaling portal, *Technical report*.

Guzzetti, F., Cardinali, M. and Reichenbach, P. (1994). The avi project: A bibliographical and archive inventory of landslides and floods in italy, *Environ Manage* **18**: 623–633.

Guzzetti, F., Peruccacci, S., Rossi, M. and Stark, C. (2007). Rainfall thresholds for the initiation of landslides in central and southern europe, *Meteorol Atmos Phys* **98**: 239–267.

Guzzetti, F., Peruccacci, S., Rossi, M. and Stark, C. (2008). The rainfall intensity/duration control of shallow landslides and debris flows: an update, *Landslides* **5**: 3–17.

Hall, J., Arheimer, B., Borga, M., Brázdil, R., Claps, P., Kiss, A., Kjeldsen, T., Kriaučiūnienė, J., Kundzewicz, Z., Lang, M., Llasat, M., Macdonald, N., McIntyre, N., Mediero, L., Merz, B., Merz, R., Molnar, P., Montanari, A., Neuhold, C., Parajka, J., Perdigão, R., Plavcová, L., Rogger, M., Salinas, J., Sauquet, E., Schär, C., Szolgay, J., Viglione, A. and Blöschl, G. (2014). Understanding flood regime changes in europe: a state-of-the-art assessment, *Hydrol Earth Syst Sci* **18**: 2735–2772.

Hawkins, E. and Sutton, R. (2011). The potential to narrow uncertainty in projections of regional precipitation change, *Clim Dynam* **37**: 407–418.

Haylock, M., Hofstra, N., Tank, A. K., Klok, E., Jones, P. and New, M. (2008). A european daily high-resolution gridded data set of surface temperature and precipitation for 1950-2006, *J Geophys Res* **113**: D20119.

Herbst, P. and Riepler, F. (2006). 14c evidence for an early to pre-würmian age for parts of the salzburger seeton, urstein, salzach valley, austria, *Austrian Journal of Earth Sciences* **99**: 57–61.

Hertig, E. and Jacobeit, J. (2014). Considering observed and future non-stationarities in statistical downscaling of mediterranean precipitation, *Theor Appl Climatol* pp. 1–17.

Hertig, E., Seubert, S., Paxian, A., Vogt, G., Paeth, H. and Jacobeit, J. (2013). Changes of total versus extreme precipitation and dry periods until the end of the twenty-first century: statistical assessments for the mediterranean area, *Theor Appl Climatol* **111**: 1–20.

Hewitson, B. and Crane, R. (2006). Consensus between gcm climate change projections with empirical downscaling: precipitation downscaling over south africa, *Int J Climatol* **26**: 1315–1337.

Hoy, A., Schucknecht, A., Sepp, M. and Matschullat, J. (2014). Large-scale synoptic types and their impact on european precipitation, *Theor Appl Climatol* **116**: 19–35.

Huang, J., Huang, R., Ju, N., Xu, Q. and He, C. (2015). 3d webgis-based platform for debris flow early warning: A case study, *Eng Geol* **197**: 57–66.

Huard, D., Mailhot, A. and Duchesne, S. (2010). Bayesian estimation of intensit-duration-frequency curves and of the return period associated to a given rainfall event, *Stoch Env Res Risk A* **24**: 337–347.

Huggel, C., Allen, S., Clague, J., Fischer, L., Korup, O. and Schneider, D. (2013). Detecting potential climate signals in large slope failures in cold mountain regions, *in* C. Margottini, P. Canuti and K. Sassa (eds), *Landslide Science and Practice*, Springer Berlin Heidelberg, pp. 361–367.

Huggel, C., Clague, J., O. and Korup (2012). Is climate change responsible for changing landslide activity in high mountains?, *Earth Surf Proc Land* **37**: 77–91.

Huggel, C., Salzmann, N., Allen, S., Caplan-Auerbach, J., Fischer, L., Haeberli, W., Larsen, C., Schneider, D. and Wessels, R. (2010). Recent and future warm extreme events and high-mountain slope stability, *Philos T Roy Soc A* **368**: 2435–2459.

Hungr, O., Leroueil, S. and Picarelli, L. (2014). The varnes classification of landslide types, an update, *Landslides* **11**: 167–194.

Hurford, A., Priest, S., Parker, D. and Lumbroso, D. (2012). The effectiveness of extreme rainfall alerts in predicting surface water flooding in england and wales, *Int J Climatol* **32**: 1768–1774.

Huth, R., Beck, C., Philipp, A., Demuzere, M., Ustrnul, Z., Cahynová, M., Kyselý, J. and Tveito, O. (2008). Classifications of atmospheric circulation patterns, *Ann NY Acad Sci* **1146**: 105–152.

Ibsen, M. and Casagli, N. (2004). Rainfall patterns and related landslide incidence in the porretta-vergato region, italy, *Landslides* **1**: 143–150.

Ionita, M., Dima, M., Lohmann, G., Scholz, P. and Rimbu, N. (2014). Predicting the june 2013 european flooding based on precipitation, soil moisture, and sea level pressure, *J Hydrometeorology* **16**: 598–614.

IPCC (2012). Managing the risks of extreme events and disasters to advance climate change adaptation, *A special report of working group I and II of the Intergovernmental Panel on Climate Change*, Cambridge University Press, Cambridge UK.

Isotta, F., Frei, C., Weilguni, V., Tadić, M. P., Lassègues, P., Rudolf, B., Pavan, V., Cacciamani, C., Antolini, G., Ratto, S., Munari, M., Micheletti, S., Bonati, V., Lussana, C., Ronchi, C., Panettieri, E., Marigo, G., G. and Vertačnik (2014). The climate of daily precipitation in the alps: development and analysis of a high-resolution grid dataset from pan-alpine rain-gauge data, *Int J Climatol* **34**: 1657–1675.

Jacob, D., Petersen, J., Eggert, B., Alias, A., Christensen, O., Bouwer, L., Braun, A., Colette, A., Déqué, M., Georgievski, G., Georgopoulou, E., Gobiet, A., Menut, L., Nikulin, G., Haensler, A., Hempelmann, N., Jones, C., Keuler, K., Kovats, S., Kröner, N., Kotlarski, S., Kriegsmann, A., Martin, E., van Meijgaard, E., Moseley, C., Pfeifer, S., Preuschmann, S., Radermacher, C., Radtke, K., Rechid, D., Rounsevell, M., Samuelsson, P., Somot, S., Soussana, J.-F., Teichmann, C., Valentini, R., Vautard, R., Weber, B. and Yiou, P. (2014). Euro-cordex: new high-resolution climate change projections for european impact research, *Reg Environ Change* **14**: 563–578.

Jacobeit, J., Hertig, E., Seubert, S. and Lutz, K. (2014). Statistical downscaling for climate change projections in the mediterranean region: methods and results, *Reg Environ Change* **14**: 1891–1906.

Jaiswal, P. and van Westen, C. (2009). Estimating temporal probability for landslide initiation along transportation routes based on rainfall thresholds, *Geomorphology* **112**: 96–105.

Jeong, D., St-Hilaire, A., Ouarda, T. and Gachon, P. (2012). Cgcm3 predictors used for daily temperature and precipitation downscaling in southern québec, canada, *Theor Appl Climatol* **107**: 389–406.

Joetzjer, E., Douville, H., Delire, C. and Ciais, P. (2013). Present-day and future amazonian precipitation in global climate models: Cmip5 versus cmip3, *Clim Dynam* **41**: 2921–2936.

Jomelli, V., Brunstein, D., Déqué, M., Vrac, M. and Grancher, D. (2009). Impacts of future climatic change (2070-2099) on the potential occurrence of debris flows: a case study in the massif des ecrins (french alps), *Climatic Change* **97**: 171–191.

Jomelli, V., Pech, V., Chochillon, C. and Brunstein, D. (2004). Geomorphic variations of debris flows and recent climatic change in the french alps, *Climatic Change* **64**: 77–102.

Kain, J., Weiss, S., Bright, D., Baldwin, M., Levit, J., Carbin, G., Schwartz, C., Weisman, M., Droegemeier, K., Weber, D. and Thomas, K. (2008). Some practical considerations regarding horizontal resolution in the first

generation of operational convection-allowing nwp, *Weather Forecast* **23**: 931–952.

Kannan, S. and Ghosh, S. (2011). Prediction of daily rainfall state in a river basin using statistical downscaling from gcm output, *Stoch Env Res Risk A* **25**: 457–474.

Kenawy, A., López-Moreno, J. and Vicente-Serrano, S. (2013). Summer temperature extremes in northeastern spain: Spatial regionalization and links to atmospheric circulation (1996-2006), *Theor Appl Climatol* **113**: 387–405.

Kendall, M. (1970). *Rank correlation methods*, 4th edition edn, Griffin.

Kendon, E., Jones, R., Kjellström, E. and Murphy, J. (2010). Using and designing gcm-rcm ensemble regional climate projections, *J Climate* **23**: 6485–6503.

Khan, S., Kamp, U. and Owen, L. (2013). Documenting five years of landsliding after the 2005 kashmir earthquake, using repeat photography, *Geomorphology* **197**: 45–55.

Khazai, B., Anhorn, J., Brink, S., Girard, T., Jimee, G., Parajuli, B., Wagle, S., Khanal, O., Shresta, S. and Manandhar, R. (2015). Emergent issues and vulnerability factors in temporary and intermediate shelters following the 2015 nepal earthquake, *Technical report*, CEDIM Report No. 4, Shelter Report Following Field Mission.

Kienberger, S., Lang, S. and Zeil, P. (2009). Spatial vulnerability units - expert-based spatial modelling of socio-economic vulnerability in the salzach catchment, austria, *Nat Hazard Earth Sys* **9**: 767–778.

Kim, J., Lee, K., Jeong, S. and Kim, G. (2014). Gis-based prediction method of landslide susceptibility using a rainfall infiltration-groundwater flow model, *Eng Geol* **182**: 63–78.

King, D., Skipper, A. and Tawhai, W. (2008). Māori environmental knowledge of local weather and climate change in aotearoa - new zealand, *Climatic Change* **90**: 385–409.

Kirschbaum, D., Adler, R., Adler, D., Peters-Lidard, C. and Huffman, G. (2012). Global distribution of extreme precipitation and high-impact landslides in 2010 relative to previous years, *J Hydrometeorology* **13**: 1536–1551.

Kirschbaum, D., Adler, R., Hong, Y., Hill, S. and Lerner-Lam, A. (2010). A global landslide catalog for hazard applications: method, results, and limitations, *Nat Hazards* **52**: 561–575.

Kirschbaum, D., Adler, R., Hong, Y., Kumar, S., Peters-Lidard, C. and Lerner-Lam, A. (2012). Advances in landslide nowcasting: evaluation of a global and regional modeling approach, *Environmental Earth Sciences* **66**: 1683–1696.

Kirschbaum, D., Stanley, T. and Zhou, Y. (2015). Spatial and temporal analysis of a global landslide catalog, *Geomorphology* **249**: 4–15.

Kjellström, E., Nikulin, G., Hansson, U., Strandberg, G. and Ullerstig, A. (2011). 21st century changes in the european climate: uncertainties derived from an ensemble of regional climate model simulations, *Tellus A* **63**: 24–40.

Klein Tank, A. and Können, G. (2003). Trends in indices of daily temperature and precipitation extremes in europe, 1946-99, *J Climate* **16**: 3665–3680.

Klein Tank, A., Zwiers, F. and Zhang, X. (2009). Guidelines on analysis of extremes in a changing climate in support of informed decisions for adaptation, *Technical report*, WCDMP-No. 72, WMO-TD No. 1500.

Knutti, R., Masson, D. and Gettelman, A. (2013). Climate model genealogy: Generation cmip5 and how we got there, *Geophys Res Lett* **40**: 1194–1199.

Köplin, N., Schädler, B., Viviroli, D. and Weingartner, R. (2014). Seasonality and magnitude of floods in switzerland under future climate change, *Hydrol Process* **28**: 2567–2578.

Kunkel, K., Changnon, S. and Angel, J. (1994). Climatic aspects of the 1993 upper mississippi river basin flood, *B Am Meteorol Soc* **75**: 811–822.

Labadie, J. (2011). Emergency managers confront climate change, *Sustainability* **3**: 1250.

Lainas, S., Sabatakakis, N. and Koukis, G. (2015). Rainfall thresholds for possible landslide initiation in wildfire-affected areas of western greece, *B Eng Geol Environ* pp. 1–14.

Lang, S., Kääb, A., Pechstädt, J., Flügel, W., Zeil, P., Lanz, E., Kahuda, D., Frauenfelder, R., Casey, K., Füreder, P., Sossna, T., Wagner, I., Janauer, G., Exler, N., Boukalova, Z., Tapa, R., Lui, J. and Sharma, N. (2011). Assessing components of the natural environment of the upper danube and upper brahmaputra river basins, *Advances in Science Research* **7**: 21–36.

Lauer, A. and Hamilton, K. (2013). Simulating clouds with global climate models: A comparison of cmip5 results with cmip3 and satellite data, *J Climate* **26**: 3823–3845.

Lempert, R. and Schlesinger, M. (2000). Robust strategies for abating climate change, *Climatic Change* **45**: 387–401.

Lenoir, J., Gégout, J., Marquet, P., de Ruffray, P. and Brisse, H. (2008). A significant upward shift in plant species optimum elevation during the 20th century, *Science* **320**: 1768–1771.

Liao, Z., Hong, Y., Kirschbaum, D., Adler, R., Gourley, J. and Wooten, R. (2011). Evaluation of trigrs (transient rainfall infiltration and grid-based regional slope-stability analysis)'s predictive skill for hurricane-triggered landslides: a case study in macon county, north carolina, *Nat Hazards* **58**: 325–339.

Lin, C., Shieh, C., Yuan, B., Shieh, Y., Liu, S. and Lee, S. (2004). Impact of chi-chi earthquake on the occurrence of landslides and debris flows: example from the chenyulan river watershed, nantou, taiwan, *Eng Geol* **71**: 49–61.

Liu, L., Hong, Y., Hocker, J., Shafer, M., Carter, L., Gourley, J., Bednarczyk, C., Yong, B. and Adhikari, P. (2012). Analyzing projected changes and trends of temperature and precipitation in the southern usa from 16 downscaled global climate models, *Theor Appl Climatol* **109**: 345–360.

Lu, P., Stumpf, A., Kerle, N. and Casagli, N. (2011). Object-oriented change detection for landslide rapid mapping, *IEEE Geosci Remote S* **8**: 701–705.

Luna, B. Q., Blahut, J., van Westen, C., Sterlacchini, S., van Asch, T. and Akbas, S. (2011). The application of numerical debris flow modelling for the generation of physical vulnerability curves, *Nat Hazard Earth Sys* **11**: 2047–2060.

Maddox, R., Chappell, C. and Hoxit, L. (1979). Synoptic and meso-α aspects of flash flood events, *B Am Meteorol Soc* **60**: 115–123.

Malek, Ž., Scolobig, A. and Schröter, D. (2014). Understanding land cover changes in the italian alps and romanian carpathians combining remote sensing and stakeholder interviews, *Land* **3**: 52–73.

Malet, J., Durand, Y., Remaître, A., Maquaire, O., Etchevers, P., Guyomarch, G., Déqué, M. and van Beek, L. (2007). Assessing the influence of climate change on the activity of landslides in the ubaye valley, *in* R. McInnes, J. Jakeways, H. Fairbank and E. Mathie (eds), *Proceedings of the International Conference on Landslides and Climate Change — Challenges and Solutions*, Wiley, United Kingdom, pp. 195–205.

Maraun, D. (2013). Bias correction, quantile mapping, and downscaling: Revisiting the inflation issue, *J Climate* **26**: 2137–2143.

Maraun, D., Wetterhall, F., Ireson, A., Chandler, R., Kendon, E., Widmann, M., Brienen, S., Rust, H., Sauter, T., Themeβl, M., Venema, V., Chun, K., Goodess, C., Jones, R., Onof, C., Vrac, M. and Thiele-Eich, I. (2010). Precipitation downscaling under climate change: Recent developments to bridge the gap between dynamical models and the end user, *Rev Geophys* **48**: RG3003.

Marchi, L., Borga, M., Preciso, E. and Gaume, E. (2010). Characterisation of selected extreme flash floods in europe and implications for flood risk management, *J Hydrol* **394**: 118–133.

Marra, F., Nikolopoulos, E., Creutin, J. and Borga, M. (2014). Radar rainfall estimation for the identification of debris-flow occurrence thresholds, *J Hydrol* **519**: 1607–1619.

Marsh, P., Brooks, H. and Karoly, D. (2009). Preliminary investigation into the severe thunderstorm environment of europe simulated by the community climate system model 3, *Atmos Res* **93**: 607–618.

Martelloni, G., Segoni, S., Fanti, R. and Catani, F. (2011). Rainfall thresholds for the forecasting of landslide occurrence at regional scale, *Landslides* .

Mason, S. and Graham, N. (1999). Conditional probabilities, relative operating characteristics and relative operating levels, *Weather Forecast* **14**: 713–725.

Mateos, R., García-Moreno, I. and Azañón, J. (2012). Freeze-thaw cycles and rainfall as triggering factors of mass movements in a warm mediterranean region: the case of the tramuntana range (majorca, spain), *Landslides* **9**: 417–432.

Matsuura, S., Asano, S., Okamoto, T. and Takeuchi, Y. (2003). Characteristics of the displacement of a landslide with shallow sliding surface in a heavy snow district of japan, *Eng Geol* **69**: 15–35.

Maurer, E. and Hidalgo, H. (2008). Utility of daily vs. monthly large-scale climate data: an intercomparison of two statistical downscaling methods, *Hydrol Earth Syst Sci* **12**: 551–563.

McBean, G. (2013). Hydrometeorological hazards, *in* P. Bobrowsky (ed.), *Encyclopedia of Natural Hazards*, Springer Netherlands, Dordrecht, pp. 497–508.

McCabe, G., Hay, L. and Clark, M. (2007). Rain-on-snow events in the western united states, *B Am Meteorol Soc* **88**: 319–328.

Melchiorre, C. and Frattini, P. (2012). Modelling probability of rainfall-induced shallow landslides in a changing climate, otta, central norway, *Climatic Change* **113**: 413–436.

Melillo, M., Brunetti, M., Peruccacci, S., Gariano, S. and Guzzetti, F. (2014). An algorithm for the objective reconstruction of rainfall events responsible for landslides, *Landslides* .

Merz, B., Aerts, J., Arnbjerg-Nielsen, K., Baldi, M., Becker, A., Bichet, A., Blöschl, G., Bouwer, L., Brauer, A. and et al., F. C. (2014). Floods and climate: emerging perspectives for flood risk assessment and management, *Nat Hazard Earth Sys* **14**: 1921–1942.

Merz, R. and Blöschl, G. (2003). Regional flood risk-what are the driving processes?, *Water Resources Systems - Hydrological Risk, Management and Development*, IAHS Publ, Sapporo, Japan, pp. 49–58.

Merz, R. and Blöschl, G. (2008). Flood frequency hydrology: 1. temporal, spatial, and causal expansion of information, *Water Resour Res* **44**: W08432.

Meyer, N., Dyrrdal, A., Frauenfelder, R., Etzelmaller, B. and Nadim, F. (2012). Hydrometeorlogical threshold conditions for debris flow initiation in norway, *Nat Hazard Earth Syst Sci* **12**: 3059–3073.

Meyer, R. (2011). The public values failures of climate science in the us, *Minerva* **49**: 47–70.

Min, S., Zhang, X., Zwiers, F. and G.C.Hegerl (2011). Human contribution to more-intense precipitation extremes, *Nature* **470**: 378–381.

Modrick, T. and Georgakakos, K. (2015). The character and causes of flash flood occurrence changes in mountainous small basins of southern california under projected climatic change, *J Hydrol- Regional Studies* **3**: 312–336.

Molini, L., Parodi, A., Rebora, N. and Craig, G. (2011). Classifying severe rainfall events over italy by hydrometeorological and dynamical criteria, *Q J Roy Meteor Soc* **137**: 148–154.

Murphy, J., Sexton, D., Jenkins, G., Booth, B., Brown, C., Clark, R., Collins, M., Harris, G., Kendon, E., Betts, R., Brown, S., Boorman, P., Howard, T., Humphrey, K., McCarthy, M., McDonald, R., Stephens, A., Wallace, C., Warren, R., Wilby, R. and Wood, R. (2009). Uk climate projections science report: Climate change projections, *Technical report*.

Nakicenovic, N., Alcamo, J., Davis, G., de Vries, B., Fenhann, J., Gaffin, S., Gregory, K., Grbler, A., Jung, T., Kram, T., Rovere, E. L., Michaelis, L., Mori, S., Morita, T., Pepper, W., Pitcher, H., Price, L., Raihi, K., Roehrl, A., Rogner, H., Sankovski, A., Schlesinger, M., Shukla, P., Smith, S., Swart, R., van Rooijen, S., Victor, N. and Dadi, Z. (2000). Ipcc special report on emissions scenarios, *Technical report*.

Nash, J. and Sutcliffe, J. (1970). River flow forecasting through conceptual models part i âĂŤ a discussion of principles, *J Hydrol* **10**: 282–290.

Niall, S. and Walsh, K. (2005). The impact of climate change on hailstorms in southeastern australia, *Int J Climatol* **25**: 1933–1952.

Nied, M., Pardowitz, T., Nissen, K., U.Ulbrich, Hundecha, Y. and Merz, B. (2014). On the relationship between hydro-meteorological patterns and flood types, *J Hydrol* **519**: 3249–3262.

Nikolopoulos, E., Crema, S., Marchi, L., Marra, F., Guzzetti, F. and Borga, M. (2014). Impact of uncertainty in rainfall estimation on the identification of rainfall thresholds for debris flow occurrence, *Geomorphology* **221**: 286–297.

Nikulin, G., Kjellström, E., Hansson, U., Strandberg, G. and Ullerstig, A. (2011). Evaluation and future projections of temperature, precipitation and wind extremes over europe in an ensemble of regional climate simulations, *Tellus A* **63**: 41–55.

Nolin, A. and Daly, C. (2006). Mapping "at risk" snow in the pacific northwest, *J Hydrometeorology* **7**: 1164–1171.

Norbiato, D., Borga, M. and Dinale, R. (2009). Flash flood warning in ungauged basins by use of the flash flood guidance and model-based runoff thresholds, *Meteorol Appl* **16**: 65–75.

Nuissier, O., Ducrocq, V., Ricard, D., Lebeaupin, C. and Anquetin, S. (2008). A numerical study of three catastrophic precipitating events over southern france. i: Numerical framework and synoptic ingredients, *Q J Roy Meteor Soc* **134**: 111–130.

Nuissier, O., Joly, B., Joly, A., Ducrocq, V. and Arbogast, P. (2011). A statistical downscaling to identify the large–scale circulation patterns

associated with heavy precipitation events over southern france, *Q J Roy Meteor Soc* **137**: 1812–1827.

OMIV-Coordinator (2012). The barcelonnette area.
URL: *http://eost.u-strasbg.fr/omiv/barcelo_area_torrential_hazard.php*

Ouarda, T. and El-Adlouni, S. (2011). Bayesian nonstationary frequency analysis of hydrological variables, *J Am Water Resour As* **47**: 496–505.

Panziera, L., Germann, U., Gabella, M. and Mandapaka, P. (2011). Noranowcasting of orographic rainfall by means of analogues, *Q J Roy Meteor Soc* **137**: 2106–2123.

Parajka, J., Kohnová, S., Bálint, G., Barbuc, M., Borga, M., Claps, P., Cheval, S., Dumitrescu, A., Gaume, E., Hlavčová, K., Merz, R., Pfaundler, M., Stancalie, G., Szolgay, J. and Blöschl, G. (2010). Seasonal characteristics of flood regimes across the alpine - carpathian range, *J Hydrol* **394**: 78–89.

Paranunzio, R., Laio, F., Nigrelli, G. and Chiarle, M. (2016). A method to reveal climatic variables triggering slope failures at high elevation, *Nat Hazards* **76**: 1039–1061.

Pattison, I. and Lane, S. (2012). The relationship between lamb weather types and long-term changes in flood frequency, river eden, uk, *Int J Climatol* **32**: 1971–1989.

Pavlova, I., Jomelli, V., Brunstein, D., Grancher, D., Martin, E. and Déqué, M. (2014). Debris flow activity related to recent climate conditions in the french alps: A regional investigation, *Geomorphology* **219**: 248–259.

Perdigão, R. and Blöschl, G. (2014). Spatiotemporal flood sensitivity to annual precipitation: Evidence for landscape-climate coevolution, *Water Resour Res* **50**: 5492–5509.

Peterson, T., Zhang, X., Brunet-India, M. and Vázquez-Aguirre, J. (2008). Changes in north american extremes derived from daily weather data, *J Geophys Res* **113**: D07113.

Petley, D. (2012). Global patterns of loss of life from landslides, *Geology* **40**: 927–930.

Petley, D., Dunning, S. and Rosser, N. (2005). The analysis of global landslide risk through the creation of a database of worldwide landslide fatalities, *in* C. R. H. O, F. R and E. E (eds), *Landslide risk management*, Balkema, Amsterdam, pp. 367–374.

Petrow, T., Zimmer, J. and Merz, B. (2009). Changes in the flood hazard in germany through changing frequency and persistence of circulation patterns, *Nat Hazard Earth Sys* **9**: 1409–1423.

Pettitt, A. (1979). A non-parametric approach to the change-point problem, *J Roy Stat Soc C-App* **28**: 126–135.

Philipp, A., Bartholy, J., Beck, C., Erpicum, M., Esteban, P., Fettweis, X., Huth, R., James, P., Jourdain, S., Kreienkamp, F., Krennert, T., Lykoudis, S., Michalides, S., Pianko-Kluczynska, K., Post, P., Álvarez,

D., Schiemann, R., Spekat, A. and Tymvios, F. (2010). Cost733cat - a database of weather and circulation type classifications, *Phys Chem Earth* **35**: 360–373.

Pierce, D., Das, T., Cayan, D., Maurer, E., Miller, N., Bao, Y., Kanamitsu, M., Yoshimura, K., Snyder, M., Sloan, L., Franco, G. and Tyree, M. (2013). Probabilistic estimates of future changes in california temperature and precipitation using statistical and dynamical downscaling, *Clim Dynam* **40**: 839–856.

Pistotnik, G., Schneider, S. and Wittmann, C. (2011). Detection of convective initiation by objective analysis methods and its use for precipitation nowcasting, *6th European Conference on Severe Storms, Palma de Mallorca, Spain, 3–7 October 2011*.

Powell, T., Hanfling, D. and Gostin, L. (2012). Emergency preparedness and public health: The lessons of hurricane sandy, *JAMA-J Am Med Assoc* **308**: 2569–2570.

Powers, D. (2011). Evaluation: from precision, recall and f-measure to roc, informedness, markedness & correlation, *Journal of Machine Learning Technologies* **2**: 37–67.

Prudhomme, C. and Genevier, M. (2011). Can atmospheric circulation be linked to flooding in europe?, *Hydrol Process* **25**: 1180–1190.

Pulquério, M., Garrett, P., Santos, F. and Cruz, M. (2015). On using a generalized linear model to downscale daily precipitation for the center of portugal: an analysis of trends and extremes, *Theor Appl Climatol* **120**: 147–158.

Raff, D., Pruitt, T. and Brekke, L. (2009). A framework for assessing flood frequency based on climate projection information, *Hydrol Earth Syst Sci* **13**: 2119–2136.

Rajczak, J., Pall, P., C. and Schär (2013). Projections of extreme precipitation events in regional climate simulations for europe and the alpine region, *J Geophys Res-Atmos* **118**: 3610–3626.

Rajeevan, M., Unnikrishnan, C. and Preethi, B. (2012). Evaluation of the ensembles multi-model seasonal forecasts of indian summer monsoon variability, *Clim Dynam* **38**: 2257–2274.

Ramesh, A. (2013). *Response of flood events to land use and climate change*, University of Vienna, Austria, Springer Theses Series.

Reeves, J., Chen, J., Wang, X., Lund, R. and Lu, Q. (2007). Review and comparison of changepoint detection techniques for climate data, *Journa of Applied Meteorology and Climatology* **46**: 900–915.

Remaître, A. and Malet, J. (2010). The effectiveness of torrent check dams to control channel instability: example of debris-flow events in clay shales, *in* C. Garcia and M. Lenzi (eds), *Check dams, morphological adjustments and erosion control in torrential streams*, Nova Science Publishers New York, pp. 211–237.

Remaître, A., Malet, J. and Maquaire, O. (2011). Geomorphology and kinematics of debris flows with high entrainment rates: A case study in the south french alps, *C R Geosci* **343**: 777–794.

Riemann-Campe, K., Fraedrich, K. and Lunkeit, F. (2009). Global climatology of convective available potential energy (cape) and convective inhibition (cin) in era-40 reanalysis, *Atmos Res* **93**: 534–545.

Romps, D., Seeley, J., Vollaro, D. and Molinari, J. (2014). Projected increase in lightning strikes in the united states due to global warming, *Science* **346**: 851–854.

Rosi, A., Lagomarsino, D., Rossi, G., Segoni, S., Battistini, A. and Casagli, N. (2015). Updating ews rainfall thresholds for the triggering of landslides, *Nat Hazards* **78**: 297–308.

Rousseeuw, P. (1987). Silhouettes: a graphical aid to the interpretation and validation of cluster analysis, *J Comput Appl Math* **20**: 53–65.

Rousselot, M., Durand, Y., Giraud, G., Mérindol, L., Dombrowski-Etchevers, I., Déqué, M. and Castebrunet, H. (2012). Statistical adaptation of aladin rcm outputs over the french alps: application to future climate and snow cover, *The Cryosphere* **6**: 785–805.

Rulli, M., Meneguzzo, F. and Rosso, R. (2007). Wind control of storm-triggered shallow landslides, *Geophys Res Lett* **34**: L03402.

Rummukainen, M. (2015). Our commitment to climate change is dependent on past, present and future emissions and decisions, *Climate Res* **64**: 7–14.

Saba, S., van der Meijde, M. and van der Werff, H. (2010). Spatiotemporal landslide detection for the 2005 kashmir earthquake region, *Geomorphology* **124**: 17–25.

Saez, J., Corona, C., Stoffel, M. and Berger, F. (2013). Climate change increases frequency of shallow spring landslides in the french alps, *Geology* **41**: 619–622.

Saez, J., Corona, C., Stoffel, M., Schoeneich, P. and Berger, F. (2012). Probability maps of landslide reactivation derived from tree-ring records: Pra bellon landslide, southern french alps, *Geomorphology* **138**: 189–202.

Salvati, P., Bianchi, C., Rossi, M. and Guzzetti, F. (2010). Societal landslide and flood risk in italy, *Nat Hazard Earth Sys* **10**: 465–483.

Schiemann, R. and Frei, C. (2010). How to quantify the resolution of surface climate by circulation types: An example for alpine precipitation, *Phys Chem Earth* **35**: 403–410.

Schmidli, J., Goodess, C., Frei, C., Haylock, M., Hundecha, Y., Ribalaygua, J. and Schmith, T. (2007). Statistical and dynamical downscaling of precipitation: An evaluation and comparison of scenarios for the european alps, *J Geophys Res-Atmos* **112**: D4.

Schneuwly-Bollschweiler, M. and Stoffel, M. (2012). Hydrometeorological triggers of periglacial debris flows in the zermatt valley (switzerland) since 1864, *J Geophys Res-Earth* **117**: F02033.

Schwarz, M., Preti, F., Giadrossich, F., Lehmann, P. and Or, D. (2010). Quantifying the role of vegetation in slope stability: A case study in tuscany (italy), *Ecol Eng* **36**: 285–291.

Segoni, S., Rossi, G., Rosi, A. and Catani, F. (2014). Landslides triggered by rainfall: A semi-automated procedure to define consistent intensity-duration thresholds, *Comput Geosci* **63**: 123–131.

Seibert, J. and Vis, M. (2012). Teaching hydrological modeling with a user-friendly catchment-runoff-model software package, *Hydrol Earth Syst Sci* **16**: 3315–3325.

Seltzer, M., Passarelli, R. and Emanuel, K. (1985). The possible role of symmetric instability in the formation of precipitation bands, *J Atmos Sci* **42**.

Sene, K. (2013). Debris flows, *Flash Floods*, Springer, Netherlands, pp. 271–291.

Shapiro, M., Shukla, J., Brunet, G., Nobre, C., Béland, M., Dole, R., Trenberth, K., Anthes, R., Asrar, G. and Barrie, L. (2010). An earth-system prediction initiative for the twenty-first century, *B Am Meteorol Soc* **91**: 1377–1388.

Sillmann, J., Kharin, V., Zhang, X., Zwiers, F. and Bronaugh, D. (2013). Climate extremes indices in the cmip5 multimodel ensemble: Part 1. model evaluation in the present climate, *J Geophys Res-Atmos* **118**: 1716–1733.

Slomp, R. (2012). Flood risk and water management in the netherlands.

Smith, J., Baeck, M., Ntelekos, A., Villarini, G. and Steiner, M. (2011). Extreme rainfall and flooding from orographic thunderstorms in the central appalachians, *Water Resour Res* **47**: W04514.

Stanzel, P., Kahl, B., Haberl, U., Herrnegger, M. and Nachtnebel, H. (2008). Continuous hydrological modelling in the context of real time flood forecasting in alpine danube tributary catchments, *IOP Conference Series: Earth Environmental Science*, Vol. 4, p. 012005.

Steele-Dunne, S., Lynch, P., McGrath, R., Semmler, T., Wang, S., Hanafin, J. and Nolan, P. (2008). The impacts of climate change on hydrology in ireland, *J Hydrol* **356**: 28–45.

Steinschneider, S. and Brown, C. (2013). A semiparametric multivariate, multisite weather generator with low-frequency variability for use in climate risk assessments, *Water Resour Res* **49**: 7205–7220.

Stoffel, M., Tiranti, D. and Huggel, C. (2014). Climate change impacts on mass movements âĂŤ case studies from the european alps, *Sci Total Environ* **493**: 1255–1266.

Street, R., Steynor, A., Bowyer, P. and Humphrey, K. (2009). Delivering and using the uk climate projections 2009, *Weather* **64**: 227–231.

Sun, Q., Miao, C. and Duan, Q. (2015). Comparative analysis of cmip3 and cmip5 global climate models for simulating the daily mean, maximum, and minimum temperatures and daily precipitation over china, *J Geophys Res-Atmos* **120**: 4806–4824.

Sunyer, M., Madsen, H. and Ang, P. (2012). A comparison of different regional climate models and statistical downscaling methods for extreme rainfall estimation under climate change, *Atmos Res* **103**: 119–128.

Tall, A., Patt, A. and Fritz, S. (2013). Reducing vulnerability to hydrometeorological extremes in africa. a qualitative assessment of national climate disaster management policies: Accounting for heterogeneity, *Weather and Climate Extremes* **1**: 4–16.

Tang, C., van Asch, T., Chang, M., Chen, G., Zhao, X. and Huang, X. (2012). Catastrophic debris flows on 13 august 2010 in the qingping area, southwestern china: The combined effects of a strong earthquake and subsequent rainstorms, *Geomorphology* **139-140**: 559–576.

Tao, F. and Zhang, Z. (2011). Impacts of climate change as a function of global mean temperature: maize productivity and water use in china, *Climatic Change* **105**: 409–432.

Tao, J. and Barros, A. (2013). Prospects for flash flood forecasting in mountainous regions - an investigation of tropical storm fay in the southern appalachians, *J Hydrol* **506**: 69–89.

Tapiador, F., Turk, F., Petersen, W., Hou, A., García-Ortega, E., Machado, L., Angelis, C., Salio, P., Kidd, C., Huffman, G. and de Castro, M. (2012). Global precipitation measurement: Methods, datasets and applications, *Atmos Res* **104–105**: 70–97.

Tarolli, P., Borga, M., Morin, E. and Delrieu, G. (2012). Analysis of flash flood regimes in the north-western and south-eastern mediterranean regions, *Nat Hazard Earth Sys Sci* **12**: 1255–1265.

Taylor, K., Stouffer, R. and Meehl, G. (2011). An overview of cmip5 and the experiment design, *B Am Meteorol Soc* **93**: 485–498.

Teng, J., Chiew, F., Timbal, B., Wang, Y., Vaze, J. and Wang, B. (2012). Assessment of an analogue downscaling method for modelling climate change impacts on runoff, *J Hydrol* **472–473**: 111–125.

Teutschbein, C. and Seibert, J. (2012). Bias correction of regional climate model simulations for hydrological climate-change impact studies: Review and evaluation of different methods, *J Hydrol* **456-457**: 12–29.

Teutschbein, C., Wetterhall, F. and Seibert, J. (2011). Evaluation of different downscaling techniques for hydrological climate-change impact studies at the catchment scale, *Clim Dynam* **37**: 2087–2105.

Themeβl, M., Gobiet, A. and Heinrich, G. (2012). Empirical-statistical downscaling and error correction of regional climate models and its impact on the climate change signal, *Climatic Change* **112**: 449–468.

Thornthwaite, C. (1948). An approach toward a rational classification of climate, *Geogr Rev* **38**: 55–94.

Tian, W. and de Wilde, P. (2011). Uncertainty and sensitivity analysis of building performance using probabilistic climate projections: A uk case study, *Automat Constr* **20**: 1096–1109.

Timalsina, N., Alfredsen, K. and øA. Killingtveit (2015). Impact of climate change on ice regime in a river regulated for hydropower, *Can J Civil Eng* **42**: 634–644.

Timbal, B., Fernandez, E. and Li, Z. (2009). Generalization of a statistical downscaling model to provide local climate change projections for australia, *Environ Model Softw* **24**: 341–358.

Tiranti, D., Rabuffetti, D., Salandin, A. and Tararbra, M. (2013). Development of a new translational and rotational slides prediction model in langhe hills (north-western italy) and its application to the 2011 march landslide event, *Landslides* **10**: 121–138.

Tobin, C., Nicotina, L., Parlange, M., Berne, A. and Rinaldo, A. (2011). Improved interpolation of meteorological forcings for hydrologic applications in a swiss alpine region, *J Hydrol* **401**: 77–89.

Toreti, A., Schneuwly-Bollschweiler, M., Stoffel, M. and Luterbacher, J. (2013). Atmospheric forcing of debris flows in the southern swiss alps, *J Appl Meteorol Clim* **52**: 1554–1560.

Trapp, R., Diffenbaugh, N. and Gluhovsky, A. (2009). Transient response of severe thunderstorm forcing to elevated greenhouse gas concentrations, *Geophys Res Lett* **36**: L01703.

Tropeano, D., Turconi, L. and Sanna, S. (2004). Debris flows triggered by the 29 august 2003 cloudburst in val canale, eastern italian alps, *Proceedings of the 10th Internationales Symposion InterPraevent 2004, Riva del Garda, Italy*, pp. 121–132.

Tukey, J. (1977). *Exploratory data analysis*, Addison–Wesley.

Turkington, T., Ettema, J., van Westen, C. and Breinl, K. (2014). Empirical atmospheric thresholds for debris flows and flash floods in the southern french alps, *Nat Hazard Earth Sys* **14**: 1517–1530.

Turkington, T., Remaître, A., Ettema, J., Hussin, H. and van Westen, C. (2016). Assessing debris flow activity in a changing climate, *Climatic Change* **137**: 293–305.

Ulbrich, U., Brücher, T., Fink, A., Leckebusch, G., Krüger, A. and Pinto, J. (2003). The central european floods of august 2002: Part 1 - rainfall periods and flood development, *Weather* **58**: 371–377.

Uppala, S., Køallberg, P., Simmons, A., Andrae, U., Bechtold, V., Fiorino, M., Gibson, J., Haseler, J., Hernandez, A., Kelly, G., Li, X., Onogi, K., Saarinen, S., Sokka, N., Allan, R., Andersson, E., Arpe, K., Balmaseda, M., Beljaars, A., van de Berg, L., Bidlot, J., Bormann, N., Caires, S., Chevallier, F., Dethof, A., Dragosavac, M., Fisher, M., Fuentes, M., Hagemann, S., Hólm, E., Hoskins, B., Isaksen, L., Janssen, P., Jenne, R., McNally, A., Mahfouf, J., Morcrette, J., Rayner, N., Saunders, R., Simon, P., Sterl, A., Trenberth, K., Untch, A., Vasiljevic, D., Viterbo, P. and Woollen, J. (2005). The era-40 re-analysis, *Q J Roy Meteor Soc* **131**: 2961–3012.

van Asch, T., Buma, J. and van Beek, L. (1999). A view on some hydrological triggering systems in landslides, *Geomorphology* **30**: 25–32.

van Asch, T., Tang, C., Alkema, D., Zhu, J. and Zhou, W. (2013). An integrated model to assess critical rainfall thresholds for run-out distances of debris flows, *Nat Hazards* pp. 1–13.

van den Besselaar, E., Tank, A. K. and Buishand, T. (2013). Trends in european precipitation extremes over 1951-2010, *Int J Climatol* **33**: 2682–2689.

van den Heuvel, F., Goyette, S., Rahman, K. and Stoffel, M. (2016). Circulation patterns related to debris-flow triggering in the zermatt valley in current and future climates, *Geomorphology* .

van der Linden, P. and Mitchell, J. (2009). Ensembles: Climate change and its impacts: Summary of research and results from the ensembles project, *Technical report*.

van Oldenborgh, G. L., Drijfhout, S., van Ulden, A., Haarsma, R., Sterl, A., Severijns, C., Hazeleger, W. and Dijkstra, H. (2009). Western europe is warming much faster than expected, *Clim Past* **5**: 1–12.

van Stokkom, H., Smits, A. and Leuven, R. (2005). Flood defense in the netherlands, *Water Int* **30**: 76–87.

van Vuuren, D. and Carter, T. (2014). Climate and socio-economic scenarios for climate change research and assessment: reconciling the new with the old, *Climatic Change* **122**: 415–429.

van Westen, C., van Asch, T. and Soeters, R. (2006). Landslide hazard and risk zonation-why is it still so difficult?, *B Eng Geol Environ* **65**: 167–184.

Vano, J., Kim, J., Rupp, D. and Mote, P. (2015). Selecting climate change scenarios using impact-relevant sensitivities, *Geophys Res Lett* **42**: 5516–5525.

Vaze, J., Post, D., Chiew, F., Perraud, J., Viney, N. and Teng, J. (2010). Climate non-stationarity - validity of calibrated rainfall-runoff models for use in climate change studies, *J Hydrol* **394**: 447–457.

Vennari, C., Gariano, S., Antronico, L., Brunetti, M., Iovine, G., Peruccacci, S., Terranova, O. and Guzzetti, F. (2014). Rainfall thresholds for shallow landslide occurrence in calabria, southern italy, *Nat Hazard Earth Sys* **14**: 317–330.

Viglione, A., Chirico, G., Komma, J., Woods, R., Borga, M. and Blöschl, G. (2010). Quantifying space-time dynamics of flood event types, *J Hydrol* **394**: 213–229.

Vormoor, K., Lawrence, D., Heistermann, M. and Bronstert, A. (2015). Climate change impacts on the seasonality and generation processes of floods – projections and uncertainties for catchments with mixed snowmelt/rainfall regimes, *Hydrol Earth Syst Sci* **19**: 913–931.

Wagener, T., McIntyre, N., Lees, M., Wheater, H. and Gupta, H. (2003). Towards reduced uncertainty in conceptual rainfall-runoff modelling: dynamic identifiability analysis, *Hydrol Process* **17**: 455–476.

Wang, W., Chen, M. and Kumar, A. (2010). An assessment of the cfs real-time seasonal forecasts, *Weather Forecast* **25**: 950–969.

Wang, X. (2008). Accounting for autocorrelation in detecting mean shifts in climate data series using the penalized maximal t or f test, *J Appl Meteorol Clim* **47**: 2423–2444.

Wang, X. and Feng, Y. (2010). Rhtestv3 user manual, *Technical report*. **URL:** *http://cccma.seos.uvic.ca/ETCCDMI/software.shtml*

Wardah, T., Bakar, S. A., Bardossy, A. and Maznorizan, M. (2008). Use of geostationary meteorological satellite images in convective rain estimation for flash-flood forecasting, *J Hydrol* **356**: 283–298.

Weatherhead, E., Gearheard, S. and Barry, R. (2010). Changes in weather persistence: Insight from inuit knowledge, *Global Environ Change* **20**: 523–528.

Weaver, C., Lempert, R., Brown, C., Hall, J., Revell, D. and Sarewitz, D. (2013). Improving the contribution of climate model information to decision making: the value and demands of robust decision frameworks, *Wiley Interdisciplinary Reviews: Climate Change* **4**: 39–60.

Wijngaard, J., Tank, A. K. and Können, G. (2003). Homogeneity of 20th century european daily temperature and precipitation series, *Int J Climatol* **23**: 679–692.

Wilks, D. (2011). *Statistical methods in the Atmospheric Sciences -3rd ed*, International Geophysics Series, 100. Elsevier.

Willems, P. and Vrac, M. (2011). Statistical precipitation downscaling for small-scale hydrological impact investigations of climate change, *J Hydrol* **402**: 193–205.

Winter, M., Dent, J., Macgregor, F., Dempsey, P., Motion, A. and Shackman, L. (2010). Debris flow, rainfall and climate change in scotland, *Q J Eng Geol Hydroge* **43**: 429–446.

Wood, A., Leung, L., Sridhar, V. and Lettenmaier, D. (2004). Hydrologic implications of dynamical and statistical approaches to downscaling climate model outputs, *Climatic Change* **62**: 189–216.

Wood, J., Harrison, S. and Reinhardt, L. (2015). Landslide inventories for climate impacts research in the european alps, *Geomorphology* **228**: 398–408.

Wood, J., Harrison, S., Turkington, T. and Reinhardt, L. (2016). Landslides and synoptic weather trends in the european alps, *Climatic Change* .

Wu, Y., Lan, H., Gao, X., Li, L. and Yang, Z. (2015). A simplified physically based coupled rainfall threshold model for triggering landslides, *Eng Geol* **195**: 63–69.

Zêzere, J., Trigo, R. and Trigo, I. (2005). Shallow and deep landslides induced by rainfall in the lisbon region (portugal): assessment of relationships with the north atlantic oscillation, *Nat Hazard Earth Sys* **5**: 331–344.

Zhang, X. and Yang, F. (2004). *RClimDex (1.0) User Manual*, Climate Research Branch, Environment Canada, Downsview, Ontario, Canada.

Zhuang, J., Cui, P., Wang, G., Chen, X., Iqbal, J. and Guo, X. (2015). Rainfall thresholds for the occurrence of debris flows in the jiangjia gully, yunnan province, china, *Eng Geol* **195**: 335–346.

Zolina, O., Kapala, A., Simmer, C. and Gulev, S. (2004). Analysis of extreme precipitation over europe from different reanalyses: a comparative assessment, *Global Planet Change* **44**: 129–161.

Zorita, E. and von Storch, H. (1999). The analog method as a simple statistical downscaling technique: Comparison with more complicated methods, *J Climate* **12**: 2474–2489.

Appendix A

A

A.1 Climate indices abbreviations

TMin > 20°C (days): The number of days with the minimum temperature greater than 20°C

TMax > 25°C (days): The number of days with the maximum temperature greater than 25°C

TMax < 0°C (days): The number of days with the maximum temperature less than 0°C

TMin < 0°C (days): The number of days with the minimum temperature less than 0°C

GSL (days) : Growing season length, days from first instance in a years of six consecutive days with daily mean temperature > 5°C till six consecutive days with daily mean temperature < 5°C)

Max TMax (°C): Monthly maximum daily maixmum temperature

Min TMax (°C): Monthly minimum daily maixmum temperature

Max TMin (°C): Monthly maximum daily minimum temperature

Min TMin (°C): Monthly minimum value of daily minimum temperature

DTR (°C): Diurnal temperature range, monthly mean difference between daily maximum and minimum temperature

Max 1dayR (mm): Monthly maximum 1-day precipitation total

Max 5dayR (mm): Monthly maximum 5-day precipitation total

Intensity (mm/day): Mean daily precipitation intensity (amount of precipitation divided by the number of days)

Days > X mm: Annunal number of days with precipitation greater than X.

Max CCD: Maximum number of consecutive days with precipitation less than 1mm

Max CWD: Maximum number of consecutive days with precipitation greater or equal to 1

R95p: The annual total amount of precipitation when the amount is greater than the 95^{th} percentile

R99p:The annual total amount of precipitation when the amount is greater than the 99^{th} percentile

Annual R (mm): Annual total precipitation

Appendix B

B

B.1 Flash events and associated return periods

Table B.1 List of flash event dates, associated 1-day (1) and 30-day (30) precipitation, return period (RP) and number of debris flows and flash floods (#).

Barcelonnette, B-1				
Date	1	30	RP	#
0/5/1979	17.3	28.7	<0.25y	5
4/06/1979	4.3	50.5	<0.25y	1
22/09/1980	27.4	50.5	<0.25y	1
28/06/1981	28.9	59.7	<0.25y	1
2/07/1981	6.6	81.6	<0.25y	1
7/06/1983	0	161.5	<0.25y	1
12/07/1983	1.9	26.8	<0.25y	4
23/08/1984	26.1	19.8	<0.25y	1
5/08/1985	50	8.9	<0.25y	1
6/08/1985	1.5	58.9	<0.25y	1
24/09/1985	2.1	37.4	<0.25y	5
6/07/1986	8.3	29	<0.25y	1
13/07/1986	40	36.1	<0.25y	5
6/08/1987	2.5	20.8	<0.25y	1
24/08/1987	14.5	60.7	<0.25y	1
1/07/1987	10	76.7	<0.25y	2
4/07/1987	2	83.7	<0.25y	1
7/71987	18.8	82.5	<0.25y	2
10/07/1987	0	2.4	<0.25y	1
11/08/1988	25	27.4	<0.25y	8
20/08/1988	16.2	27.2	<0.25y	1
20/07/1988	1.8	29	<0.25y	1
23/07/1988	0	28.7	<0.25y	1
29/09/1991	55.4	110.9	1-5y	1
6/10/1991	52.7	165.6	1-5y	1
3/11/1991	10	177.7	<0.25y	1
27/09/1992	29.6	91.6	<0.25y	1
5/11/1994	46	110.7	0.5-1y	3
19/08/1996	2.7	80.8	<0.25y	1
28/08/1997	27	60.8	<0.25y	1
12/08/2000	21.4	89.8	<0.25y	1
13/08/2000	0.8	111.2	<0.25y	1
23/11/2000	49.4	211.2	1-5 y	1
5/08/2003	2.8	36.9	<0.25y	4
8/08/2003	2.4	41.9	<0.25y	2
1/06/1992	21.8	91.2	<0.25y	1

Barcelonnette, B-1				
Date	1	30	RP	#
2/06/1992	4.1	112.7	<0.25y	2
18/06/1992	8.8	150.5	<0.25y	6
21/07/1992	4.7	85.5	<0.25y	1
10/07/1993	17.1	88.8	<0.25y	2
13/05/1994	7.5	36.6	<0.25y	1
5/07/1996	16.5	106.8	<0.25y	1
25/07/1997	0	89	<0.25y	1
22/03/2001	3	161	<0.25y	1
25/07/2001	18.8	32.2	<0.25y	1
5/06/2002	25.4	69	<0.25y	3
23/06/2002	0	95.6	<0.25y	1
27/72003	0	35.9	<0.25y	1
5/09/2004	0	62.1	<0.25y	1
19/06/2005	6.8	21.8	<0.25y	1
20/06/2005	18.6	28.6	<0.25y	1
18/7/2005	12.9	85.3	<0.25y	1
12/72007	0.2	45.8	<0.25y	1
30/06/2009	2.8	69.8	<0.25y	1
Fella River, F-5				
Date	1	30	RP	#
13/08/1991	7.6	183	<0.25y	1
1/04/1992	76.2	152	<0.25y	1
9/10/1993	102.6	464.2	0.5-1y	1
14/10/1993	65.4	578.6	0.5-1y	2
8/08/1994	22	224.8	<0.25y	1
27/12/1995	0	126.1	<0.25y	1
22/06/1996	348.8	174	>5y	40+
8/07/1996	74	667.8	0.5-1y	2
14/11/1996	87.2	289	0.25-.5y	3
15/11/1996	221.2	374.8	>5 y	2
12/09/1998	122.2	249.8	0.5-1y	1
17/08/1999	110.8	233.3	0.5-1y	1
1/11/2000	69.6	416.8	0.25-.5y	1
30/08/2003	352.6	118.7	>5y	100+
16/08/2008	207.4	288.2	1-5y	1
19/06/2011	134.6	304.2	1-5 y	10+

Appendix C

C

C.1 Quantile mapping skill

The skill of the quantile mapping for the validation and calibration datasets was in part based on the RMSE given in Table C.1. From this table, the quantile mapping improved the performance of the RCM precipitation data. In every case the RMSE was lower after the bias correction for both the validation and calibration datasets.

Table C.1 Performance skill of RCMs for the calibration (Cal) and validation (Val) datasets. Root mean squared error is given for the data both before (Raw) and after (Corr) the quantile mapping correction is applied. The abbreviations refer to RCM and driving model in Table 4.2.

			Barcelonnette						
	Driving GCM		CE	CN	GF	IP	EC		
	RCM		SM					DM	KN
RCP45	Cal	Raw	3.46	4.23	4.69	3.20	3.08	3.94	2.70
		Corr	0.76	0.51	0.50	0.50	0.55	0.61	0.49
	Val	Raw	3.31	4.25	4.78	3.19	3.03	3.84	2.58
		Corr	0.51	0.56	0.71	0.43	0.86	0.40	0.65
RCP85	Cal	Raw	3.43	4.22	4.71	3.20	3.09	3.95	2.71
		Corr	0.71	0.43	0.61	0.49	0.54	0.54	0.62
	Val	Raw	3.40	4.33	4.67	3.19	2.97	3.77	2.57
		Corr	0.59	0.57	0.71	0.55	0.79	0.56	0.70
			Fella River						
	Driving GCM		CE	CN	GF	IP	EC		
	RCM		SM					DM	KN
RCP45	Cal	Raw	6.17	5.80	5.75	6.24	6.00	4.96	5.34
		Corr	0.84	1.02	0.89	0.95	0.96	0.87	0.81
	Val	Raw	5.98	5.17	5.32	5.32	6.40	4.71	5.54
		Corr	1.05	0.71	1.42	0.59	1.35	0.87	1.22
RCP85	Cal	Raw	6.17	5.88	5.85	6.18	5.98	4.91	5.28
		Corr	0.86	1.03	0.76	0.99	0.84	0.87	0.82
	Val	Raw	5.80	4.80	4.60	5.80	6.33	4.89	5.68
		Corr	0.89	0.87	0.81	0.96	1.53	0.82	1.04

Appendix D

D

D.1 Debris-flow day probability

The debris-flow day probability is given in Table D.1 for the rain-proxy. The number of debris-flow days for the rain-proxy and QCAPE-proxy are in Table D.2 and S7 respectively, for the two base periods (1950-1979 and 1980-2009). For both study areas the absolute number of debris-flow days is greater in the second base period, while the number of days in each rain-bin is fairly consistent. The exception is for Fella River, where the highest rainfall b For Barcelonnette, there is little difference between seasons and bins for the average number of debris flows per day/day. However, for Fella River, there is clear increase in number of debris flows with higher rainfall bins (from 1-2 per day/day to 3-75 per day/day).

Table D.1 Empirical probability of debris-flow days for the rain-proxy based periods 1950-1979 and 1980-2009. The bins assume greater than the lower value and equal or less than any upper value. The unit is %.

		Probability of debris flow											
		Barclonnette						Fella River					
		Bin1	Bin2	Bin3	Bin4	Bin5	Bin6	Bin1	Bin2	Bin3	Bin4	Bin5	Bin6
All year	1950 1979	0.0	0.8	2.5	4.9	6.1	25.0	0.0	0.3	1.2	8.0	12.5	-
	1980 2009	0.1	3.4	8.2	13.3	43.5	36.4	0.1	1.0	5.1	11.8	14.3	66.7
Summer	1950 1979	0.0	1.7	4.3	9.4	7.7	50.0	0.0	0.0	1.8	6.3	20.0	-
	1980 2009	0.2	5.7	11.4	16.7	52.9	60.0	0.1	1.2	3.6	15.0	20.0	66.7

The debris-flow day probability for the QCAPE-proxy is given in Table D.3, with the number of debris-flow days and number of debris-flows per event in Table D.3.

To determine the significance of the two proxies, the probability of a debris-flow day for each of the proxy bins using the dummy dataset is compared with the actual probability in Table D.5. All of the highest bins had a significantly higher probability of debris flow day than by chance. The exception was for the rain-proxy 1950-1979 for Fella River, where

Table D.2 Number of days for each rainfall bin (precipitation), and number of days with one or more debris flow(s) observed (DF day) for the Barcelonnette Basin and the Fella River Basin. The average number of debris flows per DF day is also included for each of the bins. A refers to projections using the 1950-1979 base period, and B for the 1980-2009 base period. The first two groups show results for the two historical periods (1950-1979 and 1980-2009). All = all year, S = summer only.

			Data for debris-flow proxy											
			Barclonnette						Fella River					
			Bin1 0-10	Bin2 10-20	Bin3 20-30	Bin4 30-40	Bin5 40-50	Bin6 50+	Bin1 0-25	Bin2 25-50	Bin3 50-75	Bin4 75-100	Bin5 100-150	Bin6 150+
DFdays	All	A	0	4	4	3	2	4	1	1	1	2	1	0
		B	2	15	12	6	10	4	2	4	5	4	1	2
	S	A	0	4	3	3	1	4	1	0	1	1	1	0
		B	2	15	12	6	10	4	2	3	2	3	1	2
#DF/event	All	A	0	1.5	1.3	5	2.5	1.5	1	2	1	2.5	2	-
		B	1	1.1	1.4	1.5	1.3	1.5	1	1.5	2.6	4.3	4	140
	S	A	0	1.5	1.3	5	1	1.5	1	0	1	2	2	-
		B	1	1.1	1.4	1.5	1.3	1	1.5	1.7	3.5	2.6	4	140
Rain gauge	All	A	2211	480	158	61	33	16	3728	390	86	25	8	0
		B	2354	443	146	45	23	11	3528	393	98	34	7	3
	S	A	1170	231	69	32	13	8	2059	216	57	16	5	0
		B	1345	240	70	25	13	7	2049	252	55	20	5	3

Table D.3 Debris flow day probability based QCAPE proxy (CAPE (J/kg) and Q750 (g/kg)) for the period 1980-2009 using ERA-Interim data.The unit is %.

	Probability of debris flow											
	Barclonnette						Fella River					
	Bin1	Bin2	Bin3	Bin4	Bin5	Bin6	Bin1	Bin2	Bin3	Bin4	Bin5	Bin6
CAPE	2400 2900	2900 3400	3400 3900	3900 4400	4400 +	440 +	2600 3000	3000 3400	3400 3800	3800 4200	4200 +	4200 +
Q750	3.4	3.2	3.2	3.4	3.2	7.0	5.0	3.0	3.0	3.0	3.0	5.0
All year	1.4	1.1	1.3	1.6	1.5	50.0	0.5	0.4	0.2	0.5	3.2	6.5
Summer	1.7	1.3	1.5	2.0	0.0	50.0	0.5	0.4	0.2	0.8	0	4.8

this amount was not observed. Barcelonnette has more bins where the actual probability was significantly higher than using the dummy dataset, although this was partly due to the higher number of debris-flow days for this study area.

Table D.4 Number of days in each QCAPE bin from observations (QCAPE)1980-2009. The first two groups show the number of debris-flow days (DF days) and average number of debris flow days per bin.

		Data for debris-flow proxy QCAPE-proxy											
		Barclonnette						Fella River					
	CAPE	Bin1 2400-2900	Bin2 2900-3400	Bin3 3400-3900	Bin4 3900-4400	Bin5 4400 +	Bin6 4400 +	Bin1 2600-3000	Bin2 3000-3400	Bin3 3400-3800	Bin4 3800-4200	Bin5 4200 +	Bin6 4200 +
	Q750 (g/kg)	3.4 +	3.2 +	3.2 +	3.2 +	3.4-7.0	7.0 +	5 +	3 +	3 +	3 +	3 +	5 +
DF days	All	13	16	12	5	1	2	2	6	2	3	3	2
	Sum	13	16	11	5	0	2	2	5	2	3	0	1
#DF/ event	All	1.3	1.4	1.1	1.4	1	1	2	1.7	1.5	50	5	75
	Sum	1.3	1.4	1.1	2.6	-	1	2	1.8	1.5	50	-	144
QCAPE	All	915	1373	947	313	68	4	373	1427	1188	553	93	31
	Sum	780	1136	740	244	38	4	371	1170	930	386	29	21

Table D.5 The probability of a debris-flow day based on the proxies (Proxy) and for the 95%, 99, and 99.9% percentile for the 10,000 dummy datasets (Monte Carlo). For the no bin, the Monte Carlo results are for the 5%, 1%, and 0.1% respectively. Bin 1 is the lowest rainfall or QCAPE bin, while Bin 6 is for the highest (i.e. 50mm+ for Barcelonnette, and 150mm+ for Fella River). Unit is %

	Barcelonnette											
	Rain proxy 1950-1979				Rain proxy 1980-2009				QCAPE proxy 1980-2010			
	Proxy	Monte Carlo			Proxy	Monte Carlo			Proxy	Monte Carlo		
		0.95	0.99	0.999		0.95	0.99	0.999		0.95	0.99	0.999
Bin 6	25.00	0.00	7.14	7.14	36.40	0.00	11.11	22.22	50	0.00	25	25
Bin 5	6.1	0.00	4.55	9.09	43.50	4.76	4.76	9.52	1.50	1.47	2.94	4.41
Bin 4	4.90	2.33	2.33	4.65	13.30	2.38	4.76	4.76	1.60	1.28	1.60	1.92
Bin 3	2.50	0.96	1.92	2.88	8.20	1.47	2.21	2.94	1.30	0.84	0.95	1.16
Bin 2	0.80	0.57	0.85	1.14	3.40	1.02	1.27	1.78	1.10	0.73	0.87	1.02
Bin 1	0.00	0.37	0.49	0.56	0.10	0.70	0.84	0.94	1.40	0.77	0.98	1.20
No Bin	0.00	0.15	0.14	0.10	0.00	0.42	0.39	0.35	0.00	0.37	0.34	0.30
	Fella River											
	Rain proxy 1950-1979				Rain proxy 1980-2009				QCAPE proxy 1980-2010			
	Proxy	Monte Carlo			Proxy	Monte Carlo			Proxy	Monte Carlo		
		0.95	0.99	0.999		0.95	0.99	0.999		0.95	0.99	0.999
Bin 6	-	-	-	-	66.70	0.00	0.00	33.33	6.50	0	4	4
Bin 5	12.50	0.00	0.00	12.50	14.30	0.00	0.00	14.29	3.20	1.25	2.50	2.50
Bin 4	8.00	0.00	4.00	4.00	11.80	2.94	2.94	5.88	0.50	0.61	0.81	1.01
Bin 3	1.20	0.00	1.16	2.33	5.10	1.02	2.04	2.04	0.20	0.37	0.56	0.65
Bin 2	0.30	0.26	0.51	0.51	1.00	0.51	0.76	1.02	0.40	0.39	0.47	0.62
Bin 1	0.00	0.11	0.13	0.16	0.10	0.26	0.31	0.34	0.50	0.60	0.90	1.20
No Bin	0.00	0.03	0.01	0.00	0.00	0.12	0.10	0.07	0.00	0.14	0.11	0.09

Appendix E

E

E.1 Flood typing flow chart

Figure E.1 outlines the different steps in the methodology. The steps follows the solid black arrows. dotted lines indicate where the all or some of the parameters from the historical period model set are use the future periods.

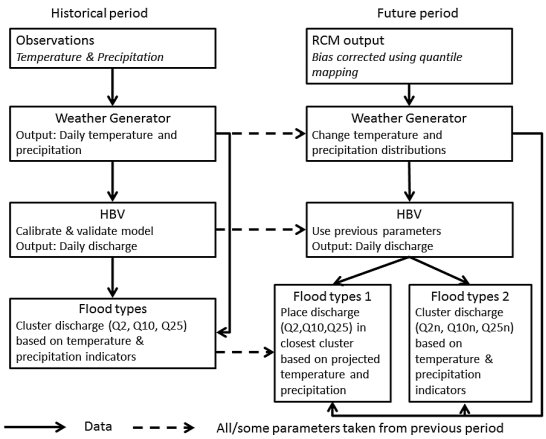

Figure E.1 Flowchart of the methodology for the historical period (left) and future period (right). The solid black lines indicate the main pathway, with dotted lines indicated that parameters from the historical period were also used. Q2, Q10, Q25 indicate discharge magnitudes based on historical return periods, while Q2n, Q10n, and Q25n indicate discharge magnitudes based on the future return periods (2, 10, 25 years). Flood type 1 and 2 refer to Approach 1 and Approach 2

E.2 Silhouette Index for future projections

The individual silhouette values for each of the future flood events are shown in Figure E.2 for Ubaye and Figure E.3 for Salzach. Values greater than 0 indicate that the flood event is most similar to flood events in the

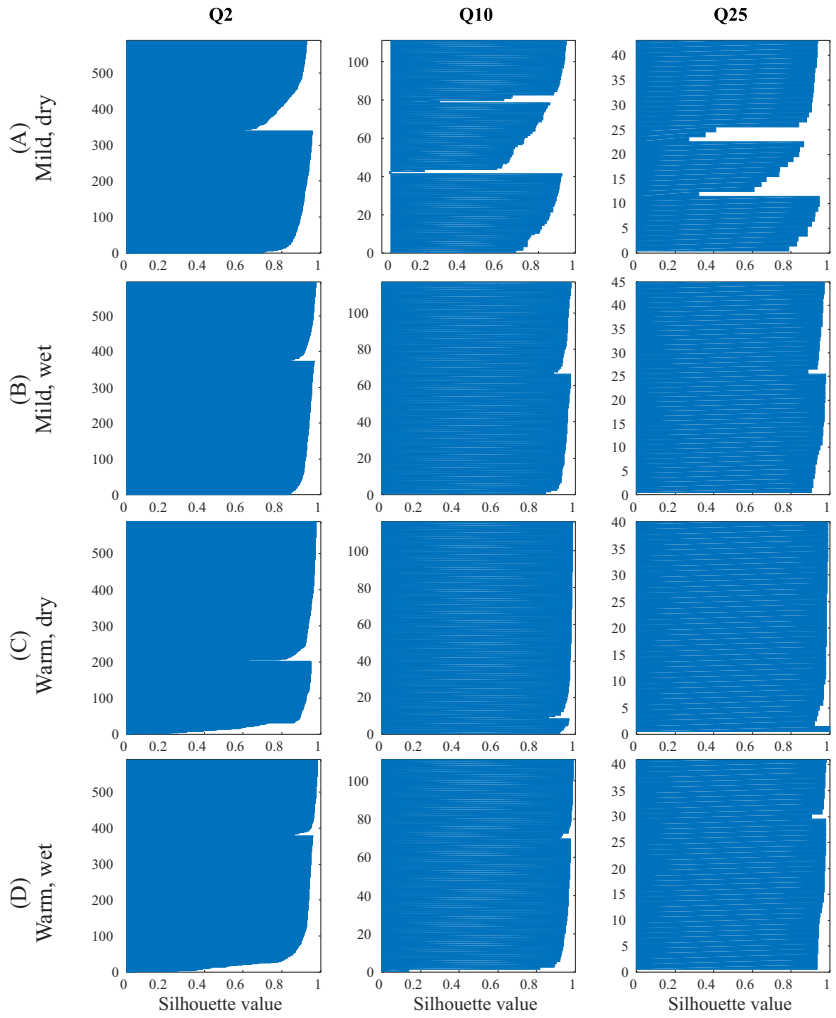

Figure E.2 The individual silhouette values for each of the flood events in Ubaye for the period 2070-2099. The four scenarios, a-d, represent the four projections selected in Figure 7.3 in the main text.

same cluster than those in the next closest cluster, with 1 being a perfect fit. Near zero values indicate no preferred cluster, and negative values indicate a poor fit.

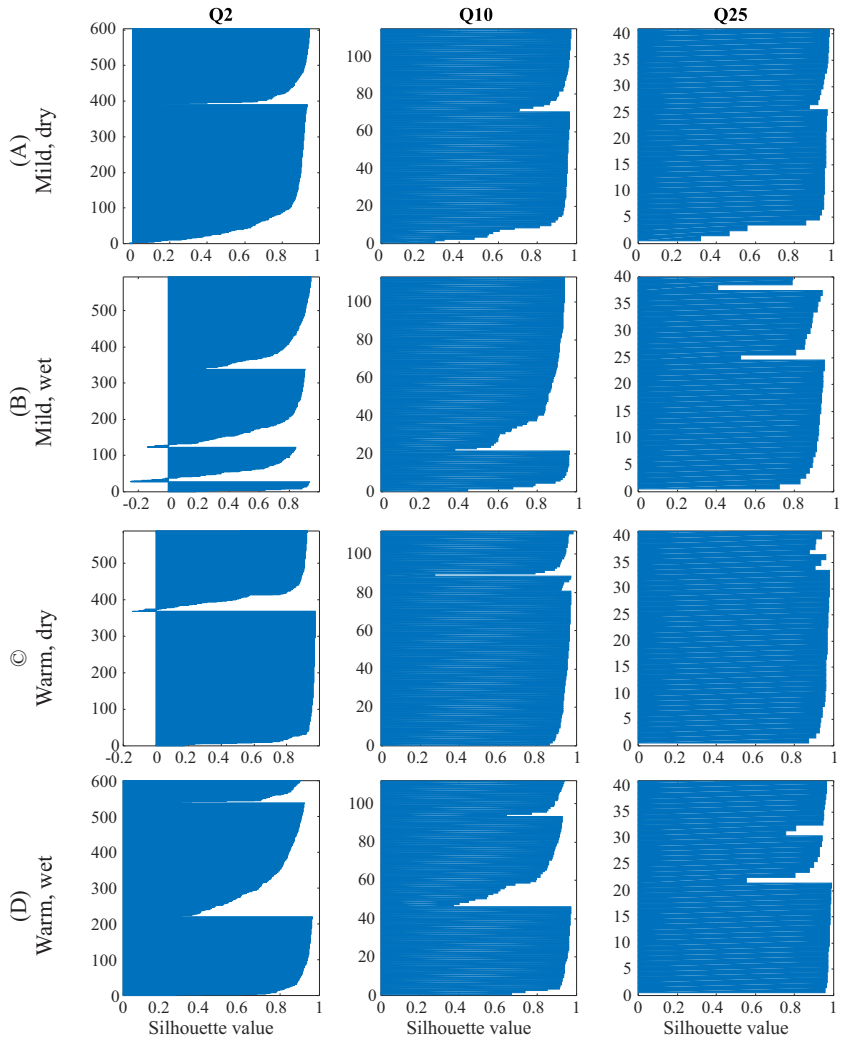

Figure E.3 The individual silhouette values for each of the flood events in Salzach for the period 2070-2099. The four scenarios, a-d, represent the four projections selected in Figure 7.3 in the main text.

Biography

Thea Turkington was born in Vancouver, Canada, and spent most of her formative years criss-crossing the Pacific between Canada and New Zealand. After completing high school in New Zealand, Thea returned to Canada in 2002 to study Physics and Earth Sciences at the University of Victoria, Canada, and received a BSc in 2007. She then travelled back to Aotearoa to train as a Meteorologist at Meteorological Service of New Zealand Limited (MetService), during which time she obtained a Postgraduate Certificate in Meteorology from Victoria University of Wellington, New Zealand. She continued working at MetService as a forecaster in the aviation department before deciding in 2010 to continue with further education. She obtained an MSc in Climate Change Science from the University of East Anglia, United Kingdom, with a thesis titled 'Future drought in Central America: a comparison of an aggressive mitigation scenario with the SRES A1B scenario using the Standardized Precipitation Index'. In 2011 she joined the CHANGES project and began the PhD journey at the University of Twente, Faculty of Geo-information Science and Earth Observation (ITC), Netherlands. From her beginning as an undergraduate student right through to her PhD studies, Thea has maintained an interest in natural hazards, extreme weather, and the climate in general.

Author's publications

Peer-reviewed journal articles

Turkington, T., Breinl, K., Ettema, J., Alkema, D., and Jetten, V. (under review). A new flood type classification method for use in climate change impact studies.

Turkington, T., Remaître, A., Ettema, J., Hussin, H. and van Westen, C. (2016). Assessing debris flow activity in a changing climate, *Climatic*

Change, 137:293–305.

Turkington, T., Ettema, J., van Westen, C. and Breinl, K. (2014). Empirical atmospheric thresholds for debris flows and flash floods in the southern french alps, *Nat Hazard Earth Sys*, 14:1517–1530.

Bharti, V., Singh, C., Ettema, J., **Turkington, T.** (2016). Spatiotemporal characteristics of extreme rainfall events over the Northwest Himalaya using satellite data, *International Journal of Climatology*.

Chen, L., van Westen, C., Hussin, H., Ciurean, R., **Turkington, T.**, Chavarro-Rincon, D., Shrestha, D. (2016). Integrating expert opinion with modelling for quantitative multi-hazard risk assessment in the Eastern Italian Alps,*Geomorphology*, 273:150–167.

Wood, J., Harrison, S., **Turkington, T.**, Reinhardt, L. (2016) Landslides and synoptic weather trends in the European Alps. *Climatic Change*, 136, 297-308

Breinl, K., **Turkington, T.** , Stowasser, M. (2014). Simulating daily precipitation and temperature: a weather generation framework for assessing hydrometeorological hazards, *Meteorological Applications*, 22: 334–347.

Breinl, K., **Turkington, T.**, Stowasser, M. (2013). Stochastic generation of multi-site daily precipitation for applications in risk management, *Journal of Hydrology*, 498:23–35.

Conference proceedings (oral presentations)

Turkington, T., Ettema, J. Malet, J.P., Remaître, A. and van Westen, C.J. (2014) Impacts of climate change on debris flows – what are some of the challenges? Conference paper for presentation: International Conference Analysis and Management of Changing Risks for Natural Hazards, Padua, Italy.

Turkington, T., Ettema, J., and van Westen C.J. (2013) Linking meteorological conditions to flood and flash flood occurrence – why is it so difficult? Conference abstract for presentation: 7th European Conference on Severe Storms, Helsinki, Finland.

Turkington, T., Breinl, K., van Westen, C.J., Malet-J.-P., Ettema, J. (2013). Analysing the problems involved in assessing hydro - meteorological triggers. Conference abstract for presentation: Geophysical Research Abstracts, vol. 15, EGU2013-1678.

Netherlands Research School for the
Socio-Economic and Natural Sciences of the Environment

D I P L O M A

For specialised PhD training

The Netherlands Research School for the
Socio-Economic and Natural Sciences of the Environment
(SENSE) declares that

Thea Anne Rex Turkington

born on 2 December 1983 in Vancouver, Canada

has successfully fulfilled all requirements of the
Educational Programme of SENSE.

Enschede, 22 September 2016

the Chairman of the SENSE board	the SENSE Director of Education
Prof. dr. Huub Rijnaarts	Dr. Ad van Dommelen

The SENSE Research School has been accredited by the Royal Netherlands Academy of Arts and Sciences (KNAW)

K O N I N K L I J K E N E D E R L A N D S E
A K A D E M I E V A N W E T E N S C H A P P E N

The SENSE Research School declares that **Ms Thea Turkington** has successfully fulfilled all requirements of the Educational PhD Programme of SENSE with a work load of 40.7 EC, including the following activities:

SENSE PhD Courses

- SENSE summer symposium - Make a change: Successful interaction with society (2014)
- Environmental research in context (2014)
- SENSE Masterclass - The Anthropocene: Anything new under the sun?
- Research in context activity: 'Contributing analysis to reviewing of IPCC chapter under coordination of the Netherlands Environmental Assessment Agency (PBL)' (2013) and 'active member of SENSE PhD Council' (2014-2016)

Other PhD and Advanced MSc Courses

- Diverse training activities in the project Changing Hydro-meteorological Risks as Analysed by a New Generation of European Scientists (CHANGES), EU FP7 Programme / Marie Curie Initial Training Network (2011-2014)

Management and Didactic Skills Training

- Supervising an MSc student with thesis entitled 'Investigation of Extreme Rainfall Events over the Northwest Himalaya Region', University of Twente (2014)
- Co-organising PhD workshops and trips, Department of Earth Systems Analysis (ESA), University of Twente (2014-2015)

Oral Presentations

- *Analysing the problems involved in assessing hydro-meteorological triggers.* European Geosciences Union General Assembly (EGU2013), 7-12 April 2013, Vienna, Austria
- *Linking meteorological conditions to flood and flash flood occurrence.* 7th European Conference on Severe Storms (ECSS2013), 3-7 June 2013, Helsinki, Finland
- *Impacts of climate change on debris flows – what are some of the challenges?* International Conference Analysis and Management of Changing Risks for Natural Hazards, 18-19 November 2014, Padua, Italy

SENSE Coordinator PhD Education

Dr. ing. Monique Gulickx

ITC dissertations

A complete list of ITC dissertations is online on the ITC website: www.itc.nl/research/phd/phd_graduates.aspx.

This dissertation has number 288.